



PREPARATION OF Cu₇S₄ NANOSTRUCTURED THIN FILMS FROM [(Et(Bu)NC(S)NC(O)C₆H₃(NO₂)-3,5)₂Cu(II) BY AEROSOL ASSISTED CHEMICAL VAPOUR DEPOSITION

Sohail Saeed^{[a],*}, Naghmana Rashid^[a], Rizwan Hussain^[b]

Keywords: Copper complex; copper sulphide (Cu₇S₄); thin film; aerosol assisted chemical vapour deposition (AA-CVD); SEM; powder XRD; *N*-[ethyl(butyl)carbamothioyl]-3,5-dinitrobenzamide ligand

The copper(II) complex of *N*-[ethyl(butyl)carbamothioyl]-3,5-dinitrobenzamide (**1**) has been synthesized and characterized by elemental analysis, IR spectroscopy and atmospheric pressure chemical ionization-mass spectrometry (MS-APCI). Thermogravimetric analysis shows the complex (**2**) decomposes in two-step to form copper sulfide. The complex was used as single-source precursor for the deposition of copper sulfide thin film by aerosol assisted chemical vapour deposition (AA-CVD) at 350 °C. Powder X-ray diffraction (p-XRD) pattern of thin film of complex showed the deposition of *monoclinic roxbyite* Cu₇S₄ and *orthorhombic anilite* Cu₇S₄ phases at 350 °C with spherical crystallites. The degree of film surface roughness was determined by atomic force microscopy (AFM). The scanning electron microscopy (SEM) and energy dispersive X-ray analysis (EDX) results showed the uniform distribution of copper sulfide in the film, which makes it useful semiconducting material on a structured surface.

Corresponding Authors

Tel.: + 0092-51 - 9250081

Fax: + 0092- 51- 9250081

E-Mail: sohail262001@yahoo.com (S.Saeed)

[a] Department of Chemistry, Research Complex, Allama Iqbal Open University, Islamabad-44000, Pakistan

[b] National Engineering & Scientific Commission, P.O. Box. 2801, Islamabad, Pakistan

successive ionic layer adsorption and reaction,¹⁶ chemical bath deposition¹⁷ and chemical vapor deposition.¹⁸

Thiourea and its alkyl derivatives are important precursors for the preparation of metal sulfide nanoparticles. Besides focusing on the applications of these ligands, special attention has been placed on their coordination chemistry to different metal atoms because of the various potential donor sites that these ligands possess.¹⁹

Introduction

Recently, nanostructured materials have attracted great attention in the fields of experimental and theoretical chemistry sciences.¹⁻³ Due to extensive dependence of the properties and application of nanostructured semiconductors on their crystal phase, size, composition and shape, synthesizing of highly tuned nanocrystals have been a challenging issue.⁴

Copper sulfides thin films and nanoparticles have been investigated for many uses including as: p-type semiconductors in solar cells,⁵⁻⁷ nanoscale switches⁸ and cathodic materials for lithium rechargeable batteries.⁹ Vaughan¹⁰ reported that in 1940 only the end member (Cu₂S) and CuS were known in the Cu-S system. By 1974 nine more copper sulfide phases had been identified^{11, 12} and in 2006 a total of fourteen copper sulfide phases were recognized.¹² Some known forms of copper sulfide include: *chalcocite* (Cu₂S), *djurleite* (Cu₃₁S₁₆ or Cu_{1.94}S), *digenite* (Cu₉S₅ or Cu_{1.8}S), *anilite* (Cu₇S₄ or Cu_{1.75}S), *covellite* (CuS) and *villamaninite* (CuS₂).⁷⁻¹³ Thin films of copper sulfide have been prepared by various methods including RF-reactive sputtering,¹⁴ spray pyrolysis,¹⁵

Arslan *et.al*²⁰ and Benzet *et.al*²¹ reported the complexation of Cu(II) and Zn(II) with thiourea derivatives and concluded that the coordination was through the sulfur and oxygen atom, using infrared spectroscopy and X-ray diffractions to determine the coordination. In addition, complexes prepared using the alkyl thiourea, such as methylthiourea, showed, using infrared spectroscopy, that the coordination also was through sulfur.²¹ Thiourea and its derivatives were used as a source of sulfur because their advantages in this regard are that they are stable for a long time, easy to synthesize, inexpensive and yield good quality crystalline semiconductor particles.

Our interest in such precursors led us to synthesize an unsymmetrical copper complex to be used as single source precursor for copper sulfide. The single source precursor can be easily synthesized in high yield from relatively inexpensive and only mildly hazardous starting materials, making them ideal for the potential large scale manufacturing of copper sulfide nanostructured thin film.

Experimental Section

Materials and Reagents

Analytical grade *N*-ethylbutyl amine (98 %), sodium thiocyanate (99%), copper(II) nitrate trihydrate (99.5 %), tetrabutylammonium bromide (TBAB) ($\geq 98\%$) and 3,5-dinitrobenzoyl chloride ($\geq 98.0\%$) were purchased from Sigma-Aldrich. Analytical grade solvents such as; tetrahydrofuran (THF), toluene, acetonitrile, *n*-hexane, dichloromethane, ethanol, methanol, chloroform, ethyl acetate and others were purchased from Sigma-Aldrich and Riedel-deHaen (Germany) whereas ethanol and acetone were dried using standard procedures.²² All the synthetic manipulations were carried out in air except for the aerosol assisted chemical vapour deposition experiment. The demonstration of AACVD was carried out under argon inert atmosphere.

Physical Measurements

Elemental analysis was carried out using Perkin Elmer CHNS/O 2400. Obtained results were within 0.4 % of the theoretical values. Infrared spectra were recorded on a Specac single reflectance Attenuated Total Reflectance (ATR) instrument (4000-400 cm⁻¹, resolution 4cm⁻¹). Atmospheric Pressure Chemical Ionization Mass Spectrometry (MS-APCI) of copper complex was recorded on a Micromass Platform II instrument. Metal analysis of the complex was carried out by Thermo iCap 6300 Inductively Coupled Plasma Optical Emission Spectroscopy (ICP-OES). Thermal stability of the copper complex was studied by thermogravimetry in an inert atmosphere, at sample heating rate of 10 °C/min, with a DuPont 2000 ATG. Melting points were recorded on Electrothermal IA9000 series digital melting point apparatus. X-ray Powder Diffraction (p-XRD) studies were performed on a Xpert diffractometer using Cu-K α radiation. The sample was mounted flat and scanned between 20 and 65° with a step size of 0.05 with various count rates. The diffraction pattern was then compared to the documented patterns in the International Center Diffraction Data (ICDD) index.

Preparation of the Ligand and Copper(II) Complex

Synthesis of N-[ethyl(butyl)carbamothioyl]-3,5-dinitrobenzamide (1)

A solution of 3,5-dinitrobenzoyl chloride (0.01 mol) in anhydrous acetone (80 ml) and 3% tetrabutylammonium bromide (TBAB) in acetone was added drop-wise to a suspension of sodium thiocyanate in acetone (50 ml) and the reaction mixture was refluxed for 45 minutes. After cooling to room temperature, a solution of *N*-butylethyl amine (0.01 mol) in acetone (25 ml) was added and the resulting mixture refluxed for 2 h. The reaction mixture was poured into five times its volume of cold water, whereupon the thiourea precipitated. The solid product was washed with water and purified by re-crystallization from an ethanol-dichloromethane mixture (1:2). Light Yellow. M.p.: 126-127 °C. Yield: 3.0g (74 %). IR ($\nu_{\max}/\text{cm}^{-1}$): 3235 (NH), 2922, 2845 (C-H), 1691(C=O),

1258 (C=S). ¹H NMR (400 MHz, CDCl₃) in δ (ppm) and *J* (Hz): δ 9.10 (t, 1H, *J* = 1.8), 8.84 (d, 2H, *J* = 1.8), 8.35(bs, 1H, CONH), 3.91(t, 2H, N-CH₂), 3.55(m, 2H, N-CH₂), 1.83(m, 2H, -CH₂-), 1.44(m, 2H, -CH₂-), 1.20(t, 3H, CH₃), 0.93(t, 3H, CH₃). *Anal. Calcd.* for C₁₄H₁₈N₄O₅S: C, 47.45; H, 5.12; N, 15.81; S, 9.05. Found: C, 47.47; H, 5.09; N, 15.82; S, 9.03.

Synthesis of bis[N-[ethyl(butyl)carbamothioyl]-3,5-dinitrobenzamide]copper(II) (2)

To a stirred solution thiourea ligand (3.54 g, 0.01 mol) in ethanol (30 ml) was added drop-wise a solution of copper nitrate (1.20 g, 0.005 mol) in ethanol (30 ml). The reaction mixture was stirred for 3h. The reaction mixture was filtered, washed with ethanol and re-crystallized from THF/acetonitrile mixture (1:1). Dark brown. Yield: 3.6 g (77 %). IR ($\nu_{\max}/\text{cm}^{-1}$): 2928, 2855(Ar-H), 1507(C-O), 1536(C-N), 1153(C-S); *Anal. Calcd.* for C₂₈H₃₄N₈O₁₀S₂Cu: C, 43.66; H, 4.45; N, 14.55; S, 8.33; Cu, 8.25. Found: C, 43.11; H, 4.02; N, 14.95; S, 8.32; Cu, 7.94. Mass (MS-APCI) (major fragment, m/z): 770[M+, C₂₈H₃₄N₈O₁₀S₂Cu].

Deposition of copper sulfide thin film by Aerosol Assisted Chemical Vapor Deposition (AA-CVD)

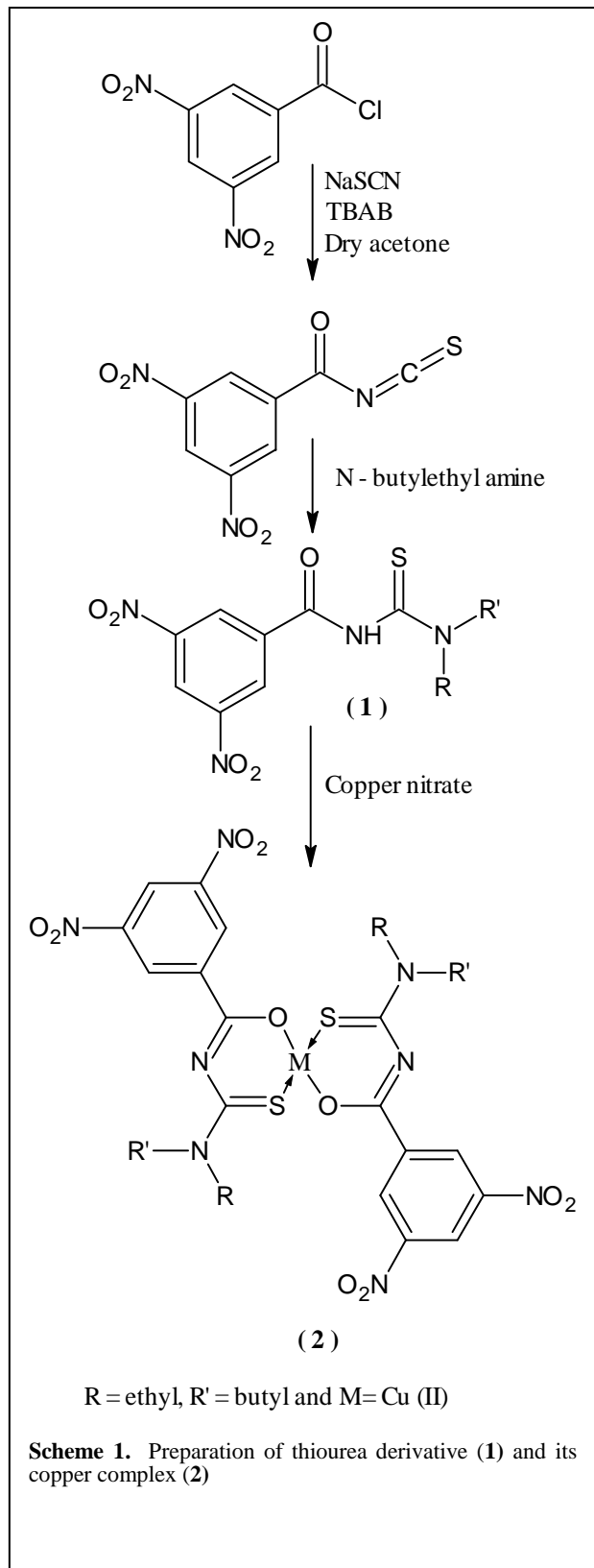
Experiments were designed according to those reported by us previously. In a typical experiment, 0.25 g of the precursor was dissolved in 15 ml tetrahydrofuran (THF) was loaded in a two-necked 100 ml round-bottom flask with a gas inlet that allowed the carrier gas (argon) to pass into the solution to aid the transport of the aerosol. This round-bottom flask was connected to the reactor tube by a piece of reinforced tubing. The argon flow rate was controlled by a Platon flow gauge. Seven soda glass substrates (approx. 1 × 2 cm) were placed inside the reactor tube, which is placed in a CARBOLITE furnace. The precursor solution in a round-bottom flask was kept in a water bath above the piezoelectric modulator of a PIFCO ultrasonic humidifier (Model No. 1077). The aerosol droplets of the precursor thus generated were transferred into the hot wall zone of the reactor by carrier gas. Both the solvent and the precursor were evaporated and the precursor vapor reached the heated substrate surface where thermally induced reactions and film deposition took place.

Results and Discussion

Most of the materials reported for photovoltaic use are either toxic or use less-abundant elements such as lead, cadmium, Indium or gallium. Less-toxic, abundant, and thus cheaper materials may be more promising even with overall lower efficiencies. Recent estimates of the annual electricity potential as well as material extraction costs and environmental friendliness led to the identification of materials that could be used in photovoltaic applications on a large scale.²³ The most promising materials include iron and copper sulfide.

Preparation and Spectroscopic Characterization

The bidentate ligand was synthesized from 3,5-dinitrobenzoyl chloride, sodium thiocyanate and *N*-butylethyl amine in anhydrous acetone. The thiourea derivative (1) and its copper complex (2) were synthesized according to the reported procedure²⁴⁻²⁹ with minor modifications as presented in **Synthesis Scheme**.



The use of phase transfer catalyst as a method of agitating a heterogeneous reaction system is gaining recognition.^{30,31} In search of improved methods to prepare the target thiourea by reacting isothiocyanates with nucleophiles, we have found that the use of tetrabutylammonium bromide (TBAB) as phase transfer catalyst (PTC) can produce isothiocyanates in good yield. The reaction proceeds via a nucleophilic addition of the secondary amine to the isothiocyanate. We have conducted our reaction using tetrabutylammonium bromide (TBAB) as phase transfer catalyst to synthesize the thiourea derivative.

Four coordinated copper(II) complex (2) were synthesized by reacting copper nitrate with *N*-[ethyl(butyl)carbamothioyl]-3,5-dinitrobenzamide (1) in ethanol. The copper(II) complex (2) obtained is green in color, air stable, non-hygroscopic in nature, soluble in tetrahydrofuran(THF), acetonitrile, dichloromethane, chloroform, DMSO, and DMF. The solid state IR spectra of thiourea derivative ligand and the metal complex in the region 4000-400 cm⁻¹ was compared and assigned on careful comparison. Thiourea ligands behave both as a monodentate and bidentate ligands, depending upon the reaction conditions. The characteristic bands of thiourea ligand are between/ near to; 3235 (NH), 2922, 2845 Ph(CH), 1691 (C=O) and 1258 (C=S), and there is a slight shift of (CN) and (CS) groups stretching frequencies due to coordination of the ligand to the copper atom. As is well known, acythiureas usually act as bidentate ligands to transition-metal ions through the acyl oxygen and sulfur atoms.³²⁻³⁴ The FTIR spectra of the complex showed significant changes when compared with the FT-IR spectra of the corresponding ligand. The IR spectra of the complex show absorption bands at $\nu_{\text{max}}/\text{cm}^{-1}$: 2928, 2855 (Ar-H), 1507 (C-O), and 1153 (C-S). The most striking changes is the N-H stretching frequency at 3235 cm⁻¹ in the free ligand, disappears completely, in agreement with both ligand and complex structure and the complexation reaction. This indicates the loss of the proton originally bonded to nitrogen atom of the (NH-CO) amide group. Another striking change is observed for the carbonyl stretching vibration. The vibrational frequency due to the carbonyl (1691 cm⁻¹) group in the free ligand is shifted towards lower frequency upon complexation, confirming ligand is coordinated to copper(II) ion through the oxygen and sulfur donor atoms.³⁵⁻³⁹ A comparative absorption pattern of the complex with the values of the free ligand demonstrate that the coordination of thiourea ligand to copper atom has a significant effect on $\nu(\text{NH})$, $\nu(\text{CO})$, and $\nu(\text{CS})$ frequencies.

The AA-CVD deposition of copper sulfide thin film from Bis[*N*-[ethyl(butyl) carbamothioyl]-3,5-dinitrobenzamide]copper(II) (2)

Thermogravimetric Analysis of Copper(II) Complex (2)

The thermogram of the complex 2 shows two stages of weight loss (Supplementary Material). The first step begins at 38 °C and accomplished at 225 °C. The second one starts at 225 °C and completed at 583 °C, with residue amounting to 29.82 % at 600 °C of the initial weight. The

residual weight (29.82 %) is higher, but considerable close to the expected composition for CuS (cal. 16.58 %), the presence of which was further supported by the XRD analysis of the residue.

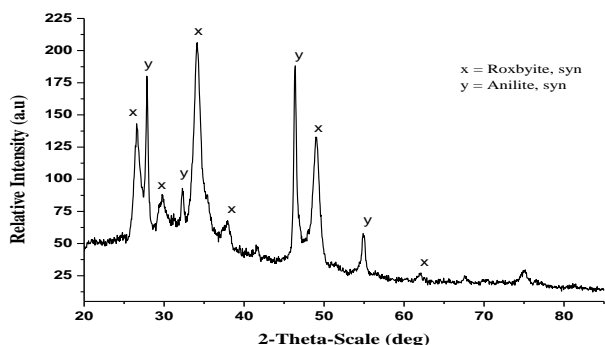


Figure 1. X-Ray diffractogram of the copper sulfide thin film obtained from complex (2)

X-ray Diffraction Studies of Deposited Nanostructured Thin Film

Using the above TGA data, the AACVD experiment was run at 350 °C. At 350 °C the XRD pattern from this film shows two types of phases (**Figure 1**). The diffraction pattern of the dominated phase is “*monoclinic roxbyite*” (Cu₇S₄) in the space group C2/m (12) with major diffraction peaks of (1600), (804), (2001) and (0160) planes (ICDD: 023-0958). The second phase is “*orthorhombic anilite*” (Cu₇S₄) in space group Pnma (62) with major diffraction peaks of (202), (220) and (224) planes (ICDD: 022-0250) and cell parameters are listed in **Table 1**.

Table 1. Powder X-ray crystal data of the decomposed material from copper complex (2)

Copper Sulfide, Cu ₇ S ₄ [ICDD:033-0489]			
Crystal System		Orthorhombic	
Space Group		Pnma	
Cell Volume		685.14Å ³	
Z		4	
Cell Parameters		a = 7.906Å	α = 90.00°
		b = 11.078Å	β = 90.00°
		c = 7.822Å	γ = 90.00°
No.	Pos. [2θ]	d-spacing d(Å)	hkl matched with Cu ₇ S ₄
1	27.6983	3.2180	202
2	29.0043	3.0760	113
3	32.1719	2.7800	220
4	37.7673	2.3800	302
5	42.0905	2.1450	321
6	44.0053	2.0560	133
7	46.2327	1.9620	224
8	54.9421	1.6698	026
9	67.3055	1.3900	440

Scanning Electron and Atomic Force Microscopic Studies of Nanostructured Thin Film

The SEM image of the film **Figure 2a** showed that the film morphology with evenly distributed small crystallites without any preferred orientation and diffusion grain boundaries. The particles with spherical appearance have good orientation and clearly well defined grain boundaries. EDX analysis of film shows that the composition as Cu:S ratio: 72.5: 27.5. The AFM image of the film (**Figure 2b**) shows the growth of closely packed crystallites onto a glass substrate with an average roughness of 11.81 nm (**Figure 2c**).

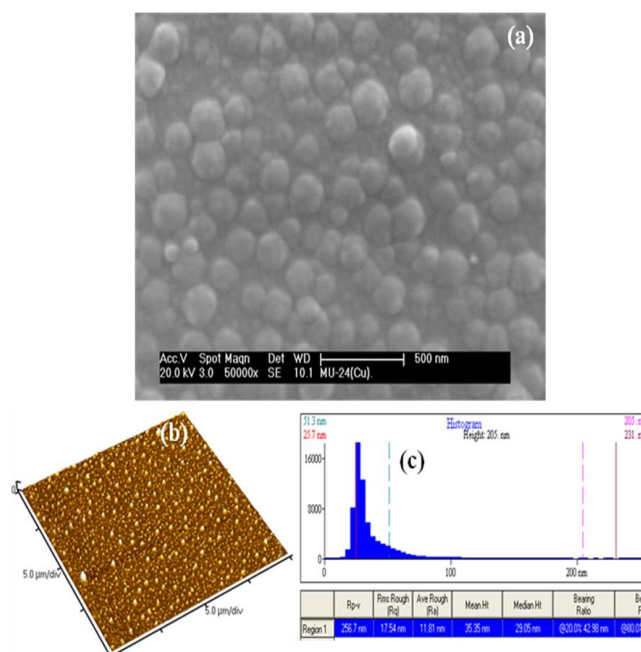


Figure 2(a) SEM image of copper sulfide thin film deposited from 2 at 350 °C, (b) AFM image in 3D view of thin film and (c) shows average roughness and Rms roughness of thin film deposited at 350 °C

Conclusions

We have successfully synthesized an unsymmetrical copper(II) complex of *Bis*[*N*-[ethyl(butyl)carbamothioyl]-3,5-dinitrobenzamide]copper(II). AA-CVD from copper (II) complex deposited monoclinic roxbyite Cu₇S₄ and orthorhombic anilite Cu₇S₄ phases at 350 °C with spherical crystallites. The composition of the deposited thin film was confirmed by EDX analysis. AFM studies showed that the average roughness of deposited film was 11.81 n.m.

Acknowledgement

S. Saeed would like to acknowledge the Higher Education Commission (HEC), Government of Pakistan for financial support.

References

- ¹Monajjemi, M.; Baei, M.T.; Mollaamin, F. *Russ. J. Inorg. Chem.*, **2008**, *53*, 1430-1437.
- ²Monajjemi, M.; Mahdavian, L.; Mollaamin, F.; Khaleghian, M. *Russ. J. Inorg. Chem.*, **2009**, *54*, 1465-1473.
- ³Zare, K.; Daroule, M.; Mollaamin, F.; Monajjemi, M. *Int. J. Phys. Sci.* **2011**, *6*, 2536-2540.
- ⁴Sun, Y.G.; Xia, Y.N. *Science* **2002**, *298*, 2176-2179.
- ⁵Lee, H.; Yoon, S.W.; Kim, E.J.; Park, J. *Nano Lett.* **2007**, *7*, 778-7784.
- ⁶Wu, Y.; Wadia, C.; Ma, W.; Sadtler, B.; Alivisatos, A.P. *Nano Lett.* **2008**, *8*, 2551-2555.
- ⁷Wadia, C.; Alivisatos, A.P.; Kammen, D.M. *Environ. Sci. Technol.* **2009**, *43*, 2072-2077.
- ⁸Sakamoto, T.; Sunamura, H.; Kawaura, H. *Appl. Phys. Lett.* **2003**, *82*, 3032-3034.
- ⁹Chung, J.S.; Sohn, H.J. *J. Power Sources* **2002**, *108*, 226-231.
- ¹⁰Vaughan, D.J.; Craig, J.R. *Mineral Chemistry of Metal Sulfides*, ed. W. B. Harland, S. O. Agrell, A. H. Cook and N. F. Hughes, Cambridge University Press, Cambridge, 1978, pp. 290-292.
- ¹¹Fleet, M.E. *Rev. Mineral. Geochem.* **2006**, *61*, 365-420.
- ¹²Koch, D.F.A.; McIntyre, R. *J. Electroanal. Chem.* **1976**, *71*, 285-296.
- ¹³He, Y.B.; Polity, A.; Osterreicher, I.; Pfisterer, D.; Gregor, R.; Meyer, B.K.; Hardt, M. *Phys. B*, **2001**, *308-310*, 1069-1073.
- ¹⁴Wang, S.Y.; Wang, W.; Lu, Z.H. *Mater. Sci. Eng., B* **2003**, *103*, 184-188.
- ¹⁵Sartale, S.D.; Lokhande, C.D. *Mater. Chem. Phys.* **2000**, *65*, 63-67.
- ¹⁶Hu, H.; Nair, P.K. *Surf. Coat. Technol.* **1996**, *81*, 183-189.
- ¹⁷Kemmler, K.; Lazell, M.; O'Brien, P.; Otway, D.J.; Park, J.H.; Walsh, J.R. *J. Mater. Sci.: Mater. Electron.* **2002**, *13*, 531-535.
- ¹⁸Moloto, M.J.; Revaprasadu, N.; O'Brien, P.; Malik, M.A. *J. Mater. Sci. Mater. Electron.* **2004**, *15*, 313-316.
- ¹⁹Arslan, H.; Flörke, U.; Kulcu, N.; Emen, M.F. *J. Coord. Chem.* **2006**, *59*, 223-228.
- ²⁰Binzet, G.; Arslan, H.; Flörke, U.; Kulcu, N.; Duran, N. *J. Coord. Chem.* **2006**, *59*, 1395-1406.
- ²¹Bailey, R.A.; Peterson, T.R. *Can. J. Chem.* **1967**, *45*, 1135-1142.
- ²²Perrin, D.D.; Armarego, W.L.F.; Perrin, D.R., *Purification of laboratory chemicals*, 3rd ed., Pergamon Press Ltd. Oxford, **1988**.
- ²³Abdelhady, A.L.; Ramasamy, K.; Malik, M.A.; O'Brien, P.; Haigh, S.J.; Raftery, J. *J. Mater. Chem.* **2011**, *21*, 17888-17895.
- ²⁴Saeed, S.; Rashid, N.; Jones, P.G.; Tahir, A. *J. Heterocycl. Chem.*, **2011**, *48*, 74-84.
- ²⁵Saeed, S.; Rashid, N.; Jones, P.G.; Ali, M.; Hussain, R. *Eur. J. Med. Chem.*, **2010**, *45*, 1323-1331.
- ²⁶Saeed, S.; Rashid, N.; Jones, P.G.; Hussain, R.; Bhatti, M.H. *Cent. Eur. J. Chem.*, **2010**, *8*, 550-558.
- ²⁷Saeed, S.; Rashid, N.; Ali, M.; Hussain, R.; Jones, P.G. *Eur. J. Chem.*, **2010**, *1*, 221-227.
- ²⁸Saeed, S.; Wong, W.-T. *J. Heterocycl. Chem.*, **2012**, *49*, 580-584.
- ²⁹Saeed, S.; Rashid, N.; Bhatti, M.H.; Jones, P.G. *Turk J. Chem.* **2010**, *34*, 761-770.
- ³⁰Ke, S.-Y.; Xue, S.-J. *ARKIVOC* **2006**, x, 63-68.
- ³¹Wei, T.B.; Chen, J.C.; Wang, X.C. *Synth. Commun.*, **1996**, *26*, 1147-1152.
- ³²Fregona, D.; Giovagnini, L.; Ronconi, L.; Marzano, C.; Trevisan, A.; Sitran, S.; Biondi, B.; Bordin, F. *J. Inorg. Biochem.*, **2003**, *93*, 181-189.
- ³³El-Reash, G.M.A.; Taha, F.I.; Badr, G. *Transit. Met. Chem.*, **1990**, *15*, 116-119.
- ³⁴Che, D.J.; Yao, X.L.; Li, G.; Li, Y.H. *J. Chem. Soc., Dalton Trans.*, **1998**, 1853-1856.
- ³⁵Richter, R.; Beyer, L.; Kaiser, J. *Z. Anorg. Allg. Chem.*, **1980**, *461*, 67-73.
- ³⁶Beyer, L.; Hoyer, E.; Liebscher, J.; Hartmann, H. *Z. Chem.*, **1980**, *21*, 81-84.
- ³⁷Irving, A.; Koch, K.R.; Matoetoe, M. *Inorg. Chim. Acta.*, **1993**, *206*, 193-198.
- ³⁸Koch, K.R.; Sacht, C.; Bourne, S. *Inorg. Chim. Acta.* **1995**, *232*, 109-115.
- ³⁹Mikami, M.; Nakagawa, I.; Shimanouchi, T. *Spectrochim. Acta* **1967**, *23A*, 1037-1053.

Received: 14.02.2013.

Accepted: 21.02.2013.



VARIATIONS IN MINERAL ELEMENT AND HEAVY METAL CONTENTS OF SOME VEGETABLES GROWN ON CRUDE OIL POST-REMEDiated AGRICULTURAL SOIL

Reginald Chibueze Ohiri^{[a]*}, Augustine Amadikwa Uwakwe^[a] and Eugene Nwaogwugwu Onyeike^[a]

Keywords: Bioaccumulation; mineral elements; heavy metals; vegetables; soil.

Variations in mineral element and heavy metal contents of some edible herbs grown on crude oil post remediated agricultural soil was carried out after four weeks of growth on the bioaugmented and natural attenuated soils. The result showed a slight decrease in all the mineral elements analyzed. However, Potassium had the highest concentration 5.5020 ± 0.1056 % and 4.7007 ± 0.6510 % for *Tallinium triangulare* and *Amarantus hybridus* planted on the bioaugmented site. Heavy metals concentration increased in all the vegetables after 4 weeks of growth with highest values of 0.0803 ± 0.0006 %, 0.0813 ± 0.0012 % and 0.8170 ± 0.0015 % for *Telfeiria occidentalis*, *Tallinium triangulare*, and *Amarantus hybridus* planted on the natural attenuated site respectively.

Corresponding Authors

Tel: +234 8038808077.

E-Mail: raycohiri@yahoo.com

[a] Department of Biochemistry, University of Port Harcourt, P. M. B. 5323 East-West Road, Choba, Rivers State, Nigeria.

Introduction

Since the rise of agriculture and forestry in the 8th millennium B.C., there has also arisen by necessity a practical awareness of soils and their management. In the 18th and 19th centuries, the industrial revolution brought increasing pressure on soil to produce raw materials demanded by commerce, while the development of quantitative science offered new opportunities for improved soil management.¹ This initial inquiry has expanded to an understanding of soil as a complex, dynamic, biogeochemical system that are vital to the life cycle of terrestrial vegetation and soil-inhabiting organisms and by extension to the human race as well. Industrial activities release substantial amount of crude oil and refined products into the environment, as a result of accidents such as storage tank leakage, oil spills during routine transportation and shipping operations or sabotage.² The contaminant load of soil and water is growing steadily each year in parallel with increasing industrialization and energy demand and therefore necessitate the need for remediation. Non-hydrocarbon compounds may also be found in crude oil and they include porphyrins and their derivatives.³ Metals that could be found in crude oil via their association with porphyrins include Nickel, Vanadium, Iron, Zinc, Cobalt, Titanium and Copper.⁴ Some priority contaminants of petroleum hydrocarbons and crude oil include Benzene, Heptane, Hexane, Isobutene, Isopentane and poly-aromatic hydrocarbons such as Benzo(a)anthracene, Benzo(a)pyrene, Benzo(b)pyrene etc.⁵ Soils subjected to petroleum hydrocarbon bioremediation are used for crop growth without possible consideration to the concentration of the recalcitrant metals and hydrocarbons in the remediated soil.

However, not all contaminants are easily treated by bioremediation using microorganisms. For example, heavy metals such as Cadmium and Lead are not readily absorbed

by microorganisms. The assimilation of metals such as Mercury into the food chain may pose a serious threat to human. Phytoremediation is useful in these circumstances, because natural plants and transgenic plants are able to bioaccumulate these toxins in their above ground parts, which can then be harvested for removal.⁶ The heavy metals in the harvested biomass may be further concentrated by incineration or even recycled for industrial use.⁷ The aim of this research is to determine the variations in mineral elements and heavy metal concentrations of vegetables namely: fluted pumpkin (*Telfairia occidentalis*), water leaf (*Tallinium triangulare*) and African spinach (*Amarantus hybridus*) grown on crude oil post-remediated soil.

Materials

Bonny light crude oil was obtained from Shell Petroleum Development Company (SPDC) flow station at Egbema, Imo State, Nigeria. Chicken drops (40 kg) was purchased from Godvine, Poultry Farm, Elioazu Obio Akpor, Rivers State, Nigeria. While, viable seeds of *Telfairia occidentalis* and healthy seedlings of *Tallinium triangulare* and *Amarantus hybridus* were purchased from Rumuokoro market, Obio Akpor Rivers State, Nigeria.

Study Area

The study area was located along Eneka-Oyigbo new link road (longitude $7^{\circ} 10''$ E and latitude $4^{\circ} 40''$ N) in Obio Akpor Rivers State, Nigeria. The soil of this area belongs to the ultisols. Approximately the entire area consisted of deep uniform sand and clay sand, with slightly humus topsoil and a topsoil pH of approximately 4.86 ± 0.12 . There was no record of oil spillage or pipeline vandalization in the study area.

Pollution and bioremediation of research site

Approximately 18 m² farmland was cleared and divided into three sites of 4 m² each with 2 m spaces in between them. These sites were polluted with 40 dm³ of bonny light

crude oil and bioremediated for 16 weeks as follows: Site A (Control site) was an unpolluted 4 m² farmland, while site B (Bioaugmented site) was a 4 m² farmland polluted with 40 dm³ of bonny light crude oil and bioaugmented with 40 kg of chicken drops. However, site C (Natural attenuated site) was polluted with 40 dm³ of bonny light crude oil.

Planting and growing of vegetables

Viable seeds of *Telfairia occidentalis* (fluted pumpkin), and healthy seedlings *Tallinium Trianglerae* (water leaf) and *Amarantus hybridus* (African spinach) were planted on the three sites and allowed to grow for 4 weeks.

Collection of plant samples

Plant leaves were collected at fourth weeks after planting with an unused sterilized razor blade into sterilized plastic bags sealed with rubber bands. All samples were labelled with a permanent water-resistance marker and were taken to the laboratory within 1 hour of collection for analysis.

Determination of mineral element and heavy metal contents of vegetable leaves

Mineral elements and heavy metal contents of vegetables leaves were determined by the emission spectroscopy method.⁸

Principle: Sample digests are burned in a carbon arc, causing each element to emit a unique wavelength of light. The density of light emitted by each element is directly proportional to the concentration of the element in the sample.

Apparatus: Arc-spark emission spectrography, Analytical weighing balance, Furnace, 10ml Porcelain crucibles, 50ml Burette, Drying oven, Wiley mill, Volumetric flasks and Pipettes.

Reagents: Lithium carbonate (LiCO₃) use for the analysis was obtained from Sigma Aldrich, MO USA.

Procedure: A quantity of 1.0 g of dried leaf samples were ground and placed in 10 ml porcelain crucibles. The crucibles were placed in a cool muffle furnace and the samples were ashed at a temperature of 500 °C for 4 hours. The crucibles were removed and allowed to cool. Then 5.0 ml of lithium carbonate buffer was added and swirled gently to dissolve the ash. The digest was transferred to a teflon boat and analysed on a direct reading arc-spark emission spectrography.

RESULTS

Mineral element content of vegetables samples

This study showed pronounced decrease in magnesium, calcium and potassium, while zinc and iron content increased (see Tables 1-3). The decrease in magnesium, calcium and potassium may be due to reduction in nutrient uptake by the vegetables caused by the presence of

petroleum hydrocarbons in the rhizosphere. Petroleum hydrocarbons may affect the uptake of many macro and micronutrients. However, the influence of petroleum hydrocarbons on the mineral element content of plants depends on the type and level of pollution and the species of plants involved.

Table 1. Mineral element content of *Telfairia occidentalis* grown on crude oil bioremediated soil (% , m/m).

	Control site	Bioaugmented site	Natural attenuated site
Mg	1.8010±0.1115 ^a	1.4027±0.0361 ^b	1.4010±0.0705 ^c
Ca	2.0033±0.0551 ^a	1.8080±0.0886 ^b	1.1033±0.0512 ^c
K	2.3103±0.0823 ^a	2.0010±0.0400 ^b	1.6037±0.0210 ^c
Zn	0.0307±0.0021 ^{ac}	0.0813±0.0038 ^b	0.0417±0.0059 ^{ac}
Fe	0.0810±0.0066 ^{abc}	0.0907±0.0021 ^{ab}	0.0713±0.0025 ^{ac}

Values are means ± standard deviations of three determinations. Mean values in each row with different superscripts differ significantly at $P = 0.05$.

Table 2. Mineral element content of *Tallinium triangulare* grown on crude oil bioremediated soil (% , m/m) .

	Control site	Bioaugmented site	Natural attenuated site
Mg	3.3353±0.2976 ^a	2.9013±0.0305 ^b	2.6347±0.5849 ^c
Ca	1.2007±0.0400 ^{ac}	1.6010±0.0790 ^b	1.3000±0.0174 ^{ac}
K	6.3027±0.1910 ^a	5.5020±0.1056 ^b	5.9030±0.1305 ^c
Zn	0.0210±0.0020 ^a	0.0600±0.0046 ^b	0.0317±0.0038 ^c
Fe	0.0500±0.0030 ^a	0.0790±0.0028 ^{bc}	0.0803±0.0070 ^{bc}

Values are means ± standard deviations of three determinations. Mean values in each row with different superscripts differ significantly at $P = 0.05$.

Table 3. Mineral element content of *Amarantus hybridus* grown on crude oil bioremediated soil (% , m/m).

	Control site	Bioaugmented site	Natural attenuated site
Mg	3.0057±0.0592 ^a	3.2023±0.0790 ^b	2.8027±0.0615 ^c
Ca	1.7020±0.0770 ^{abc}	1.9017±0.0595 ^{abc}	1.6960±0.5513 ^{abc}
K	5.1047±0.1991 ^{abc}	4.7007±0.0510 ^{abc}	4.9857±0.3095 ^{abc}
Zn	0.0613±0.0049 ^{ab}	0.0813±0.0025 ^{abc}	0.1013±0.0151 ^{bc}
Fe	0.0907±0.0032 ^{ac}	0.0683±0.0086 ^b	0.0900±0.0060 ^{ac}

Values are means ± standard deviations of three determinations. Mean values in each row with different superscripts differ significantly at $P = 0.05$.

Table 4. Heavy metal content of *Telfairia occidentalis* grown on crude oil bioremediated soil (% , m/m).

	Control site	Bioaugmented site	Natural attenuated site
Cu	ND	0.0217±0.0035 ^b	0.0113±0.0032 ^c
Pb	ND	ND	0.0813±0.0012 ^c
Cr	ND	0.0503±0.0070 ^b	0.0413±0.0009 ^c
Cd	ND	ND	0.0113±0.0015 ^c
As	ND	ND	ND

Values are means ± standard deviations of three determinations. Mean values in each row with different superscripts differ significantly at $P = 0.05$.

Table 5. Heavy metal content of *Tallinium triangulare* grown on crude oil bioremediated soil (% , m/m).

	Control site	Bioaugmented site	Natural attenuated site
Cu	0.0107±0.0006 ^{ac}	0.0303±0.0031 ^b	0.0103±0.0029 ^{ac}
Pb	ND	0.1017±0.0196 ^b	0.0803±0.0006 ^c
Cr	ND	0.0600±0.0036 ^b	ND
Cd	ND	0.0307±0.0025 ^b	0.0107±0.0006 ^c
As	ND	ND	ND

Values are means ± standard deviations of three determinations. Mean values in each row with different superscripts differ significantly at $P = 0.05$.

Table 6. Heavy metal content of *Amarantus hybridus* grown on crude oil bioremediated soil (% , m/m).

	Control site	Bioaugmented site	Natural attenuated site
Cu	0.0200±0.0030 ^{ac}	0.0417±0.0076 ^b	0.0203±0.0012 ^{ac}
Pb	ND	0.1007±0.0075 ^b	0.0817±0.0015 ^c
Cr	ND	0.0613±0.0074 ^b	0.0407±0.0042 ^c
Cd	ND	0.0205±0.0032 ^b	0.0110±0.0020 ^c
As	ND	0.0263±0.0012 ^b	ND

Values are means ± standard deviations of three determinations. Mean values in each row with different superscripts differ significantly at $P = 0.05$.

This also agrees with the work of ⁹, which stated that small concentration of diesel oil raised the content of nitrogen, potassium and sodium in oat, whereas higher concentrations depressed these elements. This may be responsible for the decrease in magnesium, calcium and potassium contents of the vegetables as observed in this study. However, the increase in iron and zinc content as observed in this study may be attributed to the availability of these nutrients in the soil caused by their presence in the crude oil. This supports the work of,⁴ which reported iron and zinc among the metals that are present in crude oil through their association with porphyrins.

The increase in heavy metal content observed in the bioaugmented and natural attenuated site may also be attributed to the presence of these metals in the crude oil (see Tables 4-6). This also corroborates the work of,⁴ which also reported that heavy metal such as copper and nickel are found in crude via their association with porphyrins.

This work also agrees with the work of ¹⁰, where an increase in cadmium concentration was observed in crude oil polluted arable soils in Isikwuato, Abia State, Nigeria. However, the concentration of cadmium observed in this research is below the Environmental Protection Agency (EPA) recommended level of 0.1mgkg⁻¹ as critical level form soil in Taiwan.¹¹

References

- ¹Sposito, G. *The chemistry of soils*, 2nd Edition, Oxford University Press, **2008**.
- ²Gonza'Lez, J. L., Serrano, A., Gallego, M. and Tejada, M. J., *J. Environ. Pollut.* **2008**, *144*, 203-209.
- ³Callot, H. J., Ocampo, R. *Geochemistry of porphyrins*. In Kadish, K. M., Smith, M., Guillard, B. (Editors.), *The Porphyrin Handbook* vol. 1. Academic Press San Diego, **2000**.
- ⁴Chicarelli, M. I, Eckardt, C. B., Owen, C. R., Maxwell, J. R., Eglinton, G., Huston, R. C., Eaton, A. N., *J. Org. Geochem.* **1990**, *15*, 266-274.
- ⁵Onwurah, I. N. E., Ogueva, V. N., Onyike, N. B., Ochonogor, A. E., Otitoju, O. F., *Int. J. Environ. Res.*, **2007**, *1*(4), 307-320.
- ⁶Meagher, R. B., *Curr. Opinion Plant Biol.*, **2000**, *3*(2), 153-162.
- ⁷Hannik, N., Rosser, S. J., French, C. E., Basran, A., Muray, J. A., Nicklin, S., Bruce, N. C., *J. Nat. Biotechnol.*, **2001**, *19*(12), 1168-1172.
- ⁸Jones, J. B. Jr., *J. Assoc. Off. Anal. Chem.*, **1975**, *58*, 764-769.
- ⁹Ziolkowskai, L., Wyszowski, H., *J. Ecol. Chem. and Eng.* **2010**, *17*(1), 37-46.
- ¹⁰Onweremadu, E. U., Duruigbo, C. I., *Int. J. Environ. Sci. Tech.*, **2007**, *4*(3), 363-366.
- ¹¹Environmental Protection Agency (EPA), *Final reports of heavy metal contents in Taiwan agricultural soils*, vol. 4 . Tapei, Taiwan. **1989**.

Received: 28.01.2013.

Accepted: 23.02.2013.



KINETIC, THERMODYNAMIC AND EQUILIBRIUM STUDIES OF RHODAMINE B ADSORPTION BY LOW COST BIOSORBENT SUGAR CANE BAGASSE

Z. M. Abou-Gamra^{[a]*} and H. A.A. Medien^[a]

Keywords: kinetics, adsorption, Lignin, Rhodamine-B, dye

The present study deals with the feasibility of removal of basic dye Rhodamine-B (RB) from aqueous solutions by using a low cost natural adsorbent lignin. Batch adsorption studies were conducted to evaluate various experimental parameters such as, contact time, initial concentration of the adsorbate, adsorbent dosage, pH and temperature. Pseudo first order and pseudo second order were used to fit the experimental data. Pseudo second order kinetics described of adsorption reasonably well. The experimental isotherms data were also modelled by the Langmuir and Freundlich equation of adsorption. Equilibrium data fitted well with the Freundlich isotherm. Lignin was shown to be a promising material for adsorption of RB from aqueous solutions.

*Corresponding Authors

E-mail: zanibabougamra@yahoo.com

[a] Chemistry Department, Faculty of Science, Ain Shams University, Abbassia, Cairo, Egypt

Introduction

Many industries such as textile, paper, rubber, plastics, paints, printing, and leather discharge coloured effluents which cause pollution in receiving water. Textile industries cause serious problem because they are major consumers of the dyes, most of which are toxic, particularly azo dye. The coloured water depletes sunlight penetration which reduces the photosynthetic activity in aquatic plants impeding their growth. Rhodamine B (RB) is used mostly in paper printing, textile dyeing, and leather industries. It is carcinogenic, and causes irritation of eyes, skin, respiratory tract and the gastrointestinal tract.¹

The removal of Rhodamine B from colour effluents is the one major environmental concern these days. Several techniques have been used such, Fenton-like,²⁻⁴ photocatalytic⁵⁻⁸ which is convenient techniques are expensive.

Adsorption process has been found to be superior technique for treating dye effluents due to simplicity and insensitivity to toxic substance. Although the activated carbon⁹⁻¹⁰ is most effective for adsorption of dye, but it has some disadvantages such as (i) high adsorbent cost, (ii) problems of regeneration and difficulties of separation of powdered activated carbon from waste water for regeneration are expensive and hence increasing need for equally effective but commercially low cost sorbents. A wide variety of materials such as animal bone,¹¹ black tea leaves,¹² cocoa,¹³ almond shell,¹⁴ mango leaves,¹⁵ saw dust.¹⁶

The present study is concerned to evaluate the efficiency of adsorbent (lignin) extracted from sugar cane bagasse for removal of Rhodamine B.

Materials and methods

Dye solution

Rhodamine B is cationic basic dye with molecular formula $C_{28}H_{31}ClN_2O_3$. It was obtained from BDH was used as received without further purification. A stock solution of RB, 479.02 mg L⁻¹, was prepared in doubled-distilled water. Solutions of desired concentration were obtained by dilution with buffer solutions.

Adsorbent

Sugar cane bagasse was obtained from a sugar cane mill, Egypt. It was wet then air dried. Lignin was extracted from bagasse by soda process as previously described.¹⁷

Experimental Methods

The reaction was followed spectrophotometrically at $\lambda_{max}=554$ nm using thermostated 292 Cecil spectrophotometer. pH of solution was conducted with a Griffin pH meter fitted with glass calomel electrode.

The efficiency of the adsorbent was evaluated by conducting laboratory batch mode studies. Specific amount of adsorbent were shaken in 50 ml of aqueous dye of different concentrations for different time periods at pH 2-8.75 and temperature 28-50 °C. At the end of predetermined time intervals, adsorbent was removed by centrifugation for 5 minutes at 1800 rpm and supernatant concentration was determined spectrophotometrically.

The surface textures of lignin before and after adsorption were observed by Scanning electron microscope (JEOL, JEM-1200X II).

Results and Discussion

Characterization of adsorbent

SEM micrograph of lignin (Figure 1) shows that the adsorbent surface is irregular, rough and highly porous indicating the possibility of its good adsorption properties.

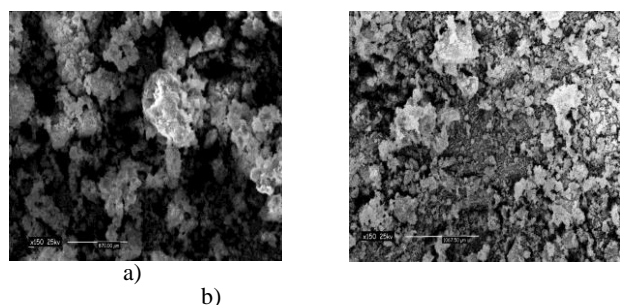


Figure 1. SEM micrographs of lignin (a) before adsorption, (b) after adsorption at pH = 3.6

Effect of contact time and Initial concentration of dye

To study the effect of dyes initial concentration and contact time on adsorption uptake, RB solution with initial concentrations 1.9-5.7 mg L⁻¹ was shaken with 0.3 g/50ml of lignin. In this case, the solution pH was 3.6 and temperature was 35 °C. The experimental results of sorption of RB on lignin at various initial concentrations are shown in Figure 2. The adsorption at different dye concentrations was rapid at the initial stages and then gradually decreases with the progress of adsorption until the equilibrium was reached. The rapid adsorption at the initial contact time can be attributed to a large number of surface sites are available for adsorption at the initial stages and after a lapse of time, the remaining surface sites are difficult to occupy because of repulsion between RB molecules of solid and bulk phases.¹⁵ Also this may be explained by rapid adsorption on outer surface followed by slower adsorption inside the pores, the same result obtained by Majid et al.¹⁴

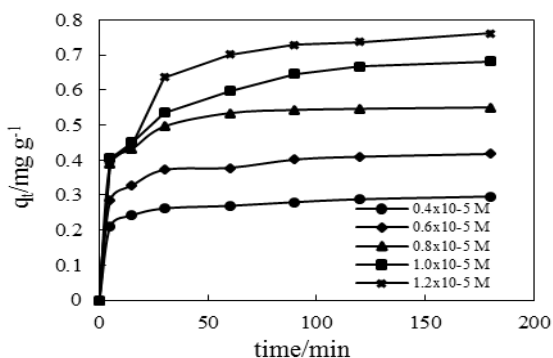


Figure 2: Effect of contact time on adsorption of Rhodamine B at different dye concentrations, adsorbent dose = 6 g L⁻¹, temp. = 35 °C, pH = 3.6.

As shown in Figure 2, the contact time needed for RB solution to reach equilibrium was 120 min. The results indicated that there was no change in the sorption capacity after 120 min, therefore 180 min was fixed as contact time for isotherm studies. The adsorption capacity increased from 0.3 to 0.8 mg g⁻¹ as the dye concentration increased from 1.9-5.7 mg L⁻¹, (Figure 2).

Effect of pH

pH is one of important factors in controlling the adsorption of dye on adsorbent. The adsorption capacity initially increased from 0.8 to 0.92 mg g⁻¹ (69.8 to 77.6%) with increasing pH, with optimal uptake at pH = 3.6-4.4, the RB uptake decreased from 0.92 to 0.125 mg g⁻¹ (77.6 to 10.4%) in the pH range of 4.4 to 8.75, this clear from (Figure 3). This may be explained on the basis of fact that at pH values lower than 4.5, the RB ions can enter into the pore structure. At a pH value higher than 4.5, the zwitterions of RB in water may increase the aggregation of RB to form a bigger molecular form (dimer) and become unable to enter into the pore structure of lignin surface. The greater aggregation of the zwitterions is due to the attractive electrostatic interaction between the carboxyl and Xanthane groups of the monomer. This is confirmed by darkness of the colour of lignin after adsorption by increasing pH till 4.1, then the colour faint by increasing pH, (Figure 3).

Similar trend was observed by other workers for RB dye in the range of pH under investigation.^{15, 18}

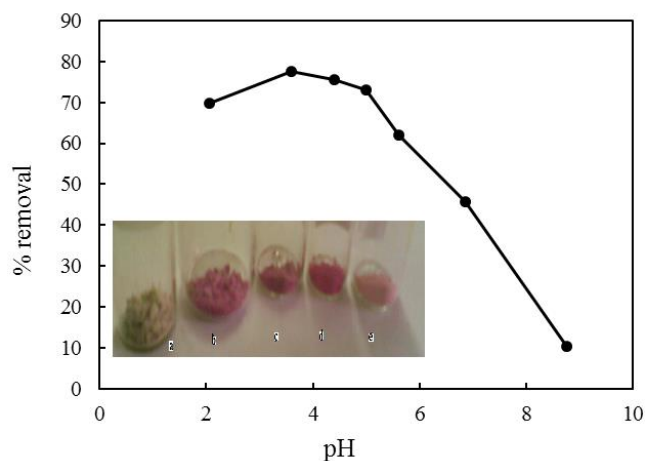


Figure 3. Effect of pH on removal of Rhodamine B, [RB] = 10⁻⁵ mol.L⁻¹, temp. = 28 °C, adsorbent dose = 4 g L⁻¹.

Effect of adsorbent dose

The adsorption capacity decreases (from 1.48 to 0.42 mg g⁻¹) with increase of adsorbent dose while adsorption percentage removal increases with increase of adsorbent dose (from 63 to 90 %) for an increase in adsorbent dose 0.1-0.5 g. The increase in the percentage colour removal was due to the increase of the available sorption surface site (Figure 4). A similar observation was previously reported for the removal of dye RB from aqueous solution by different adsorbents.^{11, 13-15, 19, 20}

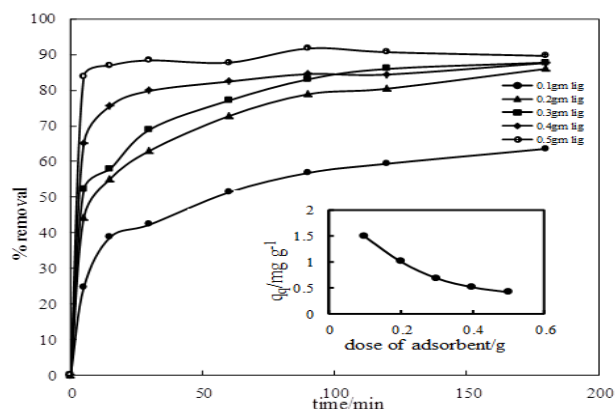


Figure 4. Effect of adsorbent dose on adsorption of Rhodamine B, $[RB] = 10^{-5}$ mol. L $^{-1}$, $T = 35$ °C, $pH = 3.6$.

Adsorption isotherm

In order to describe the adsorbate-adsorbent interaction, the isotherm data were analyzed by fitting them into Langmuir and Freundlich equations to find out the suitable model that may be used for design consideration.

Langmuir isotherm

The Langmuir adsorption mode²¹ is based on the assumption that maximum adsorption corresponds to saturated monolayer of solute molecules on the adsorbent surface. The linear form of Langmuir equation is

$$\frac{C_e}{q_e} = \left(\frac{1}{Q_m b} \right) + \left(\frac{1}{Q_m} \right) C_e \quad (1)$$

where

b is adsorption equilibrium that is related to energy of adsorption and

Q_m is the quantity of adsorbate required to form single monolayer on unit mass of adsorbent (mg g^{-1}) and

q_e is the amount of adsorbed on unit mass of the adsorbent (mg g^{-1}) when the equilibrium concentration is C_e (mg L^{-1}).

The linear plot of C_e/q_e against C_e (Figure 5) shows the adsorption obeys equation (1). The Langmuir constants Q_m and b were determined from the slope and intercept of the plot, are 1.25 mg g^{-1} and 48.78 L mg^{-1} respectively. R^2 value (0.927) suggests that the adsorption follows Langmuir model. The higher value of ($Q_m > 1$) indicates strong adsorbent- adsorbate interaction.

The essential characters of Langmuir isotherm can be expressed in term of dimensionless constant separation factor R_L ²² given by

$$R_L = \frac{1}{1 + bC_o} \quad (2)$$

where

C_o (mg L^{-1}) is the highest initial concentration of dye and

b (L mg^{-1}) is Langmuir constant.

The value of R_L in the present investigation is found to be 0.0043 showing the adsorption is favour adsorption ($0 < R_L < 1$) at the temperature studied.

Freundlich isotherm

The Freundlich isotherm considers multilayer adsorption with heterogeneous energetic distribution of active sites accompanied by interaction between adsorbed molecules.²³ The linear Freundlich isotherm is

$$\lg q_e = \lg K_f + \frac{1}{n} \lg C_e \quad (3)$$

where, K_f is Freundlich constant, which indicates the relative adsorption capacity of the adsorbent and n is a measure of the adsorption intensity or surface heterogeneity (a value closer to zero represents a more heterogeneous surface). The linear plot of $\lg q_e$ against $\lg C_e$, (Figure 6) shows that the adsorption of RB on lignin also follows Freundlich isotherm model. Freundlich constant K_f and n were 5.5 and 1.76 respectively. The value of $n > 1$ indicates favourable adsorption. Regression correlation coefficient ($R^2 = 0.978$) is better than one obtained from Langmuir isotherm ($R^2 = 0.927$) indicates that Freundlich isotherm model more fit.

Adsorption kinetics

Pseudo first order and second order models were applied to test experimental data and explain the kinetic adsorption process. Lagergren proposed a method for adsorption analysis²⁴ in the form

$$\lg(q_e - q_t) = \lg q_e - \frac{k_1}{2.303} t \quad (4)$$

where,

k_1 (min^{-1}) is the rate constant,

q_e (mg g^{-1}) is the amount of dye adsorbed on surface at equilibrium,

q_t (mg g^{-1}) is the amount of dye adsorbed on surface at time t (min).

The adsorption rate constant, k_1 and q_e were calculated from the plot of $\log(q_e - q_t)$ vs. t , (Figure 7) and are listed in Table 1.

The pseudo second order kinetic model is given by equation 5.²⁵

$$\frac{t}{q_t} = \frac{1}{k_2 q_e^2} + \frac{1}{q_e} t \quad (5)$$

where, k_2 ($\text{g mg}^{-1} \text{ min}^{-1}$) is pseudo second order rate constant. The plot of t/q_t vs t is shown in Figure 8. The values of q_e and k_2 are listed in Table 1.

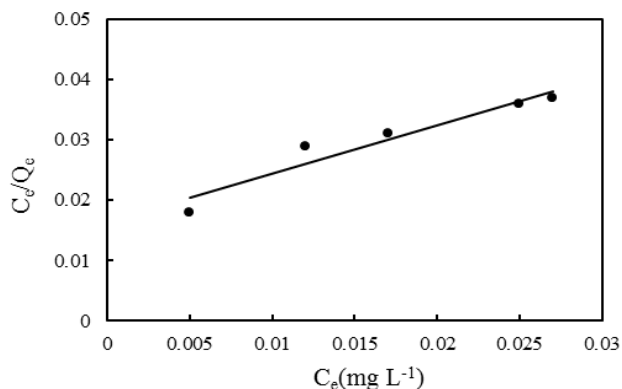
Table 1. Kinetic parameters for the adsorption of Rhodamine B on lignin

Kinetic model	[RB]=0.4x10 ⁻⁵ M	[RB]=0.6x10 ⁻⁵ M	[RB]=0.8x10 ⁻⁵ M	[RB]=10 ⁻⁵ M
Lagergren pseudo first order				
q_e (mg g ⁻¹) experimental	0.296	0.418	0.550	0.681
q_e calculated	0.076	0.127	0.165	0.335
k_1 (min ⁻¹)	0.018	0.023	0.033	0.026
R^2	0.964	0.966	0.977	0.992
Pseudo second order				
q_e calculated	0.299	0.425	0.561	0.708
k_2 (g mg ⁻¹ min ⁻¹)	0.77	0.51	0.53	0.18
R^2	0.999	0.999	0.999	0.998
Intraparticle diffusion				
k_{id} (mg g ⁻¹ min ^{-0.5})	0.007	0.011	0.015	0.026
C	0.21	0.28	0.39	0.37
R^2	0.896	0.874	0.821	0.936

Table 2. Thermodynamic parameters for the adsorption of Rhodamine B on lignin

Temperature/ K	K_e	Thermodynamic parameters		
		ΔG^0 (kJ mol ⁻¹)	ΔH^0 (kJ mol ⁻¹)	ΔS^0 (J mol ⁻¹ K ⁻¹)
301	3.47	-3.12	-29.5	-81.34
308	5.88	-4.52		
315	3.72	-3.44		
323	3.39	-3.27		

Lower correlation coefficient of pseudo first order kinetics model and the calculated q_e values are found to be lower than the experimental one comparing to pseudo second order kinetics model indicating that the applicability of pseudo second order kinetics model.

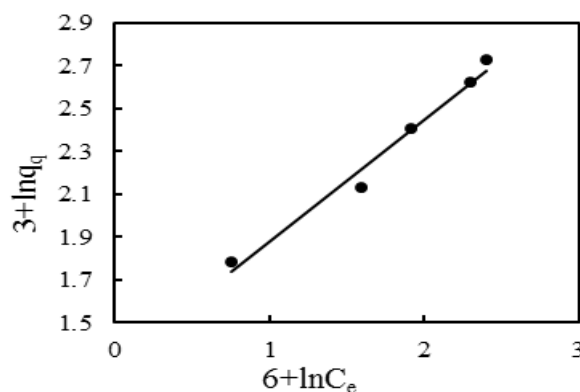
**Figure 5.** Langmuir isotherm plot for adsorption of Rhodamine B on lignin.

The kinetic results were further analyzed by the intraparticle diffusion to explain the diffusion mechanism.²⁶

$$q_t = k_{id}t^{0.5} + C \quad (6)$$

where C is the intercept and k_{id} is intraparticle diffusion rate constant (mg g⁻¹ min^{-0.5}) are listed in Table 1 which

can be evaluated from the slope of the linear plot of q_t vs $t^{0.5}$ (Figure 9). If the straight line passes through the origin, then intraparticle diffusion is the sole rate-limiting step which is not the case in (Figure 9). It may be concluded that surface adsorption and intraparticle diffusion were concurrently operating during RB interaction. Also increasing the C , value indicating increasing the boundary layer. The same results obtained by Prasad et al.²⁰

**Figure 6.** Freundlich Isotherm plot for adsorption of Rhodamine B on lignin.

The effect of temperature

The effect of temperature for RB adsorption on lignin was shown in (Figure 10). The results show that there is no consistent trend found for the relationship between temperature and amount of adsorption. Figure 10 shows that the adsorption of RB onto lignin increases with increasing temperature below 308 K, which indicates that

the adsorption is endothermic. Above 308 K, the decrease of adsorption capacity with increasing the temperature indicating that the adsorption of RB onto lignin is controlled by exothermic process. A similar temperature effect on the adsorption has been observed by Yati Yang et al²⁷ for the adsorption of methylene blue on anionic starch microsphere and Chou et al²⁸ for adsorption of reactive dye on crosslinked chitosan beads.

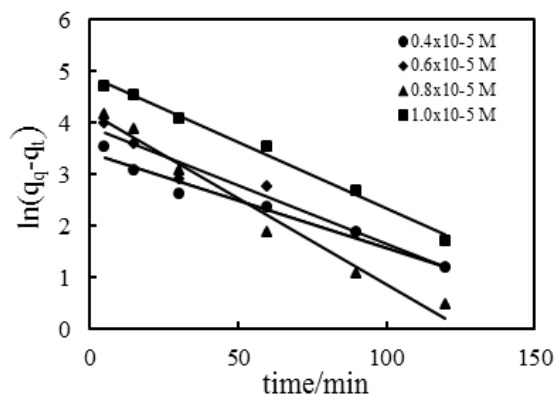


Figure 7. Lagergren pseudo first order plot for adsorption of Rhodamine B on lignin

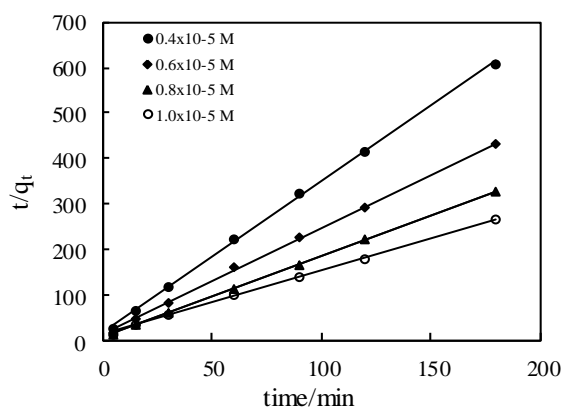


Figure 8. Pseudo second order plot for adsorption of Rhodamine B on lignin.

Thermodynamic Parameters

Thermodynamic parameters were evaluated to confirm the nature of adsorption of RB onto lignin. Thermodynamic parameters were calculated by the Van't Hoff equation.

$$\ln K_e = \frac{\Delta S^0}{R} - \frac{\Delta H^0}{RT} \quad (7)$$

From the slope and intercept of Van't Hoff plot, the value of ΔH^0 and ΔS^0 was calculated. The Gibbs free energy change ΔG^0 was calculated using the following equation are listed in Table 2.

$$\Delta G^0 = -RT \ln K_e \quad (8)$$

It is clear from Table 2 that K_e decreases by increasing temperature above 301K.

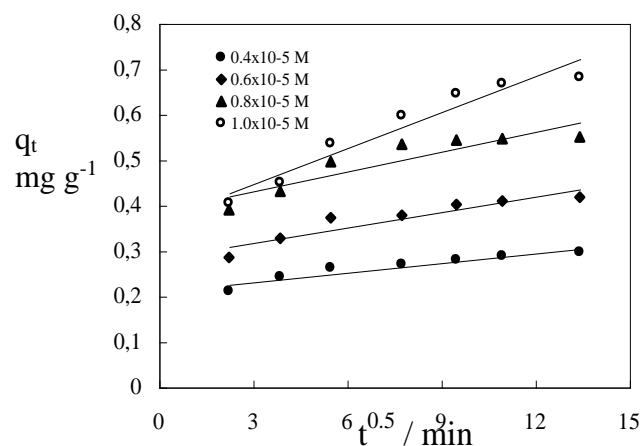


Figure 9. Intraparticle diffusion plot for adsorption of Rhodamine B on lignin.

This suggests that the adsorption process is exothermic. The negative values of free energy change indicating that the adsorption is spontaneous process. The negative value of enthalpy change suggests that adsorption is exothermic. Generally, the enthalpy change due to chemisorption takes value between 40-120 kJ mol⁻¹, which is larger due to physisorption.²⁹ Consequently, the low value of the enthalpy change indicates that the adsorption is likely due to physisorption. The low value of entropy change indicates the adsorption of RB onto lignin is favour process. The R^2 value in the plot of $\ln K_e$ vs $1/T$ was very low ($R^2 = 0.068$) for the experiments including low temperature, 301 K, which altered the trend of the temperature effect. Excluding this temperature, the plot, was closer to straight line with $R^2 = 0.853$. The values of ΔH^0 and ΔS^0 were, -29.51 kJ mol⁻¹ and -81.34 J mol⁻¹ K⁻¹ respectively, confirming that the adsorption is exothermic process at temperature above 301 K. A similar temperature effect on the adsorption has been observed by Sudipta Chatterjee.³⁰

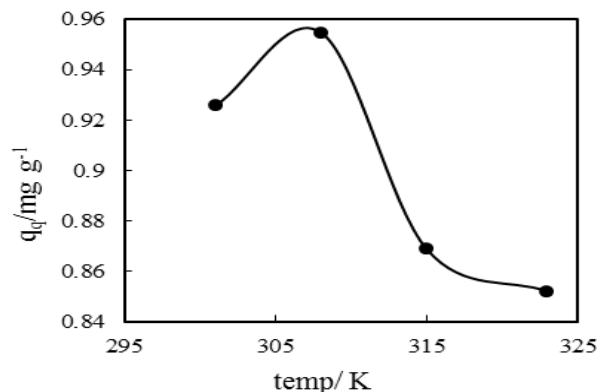


Figure 10. Effect of temperature on adsorption of Rhodamine B on lignin

Conclusion

Kinetics, equilibrium and thermodynamic of adsorption of Rhodamine B onto lignin from aqueous solution are investigated. The adsorption data is fitted Freundlich adsorption model. The kinetic data is agreed with pseudo second-order rate equation. High amount adsorbed at low pH. The adsorption is exothermic process at temperature above 28 °C.

Acknowledgements

The authors are grateful to Dr. Atef S. Darwish (lecturer of physical chemistry, Faculty of Science, Ain-Shams university, Cairo, Egypt) for preparing the adsorbent.

References

- ¹Rochat, J., Demenge, P., Rerat, J. C., *Toxicol. Eur. Res.*, **1978**, 1, 23-26.
- ²Xue, X., Hanna, K., Denga, K., *J. Hazard. Mater.*, **2009**, 166, 407-414.
- ³Xu, H. Y., Prasad, M., Xuail, H. E., Lian, W. S., Shu, Y. Q., *Sci. China. Ser E-Tech. Sci.*, **2009**, 52(10), 3054-3060.
- ⁴Medien, H. A. A., Khalil, S. M. E., *J. King Saud Univ. (Science)*, **2010**, 22(3), 147-153.
- ⁵Gondal, M. A., Chang, X., Ali, M. A., Yamani, Z. H., Zhou, Q. and Ji, Q., *Applied Catalysis A*, **2011**, 397(1-2), 192-200.
- ⁶Wilhelm, P., Stephan, D., *J. Photochem. Photobiol. A: Chem.*, **2007**, 185, 19-25.
- ⁷Byrappa, K., Subramani, A. K., Ananda, S., Lokanatha Rai, K. M., Dinesh, R. and Yoshimura, M., *Bull. Mater. Sci.*, **2006**, 29(5), 433-438.
- ⁸ Libanori, R., Giraldi, R. T., Longo, E., Edson, R. L. and Ribeiro, C., *J. Sol-Gel. Sci. Technol.*, **2009**, 49, 95-100.
- ⁹Lalitha, P., Sangeetha, S. N., *Oriental J. Chem.*, **2008**, 24(3), 983-988.
- ¹⁰Vausa, A. E., *E-J. Chem.*, **2008**, 5(4), 844-852.
- ¹¹El Haddad, M., Mamouni, R., Saffaj, N. and Lazar, S., *Global J. Human Soc. Sci. Geography Environ. Geo Sci.*, **2012**, 12(10), 18-29.
- ¹²Abul Hossain, M., Atiqur. R. M., *Orbital Elec. J. Chem. Campo Grande*, **2012**, 4(3), 187-201.
- ¹³Theivarasu, C., Mylsamy, S., *Int. J. Eng. Sci. Technol.*, **2010**, 2(11), 6284-6292.
- ¹⁴Aliabadi, M., Khazaei, I., Hajiabadi, M. and Shahrzad, F., *J. Bio. & Env. Sci.*, **2012**, 2(9), 39-44.
- ¹⁵ Khan, T. A., Sharma, S. and Ali, I., *J. Toxicol. Environ. Health Sci.*, **2011**, 3(10), 286-297.
- ¹⁶Wttek-Krowiak, A., Mittek, M., Pokomeda, K. and Szafran, R. G., *Modelski S., Chem. Process Eng.*, **2010**, 31, 409-420.
- ¹⁷Mousavioun, P., Dohrty, W. O. S., *Ind. Crops Prod.*, **2010**, 31(1), 52-58.
- ¹⁸Ramuthai, S., Nandhakumar, V., Thiruchelvi, M., Arivoli, S. and Vijayakumaran, V., *E-J. Chem.*, **2009**, 6(S1), 363-373.
- ¹⁹Ahamed, A. J., Balakrishnan, V. and Arivoli, S., *Arch. Appl. Sci. Res.*, **2011**, 3 (3), 154-166.
- ²⁰Prasad, A. L., Santhi, T., *Sustain Environ. Res.*, **2012**, 22(2), 113-122.
- ²¹Langmuir, I., *J. Am. Chem. Soc.*, **1918**, 40, 1361-1367.
- ²²Hall, K. R., Eagleton, L. C., Acrivos, A. and Vermeulen, T., *Ind. Eng. Chem. Fundam.*, **1966**, 5, 212-219.
- ²³Freundlich, H., *J. Phys. Chem.*, **1906**, 57A, 385-470.
- ²⁴Lagergren S, *Kungliga Svenska Vetenskapsakad.*, **1898**, 24, 1-39.
- ²⁵YS Ho, Mckay, G., *Adsorpt. Sci. Technol.*, **1998**, 16, 243-255.
- ²⁶Weber, W. J., Morris, J. C., *J. Am. Soc. Civil Eng.*, **1963**, 89, 31-60.
- ²⁷Yang, Y., Wei, X., Sun, P. and Wan, J., *Molecules*, **2010**, 15, 2872-2885.
- ²⁸Chiou, M. S., Li, H. Y., *J. Hazard. Mater.*, **2002**, B93, 233-248.
- ²⁹Alkan, M., Demirbas, O., Celikcapa, S. and Dogan, M., *J. Hazard. Mater.*, **2004**, B116, 135-145.
- ³⁰Chatterjee S, Woo, S. H., *J. Hazard. Mater.*, **2009**, 164, 1012-1018.

Received: 20.01.2013.

Accepted: 25.02.2013.



THE INHIBITIVE EFFECT OF DIETHYLENETRIAMINE-PENTAMETHYLENEPHOSPHONIC ACID ON THE CORROSION OF CARBON STEEL IN SEA WATER

K. Kavipriya^{[a]*}, J. Sathiyabama^[a], and S. Rajendran^[a,b], and R. Nagalakshmi^[c]

Keywords: corrosion inhibition; carbon steel; electrochemical techniques; atomic force microscopy; diethylenetriamine pentamethylenephosphonic acid

The inhibition of the corrosion of carbon steel in sea water by diethylene triamine pentamethylene phosphonic acid (DTPMP) and Ni²⁺ has been investigated using weight loss and electrochemical measurements. The results show that 70% inhibition efficiency is achieved with binary system consisting of 250 ppm of DTPMP and 50 ppm of Ni²⁺. Polarization curves indicate that the system functioned as a cathodic inhibitor. AC impedance spectra reveal that a protective film is formed on the metal surface. The protective film has been analysed by FTIR spectra. The surface morphology and the roughness of the metal surface have been analysed by atomic force microscopy.

* Corresponding Authors

E-Mail: sennikavi@yahoo.co.in

- [a] Corrosion Research Centre, PG and Research Department of Chemistry, GTN Arts College, Dindigul, Tamil Nadu, India 624005, *Email: sennikavi@yahoo.co.in
- [b] Department of Chemistry, RVS School of Engineering and Technology, Dindigul, Tamil Nadu, India 624005; Email: srnjoany@sify.com
- [c] Department of Chemistry, Aarupadai Veedu Institute of Technology, Chennai, Tamil Nadu, India 603110, Email: nagalakshmirajan@gmail.com

INTRODUCTION

Sea water is a complex natural electrolyte. Sea water contains many corrosive electrolytes such as sodium chloride, magnesium chloride, calcium chloride, etc.; hence, carbon steel immersed in sea water is corroded slowly because of chemical reactions between the metal and the electrolytes.¹⁻³ Corrosion is the gradual destruction of material, usually metal, by chemical reaction with its environment. The corrosion is severe due to the presence of chloride ions and dissolved oxygen. Sea water has been used as cooling fluid in various industries. Carbon steel is widely used in infrastructure in marine environments.⁴ It is one of the major constituents in structural steel applications including body of a ship, offshore platforms, foundation piling, sheet piling, and coastal facilities. It is also used in industry where the metal is exposed to acid corrosion. So, it is imperative to study the corrosion aspect and find out suitable corrosion inhibitors to be used in sea water. Inhibition of corrosion and scaling can be done by the application of inhibitors, which is one of the most practical and economic methods for protection against metallic corrosion.^{5,6} Corrosion inhibitors disclose that most organic substances used as corrosion inhibitors can adsorb on the metal surface employed through heteroatoms such as nitrogen, oxygen, sulphur, and phosphorus, multiple bonds or aromatic rings and block the active sites decreasing the corrosion rate.¹⁵ Several phosphonic acids have been used as corrosion inhibitor.⁷⁻⁹ Our co-workers have conducted various research works using phosphonic acids as an

inhibitor.¹⁰ Phosphonic acids are organic compounds containing R-PO(OH)₂ or R-PO(OR)₂ groups. They are effective chelating agents that are used in cooling water and desalination systems to inhibit scale formation and corrosion. Phosphonic acids are extensively used now-a-days due to their complex forming abilities, high stability under harsh conditions, and low toxicity.¹¹ They are also used as corrosion inhibitors in concrete, coating, rubber blends, acids cleaners and anti-freeze coolants.^{12,13} The inhibition efficiency of phosphonates depends on the number of phosphono groups in a molecule and also on different substituents. Compounds with a phosphonic functional group are considered to be the most effective chemical for inhibiting the corrosion process and it is well known that short-chain-substituted phosphonic acids are good corrosion inhibitors for iron and low-alloyed steels.¹⁴

The present study aims **a)** to find out the corrosion inhibition effects of diethylene triamine pentamethylene phosphonic acid (DTPMP) and Ni²⁺ system on carbon steel in sea water using weight-loss method **b)** electrochemical techniques provide information on the corrosion rate, as well as on processes at interfaces affected by additives **c)** to analyse the protective film by Fourier Transform Infrared Spectroscopy (FTIR) **d)** to study the surface morphological changes during iron corrosion by Atomic Force Microscopy (AFM) **e)** to propose a suitable mechanism of corrosion inhibition based on the results from the above studies.

EXPERIMENTAL

Preparation of Specimen

Carbon steel specimen [0.0267 % S, 0.06 % P, 0.4 % Mn, 0.1 % C and the rest iron] of dimensions 1.0 cm x 4.0 cm x 0.2 cm were polished to a mirror finish and degreased with trichloroethylene.

Weight-Loss Method

Carbon steel specimens in triplicate were immersed in 100 mL of the solutions containing various concentrations of the inhibitor in the absence and presence of Ni^{2+} (as $\text{NiSO}_4 \cdot 6\text{H}_2\text{O}$) for one day. The weight of the specimens before and after immersion was determined using a Shimadzu balance, model AY62. The corrosion products were cleaned with Clarke's solution.¹⁶ The inhibition efficiency (IE , in %) was then calculated using the equation:

$$IE = 100 \left(1 - \frac{W_2}{W_1} \right) \quad (1)$$

where W_1 is the weight loss value in the absence of inhibitor and W_2 is the weight loss value in the presence of inhibitor.

Polarization Study

Polarization studies were carried out with a CHI-electrochemical workstation with impedance model 660A. A three-electrode cell assembly was used. The working electrode was carbon steel. The exposed surface area was 1 cm^2 . A saturated calomel electrode (SCE) was used as the reference electrode and a rectangular platinum foil was used as the counter electrode.

AC impedance spectra

The instrument used for polarization study was also used for AC impedance spectra. The cell set up was the same as that was used for polarization measurements. The real part (Z') and the imaginary part (Z'') of the cell impedance were measured in ohms at various frequencies. AC impedance spectra were recorded with initial $E_{(v)} = 0 \text{ V}$, high frequency limit was $1 \times 10^5 \text{ Hz}$, low frequency limit was 1 Hz , amplitude = 0.005 V and quiet time $t_q = 2 \text{ s}$. The values of charge transfer resistance, R_t , and the double layer capacitance, C_{dl} , were calculated.

$$C_{dl} = \frac{1}{2} IIR f_{max} \quad (2)$$

where f_{max} is maximum frequency.

Surface Examination Study

The carbon steel specimens were immersed in various test solutions for a period of one day. After one day, the specimens were taken out and dried. The nature of the film formed on the surface of the metal specimen was analysed by various surface analysis techniques.

Fourier Transform Infrared Spectra (FTIR)

The FTIR spectra were recorded in a Perkin-Elmer-1600 spectrophotometer. The film formed on the metal surface was carefully removed and mixed thoroughly with KBr making the pellet.

Atomic Force Microscopy

Atomic Force Microscope (AFM) is an exciting new technique that allows surface to be imaged at higher resolutions and accuracies than ever before. The microscope used for the present study was PicoSPM Molecular Imaging, USA make. Polished specimens prior to the initiation of all corrosion experiments were examined through an optical microscope to find out any surface defects such as pits or noticeable irregularities like cracks, etc. Only those specimens, which had a smooth, pit-free surface were subjected for AFM examination. The protective film formed on the carbon steel specimens after immersion in the inhibitor systems for different time durations were examined for a scanned area of $30 \times 30 \mu\text{m}^2$ and $15 \times 15 \mu\text{m}^2$. The two-dimensional and three-dimensional topography of surface films gave various roughness parameters of the film.

RESULTS AND DISCUSSION

The physicochemical parameters of sea water used in the present study are given in Table 1.

Table 1. The physicochemical parameters of natural sea water collected in Mandapam, Tamilnadu, India.

Parameter	Value
Total dissolved salts (mg L^{-1})	78136
Electrical conductivity ($\mu\Omega^{-1} \text{ cm}^{-1}$)	70788
pH	7.82
Total hardness (CaCO_3 equivalent)	24500
Calcium as Ca^{2+} (mg L^{-1})	2200
Magnesium as Mg^{2+} (mg L^{-1})	1800
Sodium as Na^+ (mg L^{-1})	9600
Chloride as Cl^- (mg L^{-1})	23100
Fluoride as F^- (mg L^{-1})	1.2
Potassium (mg L^{-1})	900
Sulphate as SO_4^{2-} (mg L^{-1})	2350

Weight-Loss Method

Table 2 gives values of the corrosion inhibition efficiencies and the corresponding corrosion rates of diethylene triamine pentamethylene phosphonic acid (DTPMP)- Ni^{2+} system in controlling corrosion of carbon steel in sea water for a period of 24 hours. The DTPMP alone has high rate of corrosion. The inhibition efficiency of DTPMP is improved by adding various concentrations of Ni^{2+} . Similar observations have been made by Umamathi et al¹⁷ where they have improved the inhibition efficiency of Na_3PO_4 on EDTA by addition of Zn^{2+} ion. Mary Anbarasi and Rajendran¹⁸ have improved the inhibition efficiency of heptane sulphonic acid by addition of Zn^{2+} ion. However, with increasing the concentration of DTPMP as well as Ni^{2+} , the maximum inhibition is achieved and the corrosion rate is decreased. It is found that 250 ppm of DTPMP and 50 ppm of Ni^{2+} has 70% inhibition efficiency. The inhibition efficiency increases with the increase of concentration of inhibitors. This behaviour could be attributed to the increase of the surface area covered by the adsorbed molecules of phosphonic acid with the increase of its concentration.

Table 2. The inhibition efficiency (*IE* %) and the corrosion rate (mm y^{-1}) of DTPMP – Ni^{2+} system determined by weight-loss method.

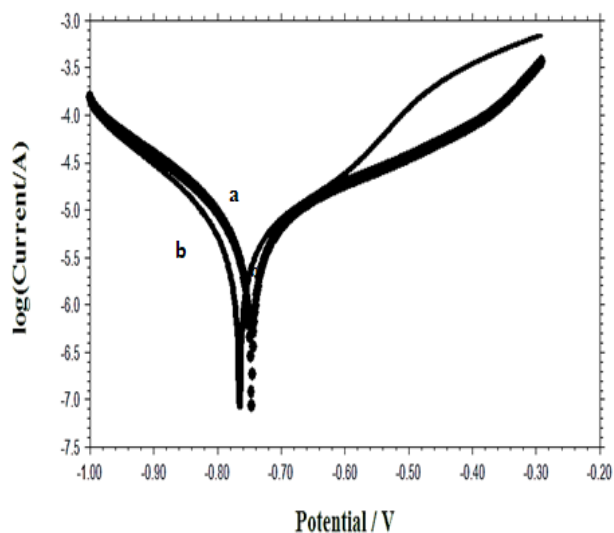
DTPMP, ppm	Ni^{2+} (ppm)					
	0		25		50	
	<i>IE</i> , %	<i>CR</i> , mm y^{-1}	<i>IE</i> , %	<i>CR</i> , mm y^{-1}	<i>IE</i> , %	<i>CR</i> , mm y^{-1}
0	-	0.1858	8	0.1709	15	0.1579
50	20	0.1486	43	0.1059	52	0.0892
100	28	0.1338	47	0.0985	56	0.0818
150	39	0.1133	52	0.0892	61	0.0725
200	46	0.1003	56	0.0818	66	0.0632
250	50	0.0929	60	0.0743	70	0.0557

Table 3. Corrosion parameters of carbon steel immersed in sea water in the presence and absence of inhibitor obtained by polarization method.

Systems	E_{corr} , mV vs SCE	I_{corr} , A cm^{-2}	b_a , mV dec^{-1}	b_c , mV dec^{-1}	<i>LPR</i> , ohm cm^2
Sea water	-746	6.351×10^{-6}	228	157	6.356×10^3
Sea water + DTPMP (250 ppm) + Ni^{2+} (50 ppm)	-765	5.238×10^{-6}	206	148	7.148×10^3

Potentiodynamic Polarization Study

Polarization study has been used to detect the formation of protective film on the metal surface.¹⁹⁻²² The polarization curves of carbon steel immersed in various test solutions are shown in Fig.1. The cathodic branch represents the oxygen reduction reaction, while the anodic branch represents the iron dissolution reaction. The corrosion parameters such as corrosion potential (E_{corr}), corrosion current density (I_{corr}), Tafel slopes (b_c and b_a) and linear polarization resistance (*LPR*) are given in Table 3.

**Figure 1.** Polarization curves of carbon steel immersed in a) sea water b) sea water + DTPMP 250 ppm + Ni^{2+} 50 ppm.

When carbon steel is immersed in sea water, the corrosion potential is -746 mV vs SCE. The formulation consisting of 250 ppm DTPMP + 50 ppm Ni^{2+} shifts the corrosion potential to -765 mV vs SCE. It shows that the corrosion potential is shifted to negative side. This suggests that the cathodic reaction is controlled predominantly.

The corrosion current density value and *LPR* value for sea water are $6.351 \times 10^{-6} \text{ A cm}^{-2}$ and $6.356 \times 10^3 \text{ ohm cm}^2$. For the formulation of 250 ppm of DTPMP and 50 ppm of Ni^{2+} , the corrosion current density value has decreased to $5.238 \times 10^{-6} \text{ A cm}^{-2}$ and the *LPR* value has increased to $7.148 \times 10^3 \text{ ohm cm}^2$. The fact that the *LPR* value increases with decrease in corrosion current density indicates adsorption of the inhibitor on the metal surface to block the active sites and inhibit corrosion and reduce the corrosion rate with the formation of a protective film on the metal surface.

AC impedance spectra

AC impedance spectra [electrochemical impedance spectra] have been used to confirm the formation of protective film on the metal surface.²³⁻²⁶ The AC impedance spectra of carbon steel immersed in sea water in the absence and presence of inhibitors are shown in Fig.2 (Nyquist plots) and Fig.3 (Bode plots). The impedance parameters namely charge transfer resistance (R_t), double layer capacitance (C_{dl}), and impedance $\lg(Z/\text{ohm})$ are given in Table 4. If a protective film is formed on the metal surface, R_t value increases and the C_{dl} value decreases.

Table 4. The AC impedance spectra of carbon steel immersed in sea water in presence of the inhibitor system

System	R_t , $\Omega \text{ cm}^2$	C_{dl} , F cm^{-2}	$\lg(Z \text{ ohm}^{-1})$
Sea water	5.426×10^1	9.3918×10^{-8}	2.010
Sea water + DTPMP (250 ppm) + Ni^{2+} (50 ppm)	2.0915×10^2	2.4365×10^{-8}	2.282

When carbon steel is immersed in sea water, R_t value is $5.426 \times 10^1 \Omega \text{ cm}^2$ and C_{dl} value is $9.3918 \times 10^{-8} \text{ F cm}^{-2}$. When DTPMP and Ni^{2+} are added to sea water, R_t value increases from $5.426 \times 10^1 \Omega \text{ cm}^2$ to $2.0915 \times 10^2 \Omega \text{ cm}^2$ and the C_{dl} value decreases from $9.3918 \times 10^{-8} \text{ F cm}^{-2}$ to $2.4365 \times 10^{-8} \text{ F cm}^{-2}$. The impedance value increases from 2.010 to 2.282. This accounts for the high *IE* of DTPMP and Ni^{2+} system and a protective film is formed on the metal surface.

In electrochemical studies, instantaneous corrosion rates are measured. But in weight-loss method, corrosion rate is measured after a longer period, in the present study after one day. After a longer period, the protective film becomes more compact and stable. This accounts for the discrepancy in IE , obtained from AC impedance spectra and from weight-loss method.

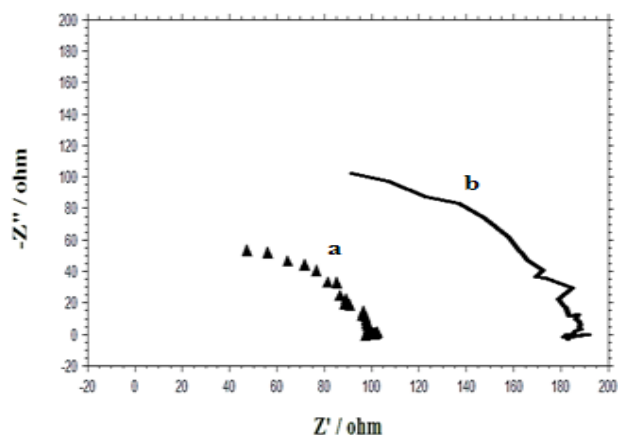


Figure 2. AC impedance spectra (Nyquist plots) of carbon steel immersed in various test solutions **a)** sea water **b)** sea water containing 250 ppm of DTPMP and 50 ppm of Ni^{2+}

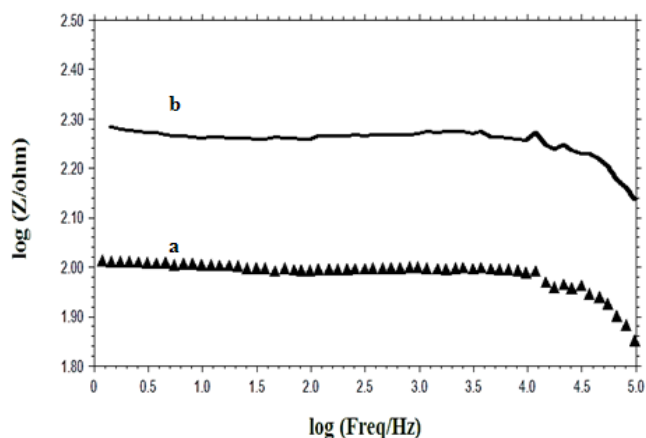
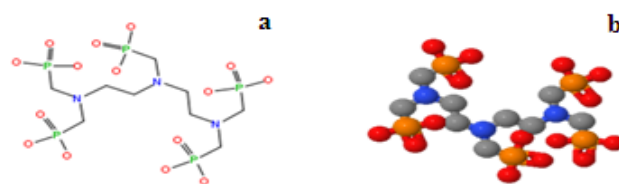


Figure 3. AC impedance spectra (Bode plots) of carbon steel immersed in various test solutions **a)** sea water **b)** sea water containing 250 ppm of DTPMP and 50 ppm of Ni^{2+}

FTIR Spectra

The structure of DTPMP is shown in Scheme 1. FTIR spectra have been used to analyse the protective film found on the metal surface.^{27,28} The FTIR spectrum (KBr) of pure DTPMP is shown in Fig. 4a. The P-O stretching frequency appears at 1058 cm^{-1} and the C-N stretching frequency appears at 1111 cm^{-1} . The FTIR spectrum of the film formed on the metal surface after immersion in sea water containing 250 ppm of DTPMP and 50 ppm of Ni^{2+} is shown in Fig. 4b. The P-O stretching frequency has shifted from 1058 cm^{-1} to 1104 cm^{-1} and the C-N stretching frequency has shifted from 1111 cm^{-1} to 1228 cm^{-1} . The shift indicates that the oxygen and nitrogen atoms of phosphonic acid are coordinated to form Fe^{2+} - DTPMP complex on the anodic sites of the metal surface. The peak at 3419 cm^{-1} is due to $-OH$ stretching. The band due to Ni-O appears at 1374 cm^{-1} . These results confirm the presence of $Ni(OH)_2$ deposited on the cathodic sites of the metal surface. Thus, FTIR spectral study leads to

the conclusion that the protective film consists of Fe^{2+} - DTPMP complex and $Ni(OH)_2$.



Scheme 1. (a) 2D Structure of DTPMP (b) 3D Structure of DTPMP

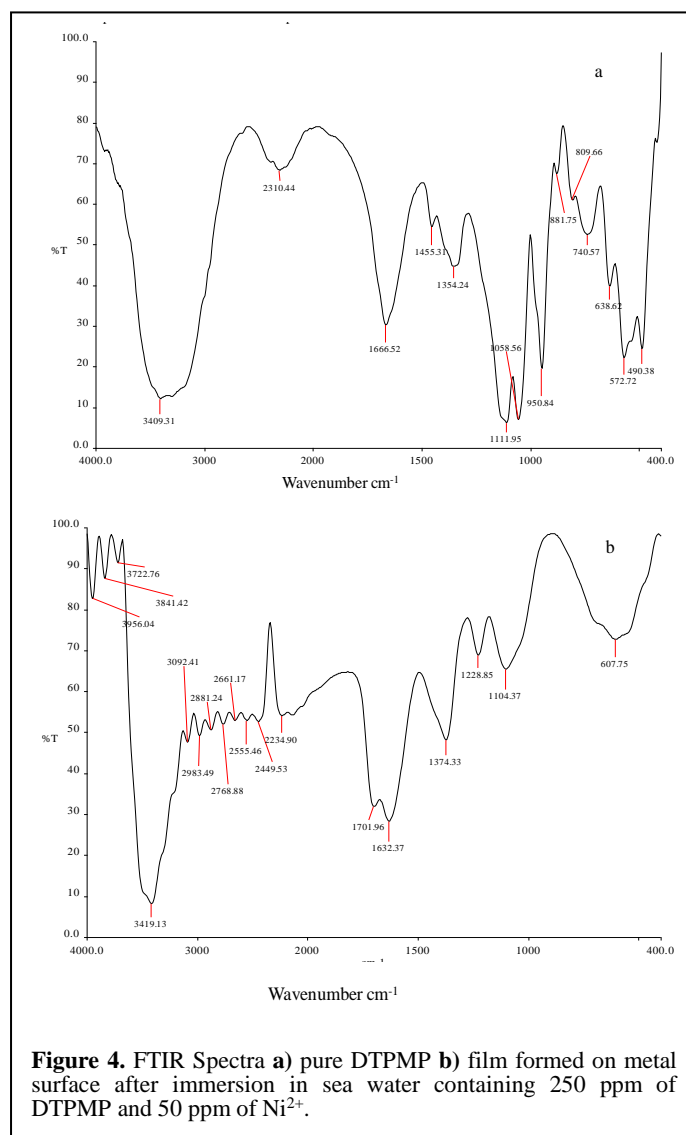


Figure 4. FTIR Spectra **a)** pure DTPMP **b)** film formed on metal surface after immersion in sea water containing 250 ppm of DTPMP and 50 ppm of Ni^{2+} .

Atomic Force Microscopy

Atomic force microscopy is a powerful technique for the gathering of roughness statistics from a variety of surfaces.²⁹ AFM is becoming an accepted method for roughness investigation.³⁰ All atomic force microscopy images were obtained on PicoSPM Molecular Imaging, USA make, AFM instrument operating in contact mode in air. The scan size of all the AFM images are $30\mu\text{m} \times 30\mu\text{m}$ areas at a scan rate of 2.4 lines per second. The two dimensional, three dimensional AFM morphologies and the AFM cross sectional profile for polished carbon steel surface (reference

sample), carbon steel surface immersed in sea water (blank sample), and carbon steel surface immersed in sea water containing 250 ppm DTPMP and 50 ppm Ni²⁺ are shown in Fig.5 (a,d,g), (b,e,h), (c,f,i) respectively.

Root Mean Square Roughness, Average Roughness and Peak-to-Valley Value: AFM image analysis was performed to obtain the average roughness, R_a (the average deviation of all points roughness profile from a mean line over the evaluation length), root – mean – square roughness, R_q (the average of the measured height deviations taken within the evaluation length and measured from the mean line), and the maximum peak-to-valley ($P-V$) height values (largest single peak-to-valley height in five adjoining sampling heights).³⁰ R_q is much more sensitive than R_a to large and small height deviations from the mean.³¹

Table 5. AFM data for carbon steel immersed in inhibited and uninhibited environments.

Samples	R_q , nm	R_a , nm	$P-V$, nm
Polished carbon steel, control	4.33	3.41	35.28
Carbon steel immersed in sea water (blank)	17.67	13.51	71.08
Carbon steel immersed in sea water containing 250 ppm DTPMP and 50 ppm Ni ²⁺	11.22	8.76	42.00

Table 5 is a summary of the average roughness (R_a), rms roughness (R_q), maximum peak to valley height ($P-V$) value for carbon steel surface immersed in different environments. The value of R_q , R_a , and $P-V$ height for the polished carbon steel surface (reference sample) are 4.33 nm, 3.41 nm, and 35.28 nm respectively. This shows that the surface is more homogenous, with some places where the height is lower than the average depth. Fig. 5 (a,d,g) displays the non-corroded metal surface. The slight roughness observed on the polished carbon steel surface is due to atmospheric corrosion. Fig. 5 (b,e,h) displays corroded metal surface with few pits. The rms roughness, average roughness, and $P-V$ height values for the carbon steel surface immersed in sea water are 17.67 nm, 13.51 nm, and 71.08 nm respectively. These values suggest that carbon steel surface immersed in sea water has a greater surface roughness than the polished metal surface, indicating that the unprotected carbon steel surface is rougher and were due to the corrosion of carbon steel in sea water environment. Fig. 5 (c,f,i) shows the carbon steel surface after immersion in sea water containing 250 ppm of DTPMP + 50 ppm Ni²⁺. The R_q , R_a , and $P-V$ height values for carbon steel surface are 11.22 nm, 8.76 nm, and 42 nm respectively. These values are considerably less in the inhibited environment compared to the uninhibited environment. These parameters confirm that the surface appears smoother. The smoothness of the surface is due to the formation of a compact protective film of Fe²⁺–DTPMP complex and Ni(OH)₂ on the metal surface, thereby inhibiting the corrosion of carbon steel. The above parameters are also somewhat greater than the AFM data of polished metal surface, which confirms the formation of film on the metal surface, which is protective in nature.

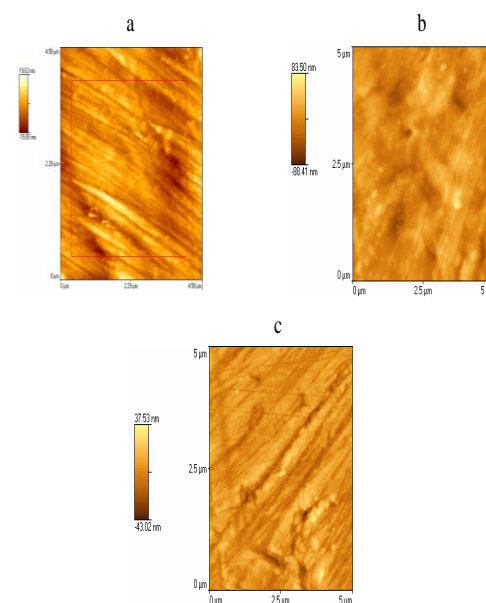


Figure 5. Two dimensional AFM images of the surface of,

- Polished carbon steel (control);
- Carbon steel immersed in sea water (blank);
- Carbon steel immersed in sea water containing DTPMP (250 ppm) + Ni²⁺ (50 ppm).

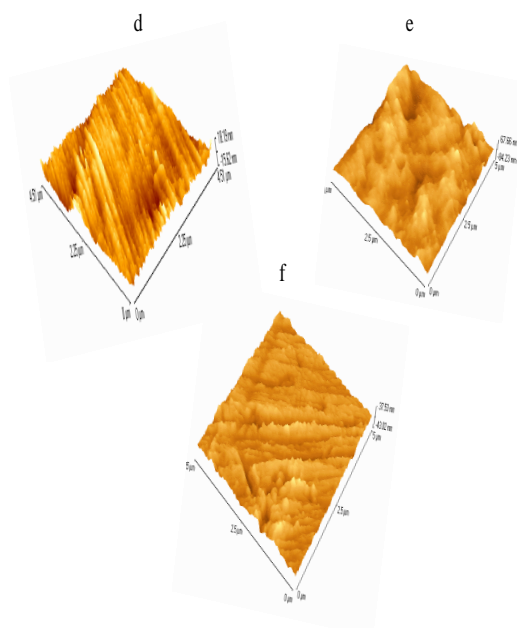


Figure 5. Three dimensional AFM images of the surface of,

- Polished carbon steel (control);
- Steel immersed in sea water (blank);
- Carbon steel immersed in sea water containing DTPMP (250 ppm) + Ni²⁺ (50 ppm).

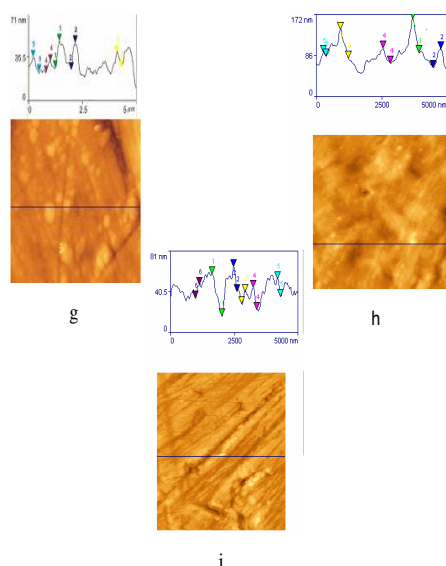


Figure 5. AFM cross-sectional images of the surface of,

(g) Polished carbon steel (control);

(h) Carbon steel immersed in sea water (blank);

(i) Carbon steel immersed in sea water containing DTPMP (250 ppm) + Ni²⁺ (50 ppm).

Mechanism of corrosion inhibition

In order to explain the above results, the following mechanism of corrosion inhibition is proposed: When carbon steel is immersed in an aqueous solution, the anodic reaction is,

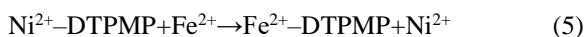


The corresponding cathodic reaction is reduction of oxygen to hydroxyl ions,



When the formulation consists of 250 ppm of DTPMP and 50 ppm Ni²⁺ in sea water, there is formation of DTPMP–Ni²⁺ complex in solution.

When carbon steel is immersed in this environment, the DTPMP–Ni²⁺ complex diffuses from the bulk of the solution to the metal surface. The DTPMP–Ni²⁺ complex is converted into DTPMP–Fe²⁺ complex on the anodic sites of the metal surface, the stability of Fe²⁺–DTPMP complex is higher than the corresponding Ni complex.



The released Ni²⁺ combines with OH⁻ to form Ni(OH)₂ on the cathodic sites of the metal surface.



The protective nature of the film is due to the presence of metal inhibitor complex and nickel hydroxide. Formation of the metal inhibitor complex fills the pores of the otherwise porous film and makes it a protective film.

Thus, the protective film consists of Fe²⁺ – DTPMP complex and Ni(OH)₂.

CONCLUSIONS

The conclusions drawn from the results may be given as: The formulation consists of 250 ppm of DTPMP and 50 ppm of Ni²⁺ has 70 % IE. Polarization study suggests that the cathodic reaction is controlled predominantly. AC impedance spectra reveal that a protective film is formed on the metal surface. FTIR spectra show that the protective film consists of Fe²⁺–DTPMP complex and Ni(OH)₂. AFM images confirm the formation of protective layer on the metal surface.

REFERENCES

- Satyanarayana, M. G. V., Kalpana, Y., Himabindu, V., Kumar, K., *Corros. Eng. Sci. Technol.*, **2012**, *47*, 38.
- Al-Baker, N., Shawabkeh, R., Rihan, R., *Corros. Eng. Sci. Technol.*, **2011**, *46*, 767.
- Durodola, B. M., Olugbuyiro, J. A. O., Moshood, S. A., Fayomi, O. S., Popoola, A. P. I., *Int. J. Electrochem. Sci.*, **2011**, *6*, 5605.
- Zou, Y., Wang, J., Zheng, Y. Y., *Corros. Sci.*, **2011**, *53*, 208.
- Khaled, K. F., Hackerman, N., *Electrochim. Acta.*, **2003**, *48*, 2715.
- Ali, S. A., Saeed, M. T., Rahman, S. V., *Corros. Sci.*, **2003**, *45*, 253.
- Amar, H., Benzakour, J., Derja, A., Villemin, D., Moreau, B., *J. Electroanal. Chem.*, **2003**, *558*, 131.
- Amar, H., Benzakour, J., Derja, A., Villemin, D., Moreau, B., Braisaz, T., Tounsi, A., *Corros. Sci.*, **2008**, *50*, 124.
- Gopi, D., Manimozhi, S., Govindaraju, K. M., *J. Appl. Electrochem.*, **2007**, *37*, 439.
- Kavipriya, K., Rajendran, S., Sathiyabama, J., Suriya Prabha, A., *Eur. Chem. Bull.*, **2012**, *1*, 366.
- Ochoa, N., Basil, G., Moran, F., Pebere, N., *J. Appl. Electrochem.*, **2002**, *32*, 497.
- Gunasekaran, G., Natarajan, R., Muralidharan, V. S., Palaniswamy, N., Appa Rao, B. V., *Anti-Corros. Methods Mater.*, **1997**, *44*, 248.
- Touir, R., Dkhireche, N., Ebn Touhami, M., Sfaira, M., Senhaji, O., Robin, J. J., Boutevin, B., Chekaoui, M., *Mater. Chem. Phys.*, **2010**, *122*, 1.
- Fang, J. L., Li, Y., Ye, X. R., Wang, Z. W., Liu, Q., *Corrosion*, **1993**, *49*, 266.
- Ramesh, S., Rajeswari, S., *Electrochim. Acta.*, **2004**, *49*, 811.
- Wranglen, G., *Introduction to corrosion and protection of Metals London: Chapman & Hall.*, **1985**, 236.
- Umamathi, Arockia Selvi, J., Agnesia Kanimozhi, S., Rajendran, S., John Amalraj, A., *Indian J. Chem. Technol.*, **2008**, *15*, 560.
- Mary Anbarasi, C., Rajendran, S., *J. Electrochem. Sci. Eng.*, **2012**, *2*, 1.
- Roque, J. M., Pandiyan, T., Cruz, J., Garcia-Ochoa, E., *Corros. Sci.*, **2008**, *50*, 616.
- Arockia Selvi, J., Rajendran, S., Ganga Sri, V., John Amalraj, A., Narayanasamy, B., *Portug. Electrochim. Acta.*, **2009**, *27*, 1.

- ²¹Nagalakshmi, R., Rajendran, S., Sathiyabama, J., Pandiarajan, M., Lydia Christy, J., *Eur. Chem. Bull.*, **2013**, 2, 150.
- ²²Agiladevi, S., Rajendran, S., Jeyasundari, J., Pandiarajan, M., *Eur. Chem. Bull.*, **2013**, 2, 84.
- ²³Sathiyabama, J., Rajendran, S., Arockia Selvi, J., Jeyasundari, J., *Open Corros. J.*, **2009**, 2, 76.
- ²⁴Shyamala Devi, B., Rajendran, S., *Eur. Chem. Bull.*, **2012**, 1, 150.
- ²⁵Rajendran, S., Paulraj, J., Rengan, P., Jeyasundari, J., Manivannan, M., *J. Dent. Oral. Hyg.*, **2009**, 1, 1.
- ²⁶Rajendran, S., Anuradha, K., Kavipriya, K., Krishnaveni, A., Angelin Thangakani, J., *Eur. Chem. Bull.*, **2012**, 1, 503.
- ²⁷Lalitha, A., Ramesh, S., Rajeswari, S., *Electrochim. Acta.*, **2005**, 51, 47.
- ²⁸Rajendran, S., Apparao, B.V., Palaniswamy, N., Periasamy, V., Karthikeyan, G., *Corros. Sci.*, **2001**, 43, 1345.
- ²⁹Singh, A. K., Shukla, S. K., Singh, M., Quraishi, M. A., *Mater. Chem. Phys.*, **2011**, 129, 68.
- ³⁰Zhang, F., Pan, J., Claesson, P. M., *Electrochim. Acta.*, **2011**, 56, 1636.
- ³¹Arockia Selvi, J., Rajendran, S., Jeyasundari, J., *Zastit. Mater.*, **2009**, 50, 91.

Received: 14.01.2013.

Accepted: 25.02.2013.



SYNTHESIS OF 2-AZETIDINONES SUBSTITUTED ISOCOUMARINS

Uday C Mashelkar^{[a]*}, Mukesh S. Jha^[a] and Beena U. Mashelkar^[a]

Keywords: 3-Formylisocoumarin, aromatic amines, acid chlorides, tri-n-butylamine, 2-azetidinones.

3-Formylisocoumarin condensed with aromatic primary amines to give Schiff bases (**2a-2d**). These Schiff bases are then reacted with acid chlorides in the presence of base in toluene to give 1,3,4-substituted 2-azetidinones.

* Corresponding Authors

E-Mail: ucmashelkar@rediffmail.com

[a] Organic Research Laboratory, S.S. & L.S. Patkar College, Goregaon (West), Mumbai 400 062, India.

INTRODUCTION

High throughput screening of the selected chemical libraries having heterocyclic or carbocyclic ring at their core is one of the most expeditious ways to search for useful medicinal activity. Heterocyclic lactones have long been a mainstay of organic synthesis due to their broad application to organic and medicinal chemistry. Isocoumarin or 1H-2-Benzopyran-1-ones constitute a small but significant group of naturally occurring lactones that is assuming growing importance in recent years. Isocoumarins constitute an important group of natural products. Equally important is the natural occurrence of 3,4-dihydro isocoumarin, the saturated lactones.

Isocoumarins have assumed importance in recent years^{1,2} majority of the naturally occurring isocoumarins and dihydro Isocoumarins occur in fungi and other microorganism and are metabolic products of the host and therefore may be playing vital part in the metabolism of these microorganisms. Few observations reported in the literature regarding the physiological activity of some of them are quiet encouraging. The heteroatom improves binding and the rigid cyclic framework, imparts rigidity, enhancing the selectivity, Nitrogen atom being one of them. There are several examples reported in literature where the presence of nitrogen atom in compounds in various form has shown tremendous therapeutic applications.

β -Lactam class of compounds has served as an important and highly successful role in the pharmaceutical industry. Miracle drugs such as Penicillins and Cephalosporins have significantly improved the human health and life expectancy. Although most Penicillin and Cephalosporin like compounds have been obtained by biosynthesis, by chemical modification of intermediates for bioassay of antibacterial activity because of growing resistance of bacteria against Penicillin and Cephalosporin like compounds and the need for medicines with more specific antibacterial activity.^{3,4} Developments in the field of β -lactams⁵⁻⁸ during the last decade have shown that the only essential

feature for the antibacterial activity in these compounds is the presence of β -lactam ring. Much attention was therefore focussed on this four membered cyclic amide and also the various substituents's attached directly to this system. The azetidinone derivatives have also been recognized as TACE inhibitors⁹ and agents with new biological activities such as anticancer,¹⁰ anticoccidal,¹¹ cardiovascular,¹² antiviral,¹³ mutagenic property,¹⁴ anticonvulsant and anti-inflammatory.^{15,16}

The biological importance of the above heterocycles led us to introduce azetidinone ring on the isocoumarin ring with an aim to increasing their biological activity.

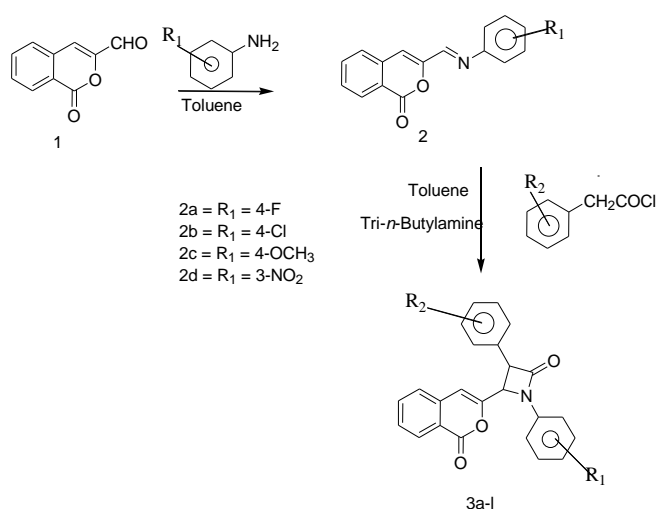
RESULTS AND DISCUSSION

The 3-formylisocoumarin was condensed with various aromatic amines in toluene to yield Schiff's bases (**2a-2d**). Reaction was monitored by TLC. After completion of reaction the product was filtered and dried to get Schiff bases (**2a-2d**) and was characterized by their physical as well as spectral data. The IR spectra of compound (**2a-2d**) showed absorption for only one carbonyl group at 1717 cm^{-1} and presence of -CH=N- band at 1618 cm^{-1} . Some other bands were observed at 1493 and 1598 cm^{-1} . $^1\text{H NMR}$ (CDCl_3) showed absence of aldehydic proton and the presence of CH=N proton at δ 8.17 ppm. These Schiff's bases (**2a-2d**) were then reacted with acid chlorides in the presence of base such as tri-n-butylamine to give 1,3,4- substituted 2-azetidinone (**3a-3l**). The IR spectra of compounds (**3a-3l**) showed absorption for two carbonyl groups at 1752 and 1739 cm^{-1} . In the $^1\text{H NMR}$ there were two doublets for $\text{C}_3\text{-H}$ and $\text{C}_4\text{-H}$ at 4.71 & 4.77 ppm. The envisaged reaction sequence is depicted in **Scheme 1**.

Structures of the compounds **3a-3l** were established by their IR and $^1\text{H NMR}$ spectra. As reported in the literature cis isomer shows higher value of coupling constant than trans isomer.¹⁷ Majority of isolated compounds are showing lower value of coupling constant confirming the trans azetidinone. One of the compound showing higher value of coupling constant confirming the presence of cis azetidinone. Few of them were showing mixture of both in which trans azetidinones containing small amount of cis azetidinones (Table 1).

Table 1. Stereochemistry of compounds (3a-3l)

Compound	R ₁	R ₂	Isolated isomer
3a	4-F	H	<i>Trans</i>
3b	4-Cl	H	<i>Trans: Cis (88: 12)</i>
3c	4-OCH ₃	H	<i>Trans</i>
3d	3-NO ₂	H	<i>Trans:Cis (91: 9)</i>
3e	4-F	4-OCH ₃	<i>Trans</i>
3f	4-Cl	4-OCH ₃	<i>Trans</i>
3g	4-OCH ₃	4-OCH ₃	<i>Trans</i>
3h	3-NO ₂	4-OCH ₃	<i>Trans</i>
3i	4-F	4-Cl	<i>Trans</i>
3j	4-Cl	4-Cl	<i>Trans</i>
3k	4-OCH ₃	4-Cl	<i>Cis</i>
3l	3-NO ₂	4-Cl	<i>Trans</i>



Scheme 1.

EXPERIMENTAL SECTION

All the compounds were identified by examination of their spectral data and physical properties. Yields refer to the isolated yields of desired products. Melting points were determined on Buchi-545 melting point apparatus and are uncorrected. Progress of the reaction was monitored on TLC. IR spectra were recorded by Perkin Elmer Spectrum-1 (FTIR) using KBr discs, ¹H NMR and ¹³C NMR was recorded in CDCl₃ using Avance 400 MHz Bruker spectrometer (chemical shift (δ) in ppm) with TMS as internal standard and mass spectra were recorded on a Thermofinigan Ion Trap GCMS Polaris Q. The dry reactions were carried out under nitrogen with magnetic/mechanical stirring.

General procedure for the synthesis of 3-arylimino-1H-isochromen-1-ones (2a-2d)

An intimate mixture of 3-formyl isocoumarin (1) (10 mmol) and corresponding aromatic primary amine (11

mmol) was refluxed in toluene (30 ml) for 6-7 hours with azeotropic removal of the water formed during the reaction. The reaction was monitored by TLC. After reaction was completed the reaction mass was cooled down to 10°C the product was filtered and washed with cold toluene to get solid products.

3-((4-fluorophenylimino)methyl)-1H-isochromen-1-one (2a): Yellow solid; Yield: 80%; m.p. 197-198°C; Anal. Calcd. for C₁₆H₁₀FNO₂; C, 71.91; H, 3.77; N, 5.24. Found: C, 71.93; H, 3.81; N, 5.30; IR (KBr, cm⁻¹): 3072 (arom-CH), 1717 (>C=O), 1618; ¹H NMR (400 MHz, CDCl₃) δ: 7.20 (s, 1H, C₄-H), 7.10-8.39 (m, 8H, Ar-H), 8.17 (s, 1H, -CH=N-); ¹³C-NMR (100.622 MHz, CDCl₃, δ/ ppm): 112.9, 115.1, 121.6, 123.6, 127.9, 130.1, 130.5, 135.8, 136.6, 143.1, 150.0, 151.1, 159.4, 161.2; Mass (m/z): 267 [M⁺].

3-((4-chlorophenylimino)methyl)-1H-isochromen-1-one (2b): Yellow solid; Yield: 82%; m.p. 212-213°C; Anal. Calcd. for C₁₆H₁₀ClNO₂; C, 67.74; H, 3.55; N, 4.94. Found: C, 67.75; H, 3.58; N, 4.97; IR (KBr, cm⁻¹): 3070(arom-CH), 1723(>C=O), 1623; ¹H NMR(400 MHz, CDCl₃) δ: 7.23 (s, 1H, C₄-H), 7.21-8.39 (m, 8H, Ar-H), 8.22 (s, 1H, -CH=N-); ¹³C-NMR (100.622 MHz, CDCl₃, δ/ ppm): 112.9, 115.1, 121.7, 123.6, 127.9, 130.2, 130.5, 135.8, 136.6, 143.2, 150.1, 151.1, 159.4, 161.3; Mass (m/z) : 283 [M⁺].

3-((4-methoxyphenylimino)methyl)-1H-isochromen-1-one (2c): Brown solid; Yield: 84%; m.p. 220-221°C; Anal. Calcd. for C₁₇H₁₃NO₃; C, 73.11; H, 4.69; N, 5.02. Found: C, 73.14; H, 4.71; N, 5.05; IR (KBr, cm⁻¹): 3067 (arom-CH), 1725 (>C=O), 1620; ¹H NMR (400 MHz, CDCl₃) δ: 3.86 (s, 3H, -OCH₃), 7.17 (s, 1H, C₄-H), 6.95-8.36 (m, 8H, Ar-H), 8.19 (s, 1H, -CH=N-); ¹³C-NMR (100.622 MHz, CDCl₃, δ/ ppm): 55.7, 112.6, 114.9, 121.9, 123.4, 127.7, 129.6, 130.3, 135.7, 136.4, 143.1, 150.0, 151.1, 159.3, 161.2; Mass (m/z) : 279 [M⁺].

3-((3-nitrophenylimino)methyl)-1H-isochromen-1-one (2d): Yellow solid; Yield: 82 %; m.p. 228-229°C; Anal. Calcd. for C₁₆H₁₀N₂O₄; C, 65.31; H, 3.43; N, 9.52. Found: C, 65.34; H, 3.48; N, 9.57; IR (KBr, cm⁻¹): 3070 (arom-CH), 1719 (>C=O), 1616; ¹H NMR (400 MHz, CDCl₃) δ: 7.25 (s, 1H, C₄-H), 7.62-8.42 (m, 8H, Ar-H), 8.40 (s, 1H, -CH=N-); ¹³C-NMR (100.622 MHz, CDCl₃, δ/ ppm): 113.2, 115.3, 121.8, 123.8, 127.6, 130.4, 130.8, 135.9, 136.8, 144.0, 143.6, 150.2, 151.4, 155.6, 159.6, 161.3; Mass (m/z): 294 [M⁺].

General procedure for the synthesis of 4-(1-oxo-1H-isochromen-3-yl)-1-aryl-3-phenylazetidin-2-ones (3a-3l)

A mixture of 3-iminoisocoumarin derivatives (10 mmol) (2a-2d), acid chlorides (20 mmol) and tri-*n*-butylamine (30 mmol) in toluene (50 ml) was refluxed for 3-4 hours. Reaction was monitored by TLC. After completion of the reaction it was then cooled to room temperature and 1:1 HCl (40-50 ml) was added. Organic layer was separated and washed with water followed by NaHCO₃ solution and finally with water and dried over

anhydrous sodium sulphate and solvent removed under reduced pressure. Compound was isolated using column chromatography (n-Hexane: Ethyl acetate = 90: 10) and thereafter it was crystallized from ethanol.

1-(4-fluorophenyl)-4-(1-oxo-1H-isochromen-3-yl)-3-phenylazetididin-2-one (3a): White solid; Yield: 54%; m.p. 147-148°C; Anal. Calcd. for C₂₄H₁₆FNO₃; C, 74.8; H, 4.18; N, 3.63. Found: C, 74.64; H, 4.08; N, 3.74; IR (KBr, cm⁻¹): 3060 (arom-CH), 1752 (>C=O), 1739 (>C=O), 1602 (C-C aromatic); ¹H NMR (400 MHz, CDCl₃) δ: 4.71 (d, 1H, *J*=2.4Hz, C₃-H), 4.77 (d, 1H, *J*=2.4Hz, C₄-H), 6.65 (s, 1H, -CH=C), 7.03-8.33 (m, 13H, Ar-H); ¹³C-NMR (100.622 MHz, CDCl₃, δ/ ppm): 60.2, 61.3, 105.3, 114.6, 119.1, 121.3, 125.7, 127.6, 128.5, 129.3, 130.1, 130.8, 133.9, 135.6, 135.9, 138.1, 151.9, 156.7, 161.3, 164.2; Mass (m/z) : 385 [M⁺].

1-(4-chlorophenyl)-4-(1-oxo-1H-isochromen-3-yl)-3-phenylazetididin-2-one (3b): White solid; Yield: 48 %; m.p. 162-163°C, Anal. Calcd. for C₂₄H₁₆ClNO₃; C, 71.73; H, 4.01; N, 3.49. Found: C, 71.85; H, 3.9; N, 3.37; IR (KBr, cm⁻¹): 3064 (arom-CH), 1758 (>C=O), 1729 (>C=O), 1598(C-C aromatic); ¹H NMR (400 MHz, CDCl₃) δ: 4.71 (d, 1H, *J*=2.4Hz, C₃-H), 4.78 (d, 1H, *J*=2.4Hz, C₄-H), 6.65 (s, 1H, -CH=C), 7.30-8.34 (m, 13H, Ar-H); ¹³C-NMR (100.622 MHz, CDCl₃, δ/ ppm): 60.2, 61.3, 105.3, 114.5, 119.2, 121.3, 125.7, 127.6, 128.6, 129.3, 130.1, 130.8, 133.9, 135.7, 135.9, 138.2, 151.9, 156.7, 161.3, 164.2; Mass (m/z) : 401 [M⁺].

1-(4-methoxyphenyl)-4-(1-oxo-1H-isochromen-3-yl)-3-phenylazetididin-2-one (3c): White solid; Yield: 49%; m.p. 159-160°C, Anal. Calcd. for C₂₅H₁₉NO₄; C, 75.55; H, 4.82; N, 3.52. Found: C, 75.60; H, 4.88; N, 3.59; IR (KBr, cm⁻¹): 3065 (arom-CH), 1759 (>C=O), 1731 (>C=O), 1603(C-C aromatic); ¹H NMR (400 MHz, CDCl₃) δ: 3.79 (s, 3H, -OCH₃), 4.67 (d, 1H, *J*=2.4Hz, C₃-H), 4.75 (d, 1H, *J*=2.4Hz, C₄-H), 6.63 (s, 1H, -CH=C), 6.87-8.33 (m, 13H, Ar-H); ¹³C-NMR (100.622 MHz, CDCl₃, δ/ ppm): 55.5, 60.2, 61.3, 105.3, 114.5, 118.4, 121.0, 125.9, 127.5, 128.2, 129.1, 129.9, 130.6, 133.8, 135.1, 136.0, 137.2, 152.0, 156.5, 161.6, 164.1; Mass(m/z) : 397 [M⁺].

1-(3-nitrophenyl)-4-(1-oxo-1H-isochromen-3-yl)-3-phenylazetididin-2-one (3d): White solid; Yield: 46%; m.p. 165-166°C, Anal. Calcd. for C₂₄H₁₆N₂O₅; C, 69.90; H, 3.91; N, 6.79. Found: C, 69.72; H, 3.75; N, 6.72; IR (KBr, cm⁻¹): 3093 (arom-CH), 1759 (>C=O), 1733 (>C=O), 1604 (C-C aromatic); ¹H NMR (400 MHz, CDCl₃) δ: 4.83 (d, 1H, *J*=2.8Hz, C₃-H), 4.89 (d, 1H, *J*=2.8Hz, C₄-H), 6.70 (s, 1H, -CH=C), 7.39-8.30 (m, 13H, Ar-H); ¹³C-NMR (100.622 MHz, CDCl₃, δ/ ppm): 60.2, 61.3, 105.3, 114.6, 118.6, 121.3, 125.9, 127.6, 128.3, 129.2, 130.1, 130.8, 133.8, 135.2, 136.1, 137.2, 138.2, 142.1, 152.1, 156.5, 161.7, 164.3; Mass (m/z) : 412 [M⁺].

1-(4-fluorophenyl)-3-(4-methoxyphenyl)-4-(1-oxo-1H-isochromen-3-yl)azetididin-2-one (3e): White solid; Yield: 53%; m.p. 184-186°C, Anal. Calcd. for C₂₅H₁₈FNO₄; C, 72.28; H, 4.37; N, 3.37. Found: C, 72.17; H, 4.24; N, 3.30; IR (KBr, cm⁻¹): 3074 (arom-CH), 1763 (>C=O), 1732 (>C=O), 1608 (C-C aromatic); ¹H NMR (400 MHz, CDCl₃) δ: 3.68 (s, 3H, -OCH₃), 4.65 (d, 1H, *J*=2.4Hz, C₃-H), 4.71 (d, 1H, *J*=2.4Hz, C₄-H), 6.63 (s, 1H, -CH=C),

6.92-7.76 (m, 12H, Ar-H); ¹³C-NMR (100.622 MHz, CDCl₃, δ/ ppm): 55.6, 60.2, 61.3, 105.4, 114.5, 118.6, 121.0, 125.9, 127.6, 128.3, 129.2, 129.9, 130.6, 133.9, 135.2, 136.1, 137.3, 153.0, 156.5, 161.6, 164.3; Mass (m/z) : 415 [M⁺].

1-(4-chlorophenyl)-3-(4-methoxyphenyl)-4-(1-oxo-1H-isochromen-3-yl)azetididin-2-one (3f): White solid; Yield: 52%; m.p. 178-180°C, Anal. Calcd. for C₂₅H₁₈ClNO₄; C, 69.53; H, 4.20; N, 3.24. Found: C, 69.60; H, 4.08; N, 3.35; IR (KBr, cm⁻¹): 3065 (arom-CH), 1766 (>C=O), 1732 (>C=O), 1607 (C-C aromatic); ¹H NMR (400 MHz, CDCl₃) δ: 3.81 (s, 3H, -OCH₃), 4.65 (d, 1H, *J*=2.4Hz, C₃-H), 4.71(d, 1H, *J*=2.4Hz, C₄-H), 6.62 (s, 1H, -CH=C), 6.93-8.30 (m, 12H, Ar-H); ¹³C-NMR (100.622 MHz, CDCl₃, δ/ ppm): 55.6, 60.2, 61.3, 105.4, 114.6, 118.7, 121.1, 125.9, 127.6, 128.3, 129.3, 129.9, 130.7, 133.9, 135.3, 136.1, 137.3, 153.0, 156.6, 161.2, 164.4; Mass (m/z) : 431 [M⁺].

1,3-bis(4-methoxyphenyl)-4-(1-oxo-1H-isochromen-3-yl)azetididin-2-one (3g): White solid; Yield: 48%; m.p. 84-86°C, Anal. Calcd. for C₂₆H₂₁NO₅; C, 73.06; H, 4.95; N, 3.28. Found: C, 72.90; H, 4.88; N, 3.17; IR (KBr, cm⁻¹): 3068 (arom-CH), 1757(>C=O), 1725 (>C=O), 1610 (C-C aromatic); ¹H NMR (400 MHz, CDCl₃) δ: 3.80 (s, 3H, -OCH₃), 3.83 (s, 3H, -OCH₃), 4.61(d, 1H, *J*=4Hz, C₃-H), 4.69 (d, 1H, *J*=4Hz, C₄-H), 6.61 (s, 1H, -CH=C), 6.87-8.33 (m, 12H, Ar-H); ¹³C-NMR (100.622 MHz, CDCl₃, δ/ ppm): 55.4, 55.6, 60.2, 61.3, 105.4, 114.4, 118.3, 121.2, 125.9, 127.7, 128.4, 129.4, 129.7, 131.0, 133.9, 135.4, 136.2, 137.3, 153.0, 156.6, 161.3, 164.6; Mass (m/z) : 427 [M⁺].

3-(4-methoxyphenyl)-1-(3-nitrophenyl)-4-(1-oxo-1H-isochromen-3-yl)azetididin-2-one (3h): White solid; Yield: 55 %; m.p. 173-175 °C, Anal. Calcd. for C₂₅H₁₈N₂O₆; C, 67.87; H, 4.10; N, 6.33. Found: C, 67.72; H, 3.97; N, 6.25; IR (KBr, cm⁻¹): 3091 (arom-CH), 1763(>C=O), 1735 (>C=O), 1612 (C-C aromatic); ¹H NMR (400 MHz, CDCl₃) δ: 3.84 (s, 3H, -OCH₃), 4.77 (d, 1H, *J*=2.8Hz, C₃-H), 4.81 (d, 1H, *J*=2.8Hz, C₄-H), 6.74 (s, 1H, -CH=C), 6.94-8.33 (m, 12H, Ar-H) ; ¹³C-NMR (100.622 MHz, CDCl₃, δ/ ppm): 55.6, 60.2, 61.3, 105.6, 114.5, 118.4, 121.3, 126.1, 127.8, 128.2, 129.6, 129.7, 131.1, 133.9, 135.6, 136.2, 137.3, 138.1, 141.2, 153.1, 156.6, 161.3, 164.4; Mass (m/z) : 442 [M⁺].

3-(4-chlorophenyl)-1-(4-fluorophenyl)-4-(1-oxo-1H-isochromen-3-yl)azetididin-2-one (3i): White solid; m.p. 150-152°C, Yield: 50%; Anal. Calcd. for C₂₄H₁₅ClFNO₃; C, 68.66; H, 3.60; N, 3.34. Found: C, 68.76; H, 3.48; N, 3.25; IR (KBr, cm⁻¹): 3075 (arom-CH), 1758 (>C=O), 1736 (>C=O), 1602 (C-C aromatic); ¹H NMR (400 MHz, CDCl₃) δ: 4.68 (d, 1H, *J*=2.4Hz, C₃-H), 4.73 (d, 1H, *J*=2.4Hz, C₄-H), 6.64 (s, 1H, -CH=C), 7.03-7.78 (m, 12H, Ar-H); ¹³C-NMR (100.622 MHz, CDCl₃, δ/ ppm): 60.2, 61.3, 105.4, 114.6, 119.1, 121.3, 125.7, 127.6, 128.8, 129.6, 130.2, 131.1, 133.9, 135.7, 135.9, 138.3, 151.9, 156.8, 161.3, 164.3; Mass (m/z) : 419 [M⁺].

1,3-bis(4-chlorophenyl)-4-(1-oxo-1H-isochromen-3-yl)azetididin-2-one (3j): White solid; Yield: 49%; m.p. 205-207°C, Anal. Calcd. for C₂₄H₁₅Cl₂NO₃; C, 66.07; H, 3.47; N, 3.21. Found: C, 65.95; H, 3.35; N, 3.15; IR (KBr,

cm⁻¹): 3081 (arom-CH), 1756 (>C=O), 1726 (>C=O), 1597(C-C aromatic); ¹H NMR (400 MHz, CDCl₃) δ: 4.69 (d, 1H, *J*=2.8Hz, C₃-H), 4.73 (d, 1H, *J*=2.8Hz, C₄-H), 6.64 (s, 1H, -CH=C), 7.31-7.78 (m, 12H, Ar-H); ¹³C-NMR (100.622 MHz, CDCl₃, δ/ ppm): 60.2, 61.3, 105.4, 114.6, 119.2, 121.4, 125.8, 127.8, 128.9, 129.6, 130.3, 131.2, 133.9, 135.8, 135.9, 138.3, 151.8, 156.9, 161.4, 164.4; Mass (m/z) : 436 [M⁺].

3-(4-chlorophenyl)-1-(4-methoxyphenyl)-4-(1-oxo-1H-isochromen-3-yl)azetid-2-one (**3k**): White solid; Yield: 53%; m.p. 197-199°C, Anal. Calcd. for C₂₅H₁₈ClNO₄; C, 69.53; H, 4.20; N, 3.24. Found: C, 69.60; H, 4.04; N, 3.17; IR (KBr, cm⁻¹): 3060 (arom-CH), 1751 (>C=O), 1725 (>C=O); ¹H NMR (400 MHz, CDCl₃) δ: 3.81 (s, 3H, -OCH₃), 5.02 (d, 1H, *J*=6Hz, C₃-H), 5.19 (d, 1H, *J*=6Hz, C₄-H), 6.33 (s, 1H, -CH=C), 6.90-8.13 (m, 12H, Ar-H); ¹³C-NMR (100.622 MHz, CDCl₃, δ/ ppm): 55.6, 60.2, 61.3, 105.6, 114.5, 118.5, 121.3, 126.1, 127.9, 128.2, 129.7, 129.9, 131.3, 133.9, 135.6, 136.3, 137.4, 138.3, 141.3, 151.3, 156.6, 161.4, 164.6; Mass (m/z) : 431[M⁺].

3-(4-chlorophenyl)-1-(3-nitrophenyl)-4-(1-oxo-1H-isochromen-3-yl)azetid-2-one (**3l**): White solid; Yield: 47%; m.p. 178-180°C; Anal. Calcd. for C₂₄H₁₅ClN₂O₅; C, 64.51; H, 3.38; N, 6.27. Found: C, 64.45; H, 3.25; N, 6.35; IR (KBr, cm⁻¹): 3099 (arom-CH), 1755 (>C=O), 1730 (>C=O), 1603 (C-C aromatic); ¹H NMR (400 MHz, CDCl₃) δ: 4.81 (d, 1H, *J*=2.4Hz, C₃-H), 4.84 (d, 1H, *J*=2.4Hz, C₄-H), 6.76 (s, 1H, -CH=C), 7.34-8.31 (m, 12H, Ar-H) ; ¹³C-NMR (100.622 MHz, CDCl₃, δ/ ppm): 60.2, 61.3, 105.3, 114.8, 118.7, 121.4, 126.1, 127.8, 128.5, 129.3, 130.2, 130.9, 134.1, 135.8, 136.3, 137.3, 138.6, 142.1, 152.2, 156.6, 161.8, 164.3; Mass (m/z) : 446 [M⁺].

CONCLUSION

In conclusion, we have synthesized novel 4-(1-oxo-1H-isochromen-3-yl)-1-aryl-3-phenylazetid-2-one derivatives starting from 3-formylisocoumarin under mild conditions.

ACKNOWLEDGEMENTS

The authors are thankful to management of Ipca Laboratories, Dr. Ashok Kumar, Dr. S. R. Soudagar, Dr. Suneel Dike, Mr. Brajesh Sharma for providing essential support.

REFERENCES

- Rama, N., Malik, A., *Indian J. Chem.* **2001**, *40B*, 372.
- Rama, N. H., Rashid, E., *Indian J. Chem.* **1998**, *37B*, 365.
- Upadhyay, A. Srivastava, S. K. Srivastava, S. D. Yadav, R. *Proc. Natl. Acad. Sci. India* **2010**, *80*, 131.
- Ikee, Y. Hashimoto, K. Nakashima, M. Hayashi, K. Sano, S. Shiro, M. Nagao, Y., *Bioorg. Med. Chem. Lett.* **2007**, *17*, 942.
- Sharma, S. D. Mehra, U., *J. Sci. Ind. Res.* **1988**, *47*, 451
- Verma, L. R. Narayanan, C. S., *Indian J. Chem.*, **1991**, *30B*, 676.
- Grochowski, E. Pupek, K., *Tetrahedron*, **1991**, *47*, 6759.
- Manhas, M. S. Wagle, D. R. Ciang, J. Bose, A. K. *Heterocycles*, **1988**, *27*, 1755.
- Rao, B. G. Bandarage, U. K. Wang, T. Come, J. H., Perola, E. Tian, Y. W. S-K., Saunders, J. O., *Bioorg. Med. Chem. Lett.* **2007**, *17*, 2250.
- Banik, B. K. Banik, I. Becker, F. F. *Bioorg. Med. Chem.*, **2005**, *13*, 3611.
- Liang, G-B. Qian, X. Feng, D. Fisher, M. Crumley, T. Darkin-Rattray, S. J. Dulski, P. M. Gurnett, A. Leavitt, P. Liberator, S. Misura, P. A. Samaras, A. S. Tamas, S. T., Schmatz, D. M. Wyvratta, M. Biftu, T. *Bioorg. Med. Chem. Lett.* **2008**, *18*, 2019.
- Takai, S. Jin, D. Muramatsu, M. Okamoto, Y. Miyazaki, M. *Pharmaco.* **2004**, *501*, 1.
- Ogilvie, W. W. Yoakim, C. Do, F. Hache, B. Lgace, L. Naud, J. Omeara, J. A. Deziel, R. *Bioorg. Med. Chem.* **1999**, *7*, 1521.
- Valette, H. Dolle, F. Bottlaender, M. Hinnen, F. Marzin, D. *Nuclear Med. Biol.* **2002**, *29*, 849.
- Kohli, P. Srivastava, S. D. Srivastava, S. K. *J. Indian. Chem. Soc.* **2008**, *85*, 326.
- Srivastava, S. K. Srivastava, S. Srivastava, S. D. *Indian J. Chem.* **1999**, *38B*, 183.
- Browne, M. Burnett, D. A. Caplen, M. A. Chen, L-Y. Clader, Domalski, J. W. Dugar, M. Pushpavanam, S. Sher, P. Vaccaro, R. Viziano, W. Zhao, M. H. *Tetrahedron Lett.* **1995**, *36*, 2555.

Received: 21.01.2013.
Accepted: 21.02.2013.



DENSITIES, VISCOSITIES AND SPEEDS OF SOUND FOR BINARY LIQUID MIXTURES OF HEXYL ACETATE AND PhX (X=F, Cl, Br, NO₂) COMPOUNDS AT DIFFERENT TEMPERATURES.

M. V. Rathnam^{*[a]}, Kavita R. Bhanushali^[a], Reema T. Sayed^[a] and M.S.S. Kumar^[b]

Keywords: density, viscosity, excess molar volume, speed of sound, hexyl acetate; halobenzenes; nitrobenzene

Densities and viscosities of binary mixtures of hexyl acetate with chlorobenzene, bromobenzene, fluorobenzene and nitrobenzene have been measured at (298.15, 303.15, 308.15 and 313.15) K over the entire composition range. Speeds of sound of these binary liquid mixtures have also been measured at 303.15 K. From the experimental density and viscosity data, the values of excess molar volume V^E , free energy of activation for viscous flow ΔG^E , while from the speed of sound data the isentropic compressibility K_s , intermolecular free length L_f , internal pressure π_i , free volume V_f , and specific acoustic impedance Z have been calculated. The excess molar volumes for these binary mixtures were negative over the whole composition range at all temperatures. The viscosity values were correlated using Frenkel and McAllister (four-body) models.

Corresponding Authors*

Tel.: +91-8976545095

Fax: 022-25337672

E-Mail: mvrathnam58@rediffmail.com

[a] Physical Chemistry Research Laboratory, B.N. Bandodkar College of Science, Thane – 400601 – India.

[b] Department of Chemistry, Zulas Bhilajirao Patil College, Deopur, Dhule, 424 002 – India.

Tel No.- 02562- 222343,

Fax No.- 02562- 220678,

E-mail: dr.mssskumar@rediffmail.com

Introduction

Hexyl acetate a short-chain ester with fruity odor, is a significant green note flavour compound and widely used in the food industry. It has been found that hexyl acetate has a potential use¹ for both the extension of shelf life and an improvement of hygienic safety of minimally processed foods. An aryl halide (also known as haloarene or halogenoarene) is an aromatic compound in which one or more hydrogen atoms directly bonded to an aromatic ring are replaced by a halide. Aryl halides are mainly used as an intermediate in pharmaceuticals and find applications in many chemical and technological processes. Nitrobenzene is used in shoe and floor polishes, leather dressings, paint solvents and other materials to mask unpleasant odors. Nitrobenzene has also been used as an inexpensive perfume for soaps. In view of these importance it is of interest to study the thermophysical properties of these chemicals, in order to understand the intermolecular interactions in their binary mixtures.

Comelli et al² investigated the excess enthalpies and excess molar volumes of diethyl carbonate with alkyl acetates at 298.15K. El-Banna³ has studied densities and viscosities of pentyl acetate and hexyl acetate each with normal alkanols. Ismadji et al^{4,5} determined densities and viscosities for binary mixtures of ethyl valerate and hexyl acetate with 1-pentanol and 1-hexanol. Arce et al⁶ determined VLE of hexyl acetate with methanol and ethanol. Likewise, there have been some reports on

physical properties for binary mixtures of aryl halides with organic solvents.⁷⁻¹² In continuation of our earlier work,¹³ we report in this paper densities and viscosities for the binary mixtures of hexyl acetate with chlorobenzene, bromobenzene, fluorobenzene and nitrobenzene at (298.15, 303.15, 308.15 and 313.15) K. Also the speeds of sound for these mixtures were determined at 303.15 K over the entire composition range. From the experimental values of density, viscosity and speed of sound, the excess molar volume V^E , the free energy of activation for viscous flow ΔG^E , isentropic compressibility K_s , intermolecular free length L_f , internal pressure π_i , free volume V_f and specific acoustic impedance have been calculated. The results of calculated excess or deviation properties viz: V^E , ΔK_s , L_f^E , π_i^E , V_f^E , Z^E were fitted to the Redlich- Kister equation.¹⁴ The viscosity data were correlated using single-parameter equation of Frenkel,¹⁵ and three-parameter equation of Mc Allister's (four-body)¹⁶ models.

Experimental

Materials : High purity and AR grade samples of hexyl acetate (Fluka AG), chlorobenzene, bromobenzene, fluorobenzene and nitrobenzene all Sigma Aldrich obtained from S.D.fine- Chem Limited, Mumbai, India were used. The claimed mass fraction purity for these chemicals range from 0.990 to 0.997. All the liquids were degassed ultrasonically and dried over 0.4 mm molecular sieves. The mass fraction purities tested by gas chromatography (HP 8610) using FID were as follows hexyl acetate (>0.994), chlorobenzene (>0.995), bromobenzene (>0.995), fluorobenzene (>0.995), and nitrobenzene (>0.997).

Methods : The compositions (mole fraction) of binary mixtures were prepared by mass in airtight glass stoppered bottles. Mass measurements accurate to ± 0.01 mg were made on a digital electronic balance (Mettler, AE, 240 Switzerland). To prevent the samples from

undergoing preferential evaporation, the mixtures were prepared by transferring aliquots via syringe into the stoppered bottles. The resulting mole fraction uncertainty was estimated to be less than ± 0.0001 .

Densities of the pure and their binary mixtures were determined using a density meter (DMA-4500 Anton Paar). The instrument was calibrated frequently before the start of the actual experiments using deionized doubly distilled water and dry air according to the established standard procedures. The instrument has a temperature sensor which measures the sample temperature right at the measuring cell. The density of the sample was measured after achieving thermal equilibrium with successive increments of 5K for a temperature range from 298.15 to 313.15 K. All measurements for each sample were made in triplicate and the results presented are the average. The average uncertainty in the density measurements was found to be less than $\pm 0.0002 \text{ g.cm}^{-3}$.

The kinematic viscosities ν were measured with an Ubbelohde viscometer. The viscometer is kept in a transparent walled water bath with a thermal stability of $\pm 0.01\text{K}$ for about 20 min to obtain thermal equilibrium. An electronic digital stopwatch with an uncertainty of $\pm 0.01\text{s}$ was used for flow time measurements. The kinematic viscosities of liquids were calculated with the measured flow time and the calibration constants using the relation $\nu = A t - B/t$, where t is the flow time in the viscometer. A and B are the viscometer constants, determined by calibrating viscometer with double distilled water and pure benzene. Dynamic viscosities η (mPa.s) were then determined by using the relation $\eta = \nu \cdot \rho$. The experimental viscosities were obtained by averaging five to six measures of flow times. The average uncertainty of dynamic viscosity values was found to be less than $\pm 0.007 \text{ mPa.s}$.

The speed of sound of pure liquids and liquid mixtures was measured with a single-crystal variable path interferometer (model F-81) supplied by Mittal Enterprises, New Delhi, India. A crystal controlled high frequency generator was used to excite the transducer at a frequency of 2 MHz. The accuracy of the velocity measurements is 0.02%. The measuring cell of interferometer has a specially designed double walled vessel with provision for temperature constancy. An electronically operated digital temperature bath (model SSI-0.3 spl) supplied by Mittal Enterprises New Delhi, operating in the temperature range -10°C to 85°C with an accuracy of $\pm 0.1 \text{ K}$ has been used to circulate water through the outer jacket of the double walled measuring cell containing the sample liquid. The instrument was calibrated by measuring the velocity in standard liquids viz AR grade benzene and carbon tetrachloride. The uncertainty in the measured speeds of sound was found to be $\pm 1 \text{ m.s}^{-1}$.

Results and Discussion

The results of density ρ , excess volume V^E , and viscosity η of the studied binary mixtures at (298.15, 303.15, 308.15 and 313.15) K are given in Table 1. From the density data, excess volumes V^E ($\text{cm}^3 \text{ mol}^{-1}$) have been calculated as

$$V^E = \frac{(x_1 M_1 + x_2 M_2)}{\rho_{12}} - \left(\frac{x_1 M_1}{\rho_1} + \frac{x_2 M_2}{\rho_2} \right) \quad (1)$$

where

x , M , and ρ are the mole fraction, molar mass, and density, respectively of pure components 1 and 2 and ρ_{12} is the density of the liquid mixture.

The excess free energy of activation (ΔG^{*E} , J.mol^{-1}) for viscous flow were obtained with the expression

$$\Delta G^{*E} = RT \left[\ln(\eta\nu) - \left\{ \left[x_1 \ln(\eta_1\nu_1) + x_2 \ln(\eta_2\nu_2) \right] \right\} \right] \quad (2)$$

where η_1 , η and ν denote the viscosity, and molar volume of the pure components and their mixtures respectively.

Table 2 lists the experimental values of speed of sound u , isentropic compressibility K_s , intermolecular free length L_f , internal pressure π_i , free volume V_f , and specific acoustic impedance Z . These properties have been calculated using the following equations

$$K_s = \frac{1}{u^2 \rho} \quad (3)$$

$$L_f = K (K_s)^{1/2} \quad (4)$$

$$\pi_i = bRT \left(\frac{K\eta}{u} \right)^{1/2} \left(\frac{\rho^{2/3}}{M_{eff}^{7/6}} \right) \quad (5)$$

$$V_f = \left(\frac{M_{eff} u}{\eta k} \right)^{3/2} \quad (6)$$

$$Z = u\rho \quad (7)$$

where K is the temperature dependent Jacobson constant, b is the cubical packing fraction taken as 2 for all the liquids, R is the universal gas constant, T is the experimental temperature, $M_{eff} = \sum x_i m_i$ where, x is the mole fraction and m is the molecular weight of i^{th} component. The excess parameters such as isentropic compressibility ΔK_s , excess intermolecular free length L_f^E , excess internal pressure π_i^E , excess free volume V_f^E and excess acoustic impedance Z^E have been obtained using the general equation

$$Y^E = Y_m - x_1 Y_1 - x_2 Y_2 \quad (8)$$

where Y^E refers to deviation or excess property in question, Y_m refers to the property of mixture $x_1 Y_1$ and $x_2 Y_2$ refer to the mole fraction and specific property of the pure components of 1 and 2 respectively.

Table 1. Values of Density ρ , Excess Volume V^E , Viscosity η for the Binary Liquid Mixtures.

x_1	ρ , g.cm ⁻³	V^E , cm ³ .mol ⁻¹	η , mPa.s	ρ , g.cm ⁻³	V^E , cm ³ .mol ⁻¹	η , mPa.s
Hexyl acetate (1) + Chlorobenzene (2)						
T/K = 298.15			T/K = 303.15			
0.0000	1.0999		0.758	1.0951		0.700
0.0635	1.0776	-0.074	0.805	1.0733	-0.118	0.740
0.1334	1.0559	-0.260	0.843	1.0518	-0.323	0.774
0.2071	1.0350	-0.481	0.880	1.0309	-0.542	0.803
0.2872	1.0146	-0.785	0.917	1.0103	-0.821	0.834
0.3797	0.9925	-1.075	0.954	0.9882	-1.107	0.866
0.4770	0.9710	-1.340	0.991	0.9669	-1.393	0.894
0.5875	0.9471	-1.388	1.026	0.9433	-1.479	0.924
0.7081	0.9223	-1.230	1.057	0.9189	-1.378	0.953
0.8407	0.8961	-0.738	1.077	0.8928	-0.898	0.971
1.0000	0.8676		1.071	0.8635		0.960
Hexyl acetate (1) + Bromobenzene (2)						
T/K = 308.15			T/K = 313.15			
0.0000	1.0900		0.665	1.0849		0.620
0.0635	1.0687	-0.161	0.700	1.0642	-0.214	0.650
0.1334	1.0473	-0.371	0.733	1.0430	-0.439	0.676
0.2071	1.0273	-0.688	0.758	1.0230	-0.752	0.701
0.2872	1.0069	-0.992	0.783	1.0034	-1.148	0.723
0.3797	0.9855	-1.369	0.809	0.9817	-1.487	0.747
0.4770	0.9638	-1.609	0.836	0.9600	-1.723	0.772
0.5875	0.9403	-1.713	0.865	0.9368	-1.865	0.796
0.7081	0.9153	-1.518	0.892	0.9122	-1.728	0.821
0.8407	0.8893	-1.048	0.910	0.8860	-1.218	0.835
1.0000	0.8593		0.898	0.8552		0.824
Hexyl acetate (1) + Bromobenzene (2)						
T/K = 298.15			T/K = 303.15			
0.0000	1.4880		1.114	1.4816		1.008
0.0667	1.4255	-0.021	1.136	1.4220	-0.230	1.021
0.1375	1.3685	-0.418	1.148	1.3656	-0.679	1.029
0.2147	1.3130	-1.062	1.158	1.3092	-1.248	1.039
0.2981	1.2586	-1.894	1.165	1.2550	-2.099	1.047
0.3873	1.2030	-2.631	1.169	1.2000	-2.900	1.051
0.4842	1.1440	-3.078	1.171	1.1421	-3.476	1.054
0.5941	1.0789	-3.099	1.168	1.0770	-3.508	1.050
0.7152	1.0098	-2.509	1.157	1.0072	-2.825	1.036
0.8477	0.9391	-1.334	1.132	0.9361	-1.574	1.011
1.0000	0.8676		1.071	0.8635		0.960
T/K = 308.15			T/K = 313.15			
0.0000	1.4752		0.947	1.4689		0.892
0.0667	1.4161	-0.256	0.956	1.4120	-0.415	0.897
0.1375	1.3609	-0.795	0.965	1.3575	-1.014	0.903
0.2147	1.3053	-1.432	0.972	1.3026	-1.718	0.909
0.2981	1.2518	-2.353	0.978	1.2489	-2.629	0.913
0.3873	1.1973	-3.212	0.982	1.1934	-3.388	0.915
0.4842	1.1393	-3.784	0.984	1.1355	-3.966	0.913
0.5941	1.0743	-3.831	0.980	1.0729	-4.312	0.908
0.7152	1.0043	-3.115	0.969	1.0061	-4.083	0.896
0.8477	0.9330	-1.817	0.945	0.9355	-2.986	0.872
1.0000	0.8593		0.898	0.8552		0.824

Table 1. (cont.)

Hexyl acetate (1) + Fluorobenzene (2)						
x_1	$T/K = 298.15$			$T/K = 303.15$		
0.0000	1.0180		0.564	1.0128		0.514
0.0602	1.0032	-0.043	0.616	0.9986	-0.091	0.559
0.1243	0.9890	-0.110	0.664	0.9845	-0.161	0.603
0.1959	0.9746	-0.192	0.713	0.9703	-0.257	0.648
0.2740	0.9601	-0.252	0.763	0.9557	-0.296	0.691
0.3627	0.9455	-0.351	0.813	0.9412	-0.397	0.735
0.4592	0.9312	-0.451	0.864	0.9272	-0.528	0.779
0.5693	0.9163	-0.513	0.918	0.9121	-0.551	0.823
0.6926	0.9010	-0.497	0.972	0.8968	-0.519	0.869
0.8358	0.8850	-0.400	1.030	0.8810	-0.440	0.917
1.0000	0.8676		1.071	0.8635		0.960
x_1	$T/K = 308.15$			$T/K = 313.15$		
0.0000	1.0069		0.494	1.0014		0.460
0.0602	0.9934	-0.144	0.533	0.9884	-0.181	0.495
0.1243	0.9794	-0.210	0.569	0.9748	-0.277	0.526
0.1959	0.9656	-0.334	0.606	0.9610	-0.390	0.559
0.2740	0.9514	-0.406	0.645	0.9469	-0.462	0.595
0.3627	0.9368	-0.481	0.684	0.9324	-0.535	0.630
0.4592	0.9228	-0.596	0.726	0.9185	-0.649	0.668
0.5693	0.9077	-0.599	0.766	0.9035	-0.650	0.706
0.6926	0.8926	-0.577	0.813	0.8886	-0.642	0.748
0.8358	0.8770	-0.508	0.858	0.8730	-0.554	0.787
1.0000	0.8593		0.898	0.8552		0.824
Hexyl acetate (1) + Nitrobenzene (2)						
x_1	$T/K = 298.15$			$T/K = 303.15$		
0.0000	1.1981		1.838	1.1934		1.625
0.0643	1.1684	-0.308	1.816	1.1654	-0.463	1.602
0.1334	1.1412	-0.877	1.776	1.1385	-1.071	1.573
0.2078	1.1144	-1.536	1.728	1.1110	-1.670	1.531
0.2905	1.0856	-2.142	1.667	1.0819	-2.251	1.480
0.3804	1.0545	-2.537	1.594	1.0506	-2.626	1.418
0.4778	1.0217	-2.714	1.513	1.0177	-2.790	1.344
0.5889	0.9854	-2.584	1.421	0.9815	-2.669	1.261
0.7099	0.9477	-2.097	1.321	0.9440	-2.204	1.176
0.8468	0.9082	-1.268	1.209	0.9049	-1.432	1.075
1.0000	0.8676		1.071	0.8635		0.960
x_1	$T/K = 308.15$			$T/K = 313.15$		
0.0000	1.1883		1.517	1.1838		1.395
0.0643	1.1617	-0.589	1.486	1.1590	-0.760	1.364
0.1334	1.1353	-1.251	1.450	1.1324	-1.416	1.330
0.2078	1.1083	-1.911	1.408	1.1050	-2.046	1.294
0.2905	1.0790	-2.481	1.359	1.0754	-2.593	1.250
0.3804	1.0470	-2.782	1.304	1.0432	-2.876	1.198
0.4778	1.0140	-2.934	1.241	1.0110	-3.134	1.139
0.5889	0.9786	-2.922	1.166	0.9758	-3.160	1.070
0.7099	0.9417	-2.554	1.084	0.9388	-2.787	0.995
0.8468	0.9025	-1.776	0.994	0.8999	-2.066	0.910
1.0000	0.8593		0.898	0.8552		0.824

The results of V^E , ΔG^{*E} , ΔK_S , L_f^E , π_i^E , V_f^E , and Z^E versus the mole fraction x_1 are graphically represented in Figures (1-7). The calculated values of these excess or deviation functions of the mixtures were fitted to Redlich-Kister¹⁴ polynomials of the form

$$Y^E = x_1 x_2 \sum_{k=0} A_k (x_1 - x_2)^k \quad (9)$$

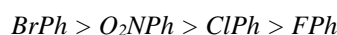
where A_k are the adjustable parameters obtained by a least squares fit method and k is the degree of the polynomial equation. Table 3 lists the parameters with the standard deviations σ . The coefficients A_k 's were used to calculate the solid curves of Figures 1-8. The standard deviations σ are defined as

$$\sigma = \left[\frac{\sum (Y_{\text{expt}}^E - Y_{\text{calc}}^E)^2}{(D - N)} \right]^{0.5} \quad (10)$$

where

D and N are the number of experimental data and equation parameters respectively.

The V^E against x_1 plots of the studied binary systems at (298.15, 303.15, 308.15 and 313.15) K are shown in Figure 1. The V^E values are negative over the whole composition range. Excess molar volumes reflect the type of interactions involving in the mixtures. For hexyl acetate + bromobenzene and hexyl acetate + nitrobenzene the negative values of V^E are large in magnitude as compared to those for hexyl acetate + fluorobenzene for which the V^E values are less in magnitude and follow the order



The V^E values at other higher temperatures follow the same trends but with different values. It is observed that there is an effect of temperature on V^E as these values increase systematically with increase in temperature. These negative values indicate the strong attractive forces involving between the liquid components. The large negative V^E for the systems of bromobenzene and nitrobenzene may be attributed to the differences in dipole moments of the liquid components leading to dipole-induced dipole interactions resulting in the formation of electron donor-acceptor complexes.^{17,18} No published data was found for the present systems with which to compare our results. However comparing the present results with our earlier published data of V^E for binary mixtures of aryl halides with several esters,¹³ it was found that the same trends were followed by the systems of bromobenzene and nitrobenzene. This further confirms that the large negative V^E values for bromobenzene and nitrobenzene may be due to the differences in the dipole moments of the pure components.

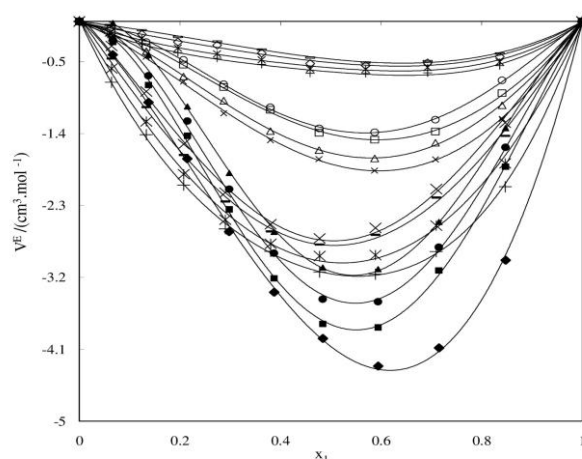


Figure 1. Curves of excess volumes V^E versus mole fraction x_1 for the binary mixtures of hexyl acetate + chlorobenzene at (o, 298.15; □, 303.15; △, 308.15; x, 313.15) K, hexyl acetate + bromobenzene at (▲, 298.15; ●, 303.15; ■, 308.15; ◆, 313.15) K, hexyl acetate + fluorobenzene at (□, 298.15; ◇, 303.15; ✕, 308.15; +, 313.15) and hexyl acetate nitrobenzene at (X, 298.1; -, 303.15; ✕, 308.15; +, 313.15) K

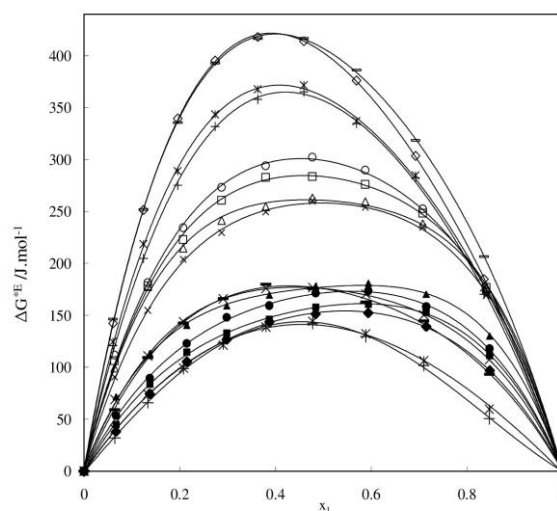


Figure 2. Curves of excess free energy of activation of viscous flow ΔG^{*E} versus mole fraction x_1 for the binary mixtures of hexyl acetate + chlorobenzene at (o, 298.15; □, 303.15; △, 308.15; x, 313.15) K, hexyl acetate + bromobenzene at (▲, 298.15; ●, 303.15; ■, 308.15; ◆, 313.15) K, hexyl acetate + fluorobenzene at (□, 298.15; ◇, 303.15; ✕, 308.15; +, 313.15) K and hexyl acetate + nitrobenzene at (X, 298.15; -, 303.15; ✕, 308.15; +, 313.15) K.

The plots of ΔG^E versus x_1 at (298.15, 303.15, 308.15 and 313.15) K are displayed in Figure 2, It is observed that the variation of ΔG^E is completely positive over the entire composition range of the mixtures. This indicates the existence of specific interactions in the liquid mixtures. The magnitude of ΔG^E is an excellent indicator of the strength of specific interactions in liquid mixtures.^{19,20} Figure 3 shows the variation of ΔK_S with mole fraction x_1 of hexyl acetate. The ΔK_S values of chlorobenzene exhibit positive deviations. For bromobenzene the ΔK_S values are slightly positive in lower mole fraction of ester ($x_1=0.2$).

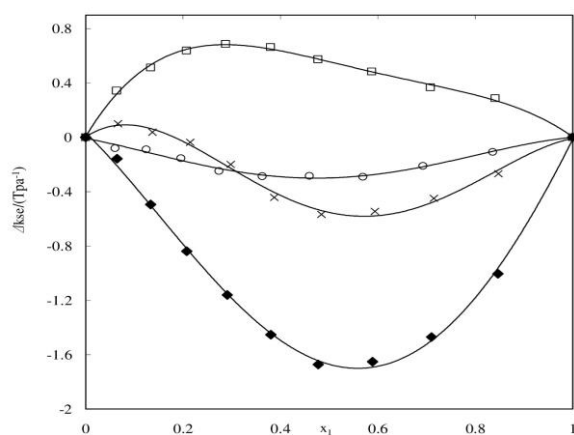


Figure 3. Deviations in isentropic compressibility ΔK_s versus mole fraction x_1 for the binary mixtures of hexyl acetate + chlorobenzene at (\square , 303.15) K, hexyl acetate + bromobenzene at (\times , 303.15) K, hexyl acetate + fluorobenzene at (\circ , 303.15) K and hexyl acetate + nitrobenzene at (\blacklozenge , 303.15) K.

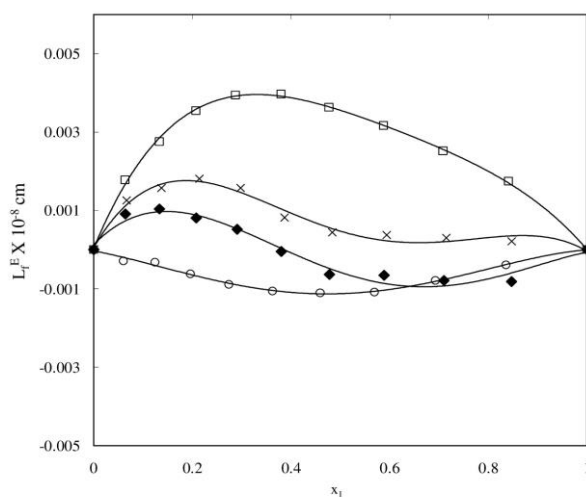


Figure 4. Plots of excess intermolecular free length L_f^E versus mole fraction x_1 for the binary mixtures of hexyl acetate + chlorobenzene at (\square , 303.15) K, hexyl acetate + bromobenzene at (\times , 303.15) K, hexyl acetate + fluorobenzene at (\circ , 303.15) K and hexyl acetate + nitrobenzene at (\blacklozenge , 303.15) K.

However, ΔK_s becomes negative as the composition of ester increases ($x_1 > 0.2$). While for fluorobenzene and nitrobenzene the ΔK_s values are completely negative over the entire composition range. The variation of the excess intermolecular free length, L_f^E versus x_1 displayed in Figure 4, shows a positive deviation in L_f^E for mixtures of chlorobenzene and bromobenzene. While for the mixtures of fluorobenzene the L_f^E values are completely negative. Where as for nitrobenzene the L_f^E values exhibit positive deviation upto $x_1 = 0.38$, but as the composition of ester increases ($x_1 > 0.38$) these values become negative. The intermolecular free length, L_f in binary liquid mixtures can be used to assess the attraction between the component molecules. These values in a binary mixture depend on concentration. For a given binary system the intermolecular free length increases with increase in concentration of ester.

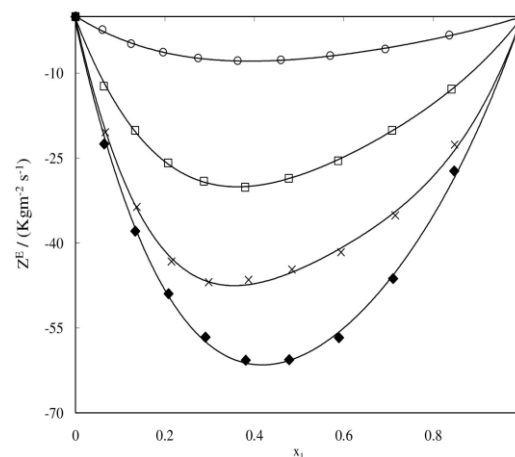


Figure 5. Plots of excess specific acoustic impedance Z^E versus mole fraction x_1 for the binary mixtures of hexyl acetate + chlorobenzene at (\square , 303.15) K, hexyl acetate + bromobenzene at (\times , 303.15) K, hexyl acetate + fluorobenzene at (\circ , 303.15) K and hexyl acetate + nitrobenzene at (\blacklozenge , 303.15) K.

The dependence of excess acoustic impedance with mole fraction x_1 is shown in Figure 5, wherein it is observed that Z^E values for all the studied systems exhibit negative deviation over the entire range of composition. The Z^E values of nitrobenzene are large negative, while these values are small negative for fluorobenzene and follow the order

$$O_2NPh > BrPh > ClPh > FPh$$

The results of the excess internal pressure, π_1^E versus mole fraction x_1 at 303.15 K are displayed in Figure 6. For the systems of chlorobenzene, bromobenzene and fluorobenzene positive π_1^E is observed, while for nitrobenzene the π_1^E values exhibit negative deviations.

The results of excess free volume, V_f^E as a function of mole fraction x_1 at 303.15 K are presented in Figure 7. Like Z^E the V_f^E values are completely negative over the entire range of composition. The V_f^E values are small negative for bromobenzene, while for fluorobenzene they are large negative and follow the order

$$FPh > ClPh > O_2NPh > BrPh$$

Viscosity Models and Interaction Parameters

The experimental viscosities of mixtures have been correlated with the one-parameter model proposed by Frenkel and three-parameter model proposed by McAllister four-body interaction. The equations of these models are

Frenkel model:

$$\log \eta = x_1^2 \log \eta_1 + x_2^2 \log \eta_2 + 2x_1x_2 \log \eta_{12} \quad (11)$$

where η is the viscosity coefficient, x_1 and x_2 are the mole fractions and η_{12} is the interaction parameter.

Table 2. Values of Speed of sound u , isentropic compressibility K_s , intermolecular free length L_f and internal pressure π_i , free volume V_f and specific acoustic impedance Z of binary liquid mixtures.

x_1	$u, \text{m.s}^{-1}$	K_s, Tpa^{-1}	$L_f \times 10^{-8} \text{cm}$	$\pi_i \times 10^6 \text{Nm}^{-2}$	$V_f \times 10^{-6} \text{m}^3 \text{mol}^{-1}$	$Z, \text{Kgm}^{-2} \text{s}^{-1}$
Hexyl acetate (1) + Chlorobenzene (2)						
x_1	$T/\text{K} = 303.15$					
0.0000	1246	588	0.5034	3.36	0.320	1365.4
0.0635	1242	604	0.5101	3.34	0.301	1333.0
0.1334	1239	619	0.5165	3.31	0.288	1303.2
0.2071	1236	635	0.5230	3.25	0.280	1274.2
0.2872	1233	651	0.5296	3.19	0.272	1245.7
0.3797	1230	669	0.5368	3.12	0.266	1215.5
0.4770	1227	687	0.5440	3.04	0.262	1186.4
0.5875	1224	708	0.5521	2.95	0.258	1154.6
0.7081	1221	730	0.5608	2.85	0.256	1122.0
0.8407	1218	755	0.5703	2.73	0.260	1087.4
1.0000	1216	783	0.5809	2.55	0.279	1050.0
Hexyl acetate (1) + Bromobenzene (2)						
x_1	$T/\text{K} = 303.15$					
0.0000	1138	521	0.4738	3.50	0.266	1686.1
0.0667	1142	540	0.4822	3.44	0.260	1623.2
0.1375	1146	558	0.4901	3.39	0.256	1565.0
0.2147	1151	577	0.4986	3.32	0.252	1506.2
0.2981	1155	597	0.5073	3.27	0.248	1449.5
0.3873	1161	618	0.5161	3.19	0.246	1393.2
0.4842	1168	642	0.5261	3.11	0.244	1333.4
0.5941	1176	671	0.5378	3.01	0.244	1266.6
0.7152	1188	704	0.5507	2.88	0.249	1196.1
0.8477	1201	741	0.5648	2.73	0.258	1124.3
1.0000	1216	783	0.5809	2.55	0.279	1050.0
Hexyl acetate (1) + Fluorobenzene (2)						
x_1	$T/\text{K} = 303.15$					
0.0000	1142	757	0.5711	3.43	0.352	1156.6
0.0602	1150	758	0.5714	3.41	0.328	1147.9
0.1243	1157	759	0.5720	3.38	0.310	1138.6
0.1959	1164	761	0.5724	3.33	0.295	1129.4
0.2740	1172	762	0.5729	3.26	0.285	1120.1
0.3627	1180	764	0.5736	3.17	0.278	1110.1
0.4592	1186	766	0.5745	3.07	0.273	1100.0
0.5693	1194	769	0.5756	2.96	0.270	1089.0
0.6926	1201	773	0.5771	2.84	0.270	1077.1
0.8358	1208	778	0.5789	2.70	0.272	1064.2
1.0000	1216	783	0.5809	2.55	0.279	1050.0

Table 2 (cont).

Hexyl acetate (1) + Nitrobenzene (2)						
x_1	$T/K = 303.15$					
0.0000	1438	405	0.4178	4.55	0.128	1716.1
0.0643	1416	428	0.4292	4.42	0.130	1650.8
0.1334	1396	451	0.4406	4.28	0.133	1589.3
0.2078	1376	475	0.4525	4.12	0.138	1528.7
0.2905	1355	503	0.4657	3.95	0.145	1466.0
0.3804	1335	534	0.4798	3.76	0.155	1402.0
0.4778	1314	569	0.4951	3.55	0.168	1337.3
0.5889	1291	611	0.5132	3.32	0.184	1267.1
0.7099	1268	659	0.5328	3.08	0.205	1197.0
0.8468	1243	715	0.5551	2.83	0.235	1124.8
1.0000	1216	783	0.5809	2.55	0.279	1050.0

Table 3. Coefficients of the Redlich-Kister Equation and Standard deviations for the Excess functions of Binary mixtures.

Function	T/K	A_0	A_1	A_2	σ
Hexyl acetate + Chlorobenzene					
V^E	298.15	-5.4063	-2.3712	2.9680	0.019
	303.15	-5.6285	-2.9548	1.6338	0.023
	308.15	-6.5757	-2.9874	1.9844	0.019
	313.15	-7.1378	-3.4807	1.0957	0.023
ΔG^{*E}	298.15	1194.65	-152.00	485.49	5.4
	303.15	1133.56	-99.70	589.25	4.3
	308.15	1042.33	-54.36	728.30	4.7
	313.15	1032.54	-11.44	559.50	2.8
ΔK_s	303.15	2.2277	-1.7165	2.1076	0.019
L_j^E	303.15	0.0142	-0.0080	0.0086	0.000
Z^E	303.15	-112.081	53.531	-45.071	0.384
π_i^E	303.15	0.2606	-0.0187	0.3137	0.004
V_j^E	303.15	-0.1520	-0.1520	-0.1200	0.001
Hexyl acetate + Bromobenzene					
V^E	298.15	-12.5120	-4.3492	11.0443	0.021
	303.15	-13.8476	-4.7303	10.0017	0.070
	308.15	-15.1538	-5.1778	9.9205	0.058
	313.15	-16.2728	-9.6783	0.9153	0.061
ΔG^{*E}	298.15	707.88	68.35	549.43	3.0
	303.15	686.60	99.88	307.11	2.0
	308.15	635.10	121.81	305.87	1.7
	313.15	613.67	86.94	155.53	1.6
ΔK_s	303.15	-2.2176	-1.5717	3.0225	0.033
L_j^E	303.15	0.0019	-0.0076	0.0128	0.000
Z^E	303.15	-178.462	69.181	-108.780	0.785
π_i^E	303.15	0.2866	0.0902	-0.1640	0.005
V_j^E	303.15	-0.1135	-0.0319	0.0219	0.001

Table 3 (cont).

Hexyl acetate + Fluorobenzene					
V ^E	298.15	-1.8815	-1.3112	-0.1815	0.012
	303.15	-2.0599	-1.1687	-0.5188	0.027
	308.15	-2.3204	-1.0362	-1.0608	0.028
	313.15	-2.5212	-1.0091	-1.5458	0.025
ΔG^{*E}	298.15	1627.78	-528.16	525.25	2.8
	303.15	1611.65	-645.80	393.60	1.5
	308.15	1422.81	-456.27	370.08	3.4
	313.15	1425.13	-411.46	264.52	4.7
ΔK_s	303.15	-1.1909	0.2125	0.6402	0.019
L_f^E	303.15	-0.0045	0.0008	0.0025	0.000
Z^E	303.15	-29.953	12.301	-6.173	0.153
π^E	303.15	0.1601	-0.3151	0.2497	0.003
V_f^E	303.15	-0.1728	0.1066	-0.0904	0.001
Hexyl acetate + Nitrobenzen					
V ^E	298.15	-10.9000	-0.5168	4.2507	0.085
	303.15	-10.9000	-0.5030	1.1008	0.089
	308.15	-10.9000	-1.2163	-4.4278	0.203
	313.15	-10.9000	-1.6922	-7.2208	0.302
ΔG^{*E}	298.15	703.09	-85.21	384.46	2.2
	303.15	702.78	-140.79	250.19	2.4
	308.15	565.87	-107.18	-43.00	2.3
	313.15	569.60	-133.71	-166.81	1.6
ΔK_s	303.15	-6.6933	-2.0456	1.5726	0.043
L_f^E	303.15	-0.0023	-0.0086	0.0081	0.000
Z^E	303.15	-239.977	69.002	-59.020	1.183
π^E	303.15	-0.1815	-0.1449	0.0945	0.004
V_f^E	303.15	-0.1310	-0.0220	-0.0313	0.000

Table 4. Adjustable Parameters and Standard Percentage Deviations of Viscosity Models for Binary Liquid Mixtures

T/K	Frenkel		McAllister (Four - body)			
	η_{12}	100 σ	ν_{1112}	ν_{1122}	ν_{2221}	100 σ
Hexyl acetate (1) + Chlorobenzene (2)						
298.15	0.1122	0.07	0.2134	0.0071	-0.0479	0.02
303.15	0.0048	0.07	0.1230	-0.1061	-0.1346	0.02
308.15	-0.0693	0.09	0.0712	-0.1915	-0.1877	0.02
313.15	-0.1559	0.07	-0.0217	-0.2451	-0.2811	0.01
Hexyl acetate (1) + Bromobenzene (2)						
298.15	0.2340	0.06	0.2187	0.1406	-0.0450	0.01
303.15	0.1203	0.06	0.0910	0.0694	-0.1743	0.01
308.15	0.0476	0.06	0.0250	0.0025	-0.2424	0.01
313.15	-0.0279	0.07	-0.0712	-0.0502	-0.3187	0.01
Hexyl acetate (1)+ Fluorobenzene (2)						
298.15	0.0272	0.17	0.1599	-0.0621	-0.1362	0.01
303.15	-0.0839	0.19	0.0304	-0.1455	-0.2355	0.01
308.15	-0.1776	0.13	-0.0272	-0.2146	-0.3180	0.01
313.15	-0.2669	0.11	-0.1141	-0.2791	-0.4074	0.02
Hexyl acetate (1)+ Nitrobenzene (2)						
298.15	0.4742	0.05	0.3635	0.3591	0.4894	0.01
303.15	0.3540	0.05	0.2351	0.2639	0.3641	0.01
308.15	0.2523	0.03	0.1321	0.2205	0.2531	0.01
313.15	0.1661	0.03	0.0367	0.1546	0.1629	0.01

McAllister four-body interaction model:

$$\ln v = x_1^4 \ln v_1 - 4x_1^3 x_2 \ln v_{1112} + 6x_1^2 x_2^2 \ln v_{1122} + 4x_1 x_2^3 \ln v_{2221} + x_2^4 \ln v_2 - \ln \left(x_1 + \frac{x_2 M_2}{M_1} \right) + 4x_1^3 x_2 \ln \left[\frac{3 + \frac{M_2}{M_1}}{4} \right] + 6x_1^2 x_2^2 \ln \left[1 + \frac{2M_2}{M_1} \right] + 4x_1 x_2^3 \ln \left[\frac{1 + \frac{3M_2}{M_1}}{4} \right] + x_2^4 \ln \left[\frac{M_2}{M_1} \right] \quad (12)$$

where v , v_1 , v_2 are the kinematic viscosities of binary mixtures and those of the pure components 1 and 2 respectively. v_{1112} , v_{1122} and v_{2221} are the model parameters which are obtained by non-linear regression.

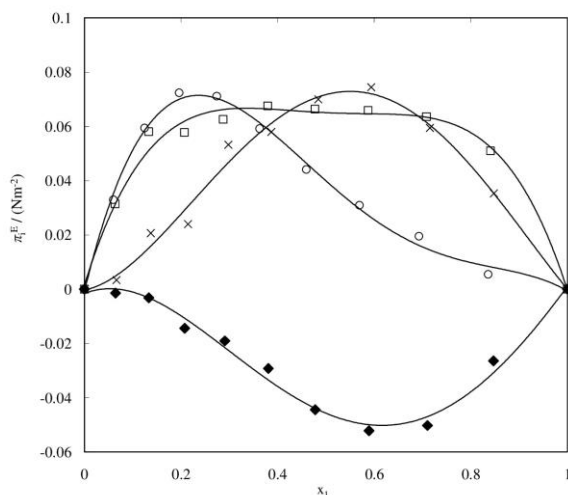


Figure 6. Plots of excess internal pressure π_i^E versus mole fraction x_1 for the binary mixtures of hexyl acetate + chlorobenzene at (\square , 303.15) K, hexyl acetate + bromobenzene at (\times , 303.15) K, hexyl acetate + fluorobenzene at (\circ , 303.15) K and hexyl acetate + nitrobenzene at (\blacklozenge , 303.15) K.

The interaction parameters and standard percentage deviations $\sigma(\%)$ of the Frenkel and McAllister models at (298.15, 303.15, 308.15 and 313.15) K for the studied mixtures are presented in Table 4. It is clear that both the models are suitable for correlating the viscosities of the binary mixtures. However, as compared to one-parameter

model of Frenkel, the McAllister's 3-parameter model gave very low $\sigma(\%)$ values. Thus it can be concluded that the McAllister model predicts the mixture viscosities of the studied binary mixtures more satisfactorily.

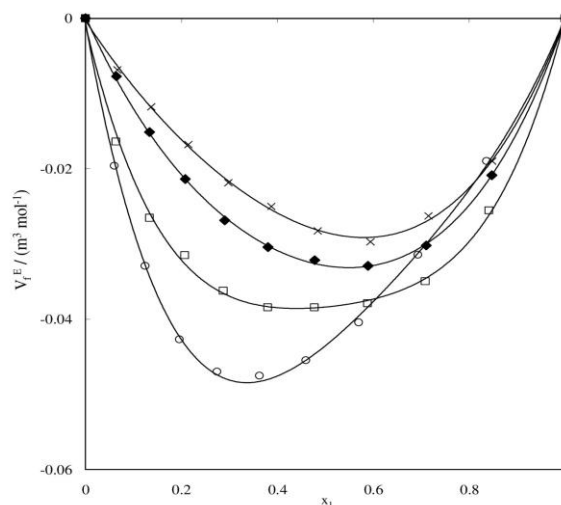


Figure 7. Plots of excess free volume V_f^E versus mole fraction x_1 for the binary mixtures of hexyl acetate + chlorobenzene at (\square , 303.15) K, hexyl acetate + bromobenzene at (\times , 303.15) K, hexyl acetate + fluorobenzene at (\circ , 303.15) K and hexyl acetate + nitrobenzene at (\blacklozenge , 303.15) K.

Conclusion

Densities, viscosities for the binary mixtures of hexyl acetate with chlorobenzene, bromobenzene, fluorobenzene and nitrobenzene have been measured at (298.15, 303.15, 308.15 and 313.15) K. While the speed of sound for these mixtures have been measured at 303.15 K. From the measured density and viscosity values, excess volume and excess free energy of activation were calculated at the respective temperatures.

From the speed of sound data isentropic compressibility K_s , intermolecular free length L_f , specific acoustic impedance Z , internal pressure π_i , free volume V_f and their corresponding excess properties (ΔK_s , L_f^E , Z^E , π_i^E , V_f^E) have been calculated at 303.15 K. The excess or deviation values were correlated using the Redlich-Kister Polynomial equation to obtain their coefficients and standard deviations. It has been observed that negative deviations were observed for excess volumes and positive deviations were observed for the excess free energy of activation of viscous flow. While the acoustic properties exhibit both positive and negative deviations for the studied mixtures. It was observed that the studied viscosity models exhibit the standard deviation values within the range of experimental errors. Better results for McAllister equation are due to number of experimental parameters.

Acknowledgement

The authors sincerely acknowledge the Hon'ble Editor and the reviewers for reviewing this research article.

References

- ¹Lanciotti, R., Belletti, N., Patrignani, F., Gianotti, A., Gardini, F., Guerzoni, M. E., *J. Agric. Food Chem.*, **2003**, *51*, 2958.
- ²Comelli, F., Ottani, S., Francesconi, R., *J. Chem. Eng. Data* **1997**, *42*(6), 1208.
- ³Mohamed M, El-Banna., *J. Chem. Eng. Data* **1997**, *42*(1), 31.
- ⁴Indraswati, N., Mudjijati, W. F., Hindarso, H., Ismadji, S., *J. Chem. Eng. Data* **2001**, *46*(1), 134.
- ⁵Djojoputro, H., Ismadji, S., *J. Chem. Eng. Data* **2005**, *50*(2), 727.
- ⁶Arce, A., Soto, A., Orge, B., Tojo, J., *J. Chem. Eng. Data* **1995**, *40*(5), 1094.
- ⁷Ali, A., Nain, A. K., Chand, D., Lal, B., *Indian J. Chem.*, **2005**, *44*(A), 311.
- ⁸Nigam, R. K., Singh. P. P., Maini, N. N., *Indian. J. Chem.*, **1970**, *8*, 998.
- ⁹Nayak, J. N., Aralaguppi, M. I., Aminabhavi, T. M., *J. Chem. Eng. Data* **2003**, *48*, 628.
- ¹⁰Joshi, S. S., Aminabhavi, T. M., Shukla. S. S., *J. Chem. Eng. Data* **1990**, *35*, 247.
- ¹¹Prasad, D. H. I., Viswanathan, S., Anand, R., *J. Chem. Eng. Data* **2000**, *45*, 764.
- ¹²Venkateswarlu, P., Dharmaraju, G., Raman, G. K., *Proc. Indian Natl. Sci. Acad. Part A.*, **1982**, *48*, 265.
- ¹³Rathnam, M. V., Rajeev Kumar R. S., Kumar M. S. S., *J. Chem. Eng. Data* **2008**, *53*, 265.
- ¹⁴Redlich, O., Kister, A. J., *Ind. Eng. Chem.*, **1948**, *40*, 345.
- ¹⁵Frenkel, Y. I., *Petroleum (London)* **1946**, *9*(1), 27.
- ¹⁶McAllister, R. A., *AIChE. J.*, **1960**, *6*, 427.
- ¹⁷Nayak, J. N., Aralaguppi, M. I., Aminabhavi, T. M., *J. Chem. Eng. Data* **2003**, *48*, 1489.
- ¹⁸Jain, P., Singh, M., *J. Chem. Eng. Data* **2004**, *49*, 1214.
- ¹⁹Reed, T. M., Taylor, T. E., *J. Phys. Chem.*, **1959**, *63*, 58.
- ²⁰Meyer, R., Meyer, M., Metzger, J., Peneloux, A., *J. Chim. Phys. Phys. Chim. Biol.*, **1971**, *63*, 406.

Received: 16.01.2013.

Accepted: 04.03.2013.



SYNTHESIS OF MAGNETITE NANOPARTICLES AND EXPLORING THEIR APPLICATION IN THE REMOVAL OF Pt²⁺ AND Au³⁺ IONS FROM AQUEOUS SOLUTIONS

Liliana Giraldo^[a] and Juan Carlos Moreno-Piraján^{[b]*}

Keywords: adsorption, Langmuir, Freundlich, magnetite, heavy metals, immersion calorimetry.

This investigation studies the adsorption of Pt²⁺ and Au³⁺ ions from nitrate solutions using nanoparticles of magnetite (Fe₃O₄) synthesized in this work. The study is carried out by the analysis of the adsorption of Pt²⁺ and Au³⁺ ions on the surface of the nanoparticles by modifying several variables: contact time, solution pH, and initial Pt²⁺ and Au³⁺ ion concentration. The highly crystalline nature of the magnetite structure with a diameter of around 10 nm was characterized with transmission electron microscopy (TEM) and X-ray diffractometry (XRD). The surface area was determined to be 117.5 m²·g⁻¹. The surface functional groups were investigated with Fourier transform-infrared spectroscopy (FTIR) as well. Batch experiments were carried out to determine the adsorption kinetics and mechanism of Pt²⁺ and Au³⁺ by these magnetite nanoparticles. The adsorption process was found to be pH dependent. The adsorption process better followed the pseudo-second-order equation and Freundlich isotherm. It has been found that the equilibrium can be attained in less than 5 min. Immersion microcalorimetry was explored as a new tool to establish the adsorption capacity of the ions under study with promising results.

* Corresponding Author

E-Mail: jumoreno@uniandes.edu.co

[a] Facultad de Ciencias, Departamento de Química, Universidad Nacional de Colombia, Carrera 30 No 45 03, Ciudad Universitaria, Bogotá, Colombia.

[b] Facultad de Ciencias, Departamento de Química, Grupo de Investigación en Sólidos Porosos y Calorimetría, Universidad de Los Andes, Bogotá, Colombia. Carrera 1 No 18 A 10, Bogotá, Colombia.

Introduction

With the development of industry, humans have tried to improve their quality of life. However, many of these advances have led to major pollution problems worldwide, within which we can mention volatile organic compounds (VOCs) and heavy metal ions. All these elements thrown into water bodies have endangered ecosystems, particularly in developing countries, where despite of controls for these emissions government agencies do not exercise such audits. Industries such as petrochemical, dye, electroplating and the tanneries are big polluters, mainly for the rivers. Today many countries have endangered ecosystems due to this uncontrolled emission of pollutants and many species are on the verge of disappearing. A critical example is the Río Bogotá (Colombia), located on the outskirts of this South American capital, which is one of the most polluted in the world due to electroplating and tanneries endanger for the river. Furthermore, Colombia is a mining country, and it has minerals such as gold, platinum, iridium and others, which are exploited irrationally, generating more pollution for the environment¹⁻⁵.

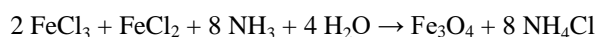
Significant global solutions have been created to remove these pollutants: among them we can mention biological systems, widely used and with some success, while other systems used include porous solids because of their wide variety, and their characteristics have been extremely useful. The removal of ions such as chromium, mercury, zinc and others is carried out by activated carbon, zeolites, and mesoporous solids, to name a few⁷⁻¹². Other systems for removing contaminants are systems through membranes, and some less used such as precipitation systems. Nanoparticles with magnetic properties have recently been explored through adsorption systems and these enable the adsorption of metal ions and can realize major disposal thereof. Today this continues to be explored in this direction with these materials that are very new, not only in the synthesis of the same but in the conditions under which they can operate to achieve a better adsorption of metal ions, which are now one of the major global problems. The key potential impact areas for nanotechnology in water treatment applications can be divided into three groups, namely treatment and remediation, sensing and detection, and pollution control^{13,14}.

In this study, magnetite nanoparticles were synthesized following literature protocols¹⁵ and their efficiency in the removal of Pt²⁺ and Au³⁺ ions were investigated. This is done through studies of adsorption capacity, kinetic effect of pH and the effect of contact time. Work plus calorimetry tests were conducted to explore this immersion technique in these investigations and whether this technique can be used for monitoring the adsorption of the ions being studied.

Experimental

Preparation and characterization of magnetite nanoparticles

In this work, magnetite nanoparticles were prepared according to published procedures in the scientific literature¹⁵⁻¹⁷. The method of co-precipitation, from aqueous solutions of Fe³⁺ and Fe²⁺ salts by addition of bases in an inert atmosphere at room temperature, is suitable for the synthesis of magnetite nanoparticles. The synthesis of magnetite nanoparticles can be represented by the overall reaction equation given below:



We adjusted the amounts of each of the reagents according to our reagents and equipment available. For the synthesis, a 1.5 M ferric chloride hexahydrate and a 2.5 M ferrous chloride tetrahydrate solution was prepared, and then 4.5 mL of FeCl₂·4H₂O and 20 mL of FeCl₃·6H₂O solutions were added to a flask. The mixture was stirred with a stirring speed of 400 rpm at a temperature of 250 °C, and the alkaline solution was added at a rate of 0.9 mL min⁻¹ from a burette with controlled speed through an automatic titrator. Several washings of the obtained solution were performed with methanol and water in a ratio of 50:50. Finally, nanoparticles were obtained by lyophilization treatment. A schematic showing the assembly used is shown in Figure 1.

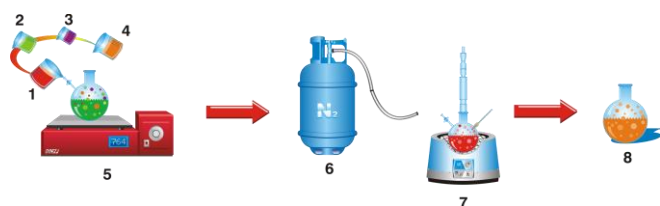


Figure 1. Synthesis equipment for producing magnetite nanoparticles: 1 FeCl₃, 2 FeCl₂, 3 NH₃, 4 H₂O, 5 reactor, 6) nitrogen, 7 heating mantle, 8 products.

Characterizations of magnetite nanoparticles

X-ray diffraction (XRD) patterns of the produced nanoparticles were recorded on a Rigaku Rotaflex X-ray diffractometer using Cu K α radiation. The X-ray tube current was 100 mA with a tube voltage of 40 kV. The 2 θ angular regions between 20 and 70° were examined at a scan rate of 0.1° min⁻¹. The determination of the morphology and size of magnetite nanoparticles was performed by transmission electron microscopy (TEM) and was carried out on a JEOL (JEM 3100 F, Japan) microscope at 200 kV. The IR spectra of the magnetic powders in KBr pellets were recorded with a Thermo Nicolet NEXUS 670 spectrophotometer in the 4000-400 cm⁻¹ range. The magnetization curves were recorded at room temperature using a vibrating sample magnetometer (VSM) characterized with a Lake Shore 7400 series VSM. Specific (BET) and external nanoparticle surface areas were measured by nitrogen adsorption and desorption at 77 K, using an Autosorb 3B (Quantachrome, MI, FL, USA) analyzer. The samples were degassed at 150 °C under N₂ flow overnight before analysis. Surface area was calculated using the BET equation. The

total pore volume, V_{pore}, was evaluated from nitrogen uptake at a relative pressure of ca. 0.97, using the adsorption branch. N₂ adsorption measurements were performed in duplicate to check the proper functioning of the equipment and the entire technique, and the average values have been presented^{18,19}.

Adsorption and desorption studies

The adsorption of Pt²⁺ and Au³⁺ ions by the magnetite nanoparticles was investigated in an aqueous solution at 25 °C. In general, the magnetite nanoparticles (5.0 mg) were put into 50.0 mL of aqueous solution containing Pt²⁺ and Au³⁺ ions (100 mgL⁻¹), the mixture was adjusted to a certain pH with NaOH or HCl and mixed by ultrasonication for several minutes until the equilibrium was established. For removal of Pt²⁺ and Au³⁺ ions from water, these were separated from the mixture with a permanent handheld magnet. The concentration of Pt²⁺ and Au³⁺ ions in the supernatant was measured by flame atomic absorption spectrometer (Ruili WFX-130).²⁰⁻²³

Tests of pH, temperature, and time effects

Tests aimed for the analysis of the pH effect were conducted at 25 °C and the initial pH of the solution was adjusted without a significant change in the initial concentration of metal ions in the solution. Standard 0.1 M HCl and 0.1 M NaOH solutions were used for pH adjustment. The effect of temperature and time was investigated as well, and adsorption tests were carried out between 15 °C and 45 °C. When adsorption equilibrium was reached, the nano-adsorbent was conveniently separated via external magnetic field and the solution was filtered to allow metal concentration measurements²¹⁻²⁵.

Kinetic studies

For the adsorption kinetic studies, the metal ion initial concentration was set to 25 mg L⁻¹ for each metal, and the experiments were carried out in a temperature incubator at 298 K, 300 rpm, and in a solution with a pH of 6.5. In order to determine the time required to reach the adsorption equilibrium, samples were analyzed for metal ion concentration at predetermined time intervals. To assure the accuracy, reliability, and reproducibility of the collected data, all batch tests were performed in triplicate and only average values were reported. Blank tests were run in parallel on metal solutions without addition of sorbent, showing that the experimental procedure does not lead to any reduction of metal concentration and pH variation unrelated to sorbent effects^{23,24}.

For all the tests, the concentration of metal ions in the supernatant was measured by a plasma-atomic emission spectrometer (ICP-AMS, Optima 3000XL, PerkinElmer).

Immersion calorimetry studies

In order to explore whether the immersion enthalpies between synthesized nanoparticles and aqueous solutions of Pt²⁺ and Au³⁺ ions at a concentration in a range between 10 and 100 mg L⁻¹, a series of calorimetric measurements were

carried out using a microcalorimeter local building immersion reported in the literature²⁶. A microcalorimeter schematic is presented in Figure 2. The equipment comprises a thermoelectric system consisting of four thermopiles, which gives a high sensitivity. These thermocouples are embedded in an aluminium block which comes without leaving any dead space and thus avoids false electrical contacts. At the centre of the aluminium block, there is a hole built by EDM, where it enters a cell in special stainless steel, with a capacity of 10 mL, and that likewise leaves no space this time to avoid bad thermal contacts. The aluminium block, or heat reservoir, is placed within a teflon joint which soon stabilizes the temperature. The teflon block has electrical connections for the sensors and electrical resistance, which is used for electric calibrations. On the inside of the microcalorimeter lid is also placed the vial holder system containing the adsorbent.

The measurement is carried out by accurately weighing milligram, 0.10 grams of magnetite, which is degassed under high vacuum to remove impurities having adhered at 90 °C for 6 hours. Once this procedure is suspended in the vacuum, we remove the heating mantle, and proceed to seal the glass ampoule. Then it is placed on the inner lid of the calorimeter, the calibration resistor is connected and the microcalorimeter is closed and we proceed to capture data using software developed in our laboratory, until the baseline stabilizes. Once this is done the ampoule is broken to produce the wetting between the magnetite and the respective solution of Pt^{2+} and Au^{3+} ions (Figure 2). These steps are performed for a range of concentrations between 10 mg L⁻¹ and 100 mg L⁻¹ for each ion. Once thermal equilibrium is re-established, it is expected that the time corresponding to equilibrate the thermometric signal is performed again and the corresponding electrical calibration finalized with each measurement. For each experiment five replicates were conducted for statistical processing.

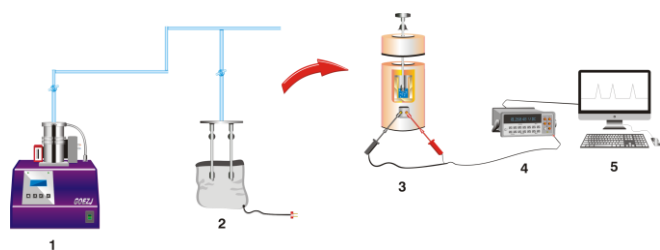


Figure 2. Set-up of microcalorimeter for immersion determinations: 1. Vacuum pump, 2. Desorption system, 3. Microcalorimeter complete, 4. Multimeter, 5. Computer.

Result and discussion

Particle characterization

Magnetite nanoparticles were characterized by XRD results as shown in Figure 3. Recorded peaks are characterized by well defined and there are no extraneous peaks, which shows that there is purity and crystallinity of the particles obtained, and the results of this study are consistent with those reported for magnetite in the literature.

Average size was determined using crystal Scherrer equation 1²⁷. To search for the particle size the most intense peak is chosen, which in this case is found to be approximately $2\theta = 35.55$ with $\kappa = 0.9$, $\lambda = 0.1540598$ nm, $FWHM = \beta$

$$MCD = \frac{k/\lambda}{bcosq} \frac{180}{\rho} \quad (1)$$

The strong and sharp peaks suggested that Fe_3O_4 crystals are highly crystalline. However, the broadening in the reflection peaks was due to the particles' size at the nano domain. All XRD patterns show a diffraction peak at $2\theta = 35.70^\circ$ which corresponds to the spinel phase of Fe_3O_4 nanoparticles. The XRD peaks of magnetic nanoparticles at $2\theta = 30.22^\circ, 43.52^\circ, 57.43^\circ$ and 63.11° were found to be in good agreement with those of previously reported 2θ values of Fe_3O_4 nanoparticles and match well with the JCPDS Card No.19-0629. The average crystallite size of nanoparticles was calculated from the lower full width at half maximum (FWHM) of (3 1 1) diffraction reflection using Scherrer's equation: $D = 0.9\lambda/\beta \cos \theta$, where D is the particle size, λ is the X-ray wavelength (nm), θ is Bragg's angle; β is the excess line broadening (radian), and the particle size of Fe_3O_4 nanoparticles was found in the range of 20–25 nm using Scherrer's equation. The intensity of all diffraction peaks at $2\theta = 35.70^\circ$ are followed by the decreasing of intensity due to formulation of more crystalline phase particles in all annealed Fe_3O_4 nanoparticles. The estimated particle size at 300 °C was estimated as ~21 nm²⁸⁻³¹.

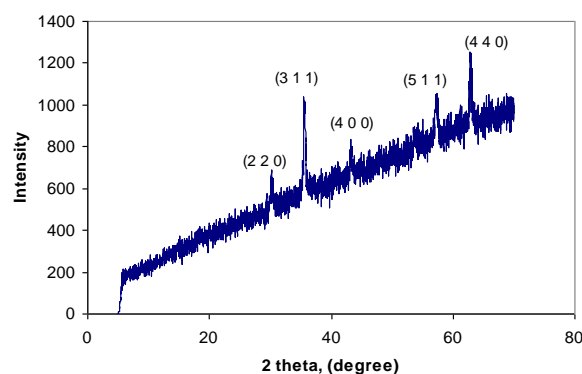


Figure 3. XRD of synthesized magnetite nanoparticles.

Figure 4 shows a transmission electron micrograph. This sample and homogeneous particles are of uniform size. The TEM image of synthesized nanoparticles reveals no presence of contaminants; this is a very important development in this research since it is necessary to have pure particles for analysis of the adsorption capacity of the ion under study. The relative size of the particles is about ~21 nm.

When performing the infrared spectrum analysis of the magnetite nanoparticles, it can be seen that the actual spectrum shows well-defined bands, confirming that particles have been obtained in a purity suitable for the present study. The spectrum shows characteristic bands between the analysed range of 4000-500 cm⁻¹. In Figure 5, the peak at ~3500 cm⁻¹ is attributed to the stretching vibrations of -OH, which is assigned to OH⁻ absorbed by

Fe_3O_4 nanoparticles, and the peak at $\sim 584.3 \text{ cm}^{-1}$ is attributed to the Fe-O bond vibration of Fe_3O_4 ³¹.

The isotherm of nitrogen adsorption (data not shown) of the particles exhibit a specific surface area measured by BET method was $117.5 \text{ m}^2 \text{ g}^{-1}$.

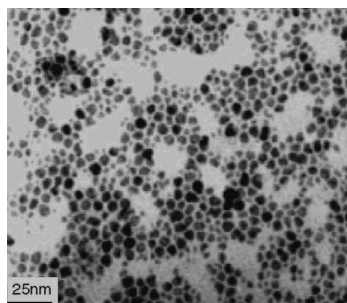


Figure 4. TEM image of synthesized magnetite nanoparticles.

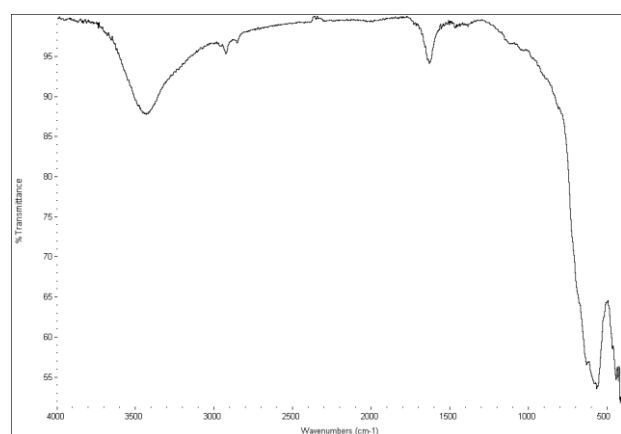


Figure 5. FTIR of synthesized magnetite nanoparticles.

Vibrating sample magnetometer (VSM) studies

Figure 6 shows the plot of the magnetization 'M' versus applied field 'H' (between -2000 Oe and $+2000 \text{ Oe}$) of the prepared Fe_3O_4 nanoparticles obtained.

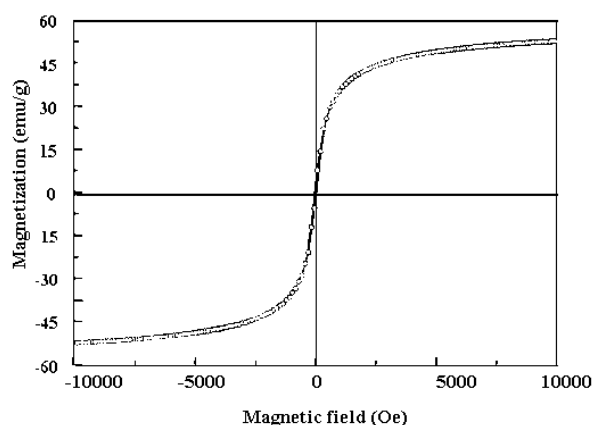


Figure 6. Magnetization curves of synthesized magnetite nanoparticles.

The VSM curve reveals the formation of a hysteresis loop for the Fe_3O_4 nanoparticles, with zero coercivity and remanance values, which exhibits superparamagnetic behaviour of Fe_3O_4 nanoparticles. On increasing the applied field from 0 to 1000 Oe , the magnetization 'M' increases sharply, and becomes nearly saturated at about 1000 Oe . It was found that all the samples of the magnetite have strong magnetic responses to a varying magnetic field. The hysteresis loops showed smooth change of magnetization with the applied field. This was reported in the literature^{32,33}.

Effect of pH

The pH of the aqueous solution is an important controlling parameter in heavy metal ion adsorption processes, as reported by several authors in the literature. Figure 7 shows the effect of a pH solution in the range 2-12 on the removal of Pt^{2+} and Au^{3+} ions from aqueous solutions by magnetite nanoparticles. As a matter of fact, at higher pH the determination of reliable adsorption capacity is not possible, due to the possible precipitation of cations as hydroxides.

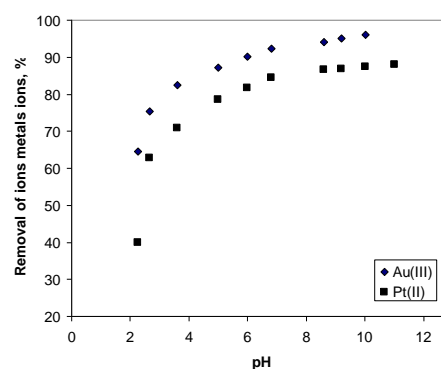
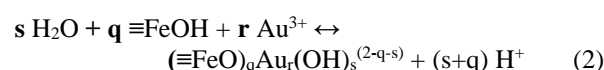


Figure 7. The effect of pH on the adsorption of Pt^{2+} and Au^{3+} ions onto magnetic Fe_3O_4 nanoparticles. $T = 298 \text{ K}$, $t = 6 \text{ h}$, adsorbent dosage = 50 mg , $V_{\text{solution}} = 50 \text{ mL}$, initial metal ion concentration = $25 \text{ mg} \cdot \text{L}^{-1}$.

Experiments were carried out at $25 \text{ }^\circ\text{C}$ with a contact time of 6 h. The adsorption efficiency increases by increasing the pH, for all the investigated cations. As an example, Au^{3+} adsorption efficiency gradually increases from 65.7% to 94.5% when the pH increases from 2 to 6.5.

The results demonstrate that the removal of the cations was mainly dependent on the proton concentration in the solution. This has been previously attributed to the formation of surface complexes between the functional groups ($\equiv\text{FeOH}$) of the sorbent and, for example, the Au^{3+} ions, with the possible reaction being expressed as follows³⁴:

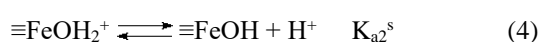
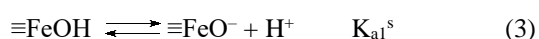


where $(\equiv\text{FeO})_q \text{ Au}_r (\text{OH})_s^{(2-q-s)}$ corresponds to the surface complexes and s , q and r are the stoichiometric coefficients. When pH increases, this equilibrium shifts in such a manner that a greater number of sites are present in the more reactive deprotonated form, thereby leading to a higher uptake of Au^{3+} .

The results show very similar trends for Pt^{2+} adsorption efficiency; this pH dependency has been attributed to the formation of surface complexes similar to those reported for Au^{3+} cations.

Furthermore, from the measured zeta potential of magnetite solution at different pH values, it appears that the magnetite surface has a positive charge at a pH below 6.0 and a negative charge when pH is higher than 6.0³⁴. This result is consistent with the experimental data reported in Figure 7.

Furthermore, it should be noted that magnetite is an amphoteric solid, which can develop charges in the protonation ($Fe-OH + H^+ \leftrightarrow Fe-OH_2^+$) and deprotonation ($Fe-OH \leftrightarrow Fe-O^- + H^+$) reactions of Fe-OH sites on the surface³⁵. The reactions can be written as:



and the corresponding acidity constants as

$$K_{a1}^s = \frac{[H^+]\{\equiv FeO^-\}}{\{\equiv FeOH\}} \quad (5)$$

$$K_{a2}^s = \frac{[H^+]\{\equiv FeOH\}}{\{\equiv FeOH_2^+\}} \quad (6)$$

where [] is the solution species concentration in mol L⁻¹ and { } is the solid surface concentration in mol g⁻¹. According to the pH of the solution, the surface is charged differently and could behave as an anion or cation exchanger. It is important to realize that negative, positive and neutral functional groups can coexist on the surface of the magnetite. At $pH < pH_{zpc}$, the $FeOH_2^+$ groups predominate over the FeO^- groups, i.e., although the surface has a net positive charge, some FeO^- groups are still present. At pH_{zpc} , the number of $FeOH_2^+$ groups equals the number of FeO^- groups, and as the pH increases, the number of FeO^- groups increases (pH_{zpc} have been calculated but not reported here). It follows that magnetite particles may adsorb either negatively or positively charged species by electrostatic attraction depending on the pH, even if, as previously reported, a complete analysis of all the pH intervals is not possible dealing with cations.

Figure 7 shows that a magnitude of adsorption can be defined according to the following order: $Pt^{2+} < Au^{3+}$. The uptake of Pt^{2+} and Au^{3+} ions onto magnetite nanoparticles occurs by physico-chemical interactions, likely represented by electrostatic attractions. In particular, the size of hydrated ionic radii seems to influence the interactions with the negative-charged adsorption site, as the greater the ion's hydration, the farther it is from the adsorbing surface and the weaker its adsorption (hydrated ionic radii: Pt^{2+} : 0.130 nm < Au^{3+} : 0.099 nm). Hence, Au^{3+} has the lowest hydrated ionic radius and the highest capability to compete with proton and, hence, the highest comparative adsorption capacity.

In the literature, results of the same order of magnitude have been reported than that obtained in this work in terms of metal adsorption capacity on the same sorbents³⁵.

Although many different sorbents can be used for the same purpose, magnetic nanosorbents possess a number of unique physical and chemical properties and they are easily dispersed in aqueous solutions. A large number of their atoms are superficial atoms, which are unsaturated and, hence, can determine high adsorption capacity towards several metal ions. Magnetic particles can be removed very quickly from a matrix using a magnetic field, but they do not retain their magnetic properties when the field is removed. This system also has several advantages compared with conventional or other nano-adsorbents such as the absence of secondary wastes and the possible recycling of the materials involved on an industrial scale. Furthermore, the magnetic particles can be tailored to separate specific metal species in water, wastes or slurries. However, from a practical point of view, there is a major drawback in the application of such nanomaterials for treating wastewater. Because the treatment of wastewater is usually conducted in a suspension of these nanoparticles, an additional separation step is required to remove them from a large volume of solution, resulting in increased operating costs. This type of system can be implemented in small towns in order to remove these precious metals efficiently and without polluting the ecosystem.

Adsorption isotherms

Adsorption isotherms of Pt^{2+} and Au^{3+} ions on magnetite nanoparticles are reported in Figure 8.

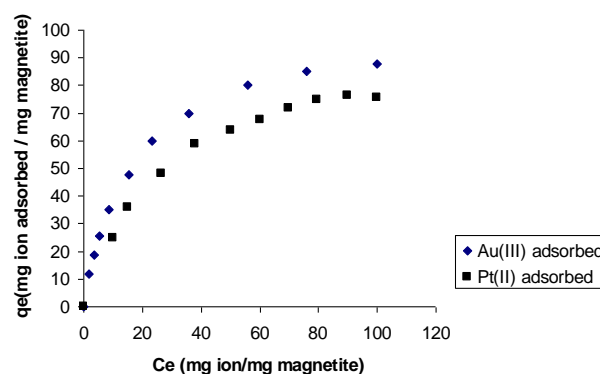


Figure 8. Pt^{2+} and Au^{3+} ions adsorption isotherms on Fe_3O_4 magnetite nanoparticles. $T=25$ °C, $pH=6.5$. Comparison between experimental data and Langmuir model. $V_{solution}= 50$ mL, initial metal ion concentration= 25 mg·L⁻¹.

Under the above-mentioned conditions, the maximum adsorption capacity resulted in being to be 80 mg g⁻¹ for Au^{3+} and then 70 mg g⁻¹ for Pt^{2+} . The uptake of Pt^{2+} and Au^{3+} ions on magnetite nanoparticles occurs by physico-chemical interactions, likely represented by electrostatic attractions, and the comparative adsorption magnitude is confirmed on the entire equilibrium concentration range.

A basic modelling analysis was carried out in order to determine the isotherm model that better describes the experimental data. In Table 1, Langmuir and Freundlich model parameters were reported, as derived from the regression analysis.

Table 1. Estimated parameters for the Langmuir and Freundlich models for isotherm of Pt²⁺ and Au³⁺ adsorption on Fe₃O₄ magnetite nanoparticles (T=25 °C).

	Langmuir equation			Freundlich		
	q _m mg g ⁻¹	b L mmol ⁻¹	r ²	k _f L ⁿ mg ¹⁻ⁿ g ⁻¹	n	r ²
Au ³⁺	86.7	7.4563	0.9788	0.06541	0.7564	0.9955
Pt ²⁺	73.5	4.8734	0.9756	0.07645	0.8765	0.9945

The Freundlich equation frequently gives an adequate description of adsorption data over a restricted range of concentration; it is usually suitable for a highly heterogeneous surface and an adsorption isotherm lacking a plateau, indicating a multilayer adsorption³⁶. Values of 1/n less than unity indicate that a significant adsorption takes place at low concentration, but the increase in the amount adsorbed with concentration becomes less significant at higher concentration and vice versa³⁷.

The essential characteristic of the Langmuir isotherms can be expressed in terms of a dimensionless constant separation factor or equilibrium parameter, R_L, which is defined as:

$$R_L = \frac{1}{(1 + bC_0)} \quad (7)$$

where *b* is the Langmuir constant and C₀ is the initial metal ion concentration. The value of R_L indicates the type of isotherm to be either favourable (0 < R_L < 1), unfavourable (R_L > 1), linear (R_L = 1) or irreversible (R_L = 0). From our study, an initial metal ion concentration of 100 mg·L⁻¹, R_L values for Pt²⁺ and Au³⁺ ion adsorption ranged from 2.77 to 1.89, therefore the adsorption process is unfavourable.

As can be observed from the data reported in Table 1, the Freundlich model shows the highest comparative value of the coefficient of determination (R²), indicating a better approximation of model parameters to the experimental counterparts. In Figure 7 the fitting of experimental data by the Langmuir model is reported.

Adsorption kinetics

In order to better analyse the rates of Pt²⁺ and Au³⁺ ion adsorption on Fe₃O₄ magnetite nanoparticles, two simple kinetic models were tested.

The pseudo-first-order rate expression, popularly known as the Lagergren equation, is generally described by the following equation³⁶:

$$\frac{dq}{dt} = k_{ad}(q_e - q) \quad (8)$$

where q_e is the amount of the metal ions adsorbed at equilibrium per unit weight of sorbent (mg g⁻¹); and *q* is the amount of metal ions adsorbed at any time (mg g⁻¹). Additionally, k_{ad} is the rate constant (min⁻¹). Integrating with appropriate boundary conditions (q = 0 for t = 0 and q = q_t for t = t), Eq. 4 takes the form:

$$\ln(q_e - q_t) = \ln q_e - k_{ad}t \quad (9)$$

However, if the intercept does not equal the natural logarithm of equilibrium uptake of metal ions, the reaction is not likely to follow a first-order path even if experimental data have a high coefficient of determination³⁶. The coefficients of determination for all metal ion adsorption kinetic tests were found to be between 0.9434 and 0.9765 and are reported in Table 2 together with the Lagergren rate constants calculated from the slope of Eq. 5³⁷.

The adsorption data were also analyzed in terms of a pseudo-second-order mechanism given follow equation^{35,36}:

$$\frac{dq}{dt} = k_2(q_e - q_t)^2 \quad (10)$$

where k₂ is the rate constant (mg·g⁻¹·min⁻¹). Integrating the above equation and applying boundary conditions (i.e. q = 0 for t = 0 and q = q_t for t = t) gives:

$$\frac{t}{q_t} = \frac{1}{h_0} + \frac{1}{q_e}t \quad (11)$$

where h₀ is the initial adsorption rate. If the second-order kinetics is applicable, the plot of t/q against *t* in Eq. 7 should give a linear relationship from which the constants q_e and h₀ can be determined. The linear model gave a good fit to the experimental data. This means that the adsorption can be described by a pseudo-second-order rate equation, hence q_e and h₀ were evaluated and are presented in Table 1. R² values are approximately the same for all the four metal ions, with values of about 0.999. At the limit at initial adsorption time, h₀ is defined as³⁵⁻³⁷:

$$h_0 = k_2q_e^2 \quad (12)$$

h₀ was calculated for the four metal ions and the values are reported in Table 1. The results obtained are similar to previous studies³⁶⁻³⁷.

Table 2. Lagergren rate equation constants and pseudo second-order rate equation constants for Pt²⁺ and Au³⁺ ion adsorption on Fe₃O₄ magnetite nanoparticles.

	q _{exp}	Pseudo-first-order equation			Pseudo-second-order equation		
		q _e (mmol g ⁻¹)	k ₁ (min ⁻¹)	r ²	q _e (mmol g ⁻¹)	k ₂ (g mmol ⁻¹ ·min ⁻¹)	r ²
Au ³⁺	0.0901	0.0877	0.3221	0.9687	0.0899	4.9876	0.9998
Pt ²⁺	0.0621	0.0658	0.2234	0.9754	0.0734	3.37456	0.9986

For all the regressions, the residual sum of squares (SSE), as the difference between the predicted values and the experimental data, can be calculated by the following equation:

$$\sum_n (q_e \text{ exp} - q_e \text{ calc})^2 \quad (13)$$

where the subscripts exp and calc refer to the experimental and the calculated q values, respectively. Hence, the higher correlation coefficient (R^2) values for the pseudo-second-order kinetic model indicated that the sorption followed a pseudo-second-order mechanism, likely controlled by chemisorption.

Effect of temperature and time

For the investigated ions, adsorption experiments were conducted varying the temperature between 15 °C and 45 °C under the following conditions: L/S = 1:6 and pH 6.5.

Figures 9a and 9b show the curves obtained for the adsorption tests at different times and temperatures for Pt^{2+} and Au^{3+} taken as an example, respectively. As can be observed, for both ions, the adsorption capacity is greater for lower temperatures, as expected, since adsorption is an exothermic process. Moreover, the increase in adsorption capacity is higher for the lowest values of temperature.

The temperature also has an effect on the time necessary to reach the equilibrium; a higher temperature, in fact, determines a lower equilibrium time.

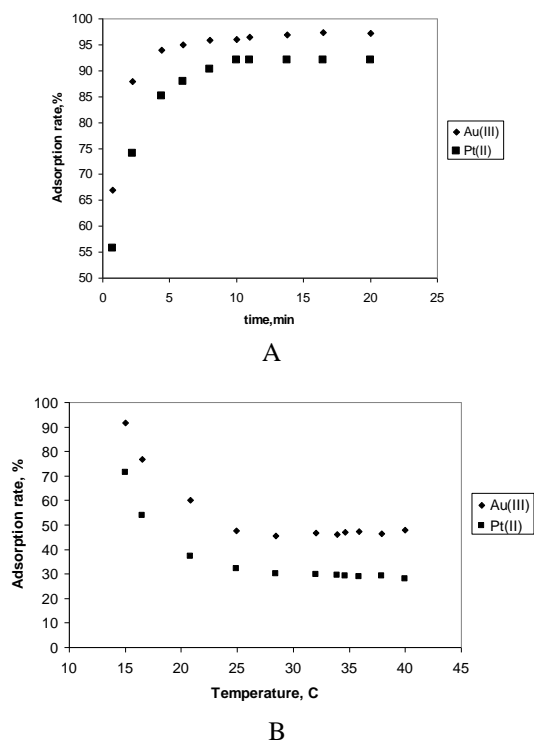


Figure 9. The effect of temperature on the adsorption of Pt^{2+} (A) and Au^{3+} (B) ions on the magnetic Fe_3O_4 nanoparticles; pH = 6.5, adsorbent dosage = 50 mg, initial metal ion concentration = 25 $mg \cdot L^{-1}$.

Immersion calorimetry

This work used the technique of immersion microcalorimetry, with the aim of analysing whether the immersion of the synthesized magnetite particles in solutions studio ions generated under some correlation.

Figure 10 shows the results obtained and show that a correlation is generated between the initial concentration of each of the solutions in the range studied and the calculated enthalpy of immersion. This makes it interesting to use in studies of adsorption microcalorimetry with such materials, since in the literature the thermodynamic variables are calculated by varying the temperature and calorimetric known from the same that this form of thermodynamic correlation is correct, produce errors which are sometimes large.

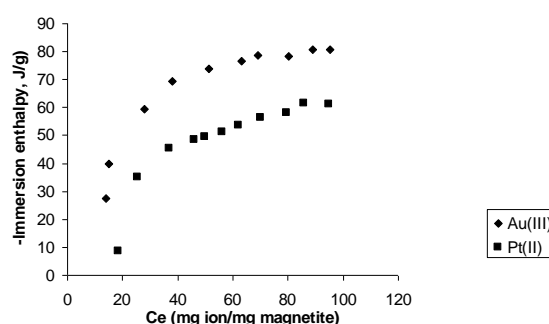


Figure 10. Immersion heats between nanoparticles of magnetite and ion solutions.

Figure 10 shows a high-energy release at low concentrations, which increases to about 60 $mg L^{-1}$ which then becomes constant, showing a behaviour similar to an isotherm from aqueous solution. It is interesting to note that the enthalpy values are higher between interaction Au^{3+} -magnetite for Pt^{2+} -magnetite; this is in accordance with that was found by the other techniques used by us in this work, where there is greater affinity between ions Au^{3+} and magnetite. These results open a very good possibility for thermodynamic studies using this technique.

Conclusion

In this work, Fe_3O_4 nanoparticles were synthesized by co-precipitation method and used for treating water artificially contaminated by metal ions, such as Pt^{2+} and Au^{3+} . Experimental results suggest that the adsorption capacity of Fe_3O_4 nanoparticles towards metal ions depends on the metal ions' electronegativity. The maximum adsorption capacity in the investigated conditions was 86.7 $mg g^{-1}$ for Au^{3+} and 76.3 $mg g^{-1}$ for Pt^{2+} . Moreover, adsorption capacity seems to be strongly dependent on pH solution and temperature. The adsorption mechanism seems to be mainly an electrostatic attraction between metal ions and nanoparticles influenced by the hydrated ionic radius of the metal cations. The Langmuir model interprets the adsorption data better. A kinetic analysis showed that the adsorption of all the investigated ions onto Fe_3O_4 nanoparticles occurs by a pseudo-second-order mechanism. In

conclusion, it is demonstrated here that the Fe_3O_4 nanoparticles with fine grain size (<10 nm) can be efficiently used as an effective, convenient and low-cost material for the removal and recovery of metals from wastewater. The adsorption process was found to follow the pseudo-second-order equation. The equilibrium data conformed better to Freundlich's isotherm. The immersion calorimetry technique presents a good chance to be employed in these studies and evaluates the thermodynamic variables.

Acknowledgements

The authors would like to gratitude the Framework Agreement between the Universidad de los Andes and the Universidad Nacional de Colombia, as well as the Agreement Statement (Acta de Acuerdo) between the Chemistry Departments of both universities.

They area especially grateful to the special fund of the Science Faculty ("Proyecto Semilla") of the Universidad de Los Andes (Colombia) for its partial funding for this research.

References

- ¹Singh, D. B., Prasad, G., Rupainwar, D. C., and Singh, V.N., *Water Air Soil Pollut.*, **1998**, *42*, 373.
- ²Jain, C. K., and Ali, I., *Water Res.*, **2000**, *34*, 4304.
- ³ World Health Organization (WHO), *Environmental Health Criteria*, **2001**, 224.
- ⁴Benjamin, M., *Water Chemistry*, McGraw Hill, New York, **2002**.
- ⁵Leon, C. A., Solar, J. M., Calemma, V. and Radovic, L. R., *Carbon*, **1992**, *30*, 797.
- ⁶Bandosz, T. J., Jagiello, J., Contescu, C., and Schwarz, J. A., *Carbon*, **1993**, *31*, 1193.
- ⁷Boehm, H. P., *Carbon*, **2002**, *40*, 145.
- ⁸Lakatos, J., Brown, S. D., and Snape, C. E., *Fuel*, **2002**, *81*, 691.
- ⁹Yacoumi, S., and Tien, C., *Kinetics of Metal Ion Adsorption from Aqueous Solutions*, Kluwer Academic Publisher, Boston, **1995**.
- ¹⁰Gabaldon, C., Marzal, P., Ferrer, J., and Seco, A., *Water Res.*, **1996**, *30*, 3050.
- ¹¹Hu, J., Lo, M., and Chen, G., *Separation and Purification Technology*, **2007**, *56*, 249.
- ¹²Lo Hu, J., and Chen, G., Iron-Based Magnetic Nanoparticles for Removal of Heavy Metals from Electroplating and Metal-Finishing Wastewater, In: *Nanotechnologies for Water Environment Applications*, Zhang C.T., Surampali Y.R., Lai K.C.K, Hu Z., Tyagi R.D., Lo M.C.I. (Eds.), American Society of Civil Engineers, Virginia, **2009**, 213-264.
- ¹³Cloete, T. E., *Nanotechnology in Water Treatment Applications*, Caister Academic Press, Norfolk, UK, **2010**.
- ¹⁴Parida, S. K., Dash, S., Patel, S., and Mishra, B. K., *Adv. Colloid Interface Sci.*, **2006**, *121*, 77.
- ¹⁵Khodabakhshi, A., Amin, M. M., and Mozaffari, M., *Iran. J. Environ. Health. Sci. Eng.*, **2011**, *8*, 189.
- ¹⁶Kang, Y. K., Risbud, S., Rabolt, J. F., and Stroeve, P., *Chem Mater.*, **1996**, *8*, 2209.
- ¹⁷Goya, G. F., Berquo, T. S., Fonseca, F. C., and Morales, M. P., *J. Appl. Phys.*, **2003**, *94*, 3520.
- ¹⁸Sudaryanto, Y., Hartono, S. B., Irawaty, W., Hindorso, H., and Ismadji, S., *Bioresour. Technol.*, **2006**, *97*, 734.
- ¹⁹Yorgun, S., Vural, N., and Demiral, H., *Microporous and Mesoporous Materials*, **2009**, *122*, 189.
- ²⁰Wang, X., Zhao, C., Zhao, P., Dou, P., Ding, Y., and Xu, P., *Bioresource Technology*, **2009**, *100*, 2301.
- ²¹Sun, Y., Ma, M., Zhang, Y., and Gu, N., *Colloids and Surfaces A: Physicochem. Eng. Aspects*, **2004**, *245*, 15.
- ²²Podzus, P. E., Debandi, M. V., and Daraio, M. E., *Physica B: Condensed Matter*, **2011**, *407*, 3131.
- ²³Lee, D., Omolade, D., Cohen, R. E., and Rubner, M. F., *Chem. Mater.* **2007**, *19*, 1427.
- ²⁴Thierry, B., Majewski, P., Ngothai, Y., and Shi, Y., *Int. J. of Nanotechnology*, **2007**, *4*, 523.
- ²⁵Kocaoba, S., and Akyuz, T., *Desalination*, **2005**, *181*, 313.
- ²⁶Giraldo, L., Huertas, J. I., Valencia, A. and Moreno J. C, *Inst Sci Technol.*, **2003**, *31*, 385.
- ²⁷ Klug, H. P., and Alexander, L. E. *X-Ray Diffraction Procedures: For Polycrystalline and Amorphous Materials*, 2nd Edition, pp. 992. Wiley-VCH, May **1974**. ISBN 0-471-49369-4.
- ²⁸Obaid, R., Subash, C. M., and Sharif, A., *Materials Chemistry and Physics*, **2012**, *132*, 196.
- ²⁹Meziani, M. J., Liu, P., Pathak, P., Lin, J., Vajandar, S.K., Allard, L.F., and Sun, Y.P., *Ind. Eng. Chem. Res.*, **2006**, *45*, 1539.
- ³⁰Boistelle, R., and Astier, J. P., *J. Cryst. Growth*, **1988**, *90*, 14.
- ³¹Ma, M., Zhang, Y., Yu, W., Shen, H., Zhang, H., and Gu, N., *Colloids and Surfaces A: Physicochem. Eng. Aspects*, **2003**, *212*, 219.
- ³²Choo, E. S. G., Tang, X. S., Sheng, Y., Shuter, B., and Xue, J., *Journal of Materials Chemistry*, **2011**, *21*, 2310.
- ³³Choo, E. S. G., Yu, B., and Xue, J. M., *Journal of Colloid and Interface Science*, **2011**, *358*, 462.
- ³⁴Hou, Y. L., Yu. H. F., and Gao, S., *J. Mater. Chem.*, **2003**, *13*, 1983.
- ³⁵Wan, S. R., Huang, J. S., Yan, H. S., and Liu, K. L., *J. Mater. Chem.*, **2006**, *16*, 298.
- ³⁶Lagergren, S., About the Theory of So-called Adsorption of Soluble Substances, *K. Svenska Vetensk-Akad. Handl.*, **1989**, *24*, 1.
- ³⁷Ho, Y. S., McKay, G., *Chem. Eng. J.*, **1998**, *70*, 115.

Received: 21.02.2013.

Accepted: 03.03.2013.



SYNTHESIS OF SOME UNSYMMETRICAL NEW SCHIFF BASES FROM AZO DYES

Asieh Yahyazadeh*, Vahid Azimi

Keywords: Schiff base, azo dye, diaminomaleonitrile, salicylaldehyde, antimicrobial, *o*-hydroxy azoaldehydes

A simple and satisfactory environment friendly procedure for synthesis of some antimicrobial azo-Schiff bases is presented. The condensation of *o*-hydroxy azoaldehydes and diaminomaleonitrile in the presence of a catalytic amount of acetic acid produced desired Schiff bases in high yields.

Corresponding Authors

Fax: +981313233262

Fax: +981313233262

E-Mail: yahyazadehphd@yahoo.com;

yahyazadeh@guilan.ac.ir

[a] Department of Organic Chemistry, University of Guilan, P.O.Box 41335-1914, Rasht, Iran

Synthesis of azo dyes precursors. A general procedure

To a solution of an aniline derivative (10 mmol) in water (5 mL), concentrated hydrochloric acid (20 mL) was added slowly with stirring. The clear solution was poured into ice-water mixture, diazotied with sodium nitrite (0.69 g, 10 mmol), dissolved in water (3.5 mL), during a period of 15 min at 0-5 °C. The cold diazo solution was added dropwise to the solution of salicylaldehyde (1.05 mL, 10 mmol) in water (50 mL) containing sodium hydroxide (0.4 g) and sodium carbonate (7.3 g) during a period of 30 min at 0-5 °C. The reaction mixture was stirred for 1 h in ice bath, allowed to warm slowly to room temperature and subsequently stirred for 4 h at this temperature. The product was collected by filtration and recrystallized from mixture of EtOH and H₂O (Scheme 1, Table 1).

INTRODUCTION

Schiff bases derived from the reaction of aromatic aldehydes and aliphatic or aromatic amines represented in important series of widely-studied organic ligands. A variety of applications such as biological,¹⁻⁴ clinical,⁵⁻⁸ analytical,⁹⁻¹² industrial¹³ and catalytical¹⁴⁻¹⁷ of Schiff bases and their metal complexes have been reported. Aromatic aldehyde Schiff bases have also attracted much attention due to their diverse biological activities, such as antimicrobial, antibacterial, antiviral, and anticancer activities.¹⁸ They are used in optical and electrochemical sensors, in various chromatographic methods and to enhance selectivity and sensitivity of the organic reagents. Schiff bases are easily characterized. They possess structural-similarities with natural biological substances. Their preparation procedures are relatively simple and have synthetic flexibility that enables tuning of suitable structural properties.¹⁹⁻²³ In the present investigation, some new Schiff bases have been in one-stage through a reaction of diaminiomaleonitrile with *o*-hydroxy azoaldehydes in the presence of acetic acid as catalyst.

Experimental Section

The UV-Vis spectra were measured on a Shimadzu UV-2100 spectrometer. The ¹H NMR (500 MHz) spectra were obtained with a Bruker 500 DRX-Avance NMR and the others (400 MHz) were registered with a Bruker 400 Avance 3 spectrometer. The IR spectra were taken with a Shimadzu 470 spectrometer using KBr pellets. Melting points of crystalline dicyano compounds were measured with a Electrothermal melting point apparatus and are not corrected. Mass spectra were recorded on a GC-MS Agilent Technologies QP-5973N MSD instrument. Typical reaction procedures and spectroscopic data for all products are described below.

5-Phenylazosalicylaldehyde 1a. Brown solid; Yield 1.76 g, 78%; M.p. 128-129 °C; IR (KBr, ν cm⁻¹): 3200 (O-H stretch), 3030 (aromatic C-H stretch), 1660 (aromatic aldehyde C=O stretch), 1618, 1568 (aromatic C=C stretch), 1478 (N=N stretch), 1280 (C-O stretch); ¹H NMR (400 MHz, CDCl₃, ppm) δ : 7.15 (d, J=8.8 Hz, 1H, H_e), 7.48-7.57 (m, 3H, H_g, H_h), 7.93 (dd, J=8.4 Hz, J=1.2 Hz, 2H, H_f), 8.21 (dd, J=8.8 Hz, J=2.4 Hz, 1H, H_d), 8.23 (d, J=2.4 Hz, 1H, H_c), 10.06 (s, 1H, H_b), 11.35 (s, 1H, H_a); UV-Vis (EtOH): λ_{\max} =240 nm, 350 nm, Exact mass (M): Calcd. for C₁₃H₁₀N₂O₂ 226.0742 found 226.0751.

5-(4-Nitrophenylazo)salicylaldehyde 1b. Orange solid; Yield 2.41 g, 89%; M.p. 184-186 °C; IR (KBr, ν cm⁻¹): 3400 (O-H stretch), 3100 (aromatic C-H stretch), 1660 (aromatic aldehyde C=O stretch), 1600, 1570 (aromatic C=C stretch), 1520 (NO₂ asymmetric stretch), 1475 (N=N stretch), 1340 (NO₂ symmetric stretch), 1280 (C-O stretch), 850 (aromatic out of plane bend); ¹H NMR (500 MHz, CDCl₃, ppm) δ : 7.21 (d, J=8.95 Hz, 1H, H_c), 8.06 (d, J=8.96 Hz, 2H, H_f), 8.26 (dd, J=8.96 Hz, J=2.3 Hz, 1H, H_d), 8.33 (d, J=2.3 Hz, 1H, H_e), 8.43 (d, J=8.94 Hz, 2H, H_g), 10.10 (s, 1H, H_b), 11.50 (s, 1H, H_a); UV-Vis (CHCl₃): λ_{\max} =255 nm, 360 nm, Exact mass (M): Calcd. for C₁₃H₉N₃O₄ 271.0593 found 271.0582.

5-(4-methylphenylazo)salicylaldehyde 1c. Brown solid; Yield 2.1 g, 87%; M.p. 150-152 °C; IR (KBr, ν cm^{-1}): 3200 (O-H stretch), 3030 (aromatic C-H stretch), 2910 (aliphatic C-H stretch), 1650 (aromatic aldehyde C=O stretch), 1618, 1600, 1567 (aromatic C=C stretch), 1478 (N=N stretch), 1278 (C-O stretch), 820, 740, 690 (aromatic out of plane bend). $^1\text{H NMR}$ (500 MHz, CDCl_3 , ppm) δ : 2.49 (s, 3H, H_h), 7.16 (d, $J = 8.7$ Hz, 1H, H_e), 7.37 (d, $J = 8.2$ Hz, 2H, H_g), 7.86 (d, $J = 8.3$ Hz, 2H, H_f), 8.21 (dd, $J = 8.8$ Hz, $J = 2.4$ Hz, 1H, H_d), 8.23 (d, $J = 2.3$ Hz, 1H, H_c), 10.07 (s, 1H, H_b), 11.34 (s, 1H, H_a); UV-Vis: (EtOH) $\lambda_{\text{max}}=240$ nm, 350 nm Exact mass (M): calcd. for $\text{C}_{14}\text{H}_{12}\text{N}_2\text{O}_2$, 240.0899 found 240.0872.

5-(4-acetylphenylazo)salicylaldehyde 1d. Brown solid; Yield 2.46 g, 92%; M.p. 176-178 °C; IR (KBr, ν cm^{-1}): 3200 (O-H stretch), 1675 (ketone C=O stretch), 1660 (aromatic aldehyde C=O stretch), 1617, 1595, 1567 (aromatic C=C stretch), 1480 (N=N stretch), 1260 (C-O stretch), 840, 735 (aromatic out of plane bend). $^1\text{H NMR}$ (500 MHz, CDCl_3 , ppm) δ : 2.71 (s, 3H, H_h), 7.19 (d, $J = 8.9$ Hz, 1H, H_e), 8 (d, $J=8.4$ Hz, 2H, H_f), 8.15 (d, $J = 8.4$ Hz, 2H, H_g), 8.25 (dd, $J = 8.9$ Hz, $J=2.2$ Hz, 1H, H_d), 8.29 (d, $J=2.1$ Hz, 1H, H_c), 10.09 (s, 1H, H_b), 11.44 (s, 1H, H_a); UV-Vis: (EtOH) $\lambda_{\text{max}}=258$ nm, 364 nm; Exact mass (M): Calcd. for $\text{C}_{15}\text{H}_{12}\text{N}_2\text{O}_3$ 268.0847 found 268.0864.

Synthesis of unsymmetrical Schiff bases. A general procedure

Different azo dyes (1mmol) in EtOH (7 mL) were added to a solution of diaminomaleonitrile (1 mmol, 0.11 g) in EtOH (7 mL) and then a catalytic amount of acetic acid (two or three drops) was added to mixture at room temperature. The reaction mixture was stirred for 2 h. The products were collected by filtration and recrystallized from ethanol (Scheme 2, Table 2).

Synthesis of 2a. Orange solid; Yield 0.30 g, 95 %; M.p. 248-250 °C; IR (KBr, ν cm^{-1}): 3300, 3400 (NH_2 stretch), 3190 (aromatic C-H stretch), 2200 (-CN stretch) 1627 (C=N stretch), 1600, 1555 (aromatic C=C stretch), 1478 (N=N stretch), 1280 (C-O stretch). $^1\text{H NMR}$ (500 MHz, DMSO, ppm) δ : 7.11 (d, $J=8.85$ Hz, 1H, H_e), 7.53 (dd, $J=8.35$ Hz, $J=9.42$ Hz, 1H, H_i), 7.57 (d, $J=7.72$ Hz, 2H, H_g), 7.85 (d, $J=7.76$ Hz, 2H, H_h), 7.87 (dd, $J = 2.54$ Hz, $J = 8.82$ Hz, 1H, H_f), 8.03 (s, 2H, H_a), 8.66 (s, 1H, H_b), 8.70 (d, $J = 2.47$ Hz, 1H, H_d), 11.24 (s, 1H, H_c); UV-Vis: (DMSO) $\lambda_{\text{max}}=257$ nm, 331 nm; Exact mass (M): Calcd. for $\text{C}_{17}\text{H}_{12}\text{N}_6\text{O}$ 316.1072 found 316.1055.

Synthesis of 2b. Orange solid; Yield 0.33 g, 92 %; M.p. 248-250 °C; IR (KBr, ν cm^{-1}): 3300, 3400 (NH_2 stretch), 3100 (aromatic C-H stretch), 2200 (-CN stretch) 1627 (C=N stretch), 1600, 1558 (aromatic C=C stretch), 1520 (NO_2 asymmetric stretch), 1480 (N=N stretch), 1340 (NO_2 symmetric stretch), 1280 (C-O stretch)); $^1\text{H NMR}$ (500 MHz, DMSO, ppm) δ : 7.13 (d, $J = 8.83$ Hz, 1H, H_e), 7.89 (d, $J=8.82$ Hz, 1H, H_f), 8.00 (d, $J = 8.84$ Hz, 2H, H_g), 8.05 (s, 2H, H_a), 8.39 (d, $J = 8.78$ Hz, 2H, H_h), 8.63 (s, 1H, H_b), 8.77 (s, 1H, H_d), 11.56 (s, 1H, H_c); UV-Vis (DMSO); $\lambda_{\text{max}}=259$ nm, 354 nm; Exact mass (M) Calcd. for $\text{C}_{17}\text{H}_{11}\text{N}_7\text{O}_3$ 361.0923 found 361.0912.

Synthesis of 2c. Yellow solid; Yield 0.28 g, 86%, M.p. 256-258 °C; IR (KBr, ν cm^{-1}): 3300, 3400 (NH_2 stretch), 3030 (aromatic C-H stretch), 2910 (aliphatic C-H stretch), 2200 (-CN stretch), 1625 (C=N stretch), 1600, 1555 (aromatic C=C stretch), 1480 (N=N stretch), 1280 (C-O stretch); $^1\text{H NMR}$ (500 MHz, DMSO, ppm) δ : 2.39 (s, 3H, H_i), 7.10 (d, $J=11$ Hz, 1H, H_e), 7.38 (d, $J=10$ Hz, 2H, H_h), 7.76 (d, $J=10$ Hz, 2H, H_g), 7.85 (dd, $J=3$ Hz, $J=11$ Hz, 1H, H_f), 8.04 (s, 2H, H_a), 8.69 (s, 1H, H_b), 8.67(d, $J=3.5$ Hz, 1H, H_d); UV-Vis (DMSO): $\lambda_{\text{max}}=252$ nm, 332 nm; Exact mass (M): Calcd. for $\text{C}_{18}\text{H}_{14}\text{N}_6\text{O}$ 330.1229 found 330.1289.

Synthesis of 2d. Yellow solid; Yield 0.28 g, 80%; M.p. 262 °C_{dec.}; IR (KBr, ν cm^{-1}): 3300, 3400 (NH_2 stretch), 1675 (ketone C=O stretch), 1625 (C=N stretch), 1600, 1557, (aromatic C=C stretch), 1480 (N=N stretch), 1260 (C-O stretch); $^1\text{H NMR}$ (500 MHz, DMSO, ppm) δ : 2.63 (s, 3H, H_i), 7.12 (d, $J = 8.8$ Hz, 1H, H_e), 7.89 (dd, $J=8.3$ Hz, $J=2.1$ Hz, 1H, H_f), 7.93 (d, $J=8.3$ Hz, 2H, H_g), 8.04 (s, 2H, H_a), 8.17 (d, $J=8.3$ Hz, 2H, H_h), 8.64 (s, 1H, H_b), 8.75(d, $J=1.9$ Hz, 1H, H_d), 11.40 (s, 1H, H_c); UV-Vis (DMSO): $\lambda_{\text{max}}=365$ nm, 549 nm; Exact mass (M): Calcd. for $\text{C}_{19}\text{H}_{14}\text{N}_6\text{O}_2$ 358.1178 found 358.1197.

Table 1. Properties of azo dye compounds

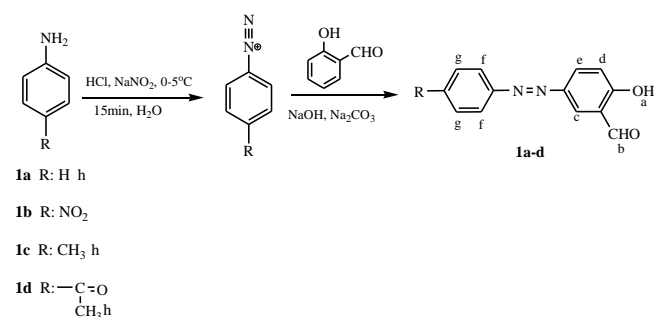
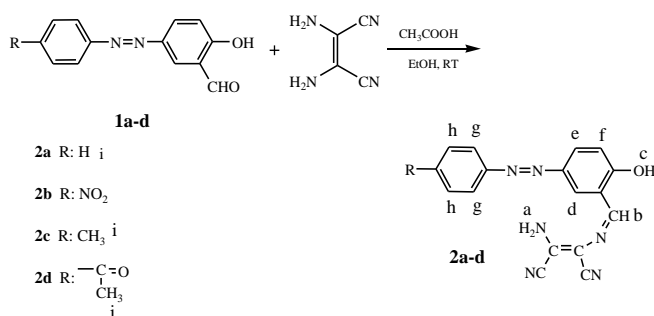
Entry	Time (h)	Yield (%)	Colour	Mp (°C)
1a	5	78	Brown solid	128-129
1b	5	89	Orange solid	184-186
1c	5	87	Brown solid	150-152
1d	5	92	Brown solid	176-178

Table 2. Properties of Schiff base compounds

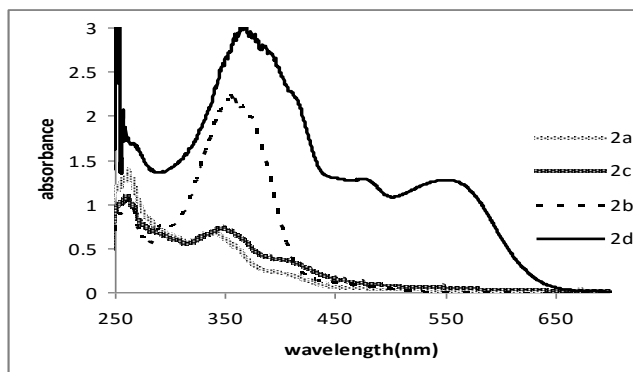
Entry	Time (h)	Yield (%)	Colour	M.p. (°C)
2a	2	95	Orange solid	248-250
2b	2	92	Orange solid	248-250
2c	2	86	Yellow solid	256-258
2d	2	80	Yellow solid	262-264

RESULTS AND DISCUSSION

Diazo coupling was accomplished selectivity at the 4-position of salicylaldehyde ring to give compounds **1** in moderate to excellent yields (78-92%) (Scheme 1) (Table 1). The electronic absorption spectra of compounds **1** and **2** show intense lowest energy charge-transfer absorption band in the UV-Vis region (240-260 nm and 340-370 nm). Electron attracting substituents such as $-\text{NO}_2$, C=O in the coupler increase the polarizability. This leads to a decrease in the energy gap between the highest occupied molecular orbital (HOMO) and lowest unoccupied molecular orbital (LUMO), thus $\pi-\pi^*$ electronic transition with lower frequency photons, results a bathochromic shift of the visible band for azo dye and Schiff bases (Figure 1).

Scheme 1. Synthetic route for azo dye derivatives **1a-d**Scheme 2. Synthetic route for Schiff base derivatives **2a-d**

All the compounds are air stable with sharp melting points indicating the purity of the compounds. The spectra analysis of the compounds is in agreement with the composition assigned to the compounds.

Figure 1. UV-Vis Absorption spectra of **2a-d** (in DMSO)

The IR spectrum of each Schiff base compound confirms the formation of imine band (---C=N---) and absence of the original aldehyde band (---C=O). A band at $1625\text{--}1627\text{ cm}^{-1}$ is assigned to the stretching vibration of the imines group (C=N). All the compounds displayed a band at $1260\text{--}1280\text{ cm}^{-1}$ assigned to (C-O) stretching vibration of the phenol-OH. The $^1\text{H NMR}$ spectra showed singlet and sharp bands at $8.63\text{--}8.69\text{ ppm}$ which further confirmed the formation of ---C=N--- bonds. Reaction of DAMN with azo aldehydes readily yields the asymmetrical Schiff base compounds **2a-d** in high yields. IR and $^1\text{H NMR}$ spectra features agree with the formula assignments.

Also, the similar IR spectra of compounds **2a-d** revealed the absence of the carbonyl group band in $1650\text{--}1660\text{ cm}^{-1}$ and appearance of a strong band in $1625\text{--}1627\text{ cm}^{-1}$ region, assignable to the $\nu(\text{C=N})$ imine group. All the compounds were analyzed by melting point, IR, UV-Vis and $^1\text{H NMR}$ spectra.

ACKNOWLEDGMENTS

The partial support of this research by the Research Committee of University of Guilan is gratefully acknowledged.

REFERENCES

- Balasubramanian, K. P., *Spectrochimica Acta Part A: Mol. Biomol. Spect.*, **2007**, 68, 50.
- Tümer, M., Ekinçi, D. and Tümer, F. A., *Spectrochimica Acta Part A: Mol. Biomol. Spect.*, **2007**, 67, 916.
- Balasubramanian, K. P., *Spectrochimica Acta Part A: Mol. Biomol. Spect.*, **2006**, 65, 678.
- Jian, L. V., *J. Inorg. Biochem.* **2006**, 100, 888.
- Huang, Z., *Thermochimica Acta*, **1998**, 320, 121.
- Taguchi, T., *J. Am. Soc. Nephrol.*, **2002**, 13, 2478.
- Khalifah, R. G., Baynes, J. W. and Hudson, B. G., *Biochem. Biophys. Res. Commun.*, **1999**, 65, 251.
- Ashish, S. P., Gupta, D. and Prasad, R., *Inter. J. Pharm.*, **2007**, 333, 79.
- Gholivand, M. B., *Talanta*, **2007**, 73, 553.
- Sivasankaran, N. M. and Selwin, J. R., *Spectrochimica Acta Part A: Mol. Biomol. Spect.*, **2007**, 70, 749.
- Fakhari, A. R., Khorrami, A. R. and Naeimi, H., *Talanta*. **2005**, 66, 813.
- Mashhadizadeh, M. H., Pour Taheri, E. and Sheikhshoae, I., *Talanta*. **2007**, 72, 1088.
- Zoubi, W. A., Kandil, F. and Chebani, M. K., *Int. J. Chem. Tech. Res.*, **2011**, 3, 1612.
- Yang, T. L., Qin, W. W. and *Spectrochimica Acta Part A: Mol. Biomol. Spect.* **2007**, 67, 568.
- Biernacka, I. K., *J. Mol. Catal. A: Chem.* **2007**, 278, 82.
- Virginie, C., *Tetrahedron Lett.*, **2007**, 48, 5561.
- Lu, X. H., *J. Mol. Catal. A: Chem.*, **2006**, 250, 62.
- Edmund, K. E., *Polyhedron*. **2007**, 26, 2559.
- Li, M. Y., Hu, P. Z. and Zhu, W. R., *Chin. Chem. Lett.*, **2003**, 14, 572.
- Danilova, T. I., *Tetrahedron: Asym.* **2004**, 15, 223.
- Tong, J., Li, Z. and Xia, C., *J. Mol. Catal. A: Chem.*, **2005**, 231, 197.
- Ibrahim, M. N., Sharif, S. E. A., *E-J. Chem.*, **2007**, 4, 531.
- Sharafudeen, K. N. and Chandrasekharan, K., *Optics Commun.*, **2012**, 10, 1016.

Received: 07.02. 2012.

Accepted: 07.03. 2013.

BEHAVIOUR OF 4-(4-ACETYLAMINOPHENYL)-4-OXO-BUT-2-ENOIC ACID TOWARDS NUCLEOPHILES AND SYNTHESIS OF VARIOUS N-HETEROCYCLES

Maher A. El-Hashash^{[a]*} and Sameh. A. Rizk^[a]

Keywords: (E)-4-aryl-4-oxo-2-butenic acid, thiophenone, furanone, benzofuranone, thiadiazole, pyridazinone, 1,2-oxazolone, benzoxazinone, quinazolinone, pyrrole, pyrazole, 1,2,4-triazine

The present work deals with the reaction of 4-(4-acetylaminophenyl)-4-oxobut-2-enoic acid (**1**) with sulfur reagents, e.g. thiophenol at different acidity of medium, phenol in the presence of concd. sulfuric acid, and phosphorous pentachloride to afford the corresponding adducts **2-6**. Reaction of the latter compounds with different electrophilic and nucleophilic reagents yields some important heterocyclic derivatives.

* Corresponding Authors

E-Mail: samehrizk2006@gmail.com

[a] Department of Chemistry, Faculty of Science, University of Ain Shams, Cairo, Egypt.

Introduction

(E)-4-Aryl-4-oxo-2-butenic acids have been shown that convenient polyelectrophilic reagents in the synthesis of heterocyclic rings for which the addition reaction of N-, S-, P- and C-nucleophiles¹⁻³ occur exclusively at the α -carbonyl electrophilic center of the molecules.

Also, they exhibit abroad spectrum of physiological activities,⁴ Alzheimer,⁵ their esters as intermediate in the field of medical science, agriculture, and perfume.⁶ The substitution pattern on the aroyl moiety influences the antiproliferative activity against the human cervix carcinoma (Hela cells)⁷ and they have activated double bond, half-wave reduction potentials ($E_{1/2}$)⁸ display good correlations with Hammett sigma value, attempts to obtain good correlations using frontier orbitals of the molecules.

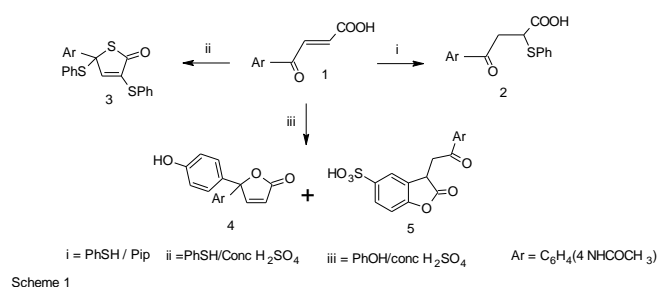
Also, they have emerged the most promising drug candidates⁹ which are selective for integrase S-1360¹⁰ and class of Human immunodeficiency virus type-1 (HIV-1) integrase inhibitors,¹¹ cytostatic activity used as an aid to study and determine factors affecting the human eye's UV filters,¹² as *Aspergillus* controller¹³ and inhibitors of phospholipase^{14a} and anticancer.¹⁵

They are used a key starting material due to their high electrophilicity, they react readily with nucleophiles including nitrogen and carbon nucleophiles afford either cyclic or normal Michael adducts.

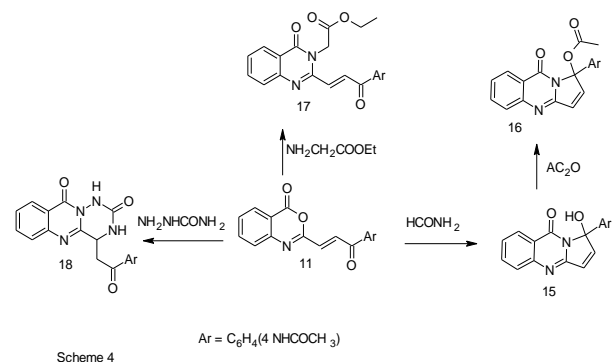
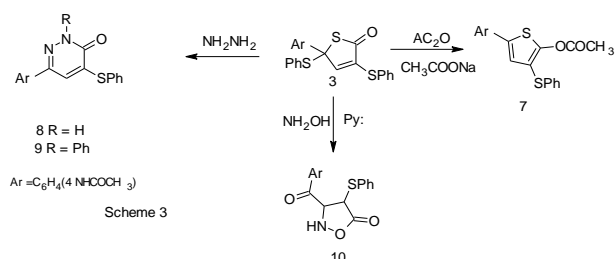
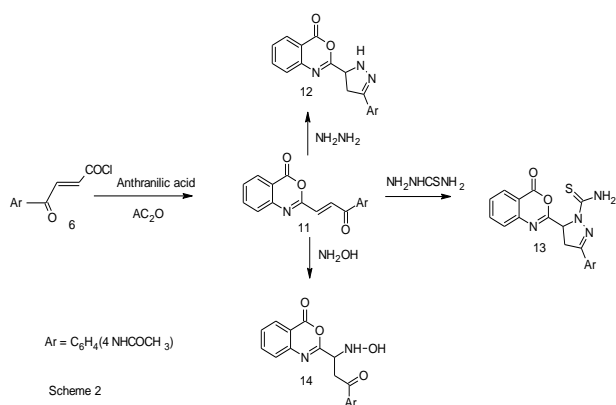
Hence, keeping these reports in view we continue our researches¹⁶ in the field of 4-(4-acetylaminophenyl)-4-oxo-2-butenic acid derivatives.

Results and Discussion

The structure of adducts that produced *via* the reaction of 4-(4-acetylaminophenyl)-4-oxo-2-butenic acid (**1**) and thiophenol was depended on acidity of the medium. So, when the acid **1** was allowed to react with thiophenol^{14,16} in the presence of few drops of piperidine (under Michael reaction condition, alkaline medium) afforded the adduct, 4-(4-acetylaminophenyl)-4-oxo-2-phenylmercapto-butanic acid (**2**). That to be differed from the behavior of the acid **1**, when it was allowed to react with thiophenol in the presence of concd. H₂SO₄ (acidic medium) afforded 2,4-diphenylmercapto-2-(4-acetylaminobenzoyl)thiophen-5-one (**3**), *via* the adduct **2** as outlined (Scheme1). Moreover, when 3-(4-acetylaminophenyl)-4-oxo-2-butenic acid (**1**) with phenol in the presence of concd. H₂SO₄ yielded¹⁴ a mixture of 2-(4-hydroxyphenyl)-2-(4-acetylaminophenyl)-5-oxofuran (**4**) and 2-oxo-3-(2-oxo-2-(4-acetylaminophenyl)ethyl)-5-benzo[b]-furan-5-sulphonic acid (**5**)



When 4-(4-acetylaminophenyl)-4-oxobut-2-enoic acid (**1**) was allowed to react with phosphorous pentachloride afforded 4-(4-acetylaminophenyl)-4-oxobut-2-enoyl chloride (**6**) as key starting material for synthesis some important heterocycles (Scheme 2).



The thiophenone **3** can be allowed to react with some electrophilic and nucleophilic reagents. Thus, it was treated with acetic anhydride in the presence of sodium acetate, hydrazine hydrate and hydroxylamine in boiling pyridine, which afforded thiophene ester **7**, pyridazinone derivatives **8** and **9** and isoxazolone derivative **10**. (Scheme 3).

The present work has succeeded in the synthesis of a series of some important heterocycles from 4-acetamido phenyl-4-oxo-2-butenic acid and in the synthesis of benzoxazinone derivative bearing α,β -unsaturated ketone moiety on aromatic substituents in the position 2, that enhances the reactivity of benzoxazinone moiety towards nitrogen nucleophiles.^{16c} Thus, when acid chloride **6** was allowed to react with anthranilic acid in the presence of acetic anhydride, it afforded benzoxazinone **11**. Reaction of the latter compound with hydrazine hydrate, thiosemicarbazide and hydroxylamine afforded 3-benzoxazinyl pyrazole derivatives **12**, **13** and hydroxylamino benzoxazinone **14** (Scheme 2).

Another aspect was the synthesis of novel quinazoline derivatives. When the benzoxazinone **11** was allowed to react with formamide, it yielded pyrrolo[1,2-b]quinazolinone **15** that was confirmed chemically by its reaction with acetic anhydride to give compound **16**. Moreover, reaction of benzoxazinone **11** with ethyl glycinate and semicarbazide afforded quinazolinone **17** and 1,2,4-triazine **18**, respectively (Scheme 4).

Experimental

All melting points are uncorrected and were determined on a Stuart electric melting point apparatus. Elemental analyses were carried out at the Microanalytical Center, National Research Center, Cairo, Egypt by Elemental Viro El Microanalysis. IR spectra (KBr) were recorded on infrared spectrometer FT-IR 400D using OMNIC program and are reported in terms of cm⁻¹. ¹H-NMR spectra were recorded on a Bruker spectrophotometer at 400 MHz using TMS as internal standard and with residual signals of the deuterated solvent $\delta=7.26$ ppm for CDCl₃ and $\delta=2.51$ ppm for DMSO-d₆. ¹³C-NMR spectra were recorded on the same spectrometer at 100 MHz and referenced to solvent signals $\delta=77$ ppm for CDCl₃ and $\delta=39.50$ ppm for DMSO-d₆. DEPT 135 NMR spectroscopy was used where appropriate to aid the assignment of signals in the ¹H spectrum. The mass spectra were recorded on Shimadzu GCMS-QP-1000 EX mass spectrometer at 70 eV using the electron ionization technique. Homogeneity of all compounds synthesized was checked by TLC.

General Procedure for the Preparation of Compounds 3

An equimolar mixture of compound **1** (2.35 g; 0.01 mol) and thiophenol (1 mL, 0.01 mol) in the presence of few drops piperidine in 30 mL benzene. The reaction mixture was refluxed for 3 h. The solid that separated after cool was filtered off, washed by petroleum ether (b.p 40-60 °C), dried and then, crystallized from ethanol.

2,4-Bis(phenylmercapto)-2-(4-acetylamino)thiophen-5-one (**3**)

Yield 74%. M.p. 150-152 °C. IR(KBr) 1613 (C=N), 1650, 1670, 1689 (CO). ¹H NMR (DMSO): δ 2.5(s, 3H, CH₃), 6.65 (s, 1H, proton of thiophene moiety), multiplet at 7.47-8.05 assigned for 14 ArH aromatic protons, acidic proton 13.1 a OH=NH proton exchanged in D₂O and Anal.: calcd. for C₂₄H₁₉NO₂S₂: C 66.82, H 4.40 N 3.24; found: C 66.75, H 4.33 N 3.10. MS: m/z 434, 431 [M], 373 [M-(NHCOCH₃)], 236 [373-(PhSCH=CH₂)].

General Procedure for the Preparation of Compounds 4 and 5

An equimolar mixture of compound **1** (2.35 g; 0.01 mol) and phenol (1g, 0.01 mol) in the presence of concd. H₂SO₄ (2 mL) in 30 mL methanol. The reaction mixture was refluxed for 3 h. The solid that separated after cool was filtered off, washed by petroleum ether (b.p. 40-60 °C), dried and then, crystallized from benzene afford **4** and ethanol afford **5**.

2-(4-Hydroxyphenyl)-2-(4-acetylamino-phenyl)-5-oxo-furan (4)

Yield 70%. M.p. 180-182 °C. IR(KBr) 1600 (C=C), 1650, 1720 (CO), 3314 (NH), 3427 (OH). ¹H NMR (DMSO): δ 2.5(s, 3H, CH₃), multiplet at 7.35 – 7.92 assigned for 10 ArH aromatic and olefinic protons, acidic protons at 13.1 OH and NH protons exchanged in D₂O and aAnal: calcd. for C₁₈H₁₅NO₄: C 69.90, H 4.85; found: C 69.75, H 4.67. MS: m/z 309 [M], 265 [M-CO₂], 248 [M-(CH₃CO+H₂O)], 175

2-Oxo-3-(2-oxo-2-(4-acetylamino-phenyl))ethyl-5-benzo[b]furan-sulphonic acid (5)

Yield 35%. M.p. 150-152 °C, IR(KBr) 3354 νNH, 2212 νCN, 1655, 1678, (cyclic amide and carboxyl group), and νC=N 1628. The EI-MS shows the molecular ion peak at m/e 392 and 389 corresponding to (M+2)⁺ (M⁺), respectively. Anal. for C₁₈H₁₅NO₇S: calcd: C 55.52, H 3.85; found: C 55.44, H 3.80.

3-(4-Acetylamino-phenyl)-4-oxobut-2-enoyl chloride (6)

A solution of 3-(4-acetamidobenzoyl)-prop-2-enoic acid (2.35 g; 0.01 mol) in phosphorous oxychloride (15 mL) was treated with PCl₅ (3 g; 0.015 mol). The reaction mixture was refluxed for 2 h. The solid that separated out on cooling was filtered off, washed with petroleum ether (b.p. 40-60 °C) and dried. Yield: 70%; M.p. 110-112 °C; IR (KBr) 1645, 1690, 1790 (CO); Anal.: calcd. for C₁₂H₁₀NO₃Cl: C 57.37, H 3.89; found: C 57.25, H 3.80.

Methyl-5-(4-acetylamino-phenyl)-2-thiophenate ester (7)

A mixture of **3** (0.01 mol), acetic anhydride (9.4 mL, 0.1 mol), and anhydrous sodium acetate (2 g) was refluxed on water bath for 2 h. The excess acetic anhydride was removed by distillation and the reaction mixture was poured onto ice/H₂O. The separated product was filtered, dried and were recrystallized from mixture of toluene-ethanol. Yield 75%. M.p. 130-132 °C. IR(KBr) 1640, 1762, 1843 (CO). ¹H NMR (DMSO-d₆): δ 2.1 (s, 6H, 2CH₃), 7.46-7.71 (m, 10H, Ar-H), 12.40 (brs, 1H, NH of acetamido moiety). Anal. calcd. for C₂₀H₁₇NS₂O₃: C 62.66, H 4.43, S 16.71; found: C 62.30, H 4.25, S 16.60 MS: m/z 325 [M-NH(O)COCH₃].

General Procedure for the Preparation of Compounds 8 and 9

A mixture of **3** (0.01 mol) and hydrazine hydrate and/or phenyl hydrazine (0.01 mol) in ethanol (40 mL) and was heated under reflux for 5 h. The reaction mixture was allowed to cool and the separated product was filtered, dried and were recrystallized from ethanol.

4-(Phenylmercapto)-6-(4-acetylamino-phenyl)-2,3-dihydro-pyridazin-3(2H)-one (8)

Yield: 70%. M.p. 230-232 °C. IR(KBr) 1640, 1687 (CO), 3285 (NH). ¹H NMR (DMSO-d₆): δ 2.5(s, 3H, CH₃), 7.35-8.00 (m, 10H, Ar-H and pyridazine), 11.90 (brs, 2H, NH of acetamido and pyridazinone moieties). Anal: calcd. for C₁₈H₁₅N₃SO₂: C 64.09, H 4.45, N 12.46, S 9.49; found: C 63.70, H 4.20, N 12.36, S 9.32. MS: m/z 337 [M], 307 [M-CH₂O], 262 [M-Ph group].

2-Pheny-4-(phenylmercapto)-6-(4-acetylamino-phenyl)-2,3-dihydropyridazin-3(2H)-one (9)

Yield: 60%. M.p. 212-214 °C. IR(KBr) 1640, 1700 (CO), 3279 (NH). ¹H NMR (DMSO-d₆): δ 2.1 (s, 3H, CH₃), 7.23-8.11 (m, 15H, Ar-H and pyridazine), 12.80 (brs, 1H, NH of acetamido moiety). Anal.: calcd. for C₂₄H₁₉N₃SO₂: C 69.73, H 4.60, N 10.16, S 7.74; found: C 69.50, H 4.30, N 9.86, S 7.52

3-(4-Acetylamino-benzoyl)-4-phenylmercapto-5-oxo-2,3,4,5-tetrahydro-1,2-oxazole (10)

A mixture of **3** (0.01 mol) and hydroxyl amine hydrochloride (1.03 g; 0.015 mol) in boiling pyridine (50 mL) and was heated under reflux for 6 h. The reaction mixture was allowed to cool, pour into ice/HCl and the product was filtered, dried, and were recrystallized from toluene. Yield 80%. M.p. 300 °C. IR(KBr) 1650, 1707, 1786 (CO), 3142 (NH). ¹H NMR (DMSO): δ 2.51 (s, 3H, CH₃), 4.87 (m, 2H, CH-CH oxazole system), multiplet at 7.63-8.00 assigned for 9 ArH aromatic protons, acidic protons 9.80 (s, 1H, NH of oxazole moiety) and 12.85 (s, 1H, NH of acetamido group), all acidic NH protons that exchanged in D₂O. Anal.: Calcd. for C₁₈H₁₆N₂SO₄: C 60.67, H 4.49, N 7.86, S 8.98; found: C 60.40, H 4.20, N 7.50, S 8.66.

2-[3-(4-Acetylamino-phenyl)-3-oxopropen-1-yl]-3,1-benzoxa-zin-4-one (11)

A solution of 3-(4-acetamidobenzoyl)-prop-2-enoic acid chloride **5** (2.5 g; 0.01 mol) and anthranilic acid (1.5 g; 0.01 mol) in 40 mL dry pyridine was refluxed for 3 h. The reaction mixture poured into ice/HCl, the solid that separated was filtered off, dried and recrystallized from ethanol. The anthranil product was refluxed with Ac₂O (5mL) for 1 h to afford **16**. Yield 75%; m.p. 130-152 °C; IR (KBr) 1660, 1683 (CO anthranil), 1780 (CO), 3220 (NH); ¹H NMR (DMSO-d₆): δ 2.5 (s, 3H, CH₃), 7.46-8.11 (m, 10H, Ar-H and olefinic), 12.40 (brs, 1H, NH of acetamido moiety) and Anal.: calcd. for C₁₉H₁₄N₂O₄: C 68.26, H 4.19, N 8.38; found: C 68.00, H 4.13, N 8.00.

2-[5-(4-Acetylamino-phenyl)-2,3,4-trihydropyrazol-3-yl]-3,1-benzoxazin-4-one (12)

A mixture of **11** (0.01 mol) and hydrazine hydrate (0.01 mol) in ethanol (50 mL) was heated under reflux for 5 h. The reaction mixture was allowed to cool and the product was filtered off, dried and recrystallized from ethanol. Yield 70%; m.p. 150-152 °C; IR(KBr) 1709, 1731 (CO), 3319 (NH); ¹H NMR (DMSO-d₆): δ 2.5 (s, 3H, CH₃), 3.2 (m, 4H, CH₂-CH-NH), 7.46-8.11 (m, 8H, Ar-H), 12.40 (brs, 1H, NH of acetamido moiety). Anal.: calcd. for C₁₉H₁₆N₄O₃: C 65.51, H 4.60, N 16.09; found: C 65.38, H 4.50, N 16.30.

2-[5-(4-Acetylamino-phenyl)-2-thiocarbamido-2,3,4-trihydro-pyrazol-3-yl]-3,1-benzoxazin-4-one (13)

A mixture of **11** (0.01 mol) and thiosemicarbazide (0.01 mol) in ethanol (50 mL) was heated under reflux for 5 h.

The reaction mixture was allowed to cool and the product was filtered off, dried and recrystallized from ethanol. Yield 70%; m.p. 112-114 °C; IR (KBr) 1709, 1735 (CO), 3423 (NH). ¹H NMR (DMSO-d₆): δ 2.5 (s, 3H, CH₃), 3.4 (m, 3H, CH₂-CH), 7.46-8.11 (m, 8H, Ar-H), 12.40 (brs, 3H, NH of acetamido and thioamide moieties) and Anal.: calcd. for C₂₀H₁₇N₅O₃: C 58.96, H 4.17, N 17.19; found: C 58.70, H 4.00, N 17.00.

2-[3-(4-Acetylamino)phenyl]-3-oxo-1-hydroxyaminopropan-1-yl]-3,1-benzoxazin-4-on (14)

A mixture of **11** (0.01 mol) and hydroxylamine hydrochloride (1.03 g; 0.015mol) was dissolved in boiling pyridine (50 mL) and heated under reflux for 6 h. The reaction mixture was allowed to cool, pour into ice/HCl, the product was filtered off, dried and recrystallized from dioxane. Yield: 70 %; M.p. 155-158 °C; IR (KBr) 1645, 1722 (CO), 3439 (NH) and (OH); ¹H NMR (DMSO-d₆): δ 2.1 (s, 3H, CH₃), 3.2 (m, 5H, CH₂CH-NHOH), 7.46-8.11 (m, 8H, Ar-H), 12.40 (brs, 1H, NH of acetamido moiety). Anal.: calcd. for C₁₉H₁₇N₃O₅: C 62.12, H 4.63, N 11.44; found: C 62.00, H 4.43, N 11.26.

1-Hydroxy-1-(4-acetylamino)phenyl-9-oxo-1,9-dihydropyrrolo[2,1-b]quinazoline (15)

A mixture of **11** (0.01 mol) and formamide (30 mL) and was heated under reflux for 3h. The reaction mixture was allowed to cool and pour into iced water. The product was filtered off, dried and recrystallized from ethanol. Yield 65 %; M.p. 185-187 °C; IR (KBr) 1660, 1716 (CO), 3438 (NH and OH); ¹H NMR (DMSO-d₆): δ 2.5 (s, 3H, CH₃) 5.5 (s, 1H, OH), 7.55-8.11 (m, 10H, Ar-H and pyrrole), 12.40 (brs, 1H, NH of acetamido group). Anal.: calcd. for C₁₉H₁₅N₃O₃: C 68.46, H 4.50, N 12.61; found: C 68.60, H 4.60, N 12.70.

1-Acetoxy-1-(4-acetylamino)phenyl-9-oxo-1,9-dihydropyrrolo[2,1-b]quinazoline (16)

A mixture of **15** (0.01 mol) and acetic anhydride (30 mL) was heated under reflux for 3 h. The reaction mixture was allowed to cool and pour into iced water. The product was filtered off, dried and recrystallized from ethanol. Yield 70%; m.p. 165-167 °C; IR (KBr) 1660, 1744, 1771 (CO), 3202 (NH). ¹H NMR (DMSO-d₆): δ 2.5 (s, 6H, 2CH₃) 7.55-8.11 (m, 10H, Ar-H and pyrrole), 12.40 (brs, 1H, NH of acetamido group) and Anal. Calc. for C₂₁H₁₇N₃O₄: C 67.20, H 4.53, N 11.20; found: C 67.30, H 4.60, N 11.30.

Ethyl 2-(2-(3-(4-acetylamino)phenyl)-3-oxopropen-1-yl)-4-oxoquinazolin-3(4H)-yl)acetate (17)

A mixture of **11** (0.01 mol) and ethyl glycinate (1.03 g ; 0.015 mol) was dissolved in boiling pyridine (50 mL) and heated under reflux for 6 h. The reaction mixture was allowed to cool, pour into ice/HCl, the product was filtered off, dried, and recrystallized from dioxane. Yield 75 %; M.p. 110-112 °C; IR (KBr) 1645, 1720, 1745 (CO), 3474 (NH); ¹H NMR (DMSO-d₆): δ 1.32 (t, 3H, CH₃), 2.1 (s, 3H, CH₃), 4.2 (q, 2H, CH₂), 5.1 (s, 2H, NCH₂CO), 7.46-8.11 (m, 10H, Ar-H and olefinic), 12.40 (brs, 1H, NH of acetamido moiety). Anal.: calcd. for C₁₉H₁₇N₃O₅: C 65.87, H 5.01, N 10.02; found: C 65.60, H 4.83, N 10.26.

1-(4-Acetylamino)phenyl)acetyl-3,4-dioxo-1,3,4-triazino[4,5-b]quinazoline (18)

A mixture of **11** (0.01 mol) and semicarbazide (1.03 g; 0.015 mol) was dissolved in boiling pyridine (50 mL) and heated under reflux for 6 h. The reaction mixture was allowed to cool, pour into ice/HCl, the product was filtered off, dried and were recrystallized from dioxane. Yield 80 %, M.p. 215-217 °C; IR (KBr) 1645, 1688 (CO), 3397, 3207 (NH); ¹H NMR (DMSO-d₆): δ 2.1 (s, 3H, CH₃), 7.46-8.00 (m, 10H, Ar-H and olefinic), 12.40 (brs, 4H, NH of acetamido and urea precursors). Anal.: calcd. for C₂₀H₁₇N₅O₄: C 61.38, H 4.34, N 17.90; found: C 61.40, H 4.43, N 17.70.

Conclusion

The present work studied the effect of the pH on the behavior of 4-(4-acetylamino)phenyl-4-oxo-but-2-enoic acid towards sulphur, carbon and nitrogen nucleophiles, producing a series of some important heterocycles, pyridazinone, benzoxazinone and quinazolinone derivatives bearing hetaryl moiety that enhances the biological effect many-fold as compared to their parent nuclei.

References

- Khachatryan, R. A., Khachatryan, R. J., Karamyan, N. V., Pansoyan, G. A. and Indzhikayan, M. G., *Chem. Heterocycl. Compd.*, **2004**, 40(4), 446-451.
- Koehler, T., Heinisch, M., Kirchner, M., Peindhardt, G., Hirschelmann, R., Nuhn, P., *Biochem. Pharmacol.* **1992**, 44(4), 805-813.
- Kolos, N. N., Kovalenko, L. Y., Shishkina, S. V., Shishkin, O. V. and Konovalova, I. S., *Chem. Heterocycl. Compd.* **2007**, 43(11), 1392-1405
- Khachikyan, D. R., Tovmasyan, N. V. and Indzhikyan, M. G., *Russ. J. Gen. Chem.* **2005**, 75(12) 1895-1898.
- Vitorovic, M. D., Juranic, I. O., Mandic, L. M. and Drakulic, B. J., *Bioorg. Med. Chem.*, **2010**, 18, 1181-1193.
- Onoue, K., Shintou, T., Zhang, C. and Isamu, I., *Chem. Lett.* **2006**, 35(1), 22-23
- Juranic, Z., Stevovic, L., Drakulic, B., Stanojkovic, T., Radulovic, S., Juranic, I. O., *J. Serb. Chem. Soc.* **1999**, 64, 505-512.
- Pastor, F. T., Drakulic, B. J., *Tetrahedron Lett.*, **2010**, 51, 734-738.
- Neamati, N. *Expert. Opin. Ther. Pat.*, **2002**, 12, 709.
- Billich, A., *Curr. Opin. Invest. Drugs*, **2003**, 4, 206.
- Cedric, M., Fabrice, B., and Philippe, C., *Tetrahedron*, **2004**, 60, 6479-6486
- Taylor, L. M., Aquilina, J. A., Jamie J. F. and Truscott, R. J. W., *Exp. Eye Res.*, **2002**, 75, 165.
- Volonterio A., Arellano, C. R. and Zanda, M., *J. Org. Chem.*, **2005**, 70, 2161.
- a) Koehler, T., Friedrich, G. and Nuhn, P., *Pharm.Chem. Martin-Luther Univ.*, **1991**, 32(1-2), 70-72.
- b) Pant, U. C., Upreti, M., Pant, S., Dandia, A., Pantai, G. K. and Goel, A. K., *Phosph. Sulf. Silicon Relat. Elem.*, **1997**, 126, 193-199.
- Takayanagi, H., Kitano, Y., Yano, T., Umeki, H., Hara, H., *Can. Pat. Appl.*, CA 2114333, **1994**;

- a) El-Hashash, M. A., Rizk, S. A., and Aburzeza, M. M., *Egypt. J. Chem.* **2011**, *54*, 3;
- b) Rizk, S.A. El-Hashash, M.A., Mostafa, K.K. *Egypt. J: Chem.*, **2008**, *51(5)* 116-121;
- c) El-hashash, M. Soliman, A., Madkour, M., *Rev. Roum. Chim.*, **1993**, *38(8)*, 955;
- d) Rizk S. A.. *Am. J. Chem.* **2011**, *1(1)*, 66-72 DOI: 10.5923/j.chemistry.20110101.01.
- e) El-Hashash, M. A., Rizk, S. A., El-Bassiouny, F. A., Darwish, K. M., *Chem. Process. Eng. Res.*, **2012**, *2*, 1032-1051.

Received: 12.02.2013.

Accepted: 10.03.2013.



ASSESSMENT OF TANNERY EFFLUENT: A CASE STUDY OF KANPUR IN INDIA

Akhand Pratap Singh^[a] and Devendra Pratap Rao^{[a]*}

Keywords: tannery, pollution, BOD, industry, potassium permanganate (KMnO₄)

The tannery effluent collected at monthly interval from January 2011 to December 2011 and analyzed for its characteristics. Samples were collected from one of the tannery from Jajmau area of Kanpur city of India. Results of the analysis showed that presence of addition chemical load like iron, calcium, magnesium, carbonate, bicarbonate, chloride and BOD were found in the discharged effluent of the above stated tannery. The analysis of various physical and chemical characteristics of tannery effluents showed variations according to month and results reveals that these are certain relationships between physico-chemical characteristics of effluents both positive and negative.

* Corresponding Author

E-Mail: devendraprataprao@yahoo.com

[a] Department of Chemistry, D.A-V. P.G. College, Kanpur-208001, U.P., India.

In the present study an attempt has been made to correlate chemical properties of polluted water discharged from tannery.

Introduction

In global scenario, Kanpur is the top and famous for tannery industries. The Kanpur city is also known for their pollution in the world. The main reason of the pollution in Kanpur is due to the Tannery. Only about 20% of the chemicals used in the tanning process are absorbed by leather. Rest of these are released as waste, which is absorbed by bioaccumulation process in cultivated crops.^{1,2} The wastes from the tannery consist of tanned and untanned solids, waste effluents, and waste gases.³ Environmental pollution is one of the major problems of the world which increases day by day due to urbanization and industrialization. Over the last few decades, large scale usage of chemicals in various human activities has grown very fast, particularly in a country like India.⁴ Ground water is of great importance for potable water supply and also serves for the agricultural irrigation and industrial production. Ground water resources are experiencing an increasing threat of pollution coming from urbanization, industrial development and agricultural activities.⁵ The global water pollution due to the increase in number of industries is a serious problem faced by the modern world.⁶ Release of the effluents in the receiving water is the major reason for water pollution. These pollutants find their way to aquatic ecosystem such as rivers and ponds and lakes, which pose a risk to the health of human and ecosystem.⁷ Almost all industries discharge water containing wastes in one stage or another during their manufacturing process. Industrial waste is not the same in every case. As a result the presence of pollutants in water alters different physico-chemical parameters from their normal prescribed levels.⁸ Negative impacts on water quality includes increase in turbidity, colour, nutrient load, addition of toxic and persistent compounds.⁹ The diversity in physical, chemical, and biological characteristics of tannery effluent is so much that each effluent habitat requires a separate study.

Materials and Experimental Methods

Samples and sampling sites

Samples were taken from one of the tannery from Jajmau area of Kanpur city of India. The study was conducted by a series of following tasks: (i) visit to tanneries and surrounding areas and (ii) on-site assessments and interviews with relevant personnel including workers, managers and other stakeholders.

The samples of effluent were collected from tannery for one month intervals from the spots fixed. The samples were collected in glass bottle (1.0 litre) and were corked immediately. All the samples were brought to the laboratory and stored at 4 °C temperatures in refrigerator till the analyses were completed. All chemical analyses were done in evening or the following days. All four or five samples of different sites were combined to get an integrated sample of the water. This sample was used for the tests given below. The sampling procedure was the same as described in Indian standard methods of sampling and test for water used in industries, I.S.I. New Delhi, India.

The physical and chemical characteristics analyzed for the effluents were colour, temperature, pH, carbonate, bicarbonate, chloride, total alkalinity, nitrite, total hardness, alkaline hardness, total solids (TS), total dissolved solids (TDS), total suspended solids (TSS), dissolved oxygen (DO), oxygen consumed by potassium permanganate, BOD, calcium, chromium, potassium, magnesium, phosphorus, sulfur, nitrogen, iron, and manganese. The pH and temperature measurements were performed for each of the above given components were the same as described in IBH hand book No.-8,¹⁰ USDA hand book no.-60,¹¹ and Laboratory methods for blue green algae.¹² Standard methods for sampling and test for water used in industries,

ISI New Delhi is 2490¹³ and as earlier used by Mohan.¹⁴ The correlations between various characteristics of effluent tested were worked out. The concentration of dissolved oxygen (DO) present in effluent samples was estimated by Winkler method. The alkalinity was analyzed by titrating against sodium thiosulfate using as indicator.¹⁵ The BOD, TDS, and TS determination of effluent samples were carried out using standard methods.¹⁶ The determination of COD was carried out according to Ademoroti.¹⁷

All data were statistically analyzed and tested for significance at 5% and 10% probability levels. For significant and highly significant 'r' values respectively one and two asterisks have been used.

Results and Discussion

The physico-chemical characteristics of the tannery effluent were found to be highly variable monthly (Table 1). The following relationships between the characteristics were found (Table 2).

Positive correlation-ships

Positive correlation-ships were observed between temperature with nitrite; pH with each total solids, total chromium, dissolved oxygen and oxygen consumed by KMnO₄; carbonate with each bicarbonate, chloride, total hardness, alkaline hardness, total solids and total suspended solid; bicarbonate with each chloride, total hardness, alkaline hardness and total solids, total dissolved solids and total suspended solids; chloride with each nitrite, total hardness, alkaline hardness, total chromium, total solids and total suspended solid; total alkalinity with each nitrite, total chromium and total dissolved solids; total hardness with each alkaline hardness, total solids, total dissolved solids and total suspended solid; nitrite with each total chromium, total dissolved solids and BOD; alkaline hardness with total suspended solid, total solid, total dissolved solid; total solids with each total dissolved solids, total suspended solid, dissolved oxygen and BOD; J.C. Akan et al. have also been studies a positive correlation between these parameters¹⁸ total dissolved solids with total suspended solid; dissolved

Table 1. The physico-chemical characteristics of the tannery effluent.

Period of sample	Characteristics of effluent												
	Colour	Temp. (°C)	pH	Carbonate	Bicarbonate	Chloride	Total alkalinity as CaCO ₃	Total Cr	Total hardness as CaCO ₃	Alkaline hardness as CaCO ₃	TS	TDS	TSS
Jan. 2011	Brown	23.7	5.2	3.1	2.0	277	1336	14.35	3500	710	1072	10460	625
Feb. 2011	Gray	24.0	4.6	2.3	1.5	341	1260	15.76	3400	670	741	10670	727
Mar. 2011	Brown	24.5	4.7	5.0	1.3	256	1372	13.70	2400	760	1062	10350	635
Apr. 2011	Light Brown	22.5	5.9	5.4	4.9	275	1436	15.35	2700	570	1970	10675	725
May. 2011	Brown	30.6	4.8	4.3	5.7	293	1251	16.65	2500	630	1862	10255	875
Jun. 2011	Brown	32.0	3.7	5.1	1.2	234	1382	13.75	2400	550	1859	10560	805
Jul. 2011	Brown	27.0	4.8	4.3	3.9	283	1347	14.25	2960	578	2065	10670	887
Aug. 2011	Brown	29.4	4.6	5.2	4.1	267	1293	16.65	3400	560	1852	10340	783
Sept. 2011	Brown	23.0	4.6	5.7	2.9	231	1380	12.76	2800	570	1870	10565	793
Oct. 2011	Brown	28.0	4.2	4.3	4.8	263	1140	16.35	2700	540	1472	10375	855
Nov. 2011	Gray	22.8	4.5	1.2	2.9	288	993	15.65	2600	630	769	10445	731
Dec. 2011	Deep Brown	20.7	4.9	1.7	5.7	267	1149	13.79	2630	576	842	10670	767

Table 1. (cont.)

Period of sample	Characteristics of effluent												
	Colour	DO	BOD	COD	[a]	Ca	K	Mg	P	S	N	Fe	Mn
		meq. L ⁻¹					mg L ⁻¹ effluent						
Jan. 2011	Brown	0.4	876	4435	2.3	575	489	385	375	240	2031	6.80	1.58
Feb. 2011	Gray	1.5	965	4485	3.2	595	665	380	145	162	1167	7.52	1.76
Mar. 2011	Brown	1.7	886	4815	1.6	535	940	364	276	292	1074	5.85	0.50
Apr. 2011	Light Brown	0.2	835	4515	1.6	575	689	362	256	264	1068	6.75	2.85
May. 2011	Brown	0.5	935	4456	2.2	650	849	385	194	83	1167	5.30	1.90
Jun. 2011	Brown	0.7	856	4845	2.7	535	972	364	183	635	1179	6.50	3.82
Jul. 2011	Brown	1.5	945	4879	2.3	570	764	352	62	84	1176	7.75	0.87
Aug. 2011	Brown	1.8	985	4750	3.2	556	872	379	182	182	1085	6.45	2.45
Sept. 2011	Brown	0.3	1125	4625	2.5	575	870	355	169	172	1065	5.70	1.40
Oct. 2011	Brown	0.6	945	4435	2.2	535	962	352	132	175	1165	7.30	0.80
Nov. 2011	Gray	1.2	958	4345	3.6	680	582	372	143	162	1056	5.45	2.30
Dec. 2011	Deep Brown	1.8	923	4390	2.1	570	868	342	147	252	1345	6.50	0.75

^a Oxygen consumed by KMnO₄ in 3 hrs.

Table 2. Correlation coefficients.

Variables	pH	CO ₃ ²⁻	HCO ₃ ⁻	Cl ⁻	Total Alkalinity	NO ₂ ⁻	Total Cr	Total Hardness	Alkaline Hardness	TS	TDS	TSS
Temp.	-0.88*	+0.79	+0.919*	+0.034	-0.256	+0.856*	+0.866*	-0.185	+0.133	+0.053	+0.034	-0.042
pH		-0.78	-0.693**	-0.577*	-0.357**	-0.542	+0.578	-0.764*	-0.978**	+0.787	-0.497	-0.878*
CO ₃ ²⁻			+0.882*	+0.877*	+0.166	+0.442	+0.645*	+0.787*	+0.977*	+0.844*	+0.388	+0.822*
HCO ₃ ⁻				+0.683*	+0.353	+0.387	+0.432	+0.876	+0.958*	+0.833*	-0.598	+0.897*
Cl ⁻					-0.022	+0.863*	+0.654*	+0.565	+0.787	+0.643*	+0.186	+0.586
Total Alkalinity						+0.577	+0.675	-0.553*	+0.296	+0.415*	+0.765	+0.544*
NO ₂ ⁻							+0.234	+0.528*	-0.615*	+0.966*	+0.616	+0.397
Total Cr								+0.342	+0.543	+0.675	+0.342	+0.345
Total Hardness									+0.822*	+0.875*	+0.565	+0.833*
Alkaline Hardness										+0.323	+0.434	+0.866*
TS											+0.612	+0.844*
TDS												+0.686*

Table 2 . (cont.)

Variables	DO	BOD	COD	O ₂ consumed by KMnO ₄	Ca	K	Mg	P	S	N	Fe	Mn
Temp.	-0.133	-0.155*	-0.078	-0.168	-0.279**	-0.412**	+0.292	-0.191	-0.143	+0.317	+0.435	-0.471**
pH	+0.858*	-0.038	-0.086	+0.953*	+0.257	+0.286*	+0.270	-0.313**	+0.032	+0.238	+0.317*	-0.196*
CO ₃ ²⁻	-0.978**	+0.044	+0.136	-0.957**	-0.375	-0.033	-0.191	+0.066	+0.062	-0.146	-0.456**	+0.126*
HCO ₃ ⁻	-0.986**	+0.231*	+0.326*	-0.945**	+0.355*	-0.434*	-0.218*	+0.171	+0.091	-0.383**	-0.494*	+0.124*
Cl ⁻	-0.822*	-0.066	-0.147	-0.202	+0.322*	-0.355**	-0.236*	-0.029	+0.031	-0.169	-0.459*	+0.178*
Total Alkalinity	-0.055	+0.244*	+0.068*	-0.076	+0.244	+0.075	+0.281	+0.328	+0.298*	-0.189*	-0.329*	+0.046
NO ₂ ⁻	+0.545*	+0.775*	+0.871*	-0.964**	-0.658**	-0.566**	-0.860**	-0.524**	-0.115	+0.139*	-0.937**	-0.581**
Total Cr	-0.678*	+0.256*	+0.045*	-0.784**	-0.765*	-0.756**	-0.645**	-0.657**	+0.432*	+0.875*	+0.835*	+0.463*
Total Hardness	-0.646	+0.075	+0.189	-0.724*	-0.197	-0.168*	-0.089	+0.143	+0.163	-0.211	-0.538**	+0.289*
Alkaline Hardness	-0.966*	+0.233*	+0.742*	-0.928**	-0.357**	-0.484**	+0.323*	+0.170	+0.071	-0.313*	-0.465**	+0.132
TS	+0.864*	+0.119	+0.267	-0.946*	-0.353**	-0.168	-0.260*	+0.152	+0.034	-0.150	-0.398**	-0.054
TDS	-0.478	+0.232*	+0.063*	-0.313	-0.256	-0.298*	+0.093	+0.459*	+0.169	+0.139	-0.186	-0.186*
TSS	-0.877*	+0.143*	+0.647*	-0.778**	-0.364**	-0.321*	-0.355*	+0.143	-0.093	+0.049	-0.511**	+0.128
DO		+0.044	-0.180	+0.957**	+0.357*	+0.313*	+0.244*	-0.094	-0.136*	+0.228*	+0.486*	+0.045
BOD			+0.357*	-0.132	-0.063	+0.068	+0.051	+0.112	+0.029	+0.061	+0.262	+0.126
COD				+0.243	+0.087	+0.352*	+0.675*	+0.142*	-0.812**	+0.087	+0.176*	+0.064
O ₂ cons. ^a					+0.322*	+0.290*	+0.280*	-0.022	+0.032	+0.384*	-0.378*	-0.197
Ca						+0.592*	+0.568*	+0.186	+0.651*	+0.271*	+0.025	+0.434*
K							-0.134*	-0.061	+0.184	+0.255	+0.183	+0.126
Mg								+0.514*	+0.759*	+0.275	+0.358*	+0.386*
P									+0.487*	+0.219*	+0.296*	+0.519*
S										-0.071	-0.290**	+0.433*
N											-0.045	-0.097
Fe												+0.079

^a O₂ consumed by KMnO₄.

oxygen with oxygen consumed by KMnO_4 ; calcium with each potassium, phosphorus, nitrogen, iron, magnesium and sulfur; magnesium with sulfur, nitrogen, iron and manganese.

Negative correlation-ships

Negative correlation-ships were observed between pH with each carbonate, bicarbonate, chloride, total hardness, alkaline hardness, total dissolved solids and total suspended particles; carbonate with dissolved oxygen calcium potassium, magnesium, nitrogen, iron and oxygen consumed by KMnO_4 ; chloride with potassium, magnesium, phosphorus, dissolved oxygen, oxygen consumed by KMnO_4 , and BOD; nitrite with each oxygen consumed by KMnO_4 , potassium, magnesium, phosphorus, sulfur, iron and manganese; total solids with oxygen consumed by KMnO_4 , calcium, potassium, magnesium, nitrogen, iron and manganese. Similar results have also observed by Piyush et al. during their study of impact of distillery effluent on seed germination behaviour.¹⁹

Conclusion

The assessment of the tannery industry effluent is carried out and observed that the tannery industry effluent was brown, turbid, and had an offensive odour. The pH of the effluent was found to be in acidic range. The physical parameters studied in the effluent namely total hardness, total suspended and dissolved solids were at higher level. The chemical parameters namely COD, BOD, carbonate, bicarbonate, calcium, magnesium, chloride, potassium, nitrite, sulfur, and chromium, is found to be much above the permissible limits prescribed by the Bureau of Indian Standards (2009). Tanneries pollution readily accelerates to cause deterioration in ground water quality. The poor quality of water resists its use for our daily life and also for aquatic life. This study will helpful for developing new techniques for the treatment of effluent.

Acknowledgements

The authors are thankful to the Secretary, Board of Management, D.A-V. P.G. College, Kanpur, U.P., India for providing laboratory facilities and department of chemistry for various equipments.

References

- ¹Sahu, R. K., Katiyar, S., Yadav, A. K., Kumar, N., Srivastava, J., *CLEAN Soil Air Water*, **2008**, 36, 517.
- ²United Nations Industrial Development Organization, UNIDO, *Cost of Tanned Waste Treatment*, 15th Session of the Leather and Leather Products Industry Panel Leon, Mexico, **2005**.
- ³Ogbonna, J. O., Lawal, F. A., Owoeye, L. D., Udeh, M. U. "Chemical Characteristics and Fertilizing value of Primary Sludge from Tannery Effluent Treatment Plant", 6th Ann. Natl. Conf. Nigerian Inst. Sci. Technol. Univ. Ibadan, 24-27th, **2008**.
- ⁴Mustafa, S., Ahmad, T., Naum, A., Shah, K. H., Wassum, M., *Water, Air and Soil Pollution*, **2010**, 210, 43.
- ⁵Hema, S., Subramani, T., Elango, L., *I. J. Inv. Sci.*, **2010**, 1, 1.
- ⁶Ganesh, S., Baskaran, L., *Iranian J. Environmental Health Sci. Eng.*, **2009**, 6, 17.
- ⁷Rehman, A., Anjum, M. S., *Water, Air and Soil Pollution*, **2010**, 205, 149.
- ⁸Shamoune, M. N., Louhab, K., Boukhiar, A., *I. J. Environmental Res.*, **2008**, 3, 229.
- ⁹Ahmed, W. A., Zakaria, Z. A., Razali, F., Samin, J., *Water, Air and Soil Pollution*, **2009**, 204, 195.
- ¹⁰IBH Hand Book No. 8, "Method for Physical and chemical analysis of fresh waters," Blackwell Scientific Publications Oxford Edinburgh London Melbourne, **1978**.
- ¹¹Richards, L. A., "Diagnosis and improvement of saline and alkali soils," U. S. Salinity Laboratory Staff USDA Handbook No. 60, **1954**.
- ¹²Kaushik, B. D., *Proc. A.I.A.P.C. Kanpur*, **1987**, 60.
- ¹³Indian standard institution, New Delhi, "Tolerance limit for industrial effluents discharged into inland surface waters," IS: 2490 part-I, **1964**.
- ¹⁴Mohan, N., "Influence of water pollutants on algal flora," UGC, MRP 3-33/86 (SR-II), **1989**, 1.
- ¹⁵Trivedy, R. K., Goel, P. K., "Chemical and biological methods for water pollution studies," Environmental Publications, Kara", **1986**.
- ¹⁶APHA-AWWA-WPCF In: *Standard methods for the examination of water and waste water*. American Public Health Association, Washington, D. C 20th ed., New York, **2005**.
- ¹⁷Ademoroti C. M. A., "Standard method for water and effluents analysis," Foludex press Ltd, Ibadan, **1996**, 111.
- ¹⁸Akan, J. C., Ogugbuaja, V. O., Abdulrahman, F. I., Ayodele, J. T., *Global J. Pure and Applied Sci.*, **2009**, 15, 343.
- ¹⁹Malviya, P., Sharma, A., *J. Environmental Biology*, **2011**, 32, 91.

Received: 17.02.2013.

Accepted: 10.03.2013.



A CONVENIENT WAY FOR THE PREPARATION OF NOVEL THIOUREA DERIVATIVES CONTAINING BIOLOGICALLY ACTIVE QUINAZOLINE MOIETY

Sohail Saeed^{[a,b]*} and Rizwan Hussain^[b]

Keywords: Heterocyclic thiourea derivatives, quinazolin-4(3H)-one moiety, phenyl isothiocyanates

A series of new thiourea derivatives containing quinazolin-4(3H)-one framework (**3a-d**) was successfully synthesized and characterized by IR, ¹H NMR, ¹³C NMR spectroscopy, ESI mass spectrometry and elemental analysis. Variation in the functional group at the phenyl ring led to set of compounds bearing quinazolin-4(3H)-one accommodated substituted phenyl thioureas.

Corresponding Authors

Tel: + 0092-51 - 9250081

Fax: + 0092-51 - 9250081

E-Mail: sohail262001@yahoo.com

[a] Department of Chemistry, Research Complex, Allama Iqbal Open University, Islamabad-44000, Pakistan

[b] National Engineering & Scientific Commission, P.O. Box. 2801, Islamabad, Pakistan

Introduction

Thioureas are potentially very versatile ligands, able to coordinate to a range of metal centers as neutral ligands, monoanions or dianions.¹⁻⁹ In addition, the oxygen, nitrogen and sulfur donor atoms provide a multitude of bonding possibilities. The coordination chemistry of substituted thioureas has led to some interesting practical applications, including liquid-liquid extraction, pre-concentration and highly efficient chromatographic separation, fluorimetric detection of the platinum group metals, and the selective on-line pre-concentration of ultra-traces of Pd, followed by its determination using graphite furnace atom absorption spectrometry.^{10,11}

Thiourea and its derivatives have found extensive applications in the fields of medicine, agriculture and analytical chemistry. They are known to exhibit a wide variety of biological activities such as antiviral, antibacterial, antifungal,¹² antitubercular, herbicidal, insecticidal,¹³ and to act as chelating agents,¹⁴ in catalysis,¹⁵ in anion recognition¹⁶ and to play a role in some epoxy resin curing agents containing amino functional groups.¹²

Substituted thioureas are an important class of compounds, precursors or intermediates towards the synthesis of a variety of heterocyclic systems such as imidazole-2-thiones,¹⁷ 2-imino-1,3-thiazolines,¹⁸ pyrimidine-2-thiones and (benzothiazolyl)-4-quinazolinones¹⁹ N-(Substituted phenyl)-N-phenylthioureas have been developed as anion-binding sites in a hydrogen-bonding receptor,²⁰ calixarenes containing thioureas as neutral receptors towards α,α -dicarboxylate anions,²¹ and N-4-substituted-benzyl-N-*tert*-butylbenzyl thioureas as vanilloid receptor ligands and antagonists in rate DRG neurons.²² As part of our research on biological activity and coordination chemistry of thioureas,²³⁻³⁰ we are interested in the study of the influence

of non-covalent interactions, especially hydrogen bonds and π - π stacking interactions, on the coordination modes of thiocarbonyl donor groups with transition metal ions.

Since varying substituents is a common method for drug design in medicinal chemistry and a useful medical value of substituted thiourea derivatives containing quinazolin moiety, we aimed to synthesize new thiourea derivatives and to investigate their antimicrobial and antitumor activities. Based on these reports, we herein report the synthesis and characterization of a series of novel thiourea derivatives bearing quinazolin moiety. However, a thorough investigation relating structure and activity of thiourea derivatives and their stability under biological conditions is required.

Experiments

Chemicals and measurements

Synthetic starting material, reagents and solvents were of analytical reagent grade or of the highest quality commercially available and were purchased from Aldrich Chemical Co., Merck Chemical Co. and were dried when necessary. Melting points were recorded on Electrothermal IA9000 series digital melting point apparatus. The proton NMR and ¹³C spectra were recorded in DMSO-*d*₆ solvent on Jeol ECS- 400 and 300 MHz spectrophotometer using tetramethylsilane as an internal reference, respectively. The apparent resonance multiplicity is described as s (singlet), br s (broad singlet), d (doublet), dd (doublet of doublets), t (triplet), q (quartet) and m (multiplet). Infrared measurements were recorded in the range 400 - 4000 cm⁻¹ on spectrum 2000 by Perkin Elmer. Thin layer chromatography (TLC) analysis were carried out on 5 × 20 cm plate coated with silica gel GF₂₅₄ type 60 (25-250 mesh) using an ethyl acetate-petroleum ether mixture (1:2) as solvent.

Procedures for the synthesis of compounds (3a-d)

Intermediate-1 was synthesized by following the Niementowski hetero cyclization reaction of 2-amino-5-nitrobenzoic acid with benzoyl chloride using pyridine as a

solvent as reported earlier.³¹ Yielded intermediate-1 was followed by nucleophilic substitution reaction by using ethylene diamine as a nucleophile to yield intermediate-2. The synthesized intermediate-2 was dissolved in DMF and equimolar amount of the substituted phenyl isothiocyanate were added drop-wise to it and anhydrous acetone was also added in an equimolar amount. After the completion of the addition, the reaction mixture was refluxed for about 6-8 hours. The status of the reaction was monitored by TLC using ethanol: ethyl acetate (1.0: 9.0) as an eluent. After complete conversion, the reaction mixture was poured in crushed ice to separate the product. The obtained product was filtered, washed and dried.

1-[2-(6-Nitro-4-oxo-2-phenyl-4H-quinazolin-3-yl)-ethyl]-3-p-tolyl-thiourea (3a)

Elemental analysis for C₂₄H₂₁N₅O₃S (MW = 459.14) in wt % calc. C=62.73, H= 4.61, N=15.24, S=6.98 and found to be C= 62.75, H=4.68, N=15.25, S= 6.96. m.p. 175°C, yield 69 %. IR (KBr, cm⁻¹): 3352.68 (-NH str.), 1683.08 (C=O str.), 1504.75 (ArC-H str.), 1339.44 (-NO₂ str.), 1284.71 (C=S str.); ¹H NMR (400 MHz, DMSO-*d*₆, δppm): 12.35 (1H, s, -NH, exchangeable with D₂O), 10.84 (1H, s, -NH, exchangeable with D₂O), 7.03-8.86 (12H, m, Ar-H), 3.12 (2H, q, -CH₂), 2.79 (2H, t, -CH₂); 2.41 (3H, s, -CH₃); ¹³C NMR (300 MHz, DMSO-*d*₆, δppm): 166.47 (C=O), 165.79 (C=O), 145.25 (C=N, quinazolinone ring), 142.40 (C-NO₂), 135.49-120.67 (Ar-C), 41.54 (CH₂), 39.46 (-CH₂), 22.36 (-CH₃); TOF-MS (m/z): 460.34 (M+1, 12%), 144.20 (100%).

1-[2-(6-Nitro-4-oxo-2-phenyl-4H-quinazolin-3-yl)-ethyl]-3-m-tolyl-thiourea (3b)

Elemental analysis for C₂₄H₂₁N₅O₃S (MW = 459.14) in wt % calc. C=62.73, H= 4.61, N=15.24, S=6.98 and found to be C= 62.76, H=4.69, N=15.25, S= 6.95. m.p. 180-181 °C, yield 73%. IR (KBr, cm⁻¹): 3351.23 (-NH str.), 1683.19 (C=O str.), 1505.18 (ArC-H str.), 1339.34 (-NO₂ str.), 1284.47 (C=S str.); 1160.31 (C-N str.); ¹H NMR (400 MHz, DMSO-*d*₆, δppm): 12.29 (1H, s, -NH, exchangeable with D₂O), 10.78 (1H, s, -NH, exchangeable with D₂O), 6.92-8.92 (12H, m, Ar-H), 3.11 (2H, q, -CH₂), 2.77 (2H, t, CH₂); 2.51 (3H, s, -CH₃); ¹³C NMR (300 MHz, DMSO-*d*₆, δppm): 166.53 (C=O), 165.83 (C=O), 145.28 (C=N, quinazolinone ring), 142.37 (C-NO₂), 133.88-121.64 (Ar-C), 41.23 (CH₂), 39.83 (-CH₂), 22.61 (-CH₃); TOF-MS (m/z): 460.09 (M+1, 13%), 144.58 (100%).

1-[2-(6-Nitro-4-oxo-2-phenyl-4H-quinazolin-3-yl)-ethyl]-3-phenyl-thiourea (3c)

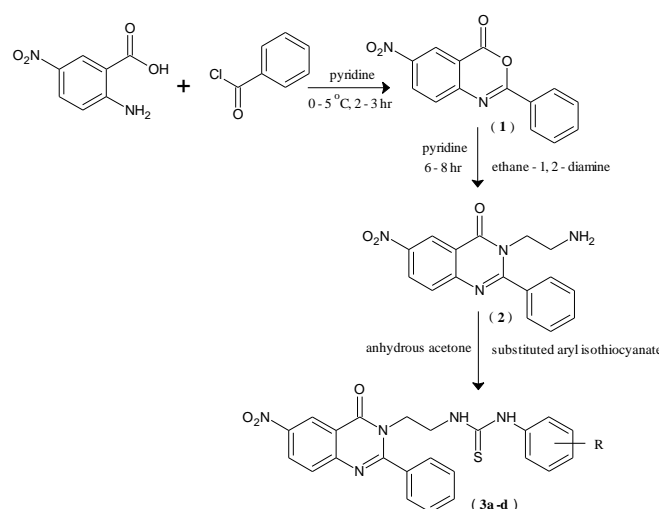
Elemental analysis for C₂₃H₁₉N₅O₃S (MW = 445.49) in wt % calc. C=62.03, H= 4.29, N=15.73, S=7.20 and found to be C= 62.06, H=4.33, N=15.71, S= 7.21. m.p. 208°C, yield 70.4 %. IR (KBr, cm⁻¹): 3352.88 (-NH str.), 1682.32 (C=O str.), 1504.80 (ArC-H str.), 1339.53 (-NO₂ str.), 1284.48 (C=S str.); ¹H NMR (400 MHz, DMSO-*d*₆, δppm): 12.06 (1H, s, -NH, exchangeable with D₂O), 10.87 (1H, s, -NH, exchangeable with D₂O), 7.13-8.81 (13H, m, Ar-H), 3.05 (2H, q, -CH₂), 2.83 (2H, t, -CH₂); ¹³C NMR (300 MHz, DMSO-*d*₆, δppm): 166.51 (C=O), 165.83 (C=O), 145.22 (C=N, quinazolinone ring), 142.37 (C-NO₂), 134.35-121.77 (Ar-C), 40.62 (-CH₂), 39.37 (-CH₂); TOF-MS (m/z): 445.42 (M+1, 14 %), 144.73 (100%).

1-[2-(6-Nitro-4-oxo-2-phenyl-4H-quinazolin-3-yl)-ethyl]-3-o-tolyl-thiourea (3d)

Elemental analysis for C₂₄H₂₁N₅O₃S (MW = 459.14) in wt % calc. C=62.73, H= 4.61, N=15.24, S=6.98 and found to be C= 62.73, H=4.64, N=15.25, S= 6.96. m.p. 182-183 °C, yield 89 %. IR (KBr, cm⁻¹): 3353.64 (-NH str.), 1685.20 (C=O str.), 1504.55 (ArC-H str.), 1340.11 (-NO₂ str.), 1284.58 (C=S str.); ¹H NMR (400 MHz, DMSO-*d*₆, δppm): 11.92 (1H, s, -NH, exchangeable with D₂O), 10.93 (1H, s, -NH, exchangeable with D₂O), 6.95-8.92 (12H, m, Ar-H), 2.72 (2H, t, -CH₂); 2.42 (3H, s, -CH₃); ¹³C NMR (300 MHz, DMSO-*d*₆, δppm): 1673.13 (2H, q, -CH₂), 49 (C=O), 166.73 (C=O), 145.19 (C=N, quinazolinone ring), 142.67 (C-NO₂), 132.82-121.86 (Ar-C), 40.57 (-CH₂), 39.43 (-CH₂), 21.96 (-CH₃); TOF-MS (m/z): 460.13 (M+1, 14%), 144.49 (100%).

Results and Discussion:

Quinazoline-4-one based derivatives were prepared by a series of reaction as illustrated in scheme. The intermediate-1 and intermediate-2 was synthesized by following the procedure reported earlier.³¹ Intermediate-3 was confirmed by C-O stretching of benzoxacine moiety observed at 1178 cm⁻¹ along with C=O stretching of cyclic ketone at 1772 cm⁻¹.



Scheme. Schematic diagram for the synthesis of target compounds (3a-d); 3a-d: R =3a= 3-CH₃, 3b; 4-CH₃, 3c; H, 3d; 2-CH₃

Reaction of intermediate-1 with ethylene diamine as a nucleophile leads to yield intermediate-2. Successful formation of intermediate-2 was confirmed by -NH₂ stretching frequencies observed at 3315 cm⁻¹ and disappearance of C-O stretching frequency at 1178 cm⁻¹. Reactions of the intermediate-2, [3-(2-aminoethyl)-6-nitro-2-phenylquinazolin-4(3H)-one], with different phenyl isothiocyanate derivatives were carried out by using DMF as a solvent along with equimolar amount of triethyl amine, resulted in the synthesis of final compounds (**Scheme**). ¹H NMR spectra of compound-3c revealed signals in the downfield region at 12.06 δppm and 10.87 δppm as a singlet indicating the presence of two protons of thiourea in the linkage at N3 position of quinazolinone moiety. Two aromatic protons adjacent to the -NO₂ group were observed in the downfield region between 8.81 to 8.66 δppm as a singlet and doublet, respectively. While remaining 11

aromatic protons were observed as a multiplet in the aromatic region between 7.13 to 7.92 δ ppm. In ^{13}C NMR spectra of final compound **3c**, two downfield peaks were obtained at 166.51 and 165.83 δ ppm, accounting for a C=S and C=O present in the compound, respectively. Carbon attached with Nitrogen heteroatom on both side in the quinazolinone moiety was observed in the downfield region at 145.23 δ ppm. Further the aromatic carbon attached with the nitro group was observed in the downfield region at 141.91 δ ppm. Peaks between 138.56-121.77 δ ppm were for the rest aromatic carbons. Peaks for aliphatic carbon present in the final structure were observed at 40.62 and 39.37 δ ppm.³²

References

- ¹Handerson, W., Nicholson, B. K., Dinger, M. B. and Bennett, R. L., *Inorg. Chim. Acta*, **2002**, 338, 210.
- ²Sacht, C.; Datt, M. S.; Otto, S. and Roodt, A. *J. Chem. Soc. Dalton Trans.*, **2000**, 4579.
- ³Lipowska, M.; Hayes, B. L.; Hansen, L.; Taylor, A. and Marzilli, L. G. *Inorg. Chem.*, **1996**, 35, 4227.
- ⁴Zuckerman, R. L. and Bergman, R. G. *Organometallics*, **2000**, 19, 4795.
- ⁵Henderson, W.; Kemmitt, R. D. W.; Mason, S.; Moore, M. R.; Fawcett, J. and Russell, D. R. *J. Chem. Soc. Dalton Trans.*, **1992**, 59.
- ⁶Arslan, H.; Külcü, N. and Flörke, U. *Trans. Metal Chem.*, **2003**, 32(7), 816-820.
- ⁷Binzet, G.; Arslan, H.; Flörke, U.; Külcü, N. and Duran, N., *J. Coord. Chem.*, **2006**, 59(12), 1395-1399.
- ⁸Ugur, D.; Arslan, H. and Külcü, N., *Russ. J. Coord. Chem.*, **2006**, 32(9), 669-6674.
- ⁹Emen, M.F.; Arslan, H.; Külcü, N.; Flörke, U. and Duran, N. *Polish. J. Chem.*, **2005**, 79(10), 1615-1620.
- ¹⁰Kemp, G., Roodt, A., Purcell, W. and Koch, K. R. *J. Chem. Soc. Dalton Trans.*, **1997**, 23, 4481-4483.
- ¹¹Koch, K. R., Sacht, C., Grimmacher T. and Bourne, S., *S. Afr. J. Chem.*, **1995**, 48 (1-2), 71.
- ¹²Saeed, S., Rahid, N., Tahir, A., Hussain, R. and Jones, P. G., *Acta Crystallogr.*, **2009**, E65, o2568-o2569.
- ¹³Zhang, Y. M.; Wei, T. B., Xian, L. and Gao, L. M. *Phosphorus, Sulfur Silicon Relat. Elem.*, **2004**, 179, 2007.
- ¹⁴Arslan, H., Duran, N., Borekci, G., Ozer, C. K. and Akbay, C. *Molecules*, **2009**, 14, 519-527.
- ¹⁵Gu, C.-L., Liu, L., Zhao, J.-L., Wang, D. and Chen, Y.-J. *Tetrahedron*, **2007**, 18, 455-463.
- ¹⁶Saeed, S., Bhatti, M. H., Yunus, U. and Jones, P. G., *Acta Crystallogr.*, **2008**, E64, o1369.
- ¹⁷D'hooghe, M., Waterinckx, A. and De Kimpe, N. *J. Org. Chem.*, **2005**, 70, 227-232.
- ¹⁸Jain, V. K. and Rao, J. T., *J. Inst. Chem. (India)*, **2003**, 75, 24-26.
- ¹⁹Lakhan, R. and Ral, B. J. *J. Chem. Eng. Data*, **1986**, 31, 501-502.
- ²⁰Saeed, A. and Parvez, M. *Cent. Eur. J. Chem.*, **2005**, 3(4), 780-791.
- ²¹Nie, L., Li, Z., Han, J., Zhang, X., Yang, R., Liu, W. X., Wu, F. Y., Xie, J. W., Zhao, Y. F. and Jiang, Y. B. *J. Org. Chem.*, **2004**, 69, 6449-6454.
- ²²Park, H., Choi, J., Choi, S., Park, M., Lee, J., Suh, J. Y., Cho, H., Oh, H.U., Lee, J., Kang, S. U., Lee, J., Kim, H. D., Park, Y. H., Jeong, Y. S., Choi, J. K. and Jew, J. S., *Bioorg Med. Chem. Lett.*, **2004**, 14, 787-791.
- ²³Saeed, S., Rashid, N., Jones, P. G., Tahir, A., *J. Heterocyclic Chem.*, **2011**, 48, 74-84.
- ²⁴Saeed, S., Rashid, N., Hussain, R., Jones, P. G., *Eur. J. Chem.*, **2011**, 2(1), 77-82.
- ²⁵Saeed, S., Rashid, N., Jones, P. G., Ali, M., Hussain, R. *Eur. J. Med. Chem.*, **2010**, 45, 1323-1331.
- ²⁶Saeed, S., Rashid, N., Jones, P. G., Hussain, R., Bhatti, M. H. *Cent. Eur. J. Chem.*, **2010**, 8(3), 550-558.
- ²⁷Saeed, S.; Rashid, N.; Jones, P.G.; Yunus, U. *J. Heterocycl. Chem.*, **2010**, 47, 908-912.
- ²⁸Saeed, S., Rashid, N., Ali, M., Hussain, R., Jones, P. G., *Eur. J. Chem.*, **2010**, 1(3), 221-227.
- ²⁹Saeed, S., Rashid, N., Ali, M., Hussain, R., *Eur. J. Chem.* **2010**, 1(3), 200-205.
- ³⁰Saeed, S., Rashid, N., Bhatti, M. H, Jones, P. G., *Turk J. Chem.* **2010**, 34, 761-770.
- ³¹Rana, A. M., Desai, K. R, Jauhari, S. *Med. Chem. Res.*, **2013**, 22, 225-233.
- ³²Silverstein, R. M. and Webster, F. X. *Spectrometric identification of organic compounds*, John Wiley & Sons, Canada 6th ed., **1997**, 79-223.

Received: 16.02.2013.

Accepted: 10.03.2013.



PREDICTIONS FOR THE YIELD OF NATURAL GAS WITH THE GRAY MODEL AND THE GENETIC ALGORITHM

Lu Hongjie^[a] and Linda Zhang^[b]

Keywords: prediction, natural gas, China, gray model, genetic algorithm

The gray model and the genetic algorithm for predicting natural gas yield have been introduced in the present article. Two new methods for forecasting the yield of natural gas in China have also been pointed out based on the gray model and the genetic algorithm. The experimental results show that both models can predict the yield of natural gas and the experimental data are in agreement with the quantitative analytical conclusions drawn from the calculated data. This proves that two types of new models can be used to predict the yield of natural gas. It results in good economic and social benefits in China.

* Corresponding Author

Fax: 86-24-56860869

E-Mail: lindazhang362@hotmail.com

[a] Liaoning Shihua University, Fushun, Liaoning, P.R. China.

[b] SAIT Polytechnic, Calgary AB, Canada.

Introduction

Natural gas has a lot of advantages such as being clean, highly efficient, abundant and easily storable. The global natural gas production and consumption in 2005 reached 2.763×10^{12} m³ and 2.749×10^{12} m³, respectively. The demands for natural gas had gradually increased to 3.3 % of the global natural gas production every year and were 25 % of total energy. Chinese natural gas consumption was only 1.7 % of total world natural gas consumption; however Chinese increment in natural gas consumption got 20.8 %. Natural gas as a clean energy is widely used in different areas such as electricity power, car market and residential fuel, etc.¹

In the present paper, the gray model and the genetic algorithm have been discussed. Two new methods for predicting the yield of natural gas yield in China have also been explained based on the gray model and the genetic algorithm.

Discussion

The gray model (GM)²

GM (1,1) was one of the main and basic gray models. GM (1, 1) was described in details. The original sample in the sequence was listed as follows.

$$X^{(0)} = \{x^{(0)}(1), x^{(0)}(2), \dots, x^{(0)}(n)\} \quad (1)$$

New sequence based on the above equation was written as follows.

$$x^{(1)}(t) = \sum_{i=1}^t x^{(0)}(i), (i = 1, 2, \dots, n) \quad (3)$$

or

$$x^{(1)}(t) = \theta x^{(1)}(t) + (1 - \theta)x^{(1)}(t+1), \\ (t = 1, 2, \dots, n \text{ and } 0 < \theta < 1) \quad (4)$$

$$X^{(1)} = \{x^{(1)}(1), x^{(1)}(2), \dots, x^{(1)}(n)\} \quad (2)$$

$x^{(1)}$ was described as follows.

It was supposed that:

$$\frac{dx^{(1)}}{dt} + ax^{(1)} = b \quad (6)$$

$$x^{(0)}(t) + ax^{(1)}(t) = b \quad (5)$$

It was simply described as follows.

$$X^{(0)} = \left\{ \begin{array}{l} 127.40, 119.30, 122.10, 124.30, 129.30, 137.60, \\ 138.90, 142.60, 150.49, 152.98, 160.73 \end{array} \right\}$$

Two parameters (a and b) were calculated with the least square method. $x^{(0)}(t)$ and $x^{(1)}(t+1)$ were obtained as follows.

The original $x^{(0)}$ was written as follows:

$$X^{(0)}(t) = X^{(1)}(t) - X^{(1)}(t-1) = (1 - e^{-a})(x^{(0)}(1) - \frac{b}{a})e^{-at},$$

$$(t = 1, 2, \dots, n-1) \quad (7)$$

$$X^{(1)}(t+1) = (x^{(0)}(1) - \frac{b}{a})e^{-at} + \frac{b}{a},$$

$$(t = 1, 2, \dots, n-1) \quad (8)$$

$X^{(1)}$ obtained was listed as follows based on the above equation.

$$X^{(1)} = \left\{ \begin{array}{l} 127.40, 246.7, 368.8, 493.1, 622.4, 760.8, 898.9, \\ 1041.5, 1191.99, 1344.97, 1505.7 \end{array} \right\}$$

The final gray model (GM(1,1)) was gotten and described as follows.

$$X^{(1)}(t+1) = (x^{(0)}(1) - \frac{b}{a})e^{-at} + \frac{b}{a} \approx$$

$$3449.875e^{-0.033t} - 3322.475 \quad (9)$$

Table 1 showed the actual yield of natural gas and predicting the yield of natural gas based on the gray model. The experimental results presented that the actual yield of natural gas was close to predicting the yield of natural gas, so the gray model was a good model for predicting the yield of natural gas.

Table 1. The relationship between the actual yield of natural gas and predicting the yield of natural gas based on the gray model

Actual yield of natural gas (billion m ³)	Predicting the yield of natural gas (billion m ³)	Relative error (%)
127.40		
119.30	117.92	1.16
122.10	121.95	0.12
124.30	126.12	-1.46
129.30	130.43	-0.87
137.60	134.89	1.97
138.90	137.50	1.01
142.60	144.26	-1.16
150.49	149.19	0.86
152.98	154.29	-0.86
160.73	159.57	0.72
157.88	165.02	-4.52
167.65	170.66	-1.80
175.59	176.50	-0.52

The genetic algorithm for forecasting the yield of natural gas.³

The generalized Wengshi model was a model for predicting the yield of natural gas⁴. Chen Yuanqian explained more details about the generalized Wengshi model. Its model was written as follows.

$$Q = at^b e^{-\frac{t}{c}}, t = y - y_0 \quad (10)$$

where

- a - constant; $a > 0$
- b - constant, $b \geq 0$
- c - constant; $c > 0$
- y - prediction for the year
- y_0 - the beginning of the year

Yang Shuzi⁵ introduced an exponential smoothing model which could forecast the yield of natural gas. The exponential smoothing model meant that a predicted value at the time $(t+1)$ weighted average with an experimental value. The exponential smoothing model was listed as follows.

$$\bar{x}_{t+1} = a_0 x_t + (1 - a_0) \bar{x}_t, 0 \leq a_0 \leq 1 \quad (11)$$

when a_0 equals 1, $\bar{x}_{t+1} = x_t$. It means the predicted value equals the experimental value at the time (t) . When a_0 equals 0, the predicted value does not change.

Shuai Xunbo pointed out the optimal group model about predicting the yield of natural gas. The optimal

$$Q = \beta at^b e^{-\frac{t}{c}} + (1 - \beta)[a_0 x_t + (1 - a_0) \bar{x}_t];$$

$$0 \leq a_0 \leq 1; 0 \leq \beta \leq 1 \quad (12)$$

group model meant that the generalized Wengshi model connected with the exponential smoothing model together. It was written as follows.

where

- a_0 - constant
- β - weight average
- Q - the optimal group model

The optimal group model was calculated based on the genetic algorithm. There were four steps described as follows.

- (1) It made sure population size (S), crossover probability (v_c), mutation probability (p_m) and iteration condition. N types of beginning populations were determined.
- (2) Each fitness function value was computed.
- (3) Its reproduction probability was calculated based on the above fitness function value. It was supposed that crossover probability (v_c) and mutation probability (v_m) were known during the genetic process. Finally N types of new populations were gotten.
- (4) Steps (2) and (3) did not redo until its result was convergence. The final optimal group model was listed as follows.

$$Q_{calc.}(a, b, c, a_0, \beta) = \beta a t^b e^{-\frac{t}{c}} + (1 - \beta)[a_0 x_t + (1 - a_0) \bar{x}_t];$$

$$a > 0; b \geq 0; c > 0; 0 \leq a_0 \leq 1; 0 \leq \beta \leq 1 \quad (13)$$

Small pieces of natural gas field in Liaohe oilfield were forecasted. It was supposed that population size (s), crossover probability (p_c), mutation probability (p_m) and iteration number were 80, 0.60, 0.001 and 800, respectively. Table 2 showed the relationship between predicting the yield of natural gas and the optimal group model with the genetic algorithm. Experimental results showed that relative errors of the optimal group model were very low, so the optimal group model was used to predict the yield of natural gas.

Table 2. The relationship between predicting the yield of natural gas and the optimal group model with the genetic algorithm

Actual yield of natural gas (10^4 m^3)	Predicting the yield of natural gas (10^4 m^3)	Relative error, %
16.30	15.87	2.63
33.80	33.80	0
47.90	46.15	3.65
55.30	55.30	0
79.30	72.55	8.51
81.10	78.30	3.45
59.30	58.39	1.53
41.30	41.29	0.02
45.30	42.35	6.51

Conclusion

In this paper, the author has introduced that the gray model and the genetic algorithm lead to and are closely in accordance with predicting the practical experimental values. The yield of natural gas in China can be accurately estimated. The gray model and the genetic algorithm point out that predicting the yield of natural gas not only has a very important significance, but also provides a theoretical reference for chemical plants or oil companies.

It is important for Chinese government to design and utilize rightly and optimize natural resources and may increase Chinese government's benefits. This mathematical method is effective, economic, simple and convenient and thus it is suitable for chemical plants or oil companies in China.

References

- ¹Wang, B., Liu, S. W., Luo, S., Fang, J. and Suo, L., *Natural Gas and Oil*, **2008**, 26(5), 30-32.
- ²Chen, X. D. and Xie, C. Y., *J. Guizhou Educ. Coll.*, **2005**, 16(4), 4-6.
- ³Shuai, X. B., Zhou, X. G., Guan, X., Wu, B. and Zhao, S. R., *Comput. Appl. Petr.*, **2007**, 15(4), 23-25.
- ⁴Chen, Y. Q., *Reservoir Engineering Practical Methods*, Beijing, Petroleum Industry Press. **1999**.
- ⁵Yang, S. Z. *Time series analysis of engineering application*, Wuhan, Huazhong University of Science and Technology Press. **1992**.

Received: 17.12.2013.

Accepted: 11.03.2013.



CORROSION INHIBITION BY AN AQUEOUS EXTRACT OF *ALOE VERA* (L.) BURM F.(LILIACEAE)

V. Sribharathy^{[a]*}, Susai Rajendran^{[a,b]*}, P. Rengan^[c], R. Nagalakshmi^[d]

Keywords: carbon steel, corrosion inhibition, plant extract, aloe vera, seawater, green inhibitor.

An aqueous extract of *Aloe vera* (L.) Burm f. (Liliaceae) has been used as a corrosion inhibitor in controlling corrosion of carbon steel immersed in sea water. Weight loss method reveals that 4ml of the extract provide 98% inhibition efficiency. The protective film has been analyzed using Fourier transform infrared (FTIR) spectroscopy and fluorescence spectroscopy. Electrochemical studies such as potentiodynamic polarization and alternating current impedance spectra have been used to find the mechanistic aspects of corrosion inhibition.

Corresponding Authors

E-Mail: bharathy_chem@yahoo.co.in,

srmjoany@sify.com

- [a] PG and Research Department of GTN Arts College, Dindigul-624005, Tamilnadu, India. Email: srmjoany@sify.com
- [b] RVS School of Engineering & Technology, GTN Arts College, Dindigul-624005, Tamil Nadu, India.
- [c] Department of chemistry, Yadava college, Madurai, India, E.mail: akveni1972@gmail.com
- [d] Department of chemistry, Aarupadai Veedu Institute of Technology, Chennai-603110, Tamilnadu, India. Email: nagalakshmirajan@gmail.com

aldehydes,¹² amines,^{13,14} amino acids,^{15,16} nitro compounds,^{17,18} amides,^{19,20} ester,^{21,22} thio compounds,^{23,24} phosphates,^{25,26} phosphonates,^{27,28} ketones^{29,30} and carboxylic acids.³¹⁻³³

The present work investigated the inhibition efficiency of an aqueous extract of plant material, *Aloe vera* (L.) Burm f. (Liliaceae) extract, in controlling corrosion of carbon steel (CS) immersed in sea water in the absence and presence of inhibitor, using mass loss method, analyzed the protective film by Fourier transform infrared (FTIR) spectroscopy and fluorescence spectroscopy, and proposed a suitable mechanism of corrosion inhibition, based on the results of the above studies and potentiodynamic polarization and the alternating current (AC) impedance spectra.

Introduction

Plant extracts have become important as environmentally acceptable, readily available and renewable source for wide range of inhibitors.¹ In general, the plant extracts are of inhibitors with high inhibition efficiency and of non toxicant. El-Etre et al. investigated Khillah extract² for the corrosion inhibition of SX 316 steel in acid media. Lawsonia extract³ was studied for effect against acid induced corrosion of metals. Opuntia extract⁴ was investigated for the corrosion of Aluminium in acid medium and vanillin⁵ for the corrosion of mild steel in acid media. Yan Li et al Berberine isolated an alkaloid from *Captis* studied for its anticorrosion effect for mild steel corrosion in H₂SO₄ medium⁶ Fabrizio Zucchi and Ibrahim Hashi Omar⁷ have found that *Papaia*, *Poinciana pulcherrima*, *Cassia occidentalis* and *Datura stramonium* seeds, *Calotropis procera*, *Azydracta indica* and *Auforpio turkiale* sap are useful as acid corrosion inhibitors. Sethuraman and Bothi raja⁸ have studied the acid extract of *Datura metel* as corrosion inhibitor for mild steel in acid medium. Quinine⁹ has been studied for its anticorrosive effect of carbon steel in 1 M HCl by Mohamed Ismail Awad. Anthony et al. has studied the effect of caffeine against chloride corrosion of carbon steel.¹⁰ There are many methods by which corrosion can be controlled one such method is the use of inhibitors. These inhibitors when added is small quantity, decrease the rate of corrosion. Corrosion inhibitors usually contain polar groups with atoms such as nitrogen, sulphur and oxygen. Correspondingly inhibitors include a wide list of organic and inorganic compounds¹¹ containing the functional groups such as

Experimental

Preparation of plant extract

An aqueous extract was prepared by grinding 10 g of fresh extract of aloe vera (mannose-6-phosphate) gel, filtering and making up to 100 ml using double distilled water.

Preparation of specimens

Carbon steel specimens (0.0267% S, 0.06% P, 0.4% Mn, 0.1% C and the rest iron) of dimensions 1.0 cm x 4.0 cm x 0.2 cm were polished to a mirror finish and degreased with trichloroethylene.

Weight loss method

Relevant data of sea water used in the study, are given in Table1. Three mild steel specimens were immersed in 100 ml of sea water containing various concentrations of the inhibitor for one day. The weight of the specimens before and after immersion were determined using Shimadzu balance, model AY 62. The corrosion products were cleansed with Clarke's solution.³⁴

Table 1. Parameters of seawater (Cuddalore district, Tamilnadu, India)

Parameter	Value
pH	8.1
Chloride	17,600 ppm
Sulphate	3254 ppm
Total hardness	800 ppm
Calcium	160 ppm
Magnesium	100 ppm

The inhibition efficiency (IE , %) was then calculated using the equation

$$IE = 100 \left(1 - \frac{W_2}{W_1} \right) \quad (1)$$

where

W_1 = corrosion rate in the absence of the inhibitor

W_2 = corrosion rate in the presence of the inhibitors

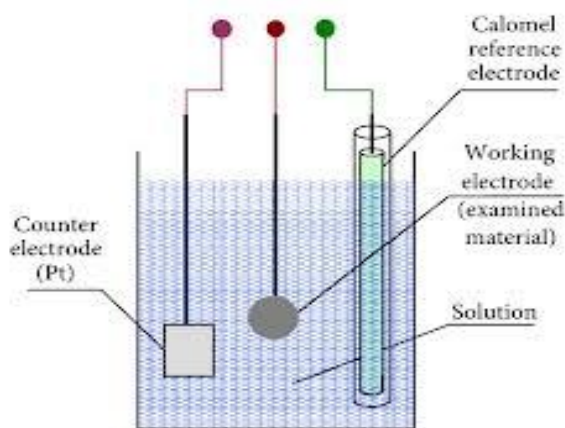
Surface Examination

The carbon steel specimens were immersed in various test solutions for a period of one day, taken out and dried. The nature of the film formed on the surface of metal specimens was analyzed by FTIR spectroscopic study.

FTIR Spectra

FTIR spectra were recorded in a Perkin – Elmer 1600 spectrophotometer. The film was carefully removed, mixed thoroughly with KBr made in to pellets and FTIR spectra were recorded.

The fluorescence spectra of the film formed on the Carbon Steel samples recorded with a Hitachi F-4500 fluorescence spectrophotometer.



Scheme 1. Three electrode cell assembly. WE - working electrode, CE - counter electrode; Reference electrode - saturated calomel electrode

Potentiodynamic Polarization

The polarization studies were carried out in a three electrode cell consisting of mild steel as working electrode (WE), a platinum wire counter electrode (CE), and a saturated calomel electrode reference electrode were used for measurements³⁵. All the potential values reported here was VS SCE (Scheme1).

The working electrode was mechanically polished on various grades of emery sheet, rinsed with double distilled water, degreased with trichloroethylene. Potentiodynamic polarization curves were recorded using an H & CH electrochemical work station impedance analyzer model CHI 660A provided with iR compensation option. Polarization curve measurements were carried out at scan rate of 0.01 V s^{-1} . The exposed area (1 cm^2) was mechanically polished with a series of emery sheets of variable grade. The samples were washed thoroughly with double distilled water before insertion in the cell. During the polarization study, the scan rate was 0.01 V s^{-1} ; hold time at E_f was 0 s and quiet time was 2 s.

AC impedance measurements

The instrument used for polarization was used for AC impedance study also. The cell set up was the same as that had been used for polarization measurements. The real part and imaginary part of the cell impedance were measured in ohms at various frequencies. The values of charge transfer resistance, R_{ct} , and the double layer capacitance, C_{dl} were calculated.

$$C_{dl} = \frac{1}{2} \pi R_t f_{max} \quad (3)$$

where

R_s - Solution resistance,

f_{max} - maximum frequency.

AC impedance spectra were recorded with dc potential $E = 0 \text{ V}$, in the frequency range $1 \times 10^5 - 10 \text{ Hz}$, amplitude = 0.005 V , and quiet time = 2 s.

Result and Discussion

Weight loss studies

Table 1 shows the values of corrosion rates and inhibition efficiencies obtained from weight loss measurements of different concentrations of aloe vera extract. 4 ml of the aloe vera offered 98 % corrosion inhibition efficiency to carbon steel immersed in 100 ml sea water. When the concentration of aloe vera was increased the inhibition efficiency decreased. This is due to the fact that when higher concentrations of aloe vera are added the protective film Fe^{2+} -mannose-6-phosphate complex formed on the metal surface goes into the solution and thus destroying the protective film. It may be considered that the protective film formed may go into transpassive state, where the film is broken³⁶.

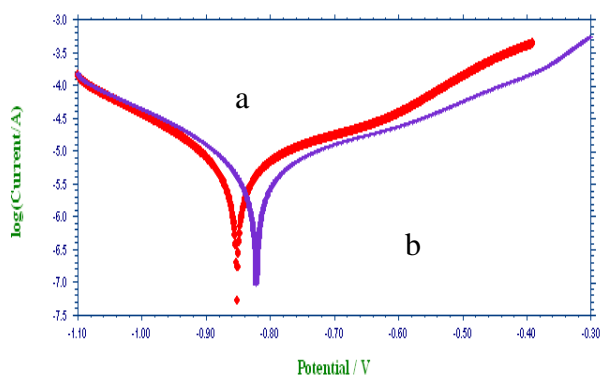
Table 2 – Corrosion rates(CR) of carbon steel immersed in sea water in the presence absence of inhibitors and the inhibition efficiencies (IE) obtained by weight loss method.

Inhibitor: Aloe vera; period of immersion: 1 day

Aloe vera extract, ml	Corrosion rate, mdd	Inhibition efficiency (IE), %
0	21.52	--
2	8.40	75
4	0.67	98
6	16.47	51
8	20.51	39

Analysis of polarization curves

The polarization study has been used to investigate the formation of protective film on metal surface³⁷⁻⁴¹. The polarization curves of carbon steel immersed in various solutions are shown in Fig 1. The corrosion parameters such as corrosion potential (E_{corr}), cathodic tafel slope and anodic tafel slope were determined from E vs $\log I$ plots Table 3. When carbon steel is immersed in sea water, the corrosion potential is -926 mV SCE. When 4 ml of aloe vera is added the corrosion potential is shifted towards the anodic side, (-882 mV SCE) indicating that the aloe vera controls the anodic reaction predominantly by forming Fe^{2+} - mannose-6-phosphate complex on the anodic sites of the metal surface. The Linear polarization resistance (LPR) value increases from 51.67×10^2 to 76.01×10^2 ohm cm^2 . This suggests that a protective film is formed on the metal surface. Further the corrosion current decreases from 7.963×10^{-6} A cm^{-2} to 5.229×10^{-6} A cm^{-2} . This suggests the inhibitive nature of this inhibitor system^{42,43}.

**Figure 1.** Polarization curves of carbon steel immersed in various test solutions: (a) Carbon steel immersed in sea water; (b) Carbon steel immersed in sea water + aloe vera 4 ml**Table 3.** Corrosion parameters of carbon steel immersed in various test solutions Inhibitor: aloe vera extract

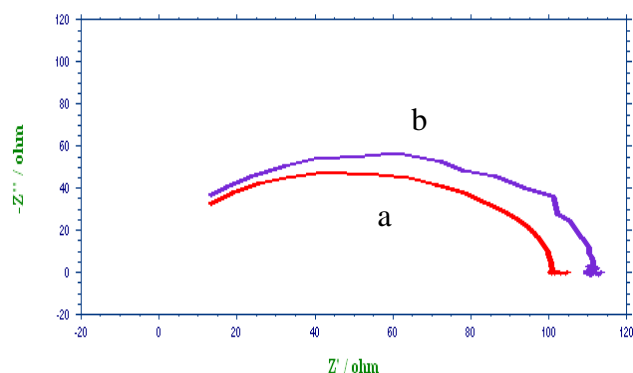
System	E_{corr} mV*	b_c mV**	b_a mV**	LPR Ohm cm^2	I_{corr} (A cm^{-2})
CS+ A	-926	153	247	51.67×10^2	7.9×10^{-6}
A + B	-882	153	226	76.01×10^2	5.2×10^{-6}

A= Sea Water, B= aloe vera 4ml,*mV vs SCE; **mV in one decade

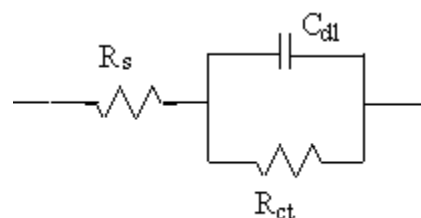
Analysis of AC Impedance spectra

AC impedance spectra have been used to detect the formation of the film formed on the metal surface. If a protective film is formed, the Charge transfer resistance increases and double layer capacitance value decreases⁴⁴⁻⁴⁶. The AC Impedance spectra of carbon steel immersed in various solutions are shown in Fig 2. The AC Impedance parameter, namely charge transfer resistance (R_{ct}) and double layer capacitance (C_{dl}) are given in Table 4.

When carbon steel is immersed in aqueous solution containing sea water, the R_{ct} value is 88 ohm cm^2 and C_{dl} value is 1.027×10^{-7} F cm^{-2} . When the inhibitor is added the R_{ct} value increases from 88 ohm cm^2 to 98 ohm cm^2 and C_{dl} value decreases from 1.027×10^{-7} F cm^{-2} to 0.923×10^{-8} F cm^{-2} . The equivalent circuit diagram is shown in Scheme 1. This suggests that a protective film is formed on the metal surface of the metal. Further there is increase in impedance $\log(Z / ohm)$, value from 2.02 to 2.05 (derived from Bode plot shown in Fig 3.)

**Figure 2.** AC Impedance parameter of carbon steel immersed in various test solutions (Nyquist plots): (a) Carbon steel immersed in Sea water; (b) Carbon steel immersed in Sea water+ aloe vera 4 ml**Table 3.** AC Impedance parameter of carbon steel immersed in various test solution

System	Nyquist plot		Bode plot
	R_{ct} , Ω cm^2	C_{dl} , F cm^{-2}	Impedance, $\log(Z/ohm)$
CS + A	88	1.02×10^{-7}	2.02
A + B	101	99.23×10^{-8}	2.05

**Scheme 2.** Equivalent electrical circuit diagram, R_s = solution resistance, R_{ct} = Charge transfer Resistance C_{dl} = Double layer capacitance

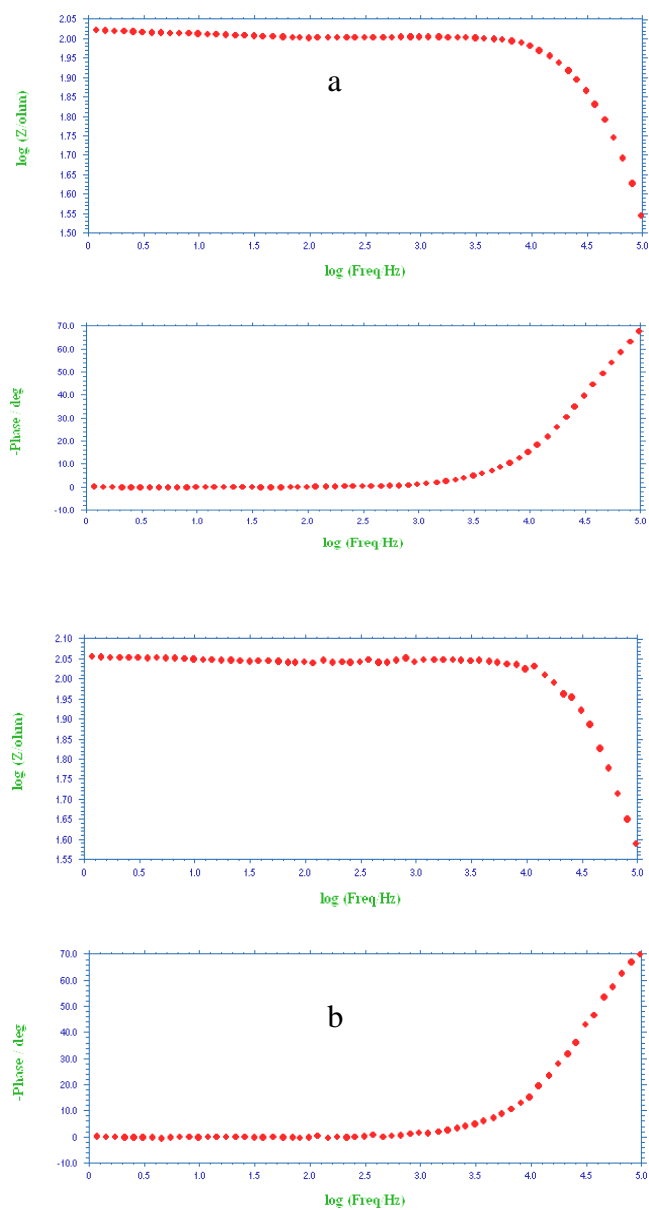
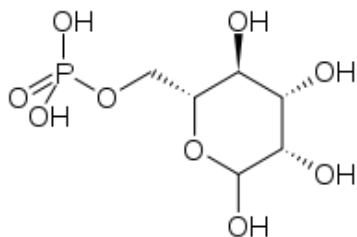


Figure 3. Bode plot of carbon steel immersed in various solutions, (a) Carbon steel immersed in sea water; (b) Carbon steel immersed in Sea water+ aloe vera 4 ml

Fourier Transfer Infrared Spectra

The main constituent of aloe vera extract is mannose-6-phosphate⁴⁷. The structure of mannose-6-phosphate is shown in Scheme 3. It contains phosphate group, hydroxyl group and ring oxygen.



Scheme 3. Mannose-6- phosphate

The aloe vera extract was evaporated to dryness to a solid mass. Its FTIR spectrum is shown in Fig 3a. The -OH stretch appeared at 3410 cm^{-1} . The aliphatic -CH stretching frequency appeared at 2936 cm^{-1} . The ring oxygen stretching frequency appeared at 1237 cm^{-1} . Phosphate stretching frequency appeared at 1060 cm^{-1} ⁴⁸⁻⁴⁹.

The FTIR spectrum of the protective film formed on the surface of the metal after immersion in the aqueous solution containing sea water and sea water containing 4ml of aloe vera is shown in Fig 3b. It is found that the -OH stretch has shifted from 3410 cm^{-1} to 3433 cm^{-1} . The aliphatic -CH₂ stretching frequency shifted from 2936 cm^{-1} to 2943 cm^{-1} . Phosphate stretching frequency shifted from 1060 cm^{-1} to 1100 cm^{-1} . The ring oxygen stretching frequency shifted from 1237.20 cm^{-1} to 1237.92 cm^{-1} . It is inferred that the active principle has coordinated with through the oxygen atom of P-O groups, OH group and ring oxygen resulting in the formation of Fe²⁺-mannose -6-phosphate complex.

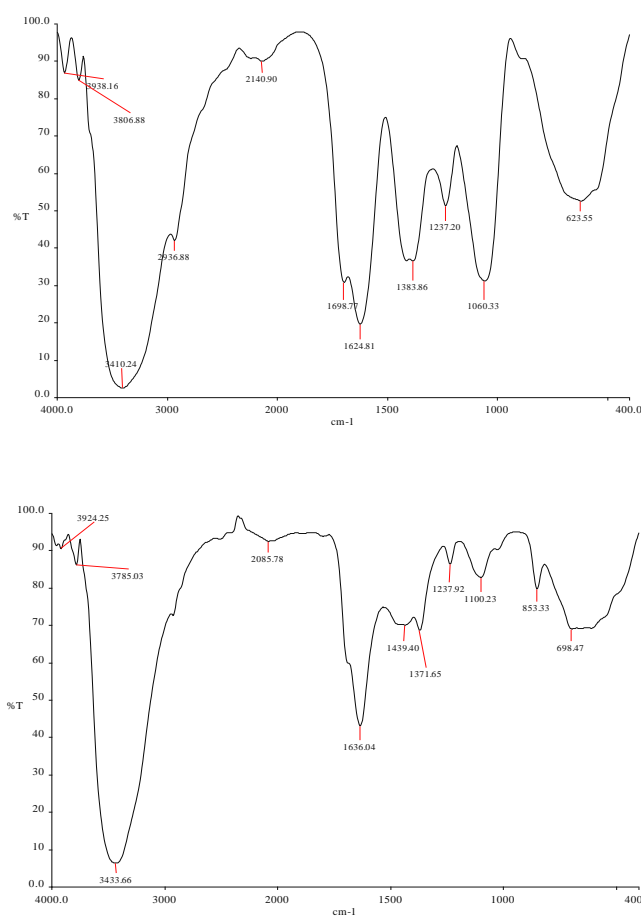


Figure 4. FTIR spectra: (a) Carbon steel immersed in Sea water (b) Carbon steel immersed in Sea water + Aloe vera 4 ml

UV-Visible adsorption spectra

The UV-Visible adsorption spectrum of aqueous solution of aloe vera is shown in Fig 5a. Peaks appear at 255 nm, 266 nm, 298 nm and 353 nm. When the Fe²⁺ (Freshly prepared FeSO₄ H₂O Solution) is added to the aqueous solution of aloe vera peak appear at 227 nm⁵⁰. This is due to Fe²⁺ - mannose-6-phosphate complex formed in solution.

Fluorescence spectra

The fluorescence spectrum ($\lambda_{ex} = 227$ nm) of the solution containing aloe vera extract and Fe^{2+} is shown in Fig 6a. A peak appears at 252 nm. This is due to Fe^{2+} -mannose-6-phosphate complex formed in solution. The fluorescence spectrum ($\lambda_{ex} = 227$ nm) of the film formed on the surface of the metal after immersion in the sea water and 4ml of aloe vera extract is shown in Fig 6b. The peak appeared at 252 nm confirming the presence of Fe^{2+} -aloe vera extract complex formed on the metal surface⁵¹.

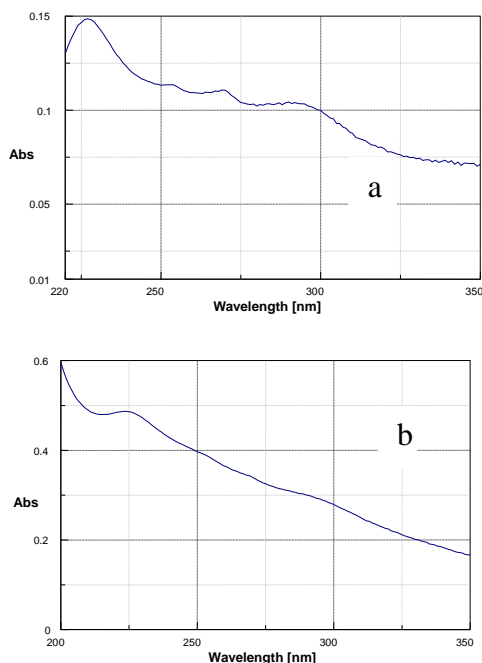


Figure 5. UV-spectra, (a) carbon steel immersed in sea water (b) film formed on metal surface after immersion solution containing sea water + aloe vera 4 ml

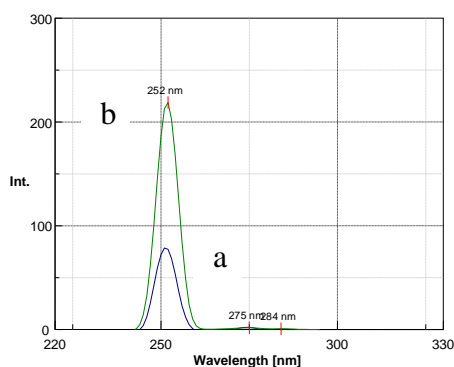


Figure 6. Fluorescence spectra, a) sea water; b) sea water + 4ml aloe vera extract

Conclusions

The main constituent of the aqueous extract of aloe vera is mannose-6-phosphate. An aqueous extract of aloe vera has excellent IE in controlling corrosion of carbon steel in aqueous solution containing sea water. The protective film consists of Fe^{2+} -aloe vera complex. It is found to be UV-fluorescent. The formulation controls the anodic reaction predominately.

References

- Tamer Soror, Y., *Eur. Chem. Bull.*, **2013**, 2(4), 150-153.
- El-Etre, A. Y., *Appl. Surf. Sci.*, **2005**, 252, 8521.
- El-Etre, A. Y., Abdallah, M., El-Tantawy Z. E., *Corros. Sci.*, **2005**, 47, 385.
- El-Etre, A.Y., *Corros. Sci.*, **2003**, 45, 2485.
- El-Etre, A.Y., *Corros. Sci.*, **2001**, 43, 1031.
- Yan Li., Peng Zhao., Qiang Liang., Baorong Hou, *Appl. Surf. Sci.*, **2005**, 252, 1245.
- Fabrizio Zucchi., Ibrahim Hashi Omar., *Surf. Tech.*, **1985**, 24, 391.
- Sethuraman, M. G., Bothi Raja, P., *Pigm. Res. Tech.*, **2005**, 34, 327.
- Mohamed Ismail Awad., *J. Appl. Electrochem.*, **2006**, 36, 1163.
- Noreen Anthony, E., Malarvizhi, P. Maheshwari, Rajendran, S., Palaniswamy, N., *Indian. J. Chem. Technol.*, **2004**, 11, 346.
- Manivannan, M., Rajendran, S., and Suriya Prabha, A., *Eur. Chem. Bull.* **2012**, 1(8), 317-29; Pandiarajan, M., Rajendran, S., Sathiyabama, J., Lydia Christy, J., Jeyasundari, J., Prabhakar, P., *Eur. Chem. Bull.* **2013**, 2(1), 1-8; Saranya, R., Rajendran, S., Krishnaveni, A., Pandiarajan, M., and Nagalakshmi, R., *Eur. Chem. Bull.*, **2013**, 2(4), 163-170; Nagalakshmi, R., Rajendran, S., Sathiyabama, J., Pandiarajan, M., and Lydia Christy, J., *Eur. Chem. Bull.*, **2013**, 2(4), 171-179; Mary Anbarasi, C., Rajendran, S., Pandiarajan, M. and Krishnaveni, A., *Eur. Chem. Bull.*, **2013**, 2(4), 197-207.
- Abdallah, M., Zaafarany, I., Fouda, A. S., *J. Mater. Eng. Perform.*, **2012**, 21(6), 995; Feng, Y., Qi, X., Jian, H.-L., Sun, R.-C., Jiang, J.-X., *Bio Resources.*, **2012**, 7(3), 3755.
- Kashkovskiy, R.V., Kuznetsov, Y., Kazansky, L. P., *Corros. Sci.*, **2012**, 64, 126.
- Hosseini, S. M. A., Salari, M., Jamalizadeh, E., Jafari, A. H., *Corros.*, **2012**, 68(7), 600.
- Gomma, G. K., Wahdan, M. H., *Mater. Chem. Phys.*, **1994**, 39(2), 142; Gowri, S., Sathiyabama, J., Rajendran, S., and Angelin Thangakani, J., *Eur. Chem. Bull.*, **2013**, 2(4), 214-219.
- Liu, P., Gao, L., Zhang, D., *J. Chin. Soc. Corros. Prot.*, **2012**, 32(2), 163; Gowri, S., Sathiyabama, J., Rajendran, S., *Eur. Chem. Bull.*, **2012**, 1(11), 470-476.
- Jayateertha, N.S., Hayavadana, N., *Res. J. Pharm. Biol. Chem. Sci.*, **2012**, 3(2), 614.
- Fernando, I. R., Daskalakis, N., Demadis, K. D., Mezei, G., *New. J. Chem.*, **2010**, 34(2), 221.
- Sliwa, A., Dive, G., Marchand-Brynaert, J., *Chem. - Asian J.*, **2012**, 7(2), 425.
- Gopiraman, M., Selvakumaran, N., Kesavan, D., Karvembu, R., *Progress Org. Coatings.*, **2012**, 73(1), 104.
- Baek, S.-Y., Kim, Y.-W., Chung, K.-W., Yoo, S.-H., *Appl. Chem. Engg.*, **2011**, 22(4), 367.
- Kalendová, A., Veselý, D., Sapurina, I., Stejskal, J., *Progress Org. Coat.*, **2008**, 63(2), 228.
- Bouklah, M., Ouassini, A., Hammouti, B., El Idrissi, A., *Appl. Surf. Sci.*, **2006**, 252(6), 2178.
- Musa, A.Y., Mohamad, A. B., Kadhum, A. A. H., Takriff, M.S., Ahmoda, W. *J. Ind. Eng. Chem.*, **2012**, 18(1), 551.
- Michael, J., Franklin, David C., White, Hugh, S., Isaacs, *Corros. Sci.*, **1992**, 33(2), 251.
- Sumanlata, Chaudhary, R. S., *Indian. J. Chem. Technol.*, **2008**, 15, 364.
- Papadaki, M., Demadis, K. D., *Comments Inorg. Chem.*, **2009**, 30(3-4), 89; Kavipriya, K., Rajendran, S., Sathiyabama, J. and Suriya Prabha, A., *Eur. Chem. Bull.*, **2012**, 1(9), 366-374.

- ²⁸Benabdellah, M., Dafali, A., Hammouti, B., Aouniti, A., Rhomari, M., Raada, A., Senhaji, O., Robin, J. J., *Chem. Eng. Commun.*, **2007**, *194*(10), 1328.
- ²⁹Ateş, E., Kizilcan, N., *Pigment Resin Technol.*, **2012**, *41*(4), 210.
- ³⁰Sherif, E. M., Park, S.-M., *Electrochim. Acta.*, **2006**, *51*(7), 1313.
- ³¹Herrag, L., Chetouani, A., Elkadiri, S., Hammouti, B., Aouniti, A., *Port. Electrochim. Acta.*, **2008**, *26*(2), 211.
- ³²Quartarone, G., Battilana, M., Bonaldo, L., Tortato, T., *Corros. Sci.*, **2008**, *50*(12), 3467.
- ³³Eddy, N. O., Abasiekong, B.O., *J. Corros. Sci. Engg.*, **2006**, 10.
- ³⁴Wranglen, G., *Introduction to corrosion and protection of metals, London: Chapman & Hall* **1985**, 236.
- ³⁵Vijaya, N., Peter Pascal Regis, A., Rajendran, S., Pandiarajan, M., and Nagalakshmi, R., *Eur. Chem. Bull.* **2013**, *2*(5), 275-278.
- ³⁶Sathyabama, J., Susai R., Arokia, S. J., John, A. A., *Indian. J. Chem. Technol.*, **2008**, *15*, 462.
- ³⁷Nagalakshmi, R., Rajendran, S., Sathiyabama, J., Pandiarajan, M., Lydia Christy, J., *Eur. Chem. Bull.*, **2012**, *1*(17), 238.
- ³⁸Sahayaraja, A., Nagalakshmi, R., Rajendran, S., Angelin Thangakani, J., Pandiarajan, M., *Eur. Chem. Bull.*, **2012**, *1*(3), 130.
- ³⁹AgilaDevi, S., Rajendran, S., Jeyasundari, J., Pandiarajan, M., *Eur. Chem. Bull.*, **2013**, *2*(2), 503.
- ⁴⁰Rajendran, S., Sridevi S. P., Anthony, N., John Amalraj, A., Sundaravivelu, N., *Anti Corros. Methods Mater.*, **2005**, *52*, 102.
- ⁴¹Felicia Rajammal Selvarani, Santhanalakshmi, S., Wilson sahayaraja, J., John Amalraj, A., and Rajendran, S., *Bull. Electrochem.*, **2004**, *20*, 561.
- ⁴²Agnesia Kanimozhi, S., Rajendran, S., *Int. J. Electrochem. Sci.*, **2009**, *4*, 353.
- ⁴³Shymala Devi, B., Rajendran, S., *Eur. Chem. Bull.*, **2012**, *1*(5), 150.
- ⁴⁴Pandiarajan, M., Prabhakaran, P., Rajendran, S., *Eur. Chem. Bull.*, **2012**, *1*(7), 238.
- ⁴⁵Rajendran, S., Mary Reenkala., Noreen Anthony., and Ramaraj, R., *Corros.Sci.*, **2002**, *44*(10), 243.
- ⁴⁶Mary anbarasi, C., Rajendran, S., *J. Electrochem. Sci. Eng*, **2012**, *2*(1), 1.
- ⁴⁷www.nature4science.com/AloeVera/1_DescriptionofAloeVera.pdf
- ⁴⁸Silverstein, R. M., Bassler, G. C., Morrill, T. C., *Spectroscopic Identification of organic compound, New York, NY, John Wiley and Sons* **1986**, 95.
- ⁴⁹Vinothkumar, K. P., Sankaranarayanan, M., Rexin Thusnavis, G., *J. Mater. Environ. Sci*, **2010**, *1*(2), 1.
- ⁵⁰Rajendran, S., Shanmugapriya, S., Rajalakshmi, T., and Amal Raj, A. J., *Corros.*, **2005**, *61*, 685.
- ⁵¹Yesu Thangam, Y., Kalanithi, M., Mary Anbarasi, C., Rajendran, S., *Arab. J. Sci. Eng.*, **2009**, *34*(2C), 49.

Received: 11.02.2013.

Accepted: 12.03.2013.



PREPARATION AND CHARACTERIZATION OF UNSATURATED POLYESTER MATERIAL BLENDED WITH CELLULOSE AND WITH ETHYL CELLULOSE.

Fadhel S. Matty, Jawad K. Al-Kafaji, Dhefah H. Badri

Keywords: unsaturated polyester, resins, mechanical, dielectric constant; cellulose and ethyl cellulose blends

Modified unsaturated polyester (MUPE) was blended with Cellulose (CIs) and with ethyl cellulose (ECIs) at ambient conditions in the presence of ethyl methyl ketone peroxide (EMKP) as hardener. The blends containing different weight percentages (5-25 %) of CIs or ECIs. Mechanical properties (impact strength, hardness, and bending) and dielectric constant were determined. The results observed that CIs increases the impact strength, hardness, and dielectric constant and decreases the bending of the MUPS, while ECIs causes an increase in the three mechanical behaviours and a decrease in the dielectric constant of the MU-PS.

* Corresponding Authors

E-Mail: dr.fadhel55@yahoo.com

[a] Chemistry Department, College of Education Ibn Al-Haithem, Baghdad University, Baghdad, Iraq.

INTRODUCTION

Unsaturated polyester resins are the group of polyester in which the acid component is part of the ester and partially composed of fumaric acid, maleic anhydride is the predominant source of this fumarate when this anhydride is incorporated in the polyester backbone and then isomerised to provide polyester¹.

Cellulose is a biopolymer consisting of D-anhydro glucose repeating units joined by α -1,4-glycosidic linkages at C-1 and C-4 positions, and each repeating unit contains three primary OH groups have the ability of hydrogen bonding and that govern the physical properties of CIs.² Ethyl cellulose is a cellulose ether distinguished by its versatility, and its molecular structure is similar to the CIs molecular structure but with 55% ethoxyl substitution and the variation in this percentage depends on its application demands.^{3,4}

Polymer blends are made by physical mixing of two or more different polymers or copolymers to produce a mixture of desirable mechanical and physical properties.⁵ Compatible polymer blends are immiscible mixtures but they exhibiting macroscopically uniform physical properties and that due to the modification of the interfacial character of the blend by the compatibiliser (polymer or copolymer) of the blend which stabilizes the morphology.⁶ Polymer blends are heterogeneous which don't form single phase system and their properties are largely dependent on the mechanical dispersion, ductility, and the degree of adhesion between the phases.⁷⁻⁹ The presence of cellulose OH groups and ethoxyl groups of ECIs in the blend can change the surface energy, polarity, wet ability, mechanical properties, and dielectric constant of the unsaturated polyester.¹⁰⁻¹¹

The aim of this work is to study the effect of CIs and ECIs on the mechanical properties (impact strength, hardness, and bending) and dielectric constant of MUPS.

Experimental

Materials

Cellulose and toluene were purchased from MERCK, ethyl cellulose from Riedel de Haen, MUPE from Enc International Corporation- South Korea, MEKP from Metric Engineering- India, and ZnO from BDH. All material were used without further purification.

Preparation of MUPE mold

The mold used for preparing the samples was a metallic plate of dimensions (20 x 15 x 1 cm). The plate was cleaned by hot caustic alkali solution and later by distilled water, then treated with a thin layer of liquid paraffin that helps to peel the samples easily.

To 100 gm of MUPE, 2 ml of MEKP as hardener was added and mixed well. The mixture was then immediately poured into the mold and left in a dark not humid place at room temperature ($\sim 25^\circ\text{C}$) for complete solidification after 24 h. The solid mold was peeled off and stored for further use.

Preparation of blended MUPE molds

The required weight present (5- 25 %) of CIs or ECIs was mixed with 100 g of MUPE at room temperature for several hours to obtain a homogeneous mixture, followed by mixing 2 ml of MEKP with the mixture and then poured immediately into the mold and left in a dark not humid place at room temperature for complete solidification after 48 h. The solid blend mold was peeled off and stored for further use.

Impact strength test

Charpy impact instrument of model IMI was used for this test which involves a pendulum swiping downing from a special height to hit the piece under test. Each sample was prepared according to ISO- 179 with fixed dimensions (55 x 10 x 10 mm). The test was carried out at room temperature

and the impact strength (I_s , in kJ m^{-2}) was obtained from equation 1:^{12,13}

$$IS = \frac{E}{A} \quad (1)$$

where

E energy of fraction
 A cross sectional area

Brinell hardness test

Hydraulic piston type LEYBOLD instrument was used for this test. The sample was prepared according to ISO-179 with fixed dimensions (5mm thickness and 20mm in diameter). The test consists of inducing the sample under test with a 5 mm diameter hardened steel ball subjected to a load of 100 and 500 N and full load was applied for 10 s.

The diameter of the indentation left in the tested material (D_1) was measured, then the Brinell hardness number (BHN , N mm^{-2}) was calculated from equation 2¹⁴:

$$BHN = \frac{F}{\frac{1}{2} \pi D \left[D - \sqrt{D^2 - D_1^2} \right]} \quad (2)$$

where

F is the load applied
 D is the indenter diameter.

Bending test

Three point-bending testers were used according to (ASTM-D790) test to determine the modulus of elasticity. The instrument type PHYWE was used to measure the deflection values. Loads ranging from 100 to 1100 gm were used for both MUPE/CIs and MUPE/ECIs blend samples. The dimensions of each rectangular sample were (135 x 10 x 10 mm). The sample was fixed between two points and a certain load (weight) was applied to the centre of the sample at room temperature. Equation 3 was used to calculate Young's modulus (E , in MPa).^{15,16}

$$E = \frac{m g L^2}{D 481} \quad (3)$$

where

g is the gravity acceleration (9.8 m/sec^2),
 m is the mass
 D is the deflection
 L is the distance between two loaded points (m), and

I is the momentum of geometric bending which could be calculated from the equation ($I = bd^3/12$).

The mass/deflection ratio was calculated from the slope of the curve.

Dielectric constant

According to ASTM- D150 the instrument used was Type Leybold – Heraeus (Germany) which represents an electrical circuit (in series connection) consists of capacitor, resistor, ammeter, coil, and frequency generator. The sample of dimensions (40 mm diameter and 5mm thickness) was placed between the capacitor plates followed by alternating the frequency of the power supplier till reaches the maximum current value which represents the resonance frequency value (f_r). After that, the (f_r) was determined with the existence of air only, i.e, without the presence of the sample.¹⁷

Dielectric constant (ϵ_r) was calculated from equation 4:

$$\epsilon_r = \frac{\epsilon}{\epsilon_0} \quad (4)$$

where

ϵ and ϵ_0 are the permittivity of the medium and the free space permittivity ($8.8 \times 10^{-12} \text{ F m}^{-1}$), respectively.

RESULTS AND DISCUSSION

Prepared blends

The use of natural polymers such as cellulose and its derivatives as reinforcements in matrix is to a chive composite or blend with improved mechanical properties and stability.¹⁸ All the prepared blends in this work were 100 % solids and homogenous with no phase separation, and they were all colourless and opaque. MUPE/ECIs blends have more smooth surfaces than those for MUPE/CIs blends, that could be due to the differences of the adhesion of CIs with the hydrophobic polymer matrix and of ECIs with the same matrix, that because CIs and ECIs have different hydrophilic degree due to their different number of primary OH groups.

Impact strength test

Impact strength test is an attempt for measuring opposition to growth of craze and that depends on the mechanism of energy absorption if the material is solid.¹⁹

Table 1. Impact strength, hardness, Young's modulus, and dielectric constant for MUPE/CIs blend at 25 °C.

MUPE, wt. %	I_s , kJ m^{-2}	BHN , N mm^{-2}	E , MPa	ϵ_r
100	4.481	118.873	8796	2.553
95	4.911	119.638	11629	2.901
90	5.859	120.849	16847	3.110
85	5.733	122.788	13840	3.400

80	5.225	124.646	13551	4.103
75	4.563	124.646	12663	3.802

Table 2. Impact strength, hardness, Young's modulus, and dielectric Constant for MUPE/ECIs blend at 25°C.

MUPE, wt. %	IS, kJ m ⁻²	BHN, N mm ⁻²	E, MPa	ϵ_r
100	4.481	118.873	8796	2.553
95	4.822	120.397	4842	2.543
90	4.997	123.512	4570	2.521
85	5.426	126.846	4486	2.481
80	4.683	129.846	4141	2.409
75	4.468	129.391	4056	2.281

From the impact strength results (Tables 1 and 2) it was found that the impact strength values of MUPE/CIs and MUPE/ECIs blends were higher than that of the unblended MUPE (Figures 1 and 2), because MUPE behaves as an elastic material in the presence of styrene in its structure, while the presence of CIs or ECIs provides a large area for the distribution of impact forces and for same extent restricts the elasticity²⁰.

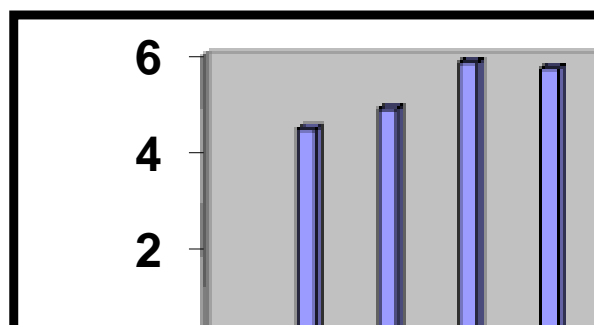


Figure 1. Impact strength for MUPE/CIs blends of CIs w% a) 0, b) 5, c) 10, d) 15, e) 20, f) 25

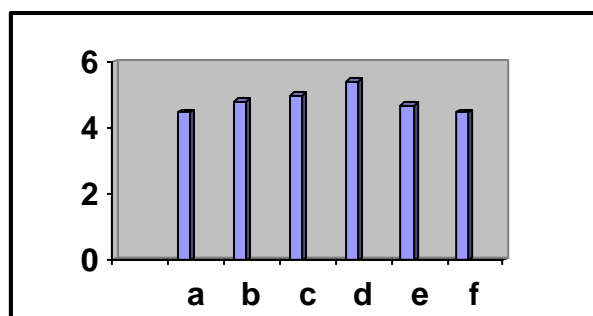


Figure 2. Impact strength for MUPE/ECIs blends of ECIs w% a) 0, b) 5, c) 10, d) 15, e) 20, f) 25

The results also observed that MUPE/CIs blends have higher impact strength than those of MUPE/ECIs blends, that could be due to the weakness of the interfacial forces between MUPE and ECIs of less free OH groups and less inter hydrogen bonds than CIs, also the bulky size of ethoxy group affects the dispersion of ECIs particles.²¹

Brinell hardness test

Hardness means the measurement of the material resistance to a localized deformation, and the ductile material absorbs more quantity of energy, also, as the concentration of the filler is increased, the ability of the filler to form chain structure in the polymeric medium becomes increasingly important.²²⁻²⁴

Hardness results (Tables 1 and 2) showed that BHN values of MUPE/CIs and MUPE/ECIs blends were higher than that of unblended MUPE, and also, blends of CIs and ECIs have good resistance to indentation (Figures 3 and 4) and that could be due to the existence of hydrogen bonds between CIs or ECIs molecules and the MUPE matrix, that leads to transfer some of the applied stress to the filler particles to obtain isotropic blend. The hardness values of MUPE/CIs blends were lower than those of MUPE/ECIs that could be due to the presence of the bulky ethoxy groups in the later.

Three points bending test

This test gives the information about the linear behaviour or Hookean behaviour when the blends are under the load influence of horizontal vector on their surfaces, and when the load is removed the material will recover its natural shape in the range of deformation, that means the material obeys Hook's law.^{25,26} The relation between the mass and deflection (Young modulus) that occurs for the samples are listed in Tables 1 and 2, and the mass against deflection was plotted in Figures 5 – 7 for pure MUPE, 25% CIs blend, and 20% ECIs blend.

The results showed a decrease in the bending of MUPE/CIs blends, while bending were increased for MUPE/ECIs blends, that may be attributed to the higher polarity and more crystallinity of MUPE/CIs blends than MUPE/ECIs blends, because the later contains a nonpolar ethyl groups.

Dielectric constant

Dielectric constant is used to determine the ability of the insulator to store electrical energy, and this constant is the ratio of the capacitance induced by two metallic plates with sample between them to the capacitance of the same plates with air or vacuum between them.²⁷

The results listed in Tables 1 and 2 observed that dielectric constants of MUPE/CIs blends were higher than those of MUPE/ECIs blends, that could be attributed to the increase in polarity which is due to the presence of the primary OH groups in the CIs molecules leading to the orientation of the segments and a some kinetic units will be observed at definite relaxation time and that gives rise to a definite values of dielectric constant, while the presence of ECIs molecules in the blend slightly decreases the dielectric constant of unblended MUPE.²⁸⁻³⁰

CONCLUSION

Cellulose and ethyl cellulose were both compatible with the MUPE used in this study. The properties of MUPE were affected by the OH groups of CIs and ECIs compounds, as

the number of these groups was increased, the intermolecular hydrogen bonds and the polarity of the blends were increased. The best impact strength results were obtained by the (90 % MUPE + 10 % Cls) and the (85 % MUPE + 15 % ECIs) the optimum results of hardness were for (75 % blends. MUPE + 25 % Cls) and (80 % MUPE + 20 % ECIs) blends. Young's modulus of MUPE/Cls blends was higher than those of unblended MUPE and MUPE/ECIs blends. The maximum value of dielectric constant was for (80 % MUPE+20 % Cls) blend.

REFERENCES

- ¹Grayson, M., Eckroth, D., *Encyclopedia of Chemical Technology*, **1982**, Vol. 18, John Wiley and sons. 3rd Ed., USA.
- ²Nevel, T. P., Zeronian, S. H., *Cellulose Chemistry and its Application*, **1987**, Wiley and Sons Inc., New York, USA.
- ³Park, J., Hans, S., Lee, I., *J. Ind. Eng. Chem.*, **2007**, 13(6), 1002-1008.
- ⁴Dong, H. , Xu, Q., Mo, S., Cai, S., Liu, L., *Colloids Surface B: Biointerface*, **2008**, 66(1), 26-33.
- ⁵Keenth, G., Senior, M., *Engineering Materials Properties and Selection*, **1996**, 5th Ed., New Jersey, Prentice-Hall Inc.
- ⁶Utracki, L., *Polymer Blend Handbook.*, **2003**, Netherlands: Kluwer Academic Publisher.
- ⁷Paul, D., Barlow, J., Kesklula, H., *Encyclopedia of Science and Engineering.*, **1988**, 2nd Ed., Vol. 12, USA, Wiley and Sons Inc.
- ⁸Chung, H., Wang, H., *Macromolecules*, **2006**, 39, 153-161.
- ⁹Sadiku, O., Sadiku, E., Adegboia, A., Biotiadora, O., *Mater. Sci. Appl.*, **2011**, 3, 30-41.
- ¹⁰Chan, L., Ong, K., Heng, P., *Pharm Res.* **2005**, 22, 422-476.
- ¹¹Nair, L., Laurein, C., *Polym. Sci.*, **2007**, 32, (8-9), 762-798.
- ¹²Rajput, R., *Material Science*, **2006**, Delhi, India: Kateria and Sons, NaiSarak.
- ¹³Bedezki, A., Mamun, A., Lucka, M., Gubowski, V., *Sci. J.* **2008**, 32, 413-422.
- ¹⁴Chandramohan, D., Marimuthu, K., *Int. J. Adv. Eng. Sci. Tech.*, **2011**, 6(1), 97-104.
- ¹⁵Hihher, R., *Mechanics of Material*, **2005**, Singapore, London, New York, Prentice-Hall Inc.
- ¹⁶Abdulkhalil, H., Bhat, I., Sartika, M., *BioResource.*, **2010**, 5(4), 2278-2298.
- ¹⁷Hameed, A. M., *Ph.D. Thesis*, Department of Appl. Sci. University of Technology, **2006**, Baghdad, Iraq.
- ¹⁸Marcovich, N., Reboredo, M., Aranguren, M., *Chemical Modification of Lignocellulose Materials: The Utilization of Natural Fibers as Polymer Reinforcement*, Sao Paulo: Lignocellulosic Plastic Composite USP and UNSEP, **1997**, 223-240.
- ¹⁹Dinakaran, K., Alagar, M., *Int. J. Polym. Mater.*, **2003**, 52, 957-966.
- ²⁰Al-Zubidy, G. M., *M.Sc. Thesis*, Chemistry Department College of Education Ibn-Al-Haithem Baghdad University, Baghdad, Iraq, **2007**.
- ²¹Al-Saadi, M. H., *Ph.D. Thesis*, Department of Appl. Sci. University of Technology. Baghdad, Iraq, **2006**.
- ²²Foro, C. L., Cicals, G. L., *The Energy Absorbing Properties of Composite Materials, Engineering Materials*, **2000**, UK.
- ²³Aravind, I., Ahn, K., Ranganathaiah, C., Thomas, S., *Ind. Eng. Chem. Res.*, **2009**, 48, 9942-9951.
- ²⁴Aruniit, A., Kers, J., Tall, K. *Agronomy Res. Biosystem Eng., Special Issue*, **2011**, 1, 23-29.B
- ²⁵Grayson, M., *Encyclopedia of Composite Material Components*, John Wiley and Sons, New York, **1983**.
- ²⁶Escamilla, G., Laviada, J., Mendzabel, E., Puig, J., *Composites Part A.*, **2002**, 33(4), 529-549.
- ²⁷McGrsamum, N., Read, B., Williams, G., *Elastic and Dielectric Effects in Polymer Solids.*, London: Wiley, **1967**.
- ²⁸Baird, M. F., *Electrical properties of Polymeric Materials*. London: Plastic Institute, **1973**,
- ²⁹Allcock, H., Lampe, F., Mark, J., *Contemporary Polymer Chemistry*, USA: Amazon Com., **2003**.
- ³⁰Schottky, W., *Dielectric Constant, Strength, and Loss Tangent*, Cafe Forums, **2008**.

Received: 16.01.2013.

Accepted: 13.03.2013.



AN EFFICIENT SYNTHESIS OF 4-ARYL-SUBSTITUTED 3,4-DIHYDROPYRIMIDIN-2(1H)-ONES USING NANOCOMPOSITE FERRITE CATALYST

Vijaykumar M. Joshi^[a], Sanjay K. Vyawahare^[b], Sunil U. Tekale^[b], Sunita B. Shinde^[b], Mohammed Fareesuddin^[b], Satish A. Dake^[b], Suresh U. Shisodia^[b] and Rajendra P. Pawar^{[b]*}

Keywords: 3, 4-Dihydropyrimidin-2(1H)-ones, Ferrite composite, Multicomponent reaction.

A simple and efficient protocol has been reported for the synthesis of 5-ethoxycarbonyl-6-methyl-4-aryl-3,4-dihydropyrimidin-2(1H)-ones using nanoparticulate ferrite composite as recyclable catalyst for one pot three component Biginelli reaction to afford the corresponding product in excellent yields.

* Corresponding Author

Fax: +91-240-2334430

E-Mail: rppawar@yahoo.com

[a] Shri Jagdishprasad Jhabarmal Timrewala University, Rajasthan, India

[b] Department of Chemistry, Deogiri College, Aurangabad-431 005, (MS) India.

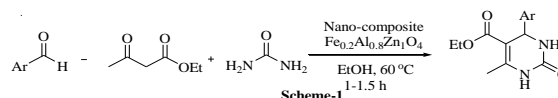
Introduction

Multi-component reactions are the efficient tools in modern synthetic organic chemistry due to their significant features such as atom economy and straight forward reaction designing. Multicomponent reactions facilitate the synthesis of compounds of biological and pharmacological importance by introducing several steps in one pot reaction.

Biginelli reaction is an important multi-component reaction that allows one pot three component synthesis of 3, 4-dihydroxypyrimidin-2-(1H)-ones and their analogues which exhibit many interesting pharmacological and biological properties. 3, 4-dihydropyrimidin-2-(1H)-ones and their derivatives possess several biological activities such as antimicrobial [1], antifungal [2], anti-inflammatory [3], enzyme inhibitory [4], antihypertensive agents [5]. They also act as channel modulators and showed antagonist activities [6]. Thus Biginelli reaction is an important multi-component reaction for the synthesis of biologically active dihydropyrimidinone derivatives.

The first Biginelli reaction was reported by Pietro Biginelli in 1893 by the condensation of an aldehyde, β -keto ester and urea or thiourea in ethanol using a catalytic amount of HCl. This classical synthesis suffered from several drawbacks including low yields (25-60 %) and prolonged reaction time. To improve the reaction; numerous improvements were suggested by different researchers using different both acidic and basic catalytic systems such as copper (II) sulfamate [7], ClSO_3H [8], EPZ10 [9], InBr_3 [10], $\text{Pb}(\text{NO}_3)_2$ [11], NaIO_4 [12], $\text{SnCl}_2 \cdot 2\text{H}_2\text{O}$ [13], Lanthanide Triflate [14], Sulfated Zirconia [15], Zeolite [16], Benzyltriethylammonium chloride [17], Ionic liquid [18], Microwave [19] etc. However, all these methods have several shortcomings which need to be modified.

Herein, we wish to report an efficient and versatile method for Biginelli reaction using nanocomposite ferrite material as a recyclable catalyst (**Scheme-1**).



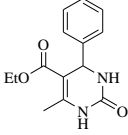
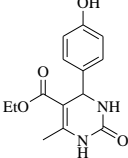
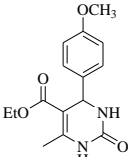
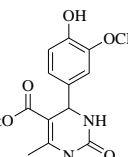
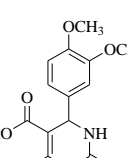
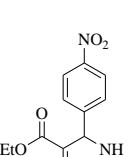
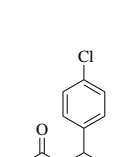
Experimental

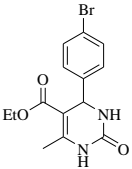
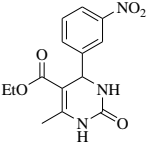
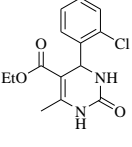
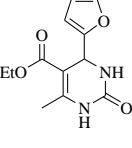
Chemicals were purchased from SD fine chemicals Ltd and used without further purification. Melting points of products were measured in open capillaries. NMR spectra were recorded 400 MHz Varian NMR spectrophotometer using tetramethylsilane (TMS) as the internal standard. All solvents were AR grade and used as received. IR spectra of the samples were recorded on Perkin IR spectrophotometer using KBr discs. Samples were scanned for mass on Shimadzu mass analyzer. The catalyst was synthesized by reported sol-gel method [20]

General procedure for the nanocomposite ferrite catalyzed synthesis of 4-aryl substituted 3, 4-dihydropyrimidin-2(1H)-ones

A mixture of aldehyde (2 mmol), ethyl acetoacetate (2 mmol), urea (3 mmol), ferrite nanocomposite $\text{Fe}_{0.2}\text{Al}_{0.8}\text{Zn}_1\text{O}_4$ (10 mol %) and 2 drops HCl in ethanol (5 mL) was heated at 60 °C for 1 hr. The progress of reaction was monitored by Thin Layer Chromatography (30 % ethyl acetate: hexane). After completion of the reaction as indicated by TLC, the reaction mixture was diluted with hot ethanol (10 mL), filtered off to separate the catalyst. The filtrate was concentrated and the product was purified by recrystallization from ethanol. Using these conditions a series of different 3, 4-dihydropyrimidin-2(1H)-ones were obtained (**Table 1**). All the synthesized compounds are reported and characterized by IR, ^1H NMR, Mass and comparison of their physical constants as reported in the literature. The spectral data of representative compounds is described below:

Table 1: Synthesis of 4-aryl substituted 5-ethoxycarbonyl-6-methyl-3,4-dihydropyrimidin-2(1H)-ones using nanoparticulate composite ferrite catalyst.

Sr. No.	Ar	Product	Time, h	Yield, %	M. p., °c	Reference
1	C ₆ H ₅		1.30	92	205-207	[17]
2	4-OH-C ₆ H ₄		1.35	94	221-222	[7]
3	4-OCH ₃ -C ₆ H ₄		1	92	198-200	[17]
4	4-OH-3-OCH ₃ -C ₆ H ₃		1.45	91	257-259	[7]
5	3,4-(OCH ₃) ₂ -C ₆ H ₃		1.15	88	172-173	[17]
6	4-NO ₂ -C ₆ H ₄		1	87	209-211	[8]
7	4-Cl-C ₆ H ₄		1.2	92	211-213	[8]

8	4-Br-C ₆ H ₄		1.5	92	212-214	[13]
9	3-NO ₂ -C ₆ H ₄		1.2	90	2085-201	[13]
10	2-Cl-C ₆ H ₄		1.2	94	213-215	[9]
11	2-Furyl		1.2	89	208-210	[10]

Yield of reactions using aldehyde (2 mmol), ethylacetoacetate (2mmol), urea or thiourea (3 mmol), nanocomposite ferrite (10 mol %) and 2 drops HCl in ethanol (5 mL) at 60 °C temperature.

5-Ethoxycarbonyl-6-methyl-4-(4-hydroxyphenyl)-3,4-dihydropyrimidin-2(1H)-one (Entry 2, Table 1). M.p. 221-222 °C; ¹H NMR (400 MHz, CDCl₃): δ ppm 1.6 (t, 3H), 1.9 (s, 3H), 4.65 (q, 2H), 5.05 (s, 1H), 5.8 (s, 2H), 5.5 (s, 1H), 6.6 (d, 2H), 7.05 (d, 2H); ¹³C NMR (100 MHz, CDCl₃): δ ppm 23.123, 24.011, 29.726, 50.001, 62.584, 117.356, 121.814, 127.645, 136.015, 145.143, 153.468, 169.542; IR (KBr) cm⁻¹ 3383, 3236, 2920, 1627, 1516, 1447.

5-Ethoxycarbonyl-6-methyl-4-(4-methoxyphenyl)-3,4-dihydropyrimidin-2(1H)-one (Entry 3, Table 1) M.p. 198-200 °C; ¹H NMR (400 MHz, CDCl₃): δ ppm 1.15 (t, 3H), 2.29 (s, 3H), 3.72 (s, 3H), 4.05 (q, 2H), 5.28 (s, 1H), 6.20 (brs, 1H, NH), 6.84 (d, 2H), 7.21 (d, 2H), 8.75 (brs, 1H, NH); ¹³C NMR (100 MHz, CDCl₃): δ ppm 14.404, 16.742, 55.47, 60.18, 67.301, 101.723, 114.154, 128.039, 136.494, 146.399, 154.021, 159.421, 165.365; IR (KBr) cm⁻¹ 3276, 3112, 2979, 2826, 1614, 1512, 1720, 1653, 1463, 1082, 842.

Results and Discussion

To find out the utility of catalyst, a mixture of 1 equivalent amount of 4-methoxybenzaldehyde, ethyl acetoacetate and 1.5 equivalent urea in water were refluxed for 10 h with different catalysts. Different catalysts such as HCl, CuCl, CuCl₂, and ferrite composite

were used to explore the reaction. After 10 h, the crude product was diluted with 5 mL ethanol and filtered off to separate the catalyst. The filtrate was concentrated and the product was purified by recrystallization in ethanol. The results are presented in **Table 2** which shows that Ferrite Composite was the best among tested catalysts, but the yields were not so high.

To check the temperature effect on the formation of product, these reactions were carried out at different temperature (**Table 3**). The maximum yield of product was obtained at temperature 60 °C. Thus, the best results were obtained using 10 mol% of the nanocomposite catalyst ferrite in ethanol at 60 °C temperature.

Table 2. Effects of the Catalysts on the formation of 4-methoxyphenyl 5-ethoxycarbonyl-6-methylpyrimidin-2(1H)-ones

Entry	Catalyst	Amount	Yield, % ^b [Ref.]
1	Free	----	39
2	HCl	1 ml	44 [21]
3	CuCl	10 mol%	63 [21]
4	CuCl ₂	10 mol%	71 [21]
5	Ferrite composite	10 mol%	92

^aReaction conditions: 4-methoxybenzaldehyde (1 mmol), ethyl acetoacetate (1 mmol), urea (1.5 mmol), ferrite composite (10 mol %) and 1 drop HCl in ethanol (2 mL), ^bIsolated yield.

Table 3. Effects of temperature on the formation of 4-methoxyphenyl-5-ethoxycarbonyl-6-methylpyrimidin-2(1H)-ones

Entry	Temperature, °C	Time, min	Yield, % ^b
1	RT	60	--
2	40	60	18
3	50	60	24
4	60	60	92
5	60 and above	60	94

^aReaction conditions: 4-methoxybenzaldehyde (1 mmol), ethyl acetoacetate (1 mmol), urea (1.5 mmol), nanocomposite ferrite catalyst (10 mol %) and 1 drop HCl in ethanol (1 mL); ^bIsolated yield.

Conclusion

In summary the present work explores a new approach for one pot three component Biginelli reaction using nano composite ferrite material as a heterogeneous catalyst in ethanol. This protocol shows several advantages, such as shorter reaction time, operational and experimental simplicity; making it an attractive process for Biginelli reaction.

Acknowledgements

The authors are thankful to the Principal **Dr. S. N. Thore**, Deogiri College, Aurangabad, for his continuous encouragement during this work.

References

- ¹Jalali, M., Mahdavi, M., Memarian, H. R., Ranibar, M., Solevmani, M., Fassihi, A., Abedi, D. *Res. Pharm. Sci.* **2012**, *7*, 243-247.
- ²Duguay, D. R., Zamora, M. T., Blacquiére, J. M., Appoh, F. E., Vogels, C. M., Wheaton, S. L., Baerlocher, F. J., Decken, A., Westcott, S. A. *Cent. Eur. J. Chem.* **2008**, *6*, 562-568.
- ³Tale, R. H., Rodge, A. H., Hatnapure, G. D., Keche, A. P., Patil, K. M., Pawar, R. P. *Med. Chem. Res.* **2012**, *21*, 4252-4260.

- ⁴Kim, J., Park, C., Ok, T., So, W., Jo, M., Seo, M., Kim, Y., Sohn, J. H., Park, Y., Ju, M. K., Kim, J., Han, S. J., Kim, T. H., Cechetto, J., Nam, J., Sommer, P., No, Z. *Bioorg. Med. Chem. Lett.* **2012**, *22*, 2119-2124.
- ⁵Atwal, K. S., Swanson, B. N., Unger, S. E. *J. Med. Chem.*, **1991**, *34*, 806-811.
- ⁶Kappe, C. O., Fabian, W. M. F., Semones, M. A. *Tetrahedron* **1997**, *53*, 2803-2816.
- ⁷Liu, C.-J., Wang, J.-D. *Molecules* **2009**, *14*, 763-770.
- ⁸Kotharkar, S. A., Nagawade, R. R., Shinde, D. B. *Ukr. Bioorg. Acta.* **2006**, *2*, 17-21.
- ⁹Lee, K.-Y., Ko K.-Y., *Bull. Korean Chem. Soc.* **2004**, *25*, 1929-1931.
- ¹⁰Fu, N. Y., Pang, M. L., Yuan, Y. F., Wang, J. T. *Chin. Chem. Lett.* **2002**, *13*, 921-922.
- ¹¹Boumoud, T., Boumoud, B., Rhouati, S., Belfaitah, A., Debache, A., Mosset, P. *E-J Chem.* **2008**, *5*, 688-695.
- ¹²Jing, X., Li, Z., Pan, X., Shi, Y., Yan, C. *J. Iran. Chem. Soc.*, **2009**, *6*, 514-518.
- ¹³Russowsky, D., Lopesa, F. A., Silvaa, V. S. S., Cantoa, K. F. S. D'Ocab, M. G. M., Godoi, M. N. *J. Braz. Chem. Soc.*, **2004**, *15*, 165-169.
- ¹⁴Ma, Y., Qian, C., Wang, L., Yang, M. *J. Org. Chem.* **2000**, *65*, 3864-3868.
- ¹⁵Reddy, B. M., Sreekanth, P. M., Lakshmanan, P. *J. Mol. Cat. A: Chem.* **2005**, *237*, 93-100.
- ¹⁶Kulkarni, M. G., Chavhan, S. W., Shinde, M. P., Gaikwad, D. D., Borhade, A. S., Dhondge, A. P., Shaikh, Y. B., Ningdale, V. B., Desai, M. P., Birhade, D. R. *Beil. J. Org. Chem.* **2009**, *5*, 1-4.
- ¹⁷Bose, D. S., Sudharshan, M., Chavhan, S. W. *Arkivoc* **2005**, *iii*, 228-236.
- ¹⁸Li, M., Guo, We-S., Wen L.-R., Li Y.-F., Yang H.-Z. *J. Mol. Cat. A: Chem.* **2006**, *258*, 133-138.
- ¹⁹Stadler, A., Kappe, C. O. *J. Chem. Soc., Perkin Trans.* **2000**, *2*, 1363-1368.
- ²⁰Mircea, S., M., Stoia, O., Stefanescu, P., Barvinschi, *J. Therm. Anal. Calorim.* **2010**, *99*, 459-464.
- ²¹Mirza-Aghayan, M., Moradi, A., Bolourtchian, M. *J. Iran. Chem. Soc.* **2010**, *7*, 269-274.

Received: 22.02.2013.

Accepted: 11.03.2013.



NEW CRITERIA AND REQUIREMENTS FOR REDUCING AND STOPPING THE GLOBAL WARMING

Csaba Muzsnay^[a]

Keywords: global warming, greenhouse effect, atmospheric water vapor (AWV), greenhouse gases, carbon-dioxide, human activities originated water vapor generators, absorption of long wave radiation, precipitate formation and transport

It has long been known that the absorption of terrestrial energy by water molecules is the largest one (60-75 %), comparing with the lower value (20-24 %) of carbon dioxide molecules. The other gases with greenhouse effect absorb this energy in much smaller extent (8-12 %). In the last 360 years, considering from the industrial revolution, the amount of water vapor resulting on the basis of eight types of major processes, by direct and indirect human activities, and getting into the atmosphere was continuously growing. These are determined, by the appearance of very numerous human activities originated water-vapor/steam generators, the continuous increase of the greenhouse effect and the climate change. The following levels of special and extraordinary behavior of the atmospheric water vapor can be distinguished: 1) molecular, 2) associative (cluster) level, 3) condensation level which can be joined to phase transformations - mainly in the clouds, 4) the level of precipitate formation followed by intense moisture transport, 5) the level of firm difference existing between the atmospheric relations of the Northern and the Southern Hemisphere, mainly due to human activities. The atmosphere near the Earth's surface (in the troposphere) has such a well delimited temperature and pressure domain, in which water with its unique property occurs in all three phases. Water vapors condense easily. The triple point of the other atmospheric components is not achieved. This unique and extraordinary feature of the water plays a determining role in the meteorological processes of the Earth and the development of the climatic relations. All this warming, among other things, is manifested in the melting of the ice of the North Pole and the elevation of the snow altitude line. The primary task is the stopping of the warming of the North Pole Region and the promotion of its cooling. Global solutions appear as mandatory needs, which are very costly to start because extensive investments are required.

* Corresponding Authors

E-Mail: cmuzsnay@chem.ubbcluj.ro

[a] Babeş-Bolyai University, Chair of Analytical Chemistry, Cluj-Napoca, Romania

effect and the climate changes, through the appearance of very numerous human activities originated water-vapor generators. The spheres and the climatic systems of the Earth in the last two centuries clearly show noticeable changes. In connection with the global warming and climate change differences of opinion took shape.^{2, 4-8}

INTRODUCTION

The global warming of the Earth's surface and that of the atmosphere already has a solid experimental basis. There are fierce discussions about the time variability of the weather and strange interpretations of the average global temperatures drop in the second half of the twentieth century. It should be mentioned that the author of this paper was able to interpret the phenomenon of global cooling during 1945-1980.¹

The increased greenhouse effect caused by constantly rising carbon dioxide content of the atmosphere is almost universally accepted, although there is no direct evidence for this. Among the triatomic molecules of atmosphere, the asymmetric water molecules, - because of their polar character, and their highest average concentration, absorb much more strongly the long-wave (terrestrial) radiation, than the symmetric, non polar molecules of carbon dioxide. The absorption of terrestrial energy by atmospheric water molecules is the largest one (60-75 %), comparing to the lower value (20-24 %) of carbon dioxide molecules. The other gases with greenhouse effect absorb this energy in a much smaller extent (8-12 %).

Considering from the industrial revolution, in the last 360 years by direct and indirect human activities, increasing amount of water vapor are getting into the atmosphere on the basis of eight types of major chemical processes.^{2a,3} These determined the continuous increase of the greenhouse

Within the framework of this paper we turn our attention to the water vapors resulted directly and indirectly from human activity, that causes weather variability and global warming which is demonstrated on the basis of a five levels theory recently published partially.^{2, 3}

Because of the special and extraordinary behavior of atmospheric water vapor the following five levels, with some energetic aspects, can be distinguished: 1) molecular, 2) associative (cluster) level, 3) condensation level which can be joined to phase transformations - mainly in the clouds, 4) the level of precipitate formation followed by intense moisture transport, 5) the level of firm difference existing between the atmospheric relations of the Northern and the Southern Hemisphere, mainly due to human activities.^{2, 9, 10}

DISCUSSION

The levels are constituted by molecular structures, energy states, phase transitions, human agglomerations, and activities, as well as differences in geographical location.

The first three levels possess mainly energetic characteristics, at which are determining the changes in energy of molecular structures or physical state of material. The presentation of all levels will happen in separate subsections

Molecular level of electromagnetic energy absorption

The small sized and simple structured molecules have the determining role in properties of the Earth's atmosphere. The larger molecules with a more complicated structure can be found only in trace amounts, and they do not get a determining role in the energy relations of the atmosphere. According to quantum-chemical calculations and on the basis of molecular spectroscopy measurements, the monatomic noble gases and the most abundant components, like nitrogen and oxygen, with symmetrical diatomic molecules - N_2 and O_2 - are capable of significant interaction only with the electromagnetic radiation of high energy - of the order of electron excitation energy.

These atoms have a spherical electron distribution, and the diatomic molecules have a non-polar character. As a result of this, they interact very limitedly with the solar radiation and their absorption of the low energy Earth radiation is completely negligible.¹¹

The special role of water vapors in the greenhouse effect is due primarily to the V- or triangle- shaped, respectively flattened (distorted) tetrahedron of asymmetric water molecules with permanent dipole moment¹². Thus, it can interact with all the visible, the microwave and the infrared components of the electromagnetic radiation, absorbing the long-wave (terrestrial) radiation. The non-symmetrical water molecule with relatively high concentrations presents big reservoirs (e. g., the oceans, seas, lakes, rivers), and is able to change the thermodynamic states in the atmosphere. Although the linear carbon dioxide molecule is non-polar in ground-state, in the course of vibrations it becomes polar and capable of interaction with radiation. Primarily it absorbs energies radiated from the surface of Earth. Both the quite large and the ever-increasing concentrations produce important greenhouse effect. At the sun's surface there's a high temperature (5250 °C) with a blackbody radiation spectrum (Fig. 1.) This light passing through the gas components of the atmosphere is absorbed in many frequencies/wavelengths obtaining the absorption bands of greenhouse (GH) gases presented.

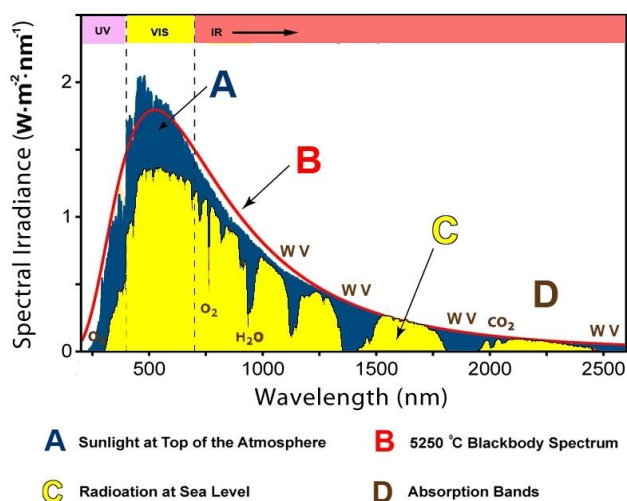


Figure 1. The solar radiation spectrum [/http://en.wikipedia.org/wiki/File:Solar_Spectrum.png](http://en.wikipedia.org/wiki/File:Solar_Spectrum.png)

The ozone appears mainly in the upper layers of air, in the middle part of the stratosphere (20-35 km altitude) attains its largest concentration, in the so called ozone shield. As a triangle shaped molecule it easy interacts with different energies of photons from sunlight. It absorbs ultraviolet radiation and thus protects the biosphere from the harmful components of sunlight. By means of his greenhouse effect a part of heat radiations is retained from the surface of the Earth. As an oxidant it is decomposed by gases with reductive character (e.g. NO), the Cl atom and the halogenated hydrocarbons catalyze the ozone disintegration. All these threaten the existence of the O_3 -layer, or diminish its thickness.

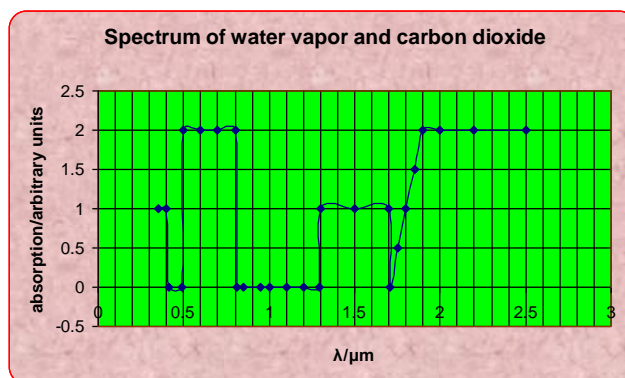


Figure 2. Schematic spectrum of water vapor and carbon dioxide. Arbitrarily, both for easier representation and better transparency of figure the maximum absorption of carbon dioxide (1) is considered as half of the value for water (2). The range of "atmospheric window" is well discernible on the figure (range between 0.8-1.3 μm).

Fig. 2. represents the 2-2 main absorption bands of atmospheric water vapors and carbon dioxide in the range of 0.1-3.0 μm . The CO_2 has between 1.3-1.7 μm a very strong absorption band and between 0.35-0.40 μm a weaker one. In addition, there are smaller absorption bands also in the range of 0.11-0.27 μm , which are not shown on the graph.^{13, 14} Between 0.5-0.8 μm the strong water vapors absorption corresponds to rotational-vibration band, while at wavelengths bigger than 2.0 μm an excessively strong absorption as a rotational band of water vapors is noticeable. At wavelength smaller than 0.5 microns, more precisely in the 0.072-0.49 microns wavelength range water vapors excel in absorbing capability.

In the range of 0.8-1.3 microns neither CO_2 nor water vapors get absorbed and through this well known "atmospheric window" the long-wave radiation from Earth's surface escapes into the space. The energy of the sun-ray, with its variety of color and wavelength, reaches the earth's surface, illuminates and warms it. IR emission from the Earth's radiation can get back into the space, but mostly it's absorbed by water vapors and carbon dioxide in the atmosphere - these substances become almost opaque for the radiation in IR. If other gases are present (e. g. CH_4 , N_2O), they also absorb, the "atmospheric window" closes more and more, all together it's warming the air layer near the Earth very effectively - in form of long wave ray - 240 $W\cdot m^{-2}$ of energy radiated out into space directly.^{13, 3}

The level of molecular association, of cluster and aerosol formation

Water molecules establish hydrogen bonds with almost all atmospheric components forming clusters. The following clusters are more frequent:

- water-water ($7 > n > 1$), where n is the total number of water molecules),
- sulfuric acid-water
- nitric acid-hydrochloric acid-water: $\text{HNO}_3\text{-HCl-H}_2\text{O}$ (see Fig. 3),
- inert gas-water
- and many others.

The stability of the above association compounds decreases with temperature increase.

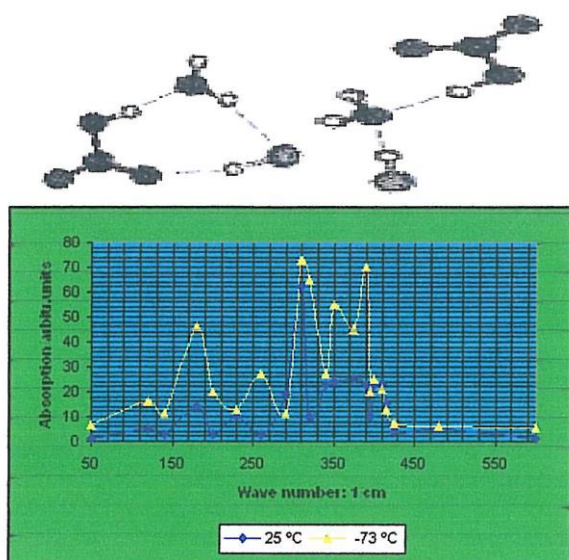


Figure 3. A spectral detail referring to $\text{HNO}_3\text{-HCl-H}_2\text{O}$ cluster at two temperatures. At $-73\text{ }^\circ\text{C}$ the cluster is stable and ring-shaped, at $25\text{ }^\circ\text{C}$ the cluster is less stable, by ring opening there is a chain formation.

The pronounced aggregation under certain conditions leads to aerosol formation. All types of these aggregations absorb terrestrial radiant energy. Aerosols absorb directly the radiant energy of the sun too.¹⁵

The level of condensation, which is connected with the phase transformation of water

Both the temperature and pressure of the atmosphere near the Earth's surface (troposphere, stratosphere) varies in a limited area in which the three phases (vapor /gas, liquid, ice /solid) of water with their special properties can be present simultaneously - at temperatures corresponding to the triple point ($T: 0.006\text{ }^\circ\text{C} = 273.156\text{ K}$ and $P_{\text{vap}}: 6.11\text{ mb}$).¹⁶ This interphasic equilibrium (See: $p = f(T)$ diagram - Fig. 4.) is established quickly especially between liquid and gaseous phases with fast evaporation of liquid water and easy condensation of vapors at greater temperatures than $0\text{ }^\circ\text{C}$ along the blue curve. At lower temperatures than $0\text{ }^\circ\text{C}$ along

the blue curve the water vapors are in equilibrium with the ice (solidified water). The nearly vertical brown line separates water (liquid) from the solid water (ice) Parallelogram delimited by coordinates: $p = 0$ to 1.0 bar and $T = -100$ to $100\text{ }^\circ\text{C}$ (the green colored area on the reduced form of Fig. 4.) represents the boundary conditions of the earth's atmosphere and the existence of water in the 1-3 states of aggregation. In this parallelogram between $-80\text{ }^\circ\text{C}$ ($p = 1\text{ b}$) and $-100\text{ }^\circ\text{C}$ ($p = 0.1\text{ b}$) the CO_2 can be condensed but only at greater pressures than the partial pressure of carbon dioxide in atmosphere. Thus, the atmosphere near the Earth's surface has such a well delimited temperature and pressure domain, in which water with its unique property occurs in all three phases.

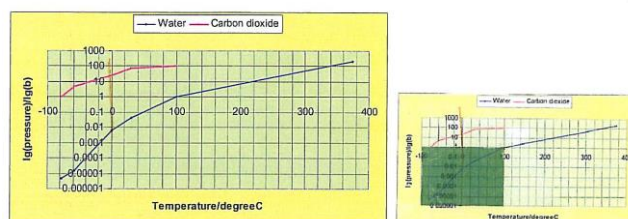


Figure 4. Pressure-temperature dependence ($p=f(T)$) for two components of air: water vapors and carbon dioxide. The pressure axis is logarithmic.

It must be emphasized that the triple point of water is objectively determinable and reproducible, but this doesn't happen in the atmosphere for the other nine basic components. The triple points of the rest of the atmospheric components - other than water - (especially of carbon dioxide) are not achieved. This unique and extraordinary feature of the water plays a determining role in the meteorological processes of the Earth and the development of the climatic relations.

The formation of precipitation, and the intense transport of humidity

The fact that only water condenses (by liquefaction or solidification) among the ten basic components of the atmosphere having a real triple point in the troposphere, is a unique and extraordinary property, that plays a decisive role in meteorological processes of the world. In the atmosphere, due to local differences in temperature and pressure it's generating either vertical transport (convection) or horizontal transport (advection) of moisture able to have three states of aggregation.¹⁷ The occurrence of storm cells involves a starting pulse: e.g. - among other things - the introduction of water vapors in the atmosphere by human contribution.

The fulfillment of at least four balance conditions ensures the understanding of the major processes in the atmosphere.^{17, 18}

1) The water balance: excess water vapors do not accumulate, but carrying both atmospheric humidity and precipitations as either to the North Pole or to the drier areas.

2) The heat balance: Most of the radiation deficit observed Earth's surface near the Arctic is compensated by the latent heat of water vapors that is released by its condensation during cooling (Fig. 5).¹⁹

3) The angular momentum balance of Earth-atmosphere system: Introduced water vapors into the atmosphere by human contribution and pumped through greenhouse energy are not lost, they also contribute to both atmospheric warming and other neighboring areas.

4) The equilibrium distribution of air masses.

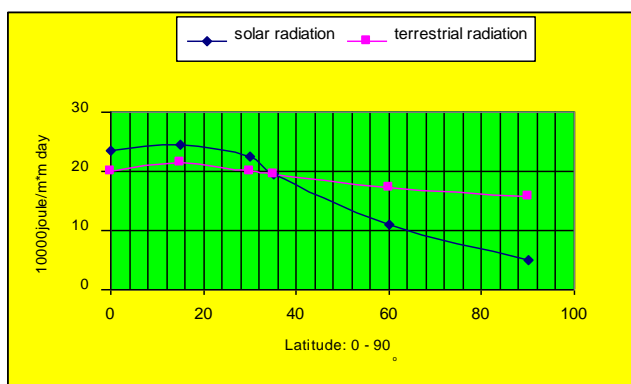


Figure 5. Variation of two types of radiant energy in function of northern latitude. At 35 ° latitude the two radiations are leveling.

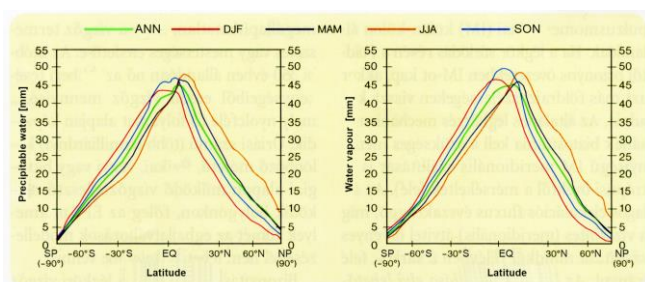


Figure 6. Water vapors column of the atmosphere (in mm) during 4 seasons of year averaged zonal, seasonal and by time, from July 1990 to June 1995 using TOVS Path – B data (right) and from 1991 to 1995 using NVT data (left). On both figures it's noticeable, that much greater quantities of water vapors stream in the direction of the North Pole than in the direction of the South Pole, mainly in summer (JJA), but in the Spring (MAM) and Autumn (SON) period. The blue curve (ANN) is averaged over the year, it also supports the previous commentary.

The distinctive difference level between the atmospheric phenomena of the Northern and the Southern hemisphere

Heating phenomena presented above is manifested in many ways, e.g. by suddenly melting of North Pole ice in the summer, but in a lesser extent ice melts at the South Pole too, and by increased thickness of snow in the mountains - especially in the northern hemisphere, because there is a clear and distinct difference between the two hemispheres of the globe. Thus: - land area is much smaller (1/4-1/3), than that covered by water (2/3-3/4), but the land on the north is more than ~ 2/5 as against 1/5 land area on the south. 90% of the population lives and works in the Northern Hemisphere and 90% of the water vapor resulting from human activities get into these parts of the atmosphere. Comparing the corresponding seasons, the northern

hemisphere has wetter seasons mainly due to human activities. This part of the atmosphere contains more vapors, being wetter than the southern one (see also the Fig. 6).²⁰

Winters are about equally wet, but summers in the Northern Hemisphere are more humid. Thus in August humidity is higher by 20%, and the average temperature is higher by 2.2 °C. Vapor content of the atmosphere in the North are higher than in the South primarily because of more extensive human activities.

The most sensitive sensor of global warming caused by water vapors, is the Arctic, with the North Pole and Greenland (Fig. 6.), and respectively the Antarctic.

Most important global tasks

1. Reducing the water vapor content in the atmosphere, not by any means, but respecting a comprehensive and continuous program of permanent reduction of water vapors emitted by mankind. - Gradual restoration of the North Pole to the frozen state it had before the beginning of the industrial revolution.
2. Stopping the warming of the Arctic, especially in summer, promoting its gradual cooling is the main task. In this way, we could avoid the further weakening of the Gulf Stream, the rise of the ocean's level and such prevent the flooding of seaside cities and settlements.^{2b, 3, 9}
3. Making serious global investments for both vapor condensation, and reducing the evaporation of water used in industry, agriculture and many other fields to obtain the formulated major goals. It involves the establishment of an overall control system for efficient operation of expected processes and technologies. When an internationally valid political decision has been reached, aiming at the complete and continuous retention from the atmosphere of all water vapors resulting from human activity - a decision that is compulsory for every nation - detailed action plans have to be developed and implemented while ensuring all reasonable and legitimate security requirements.
4. Ensuring the central role of natural sciences especially that of Chemistry and Engineering through increased contribution from scientific institutions and national scientific organizations.

CONCLUSIONS

Global warming is due not only to the increasing carbon dioxide content of atmosphere; it can be attributed to the great quantity of water vapors generated both directly and indirectly by mankind.

The global and international actions should provide concomitant reduction of the huge amounts of water vapors and carbon dioxide originated from human sources of any kind.

The amount of atmospheric water vapors resulted directly or indirectly by human activities must be condensed and stored very wisely and efficiently.

REFERENCES

- ¹Muzsnay, Cs., *17th Internat. Conf. on Chem.*, Cluj-Napoca, November 3-6, **2011**, 62.
- ²Muzsnay, Cs. *Magy. Kém. Lapja*, **2011**, *64*(9), 265-272; *Magy. Kém. Lapja*, **2011**, *64*(10), 301-306.
- ³a) Muzsnay, Cs., *15th Int. Conf. Chem., Târgu-Mureş* November 14, **2009**, 59, b) Muzsnay, Cs., and Muzsnay, Cs. jun., *15th Int. Conf. Chem., Târgu-Mureş*, November 14, **2009**, 77.
- ⁴Muzsnay, Cs., *Int. Conf. "The contexts of sustainable development, environmental protection and nature conservation in Carpathian Basin"*, Pécs, 15-th September, **2010**.
- ⁵Pentagon Report, in "*Magyar Szó*" Online, (In Hungarian) Iss. 21, 22 February, **2004**.
- ⁶Miskolczi, F. M., a) *Időjárás* **2007**, *111*(1), 1., b) *Energy Environ.* **2010**, *21*(4), 243.
- ⁷Berényi, D., *Term. Tud. Közl. (Budapest)*, **2011**, *142*(3), 101.
- ⁸Czelnai, R., *Term. Tud. Közl. (Budapest)*, **2011**, *142*(4), 148.
- ⁹Muzsnay, Cs., *16th Int. Conf. Chem., Cluj-Napoca*, November 11, **2010**, 63.
- ¹⁰Muzsnay, Cs., *Int. Conf. Environ. Progress, Cluj-Napoca*, 11th November, **2011**, 56.
- ¹¹a) Császár, A., *Term. Tud. Közl.* **2009**, *140*(2), **2009**, 60-64; b) Császár, A., Furtenbach, T. and Czakó, G., *Magy. Kém. Foly.* **2006**, *112*(4), 123-8.
- ¹²a) Chaplin, M., „*Water Structure and Behavior*”; <http://www.lsbu.ac.uk/water/molecule.html>, (<http://www.lsbu.ac.uk/water/chaplin.html>) - with regularly and frequently renewed chapters. b) Muzsnay, Cs., 1) *Stud. Univ. Babeş-Bolyai, Ser. Chem.*, V., **1984**, 29, 49. 2) *Magy. Kém. Foly.* **1987**, *93*(2), 54.
- ¹³Uherek, E., *Environmental Science Published for Everybody Round the Earth Educational Network on Climate, ESPERE Climate Encyclopedia*, **2004**, Mainz, Max Planck Institute for Chemistry; (<http://www.atmosphere.mpg.de/enid/2640>).
- ¹⁴Borşan, D., „*Fizica atmosferei*” (in Romanian) **1981**, Univ. Bucureşti, Bucureşti, 125.
- ¹⁵Gómez, P., C., Gálvez, O., Mosteo, R., G., Puzzarini, Cr., Escribano, R., *PCCP*, **2010**, *12*, 4617.
- ¹⁶Atkins, P., W., „*Physical Chemistry*”, **1992**, V. I. *Capitols: 1 and 6* (in Hungarian), Tankönyvkiadó, Budapest.
- ¹⁷Czelnai, R., *Introduction to Meteorology I. Fundamentals of Atmospheric Science (in Hungarian)*, **1993**, Nemzeti Tankönyvkiadó, a) 93-95, b) 110, c) 125, d) 122, 130, and e) 115-118.
- ¹⁸Czelnai, R., Götz, G. and Iványi Zs., *Introduction to meteorology II., The atmosphere in motion and oceans (in Hungarian)*, Nemzeti Tankönyvkiadó, Budapest 1998, a) 346-347, b) 11-14, c) 56-61, 303-307.
- ¹⁹Rákóczi, F., „*The atmosphere our living space*” (in Hungarian), **1998**, Mundus Magyar Egyetemi Kiadó, Budapest, 32-38, 40, 41, 50.
- ²⁰Hantel, M., volume editor, *Observed Global Climate in Landolt-Börnstein, New Series, Group V. Geophysics, Vol. 6*, **2005**, Springer Verlag, Berlin, a) 5-4, b) 5-12.

Received: 24.02.2013.

Accepted: 13.03.2013.



VARIATIONS IN NUTRITIONAL POTENTIALS OF SOME VEGETABLES GROWN ON CRUDE-OIL CONTAMINATED AND REMEDIATED AGRICULTURAL SOIL.

Reginald Chibueze Ohiri^{[a]*}, Augustine Amadikwa Uwakwe^[a] and Eugene Nwaogwugwu Onyeike^[a]

Keywords: Bioremediation, Proximate composition, Vitamins, vegetables.

Variations in nutritional potentials of some edible vegetables grown on crude oil post remediated agricultural soil was carried out after four weeks of growth on the bioaugmented and natural attenuated soils. The result showed variations in both the vitamin content and proximate composition of the vegetables. *Telfairia occidentalis* grown on bioaugmented site had the highest concentration of vitamins B₂, B₃ and E with an increase of 16.5425 % for vitamin B₂ and decrease of 7.8747 % and 6.6143 % for vitamins B₃ and E, while *Tallinium triangulare* grown on natural attenuated site had the highest concentration of vitamins A, B₁, B₂, B₃, B₆, C and E with decrease of 12.7558 %, 5.3239 %, 6.2900 %, 2.4000 %, 2.8834 %, 0.1508 %, and 21.4117 %. Moreover *Amarantus hybridus* grown on the natural attenuated site had the highest increase in vitamins A, B₁, B₆, C and E with decrease of 5.4216 %, 16.2200 %, 4.7159 %, 1.7580 % and 3.5965 %. Proximate composition of the vegetables showed that *Telfairia occidentalis* grown on bioaugmented site had the highest concentration of lipid, carbohydrate, moisture, and crude fibre with increase of 125.1487 %, 3.0111 %, 3.0600 % and 6.2500 % respectively, while *Tallinium triangulare* grown on bioaugmented site had the highest concentrations of lipid, carbohydrate and ash with increase of 430.0000 %, 27.7592 % and 31.2846 % respectively. However, *Amarantus hybridus* also grown on bioaugmented site had the highest concentrations of lipid, carbohydrate and moisture with increase of 349.9631%, and 1.4593% for lipid and moisture, while carbohydrate had a decrease of 12.4762% when compared to their respective controls.

Corresponding Authors

Tel: +234 8038808077.

E-Mail: raycohiri@yahoo.com

[a] Department of Biochemistry, University of Port Harcourt, P. M. B. 5323 East-West Road, Choba, Rivers State, Nigeria.

Introduction

The soil is a biologically active porous medium that developed in the uppermost layer of the earth's crust. It is one of the principal substrata of life on earth, serving as a reservoir of water and nutrients, as a medium for the filtration and breakdown of injurious wastes and as a participant in the cycling of carbon and other elements through the global ecosystem. Since the rise of agriculture and forestry in the 8th millennium B.C., there has also arisen by necessity a practical awareness of soils and their management. In the 18th and 19th centuries, the industrial revolution brought increasing pressure on soil to produce raw materials demanded by commerce, while the development of quantitative science offered new opportunities for improved soil management.¹ This initial inquiry has expanded to the understanding of soil as a complex, dynamic, biogeochemical system that are vital to the life cycle of terrestrial vegetation and soil-inhabiting organisms and by extension to the human race as well. The presence of toxic compounds in soil has increased dramatically by the accelerated rate of extraction of minerals and fossil fuels and by highly technological industrial processes¹. Notable among these extractable toxic fossil fuels are the petroleum hydrocarbons.

Petroleum like all fossil fuels primarily consists of complex mixtures of hydrocarbons. Petroleum hydrocarbons are composed of various portions of alkanes (e.g. methane, ethane, etc), aromatics (e.g. benzene, toluene, ethylene and xylene, collectively known as BTEX) and polycyclic

aromatics hydrocarbons (PAHs) (e.g. naphthalene, phenanthrene, anthracene and benzo(α)pyrene, etc). In high concentrations, the hydrocarbons molecules that make up petroleum are highly toxic to many organisms, including humans.² The dominance of petroleum products in the world economy creates the conditions for distributing large amounts of these toxicants into populated areas and ecosystem around the globe.³ Industrial activities release substantial amount of crude oil and refined products into the environment, as a result of accidents such as storage tank leakage, oil spills during routine transportation and shipping operations or sabotage.⁴ The contaminant load of soil and water is growing steadily each year in parallel with increasing industrialization and energy demand and therefore necessitate the need for remediation. The penetration of high doses of petroleum hydrocarbons into plant cells may lead to significant deviations from the norm and in some cases, even to the complete cell destruction and plant death.⁵ Plant cells subjected to high doses of these toxicants will be faced with oxidative stress, which will subsequently lead to the protective usage of its antioxidant molecules. Notable among these antioxidant molecules in plants (mainly in the leaves) are Tocopherol (Vitamin E) and Ascorbic acid (Vitamin C) and Dehydroascorbic acid (the oxidized form of ascorbic acid).⁶

Materials

Bonny light crude oil was obtained from Shell Petroleum Development Company (SPDC) flow station at Egbema, Imo State, Nigeria. Chicken drops (40kg) was purchased from Godvine, Poultry Farm, Elioze Obio Akpor, Rivers State, Nigeria. While, viable seeds of *Telfairia occidentalis* and healthy seedlings of *Tallinium triangulare* and *Amarantus hybridus* were purchased from Rumuokoro market, Obio Akpor Rivers State, Nigeria.

Study Area

The study area was located along Eneka-Oyigbo new link road (longitude 7° 10' E and latitude 4° 40' N) in Obio Akpor Rivers State, Nigeria. The soil of this area belongs to the ultisols. Approximately the entire area consisted of deep uniform sand and clay sand, with slightly humus topsoil and a topsoil pH of approximately 4.8600±0.1200. There was no record of oil spillage or pipeline vandalization in the study area.

Pollution and bioremediation of research site

Approximately 18 m² farmland was cleared and divided into three sites of 4 m² each with 2 m spaces in between them. These sites were polluted with 40 dm³ of bonny light crude oil and bioremediated for 16 weeks as follows:

Site A (Control site) was an unpolluted 4 m² farmland, while site B (bioaugmented site) was a 4 m² farmland polluted with 40 dm³ of bonny light crude oil and bioaugmented with 40 kg of chicken drops. However, site C (natural attenuated site) was polluted with 40 dm³ of bonny light crude oil.

Planting and growing of vegetables.

Viable seeds of *Telfairia occidentalis* (fluted pumpkin), and healthy seedlings *Tallinium Trianglrae* (water leaf) and *Amarantus hybridus* (African spinach) were planted on the three sites and allowed to grow for 4 weeks.

Collection of plant samples

Plant leaves were collected at fourth weeks after planting with an unused sterilized razor blade into sterilized plastic bags sealed with rubber bands. All samples were labelled with a permanent water-resistance marker and were taken to the laboratory within 1 hour of collection for analysis.

Determination of vitamin content of vegetable leaves

Pulverized leaf samples were allowed to attain atmospheric conditions after removing from the storage chamber at 4 °C. The samples were pressed carefully in different mortars and 0.10 g of each sample was weighed into a 10ml beaker for extraction. The extracted was analysed by the method of the Association of Official Analytical Chemist.⁷ The extract was concentrated to 1.0ml volume. The concentrate was injected into a Hewlett and Packard model 5890 Gas Chromatography (GC) powered with Hewlett and Packard Chemstation Rev. A09.01 (1206) software. Vitamin content was determined by a split injection method with split ratio of 20:1 and nitrogen was used as the carrier gas at an inlet temperature of 250 °C. A HPS column type of dimension (30 X 0.25)mm X 0.25µm was used. The initial temperature was 50°C and first ramping was done at 10 °C per minute for 20 minutes and maintained for 4 minutes while second ramping was done at 15 °C per minute for 4 minutes and maintained for 2 minutes. The detector temperature was 32 °C while hydrogen pressure and compressed air are 20 psi and 30 psi respectively.

Proximate analysis of vegetable leaves

Proximate analyses of vegetable leaves was carried out by the methods of the Association of Official Analytical Chemist.⁷

RESULTS AND DISCUSSIONS

Vitamin E is presently the most important lipid-soluble antioxidant that protects the cell membranes from oxidation by reacting with free radicals produced by lipid peroxidation chain reaction.⁸ Thus, the decrease in vitamin E concentration as observed in this research maybe due to the enhanced use of vitamin E in the prevention of oxidative stress induced by petroleum hydrocarbon (See tables 1-3). However, the oxidized form of vitamin E (alpha-tocopheroxyl radical) produced in this process may be recycled back to the active reduced form through reduction by other antioxidants such as ascorbate and ubiquinol.⁹

Plants are generally good sources of vitamin C (ascorbic acid), but this depends on the precise variety of the plant, the soil condition, the climate in which they grew and the length of time before analysis. However, this study showed a slight decrease in vitamin C content of the vegetables grown on the bioaugmented and natural attenuated site (See tables 1-3). This work agrees with that of,¹⁰ which reported a decrease in vitamin C concentration in *Tallinium triangulare* planted on crude oil polluted site. However, the high concentration of vitamin C as compared to vitamin E may be due to the ability of these vegetables to convert glucose into ascorbic acid through a sequence of four enzyme catalysed steps⁶. The decrease in vitamin B complex of vegetables grown on the bioaugmented and natural attenuated sites as compared to their control may be attributed to the reduction in plant nutrients caused by the presence of recalcitrant hydrocarbons in the rhizosphere of vegetables grown on both the bioaugmented and natural attenuated sites. Vitamin B₁ (thiamine) is considered as an "anti stress" vitamin because it may strengthen the human immune system.¹¹

Table 1. Vitamin content of *Telfairia occidentalis* grown on crude oil bioremediated soil (% , m/m).

	Control site	Bioaugmented site	Natural attenuated site
Vit. A	4.6816±0.0365 ^a	4.8698±0.0298 ^{bc}	4.9060±0.0066 ^{bc}
Vit. B ₁	7.1452±0.0052 ^a	7.0132±0.0008 ^{bc}	7.0182±0.0020 ^{bc}
Vit. B ₂	1.5034±0.0042 ^a	1.7521±0.0019 ^b	1.5675±0.0075 ^c
Vit. B ₃	1.8515±0.0045 ^a	1.7057±0.0071 ^b	1.6444±0.0010 ^c
Vit. B ₆	4.4349±0.0006 ^{ab}	4.4823±0.0178 ^{abc}	4.4968±0.0249 ^{bc}
Vit. C	64.0402±0.4357 ^a	62.0920±0.0358 ^{bc}	62.4789±0.0286 ^{bc}
Vit. E	7.4838±0.0324 ^a	6.9888±0.0823 ^b	6.7104±0.0022 ^c

Values are means ± standard deviations of three determinations. Mean values in each row with different superscripts (either a, b or c) differ significantly at $P = 0.05$.

Proximate analysis of vegetable samples grown on the bioaugmented and natural attenuated sites showed a pronounced decrease in protein content and a slight decrease in ash content when compared to their control (See tables 4-6). The decrease in protein content may be as a result of oxidative stress induced by the presence of petroleum hydrocarbons in these vegetables. This may have interfered with the protein synthesis or an increase in protein oxidation

and destruction of plant cells which may possibly lead to a decrease in protein content of these vegetables. The results of this study corroborates that of,¹² where a progressive reduction in the mean concentrations of protein thiol and total thiol attributed to increased oxidative protein damage due to the reactive intermediates from spent engine oil was reported.

Table 2. Vitamin content of *Tallinium triangulare* grown on crude oil bioremediated soil (% , m/m).

	Control site	Bioaugmented site	Natural attenuated site
Vit. A	3.4259±0.0064 ^a	2.9507±0.0043 ^b	2.9889±0.0118 ^c
Vit. B₁	5.0876±0.0189 ^a	4.6095±0.0024 ^b	4.7879±0.0315 ^c
Vit. B₂	4.7663±0.0107 ^a	4.3940±0.0236 ^b	4.4665±0.0376 ^c
Vit. B₃	1.3625±0.0027 ^{ac}	1.3071±0.0002 ^{bc}	1.3298±0.0341 ^{abc}
Vit. B₆	2.3028±0.0003 ^a	2.1626±0.0046 ^b	2.2364±0.0038 ^c
Vit. C	43.6426±0.0770 ^{abc}	43.5302±0.0029 ^{abc}	43.5768±0.0298 ^{abc}
Vit. E	1.6944±0.0074 ^a	1.2507±0.0041 ^b	1.3316±0.0043 ^c

Values are means ± standard deviations of three determinations. Mean values in each row with different superscripts (either a, b or c) differ significantly at P = 0.05.

Table 3 Vitamin content of *Amarantus hybridus* grown on crude oil bioremediated soil (% , m/m).

	Control site	Bioaugmented site	Natural attenuated site
Vit. A	3.2813±0.0431 ^a	3.0947±0.0079 ^{bc}	3.1034±0.0490 ^{bc}
Vit. B₁	2.9630±0.0664 ^a	2.0620±0.0002 ^b	2.4824±0.0380 ^c
Vit. B₂	4.8750±0.1123 ^{ab}	4.7045±0.0270 ^{ab}	4.4312±0.0013 ^c
Vit. B₃	1.7239±0.0005 ^a	1.5343±0.0007 ^b	1.4506±0.0066 ^c
Vit. B₆	2.8075±0.0044 ^a	2.5303±0.0020 ^b	2.6751±0.0102 ^c
Vit. C	25.9443±0.0224 ^a	25.1470±0.1288 ^b	25.4882±0.0178 ^c
Vit. E	6.2228±0.0024 ^a	5.2987±0.0587 ^b	5.9990±0.0806 ^c

Values are means ± standard deviations of three determinations. Mean values in each row with different superscripts (either a, b or c) differ significantly at P = 0.05.

Table 4. Proximate composition of *Telfairia occidentalis* grown on crude oil bioremediated soil (% , m/m).

	Control site	Bioaugmented site	Natural attenuated site
Proteins	3.2000±0.0500 ^a	2.7000±0.0100 ^b	3.1100±0.0755 ^c
Lipids	1.1933±0.0902 ^a	2.6867±0.0833 ^{bc}	2.6000±0.0800 ^{bc}
Carbohydrates	6.3100±0.3000 ^{abc}	6.5000±0.0110 ^{abc}	6.3000±0.3300 ^{abc}
Moisture	81.7000±0.2000 ^{ac}	84.2000±0.5300 ^b	81.4000±0.4400 ^{ac}
Crude fibre	3.4100±0.2152 ^{abc}	3.3000±0.0600 ^{abc}	3.1000±0.0400 ^{abc}
Ash	3.2000±0.0240 ^{ac}	3.4000±0.0510 ^b	3.2000±0.0112 ^{ac}

Values are means ± standard deviations of three determinations. Mean values in each row with different superscripts (either a, b or c) differ significantly at P = 0.05.

Table 5. Proximate composition of *Tallinium triangulare* grown on crude oil bioremediated soil (% , m/m) .

	Control site	Bioaugmented site	Natural attenuated site
Proteins	2.2300±0.1044 ^a	1.8000±0.0420 ^{bc}	2.0100±0.0794 ^{bc}
Lipids	0.3000±0.0200 ^a	1.5900±0.3606 ^b	1.4367±0.0355 ^c
Carbohydrates	4.2267±0.1168 ^a	5.4000±0.0800 ^b	4.6033±0.0751 ^c
Moisture	89.8133±0.3691 ^{abc}	88.7000±0.7600 ^{abc}	89.2000±0.5300 ^{abc}
Crude fibre	2.1067±0.0208 ^{ac}	1.6300±0.2858 ^b	2.4000±0.0820 ^{ac}
Ash	1.3000±0.0320 ^{ac}	1.7067±0.0603 ^b	1.4033±0.0116 ^{ac}

Values are means ± standard deviations of three determinations. Mean values in each row with different superscripts (either a, b or c) differ significantly at P = 0.05.

Table 6. Proximate composition of *Amarantus hybridus* grown on crude oil bioremediated soil (% , m/m).

	Control site	Bioaugmented site	Natural attenuated site
Proteins	2.9000±0.0600 ^a	2.3033±0.0208 ^b	2.5933±0.0704 ^c
Lipids	0.4067±0.0710 ^a	1.8300±0.0794 ^{bc}	1.7033±0.0404 ^{bc}
Carbohydrates	10.5000±0.1418 ^a	9.1900±0.2066 ^{bc}	8.9900±0.2751 ^{bc}
Moisture	82.2033±0.5330 ^{abc}	83.4029±0.7550 ^{abc}	82.7744±0.6997 ^{abc}
Crude fibre	1.3967±0.0153 ^a	1.2100±0.0200 ^b	1.7133±0.0603 ^c
Ash	1.7967±0.0551 ^a	2.1067±0.0351 ^b	2.3033±0.0503 ^c

Values are means ± standard deviations of three determinations. Mean values in each row with different superscripts (either a, b or c) differ significantly at P = 0.05.

However, petroleum contaminants, apart from increasing the concentration of hydrocarbon in the soil can also lead to the predominance of organic carbon over the content of nitrogen in the humus horizon, which can consequently lead to large supply of energy and proportionately decrease in the availability of nitrogen.¹³ Thus, strong competition for nitrogen occurs between microorganisms that are degrading the hydrocarbons and the plant root systems. This competition may result to acute shortage of nitrogen for plants, thereby minimizing or inhibiting the plant growth. This may also be responsible for the decrease in plant protein content and slight increase in carbohydrate content as observed in this research.

The increase in lipid content observed in these vegetables may be due to the ability of these vegetables to absorb and bioaccumulate petroleum hydrocarbon in their aerial parts (see tables 4-6). This also corroborates the work of,¹³ which reported that contamination of soil with petroleum substances may not weaken the vegetative development of crops but can cause accumulation of hydrocarbon in plants.

Petroleum hydrocarbons can also have a direct effect by producing oily films on aerial parts of the plants, thus reducing plant transpiration and respiration thereby decreasing membrane permeability, thus causing disorders in the metabolic processes, which may result in some modifications in the chemical compositions of plants.¹³ This may be responsible for the increase in lipid content of the vegetables grown on both the bioaugmented and the natural attenuated sites.

References

- ¹Sposito, G. *The chemistry of soils*, 2nd Edition, Oxford University Press, **2008**.
- ²Alexander, M. *Biodegradation and bioremediation*, Academic Press, New York, **1994**.
- ³Ojumu, T., Bello, O. O., Sonibare, J. O. and Solomon, B. O., *African J. Biotech.*, **2004**, *1*, 31-35.
- ⁴Gonzalez, J. L., Serrano, A., Gallego, M. and Tejada, M. J., *J. Environ. Pollut.* **2008**, *144*, 203-209.
- ⁵Korte, F., Kvesitadze, G., Ugrekhelidze, D., Gordeziani, M., Khatisashuili, G., Buadze, O., Zaalislwili, G. and Coulston, F., *J. Ecotoxicol. Environ. Safety.* **2000**, *47(1)*, 1-26.
- ⁶Naidu, K., *J. Nutr.*, **2003**, *2(7)*, 1-30.
- ⁷Association of Official Analytical Chemists (AOAC), *Official Methods of Analysis*. Virginia, USA., **2006**.
- ⁸Traber, M. G. and Atkinson, J., *J. Free Radic. Biol. Med.* **2007**, *43(1)*, 4-15.
- ⁹Wang, X. and Quinn, P., *Prog. Lipid Res.* **1999**, *38(4)*, 309-336.
- ¹⁰Nwaoguikpe, R. N., *Pak. J. Nutr.*, **2011**, *10(3)*, 274- 281..
- ¹¹Ambrose, M. L., Bowden, S. C. and Whelan, G., *Alchol. Clin. Exp. Res.* **2001**, *25(1)*, 112-116.
- ¹²Nwaogu, L. A. and Onyeze, G. O. C., *Nigerian J. Biochem. Mol. Biol.*, **2010**, *25(2)*, 98 - 104.
- ¹³Ziolkowskai, L., Wyzkowskii, H., *J. Ecol. Chem. and Eng.* **2010**, *17(1)*, 37 - 46.

Received: 25.02.2013.
Accepted: 14.03.2013.



CORROSION INHIBITION BY CARBOXYMETHYL CELLULOSE

N. Manimaran ^{[a]*}, S. Rajendran ^[b,c], M. Manivannan ^[d], J. Angelin Thangakani ^[e]
and A. Suriya Prabha ^[f]

Keywords: Carboxymethyl cellulose, carbon steel, ground water, SEM, AFM, F-Test, corrosion inhibition.

The inhibition efficiency (IE) of carboxymethyl cellulose (CMC)-Zn²⁺ system in controlling corrosion of carbon steel in ground water in the absence and presence of Zn²⁺ has been evaluated by weight loss method. The formulation consisting of 250 ppm CMC and 50 ppm Zn²⁺ has 98 % IE. A synergistic effect exists between CMC and Zn²⁺. Synergism has been confirmed by synergism parameter. AC impedance spectra confirm the formation of protective film on the metal surface. The nature of the protective film has been characterized by scanning electron microscopy (SEM).

Corresponding Authors

E-Mail: n.manitri@gmail.com, srmjoany@sify.com

- [a] Department of Chemistry, Yadava College, Madurai-625 014, Tamilnadu, India.
 [b] PG and Research Department of Chemistry, GTN Arts College, Dindigul-624 005, Tamilnadu, India.
 [c] Department of Chemistry, RVS School of Engineering and Technology, Dindigul-624 005, Tamil Nadu, India.
 [d] Department of Chemistry, Chettinad College of Engineering and Technology, Karur – 639 114, Tamil Nadu, India.
 [e] CEOA Matric Hr Sec School, A. Kozakulam, Madurai-17, Tamil Nadu, India.
 [f] Department of Chemistry, Shanmuganathan Engineering College, Arasampatti-622 507, Tamil Nadu, India. Chapters

The present work is undertaken:

- 1) to evaluate the inhibition efficiency(IE) of CMC in controlling corrosion of carbon steel in ground water which is collected from Yadava college which is located at Madurai, Tamil Nadu, India (**Table 1**)
- 2) to study the synergism using synergism parameters.
- 3) to understand the mechanistic aspects of corrosion inhibition and formation of protective film on the metal surface by AC impedance spectra.
- 4) to analyze the protective film formed on the metals surface by scanning electron microscopy (SEM)
- 5) to propose a suitable mechanism for corrosion inhibition process.

INTRODUCTION

Corrosion can be defined as the destruction of metals and alloys by electrochemical reaction with its environment. Corrosion occurs because of the natural tendency of the metals to return back to their thermodynamically stable native state. It cannot be avoided, but it can be controlled and prevented by using appropriate preventive measures like cathodic protection, anodic protection, coating, alloying and using inhibitors, etc. Out of these methods, the inhibitors reduce the aggressiveness of the corrosion and harmful aqueous environment. Thus prevent the metal and alloy by the forming of a protective layer on the metal surface. The applications of inhibitors are mostly find applications in cooling water system and boiler water system.^{1,2} The organic compounds containing hetero atoms like oxygen, nitrogen, phosphorus, halogen and sulphur, etc have been used as corrosion inhibitors to control the metals from corrosion.³⁻⁵ The compound carboxy methyl cellulose,⁶⁻⁸ has been used as corrosion inhibitor for mild steel in various aqueous environments. Rajendran *et al.* have been investigated that the corrosion behavior of carbon steel in presence of carboxymethyl cellulose-1-hydroxyethane-1,1-diphosphonic acid.⁹ Moreover, the application of polymers and their derivatives in corrosion controlling of metals and alloys in various aqueous environment have been investigated by various researchers.¹⁰⁻¹¹

EXPERIMENTAL

Preparation of the specimens

Carbon steel specimens (0.026 % S, 0.06 % P, 0.40 % Mn, 0.10 % C, and the rest iron) of dimensions 1.0 x 4.0 x 0.2 cm were polished to mirror finish and degreased with trichloroethylene were used for both weight-loss method and surface examination studies. The environment chosen is ground water and the physico-chemical parameter of ground water is given in **Table 1**.

Table 1. Physico-chemical parameters of ground water

Parameters	Value
pH	7.3
Total Hardness as CaCO ₃	460 ppm
Calcium	32 ppm
Magnesium	91 ppm
Nitrate	8 ppm
Chloride	270 ppm
Fluoride	0.8 ppm
Sulphate	100 ppm
Phosphate	0.46 ppm

Weight-loss method

Carbon steel specimens in triplicate were immersed in 100 mL of the ground water containing various concentrations of the inhibitor in the presence and absence of Zn^{2+} for 3 day. The corrosion product was cleaned with Clark's solution.¹² The weights of the specimens before and after immersion were determined using an analytical balance, Shimadzu AY210 model. Then the Inhibition efficiency (IE) was

$$IE(\%)=100\left(1-\frac{W_2}{W_1}\right) \quad (1)$$

calculated using the equation (1).

where

W_1 =corrosion rate (mdd) in absence of inhibitor,
 W_2 = corrosion rate (mdd) in presence of inhibitor.

The corrosion rate (CR , in mdd) was calculated using the equation

$$CR = \frac{\Delta m}{A t} \quad (2)$$

where

Δm - weight loss in mg
 A- area of the specimen in dm^2
 t- Immersion period in days

Synergism Parameter (S_I)

Synergism parameters are indications of synergistic effect existing between the inhibitors. S_I value is found to be greater than one suggesting that the synergistic effect between the inhibitors.¹³⁻¹⁴ The S_I value can be calculated using the formula as follows:

$$S_I = \frac{1-\theta_{1+2}}{1-\theta'_{1+2}} \quad (3)$$

where,

$\theta_{1+2} = (\theta_1+\theta_2) - (\theta_1\theta_2)$
 θ_1 = surface coverage of inhibitor CMC
 θ_2 = surface coverage of inhibitor Zn^{2+}
 θ'_{1+2} = combined surface coverage of inhibitor carboxymethyl cellulose (CMC) and Zn^{2+} .

AC impedance measurements

AC Impedance study was carried out in Electrochemical Impedance Analyzer model CHI 660A using a three electrode cell assembly. The working electrode was used as a rectangular specimen of carbon steel with one face of the

electrode of constant 1 cm^2 area exposed. A saturated calomel electrode (SCE) was used as reference electrode. A rectangular platinum foil was used as the counter electrode. AC impedance spectra were recorded after doing iR compensation. The real part (Z') and imaginary part (Z'') of the cell impedance were measured in ohms for various frequencies. The corrosion parameters such as charge transfer resistance (R_t) and double layer capacitance (C_{dl}) values were calculated. During the AC impedance spectra, the scan rate ($V\text{ s}^{-1}$) was 0.005; Hold time at E_f (s) was zero and quiet time (s) was 2.

Surface Characterization by Scanning Electron Microscopy (SEM)

The carbon steel immersed in blank and in the inhibitor solution for a period of one day was removed, rinsed with double distilled water, dried and observed in a scanning electron microscope to examine the surface morphology. The surface morphology measurements of the carbon steel were examined using HITACHI S-3000 H computer controlled scanning electron microscope.

RESULTS AND DISCUSSION

Analysis of results of weight loss study

The calculated inhibition efficiencies (IE) and corrosion rates (CR) of CMC in controlling corrosion of carbon steel immersed in ground water both in the absence and presence of Zn^{2+} ion are given in **Table 2**.

Table 2: Inhibition efficiencies (IE %) and Corrosion rates (CR) obtained from CMC - Zn^{2+} systems, when carbon steel is immersed in ground water

CMC ppm	Zn^{2+} , ppm			
	0		50	
	CR, mdd	IE %	CR, mdd	IE, %
0	15.15	---	12.88	15
25	13.64	10	5.30	65
50	12.57	17	3.64	76
75	11.51	24	2.12	86
100	9.85	35	1.52	90
125	8.33	45	0.91	94
250	7.88	48	0.30	98

The calculated values indicate the ability of CMC to be a good corrosion inhibitor. The IE is found to be enhanced in the presence of Zn^{2+} ion. CMC alone shows some IE . But the combination of 250 ppm CMC and 50 ppm Zn^{2+} shows 98% IE . This suggests that a synergistic effect exists between CMC and Zn^{2+} ion.¹⁵⁻²⁰

Synergism parameters (S_I)

The synergism parameters of CMC- Zn^{2+} system are given in **Table 3**. For different concentrations of inhibitors, S_I approaches 1 when no interaction between the inhibitor compounds exists. When $S_I > 1$, it points to synergistic effects. In the case of $S_I < 1$, it is an indication that the synergistic effect is not significant. From Table 4, it is observed that value of synergism parameters (S_I) calculated

from surface coverage were found to be one and above. This indicates that the synergistic effect exists between CMC and Zn^{2+} ions.²¹

Table 3: Inhibition efficiencies and synergism parameters for various concentrations of CMC- Zn^{2+} system, when carbon steel immersed in ground water

CMC, ppm	25	50	75	100	125	250
θ_1	0.10	0.17	0.24	0.35	0.45	0.48
θ_2 ($Zn^{2+}=5$ ppm)	0.07	0.07	0.07	0.07	0.07	0.07
θ_{1+2}	0.16	0.23	0.29	0.42	0.49	0.52
θ'_{1+2}	0.20	0.35	0.55	0.60	0.70	0.75
S_I	1.05	1.19	1.57	1.51	1.71	1.93
θ_1	0.10	0.17	0.24	0.35	0.45	0.48
θ_2 ($Zn^{2+}=10$ ppm)	0.10	0.10	0.10	0.10	0.10	0.10
θ_{1+2}	0.19	0.25	0.32	0.42	0.51	0.53
θ'_{1+2}	0.44	0.56	0.76	0.88	0.89	0.90
S_I	1.45	1.69	2.85	4.88	4.50	4.68
θ_1	0.10	0.17	0.24	0.35	0.45	0.48
θ_2 ($Zn^{2+}=25$ ppm)	0.12	0.12	0.12	0.12	0.12	0.12
θ_{1+2}	0.21	0.27	0.33	0.43	0.52	0.54
θ'_{1+2}	0.50	0.70	0.80	0.82	0.90	0.94
S_I	1.58	2.43	3.34	3.17	4.84	7.63
θ_1	0.10	0.17	0.24	0.35	0.45	0.48
θ_2 ($Zn^{2+}=50$ ppm)	0.15	0.15	0.15	0.15	0.15	0.15
θ_{1+2}	0.24	0.29	0.35	0.45	0.53	0.56
θ'_{1+2}	0.65	0.76	0.86	0.90	0.94	0.98
S_I	2.19	2.94	4.41	5.53	7.79	22.1

Analysis of AC impedance spectra

AC impedance spectra (electro chemical impedance spectra) have been used to confirm the formation of protective film on the metal surface. If a protective film is formed on the metal surface, charge transfer resistance (R_t) increases; double layer capacitance value (C_{dl}) decreases and the impedance $\log(Z/\text{ohm})$ value increases. The AC impedance spectra of carbon steel immersed in ground water in the absence and presence of inhibitors (CMC- Zn^{2+}) are shown in **Fig.1** to **Fig. 3**. The AC impedance parameters namely charge transfer resistance (R_t) and double layer capacitance (C_{dl}) derived from Nyquist plots are given in **Table 4**. The impedance value $\log(Z/\text{ohm})$ derived from Bode plots are also given in **Table 4**.

Table 4. Impedance parameters for corrosion of carbon steel immersed in ground water in the absence and presence of inhibitors obtained by AC impedance spectra

System	Nyquist plot		Bode plot
	$R_t, \Omega \text{ cm}^2$	$C_{dl}, \text{F cm}^{-2}$	$\log(Z/\text{ohm})$
Ground Water	1962.3	2.5989×10^{-9}	3.297
Ground Water + CMC (250 ppm) + Zn^{2+} (50 ppm)	2081.9	2.4496×10^{-9}	3.340

It is observed that when the inhibitors [CMC (250 ppm) + Zn^{2+} (50 ppm)] are added, the charge transfer resistance (R_t) increase from 1962.3 ohm cm^2 to 2081.9 ohm cm^2 . The C_{dl} value decreases from $2.5989 \times 10^{-9} \text{ F cm}^{-2}$ to $2.4496 \times 10^{-9} \text{ F cm}^{-2}$.

cm^2 . The impedance value $[\log(Z/\text{ohm})]$ increases from 3.297 to 3.340. These results lead to the conclusion that a protective film is formed on the metal surface.²²⁻²⁵

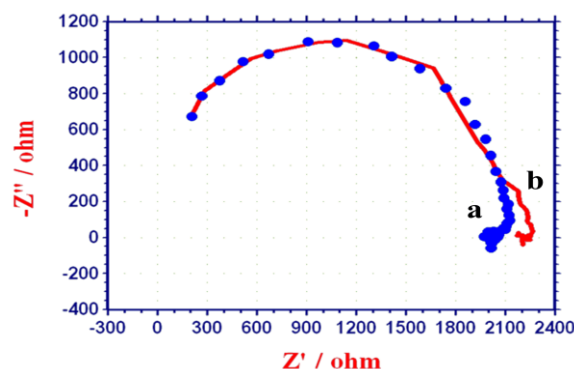


Figure 1. AC impedance spectra of carbon steel immersed in various test solutions (Nyquist plot) a) Ground water b) Ground water + CMC (250 ppm) + Zn^{2+} (50 ppm)

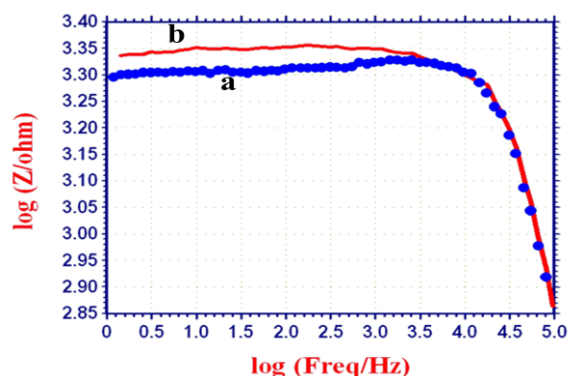


Figure 2. AC impedance spectra of carbon steel immersed in various test solutions (impedance-Bode plot) a) Ground water (blank) b) Ground water + CMC (250 ppm) + Zn^{2+} (50 ppm)

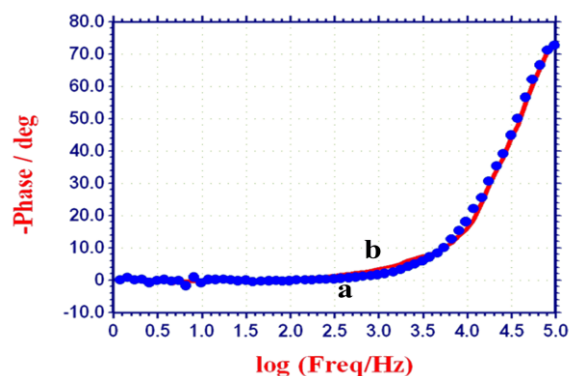


Figure 3. AC impedance spectra of carbon steel immersed in various test solutions (Phase-Bode plot) a) Ground water, b) Ground water + CMC (250 ppm) + Zn^{2+} (50 ppm)

Scanning Electron Microscopy (SEM)

SEM provides a pictorial representation of the surface. To understand the nature of the surface film in the absence and presence of inhibitors and the extent of corrosion of carbon steel, the SEM micrographs of the surface are examined.²⁶ The SEM micrograph (X 500) of a polished carbon steel

surface (control) in **Fig. 4 (a)** shows the smooth surface of the metal. This shows the absence of any corrosion products or inhibitor complex formed on the metal surface.

The SEM micrograph (X 500) of carbon steel specimen immersed in the ground water for one day is shown in **Fig. 4 (b)** and **(c)** respectively. The SEM micrograph of carbon steel surface immersed in ground water in **Fig. 4 (b)** shows the roughness of the metal surface which indicates the corrosion of carbon steel in ground water. The **Fig. 4 (c)** indicates that in the presence of 250 ppm CMC and 50 ppm Zn^{2+} mixture in ground water, the surface coverage increases which in turn results in the formation of insoluble complex on the metal surface. In the presence of CMC and Zn^{2+} , the surface is covered by a thin layer of inhibitors which effectively control the dissolution of carbon steel.²⁷

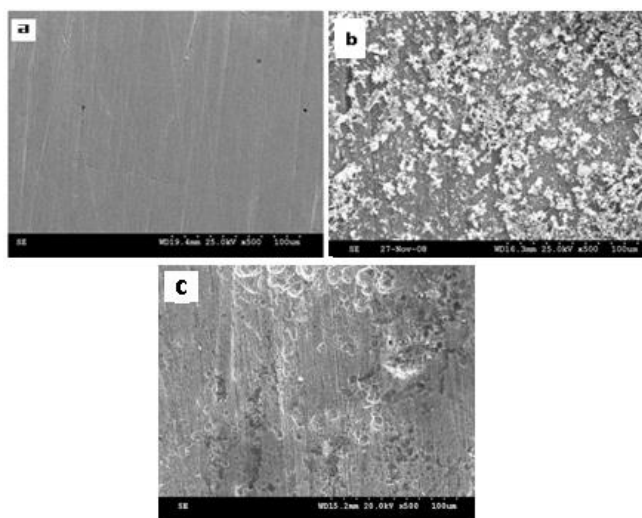
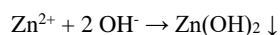
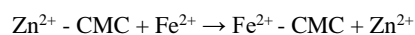


Figure 4. SEM analysis of a) Polished Carbon steel (control); b) Carbon steel immersed in ground water (Blank); c) Carbon steel immersed in ground water + 250 ppm of CMC + 50 ppm of Zn^{2+}

Mechanism of corrosion inhibition

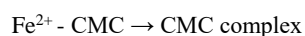
Based on the above studies the following mechanism can be proposed for corrosion inhibition process.



Protective film consists of $Fe^{2+} - CMC$ complex and $Zn(OH)_2$

At anode: $Fe \rightarrow Fe^{2+} + 2e^{-}$

At cathode: $H_2O + \frac{1}{2} O_2 + 2e^{-} \rightarrow 2 OH^{-}$



It accounts for the synergism of CMC – Zn^{2+} system.

CONCLUSIONS

The present study leads to the following conclusions:

The formulation consists of 250 ppm of CMC and 50 ppm of Zn^{2+} offers 98% IE to carbon steel immersed in ground water.

Synergistic effect of exists between CMC and Zn^{2+} .

AC impedance spectra reveal that the formation of protective film on the metal surface.

SEM study confirms the formation of protective film on the metal surface and hence the corrosion process is inhibited.

ACKNOWLEDGEMENTS

The authors are thankful to their respective managements.

REFERENCES

- Mars G., Fontana, *Corrosion Engineering* (Tata McGraw Hill Education Private Limited, New Delhi, **2005**).
- Pierre R., Roberge, *Handbook of Corrosion Engineering*, (McGraw Hill, **2000**).
- Thomas, J. G. N., *Proc. 5th Eur. Symp. Corr. Inhibitors*, Ferrara, Italy, University of Ferrara, **1981**, 453.
- Donnelly, B. E., Downie, T. C., Grzeskowiak, R., Hamburg, H. R. and Short, D., *Corr. Sci.*, **1997**, *38*, 109.
- Tadros, A. B., and Abdel-Naby Y., *J. Electroanal. Chem.*, **1988**, *224*, 433.
- Umoren, S. A., Solomon, M. M., Udosoro, I. I., Udoh, A. P., *Cellulose*, **2010**, *17(3)*, 635.
- Solomon, M. M., Umoren, S. A., Udosoro, I. I., and Udoh, A. P., *Corr. Sci.*, **2010**, *52(4)*, 1317.
- Bayol E., Gürten, A. A., Dursun M., Kayakirilmaz K., *Wuli Huaxue Xuebao/ Acta Physico - Chimica Sinica*, **2008**, *24(12)*, 2236.
- Rajendran S., Joany, R. M., Apparao, B. V., Palaniswamy N., *Bull. Electrochem.*, **2002**, *18(1)*, 25.
- Khairou, K. S., El-Sayed A., *J. Appl. Polym. Sci.*, **2003**, *88(4)*, 866.
- El-Sayed A., *Corr. Prevent. Cont.*, **1996**, *43(1)*, 27.
- Wranglen G., *Introduction to corrosion and protection of metals*, Chapman and Hall, London, **1985**, 236.
- Benita Sherine H., Jamal Abdul Nasser A., and Rajendran S., *Int. J. Eng. Sci. Technol.*, **2010**, *2(4)*, 341.
- Agnesia Kanimozhi S., and Rajendran S., *Int. J. Electrochem. Sci.*, **2009**, *4*, 353.
- Sahaya Raja A., Rajendran S., Nagalakshmi R., Angelin, T. J., Pandiarajan M., *Eur. Chem. Bull.*, **2012**, *1(3)*, 130-136.
- Bouyanzer A., Hammouti B., and Majidi L., *Mater. Lett.*, **2006**, *60(23)*, 2840.
- Satapathy, A. K., Gunasekaran G., Sahoo, S. C., Kumar A., and Rodrigues, P. V., *Corr. Sci.*, **2009**, *51(12)*, 2848.
- de Souza, F. S., Spinelli A., *Corr. Sci.*, **2009**, *51(3)*, 642.
- Sathiyabama J., Rajendran S., Selvi, J. A., Jeyasundari J., *The Open Corr. J.*, **2009**, *2*, 76.
- Nithya, A., Rajendran, S., *Bulg. Chem. Comm.*, **2010**, *42(2)*, 119.
- Manivannan M., and Rajendran S., *J. Chem. Bio. Phy. Sci.*, **2011**, *1(2)*, 241.

- ²²Joseph Raj X., and Rajendran N., *Int. J. Electrochem. Sci.*, **2011**, 6, 348.
- ²³Weihua Li, Lichao Hu, Shengtao Zhang and Baorong Hou, *Corr. Sci.*, **2011**, 53(2), 735.
- ²⁴Rajendran S., Anuradha K., Kavipriya K., Krishnaveni A., Angelin Thangakani J., *Eur. Chem. Bull.*, **2012**, 1(12), 503-510.
- ²⁵Chauhan, L. R., and Gunasekaran G., *Corr. Sci.*, **2007**, 49(3), 1143.
- ²⁶Manivannan M., Rajendran S., and Suriya Prabha A., *Eur. Chem. Bull.*, **2012**, 1(8), 317-329.
- ²⁷Fallavena T., Antonow M., Gonçalves, R. S., *Appl. Surf. Sci.*, **2006**, 253, 566.

Received: 03.02.2013.

Accepted 14.03.2013.



APPLICATION OF WOOD SAWDUST MODIFIED WITH CATIONIC SURFACTANTS FOR EFFICIENT REMOVAL OF ACIDIC DYES FROM AQUEOUS SOLUTIONS: KINETIC AND THERMODYNAMIC STUDIES

Reza Ansari ^{[a]*} and Babak Seyghali^[a]

Keywords: Removal, acidic dyes, modified sawdust, cationic surfactant, isotherm, kinetic, thermodynamic

In this paper, application of sawdust prepared from Narra wood (SD) modified with cationic surfactant of cetyltrimethylammonium bromide (SD/CTAB) was used for removal of two typical acid dyes commercially named as Acid Green 25 (AG25) and Acid Red 14 (AR14) from aqueous solutions. The effects of experimental variables, such as pH, initial dye concentration, adsorbent dose, contact time and temperature were investigated in order to find out the optimized conditions for removal of selected test dyes. Langmuir and Freundlich Isotherms were used to analyse the experimental adsorption data. Pseudo- first and second order models suggested by Lagergren, Ho & McKay were used for kinetic study. The van 't Hoff equation employed for obtaining of thermodynamic parameters. It was found that upon simple treatment of sawdust with a cationic surfactant, the adsorption capacity of sawdust for uptake of anionic dyes is improved considerably. The monolayer maximum adsorption capacity of SD/CTAB toward AG25 and AR14 dyes calculated using Langmuir isotherm model was 17.5 and 18.9 mg g⁻¹ at 298 K, respectively. Based on kinetics and thermodynamic studies, it was found that adsorption process using SD/CTAB follows pseudo second-order rate equation and the adsorption investigated system is spontaneous and endothermic in nature. Exhausted adsorbent can also be regenerated for reuse with high performance. It was found that via simple treatment of agricultural wastes such as wood sawdust with cationic surfactants it is possible to improve the sorption capacity of sawdust for removal of anionic dyes from aqueous wastes considerably.

Corresponding Authors

E-Mail: ransari@guilan.ac.ir; seyghali.babak@gmail.com

Tel: +98-1313243630-4 (Ext. 226)

Fax: +98-131-3233262

[a] Chemistry Department, Faculty of Science, University of Guilan, Rasht, Iran, POB: 41635-1914

Introduction

Dyes have been widely used in textile, paper, rubber, plastics, leather, cosmetic, pharmaceutical, and food industries, which generated huge volume of wastewater every year. The disposal of dye wastewater without proper treatment is a big challenge and has caused harms to the aquatic environment, such as reducing light penetration and photosynthesis.^{1,2} Due to the complex molecular structure, dyes are usually very difficult to be biodegraded, making them hardly eliminated under natural aquatic environment^[3]. Acid dyes are anionic compounds mainly used for dyeing nitrogen-containing fabrics like wool, polyamide, modified acryl and silk. Acid Green 25 (1,4-di-[(2-sulfono-4-methylphenyl) amino]-9,10-anthracenedione, disodium salt) (Fig. 1a) in particular belongs to the commercial acid dye often used in textile, hair dye formulation and cosmetic product.⁴ Acid Red 14 (4-hydroxy-3-(4-sulfonato-1-naphthylazo)-1-naphthalenesulfonate disodium salt) (Fig. 1b) is a synthetic azo class of dye, imparting red color to foods. Being a typical azo dye the effluent containing AR14 dye is also difficult to treat in environmental systems due to the sulfonic group, which makes it polar and soluble in water. For many years it was used as coloring material for edibles like jams and preservatives; however, most of the developed countries finally prohibited its use in edibles due to the presence of β-naphthylamine, a well-known

carcinogen in it. These dyes also cause asthma or drug intolerance, including nettle rash and water retention to many people.^{5,6} So its removal from wastewaters before its discharge in the environment seems to be very essential.

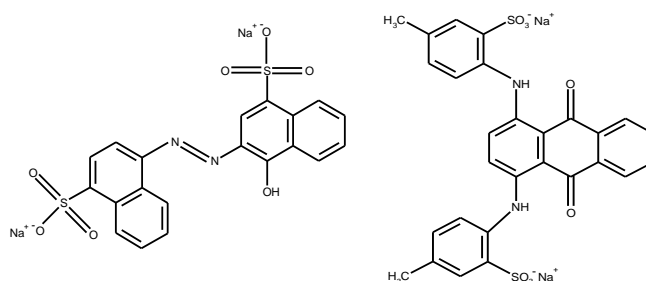


Figure 1. Molecular structure of (a) AG25 and (b) AR14 dyes.

Several physical, chemical and biological treatment methods (e.g. adsorption, coagulation-flocculation, biodegradation, ion-exchange, chemical oxidation, ozonation, reverse osmosis, membrane filtration and electrochemical methods) have been applied to remove dye molecules from such effluent. However, these processes vary in their effectiveness, cost and environmental impact.⁷⁻⁹ Adsorption has been found to be one of the promising techniques for dye wastewater treatment because of its simplicity, high efficiency, and wide-ranging availability. Different types of dye molecules can be removed very effectively by adsorption techniques and this process also removes the complete dye molecule, leaving no fragments in the wastewater.¹⁰⁻¹³ In some recent publications, different low-cost adsorbents such as chitosan, seashells, soy meal hull, palm ash and chemically modified sawdust have been used for various dyes removal from aqueous solutions.¹⁴⁻²² However, these adsorbents do not have good adsorption

capacities toward acid dye due to their negatively charged functional groups on their surfaces.²² Therefore, to improve the adsorption capacity of these adsorbents, surface modification such as cationic surfactant treatment seems to be effective. Detergents or surface-active agents are organic molecules that, when dissolved in a solvent at low concentration, have the ability to adsorb (or locate) at interfaces, thereby altering significantly the physical properties of those interfaces. This adsorption behavior can be attributed to the solvent nature and to a chemical structure for surfactants that combine both a polar and a non-polar (amphiphilic) groups into a single molecule. It has been reported that the cationic surfactants mostly quaternary ammonium salts such as hexadecyltrimethylammonium (HDTMA) or cetyltrimethylammonium bromide (CTAB) provide potential positively charged active sites for efficient removal of anionic contaminants from aqueous solutions.²³ The same improvement in cationic dye removal was observed when sawdust modified with anionic surfactant of SDS.¹⁹

In this work, the removal of two acid dyes (AG25 and AR14) from aqueous solutions was investigated using cetyltrimethylammonium bromide modified sawdust (SD/CTAB) and adsorption capacity compared with untreated sawdust (SD). The study includes an evaluation of the effects of various operational parameters such as initial dye concentration, adsorbent dose, contact time, temperature and pH on the dye adsorption process. The adsorption kinetic models, equilibrium isotherm models, thermodynamic parameters and regeneration study related with the process were also performed and are reported.

Experimental and Measurements

Materials and methods

All chemicals used were analytical reagent grades and used without further purification. All experiments were carried out in aqueous solutions prepared with distilled water. Sawdust samples (SD) from Nara wood were obtained from a local carpentry workshop (North of Iran). AG25 (C₂₈H₂₂N₂O₈S₂ · 2Na MW=622.59 g mol⁻¹), Acid red 14 dye (C₃₂H₂₂N₆O₆S₂ · 2Na, MW=696.66 g mol⁻¹) and cetyltrimethylammonium bromide (C₁₉H₄₂NBr MW=364.46 g mol⁻¹) were purchased from Merck chemical company. Solutions with concentration of 200 mg L⁻¹ for both dyes were prepared in distilled water as stock solution and the other working solutions were prepared by diluting the stock solution with distilled water to the needed concentration. AG25 and AR14 show intense absorption peaks in the visible region at 605 nm and 500 nm, respectively. A single beam Perkin-Elmer UV-Vis spectrophotometer with a glass cell (b=1.0 cm) was used for measuring all the absorption data at the maximum wavelength of each dye. A calibration curve based on Lambert-Beer law ($A=\epsilon bc$) obtained for each dye was used for quantitative analysis of the unadsorbed dye. The pH adjustments were carried out using dilute NaOH and HCl solutions (0.10 M). A pH meter (Metrohm, model 827) with a combined double junction glass electrode was used for pH measurements.

Preparation of sawdust modified by cetyltrimethylammonium bromide (SD/CTAB)

Sawdust was first washed with distilled water in order to remove any dust or impurities and then dried at temperature of about 60 °C for 5 h in an air circulating oven. In order to have uniform modification and reproducible results, sawdust particles sieved pass through a 35-50 mesh (317-508 μm) screen before surfactant treatment. 35 g of sawdust was weighed and mixed with 500 mL of CTAB solution having a concentration of 4.0 g L⁻¹. The mixture was shaken for 5 h at room temperature. The aqueous samples were then filtered, washed with distilled water in order to remove any loosely adsorbed surfactant, dried about 50 °C and sieved before use.

Adsorption experiments

Batch mode studies were conducted with treatment of different amount of adsorbent in range of 0.20 to 1.0 g with 50 mL of aqueous dye solution of dyes having different known concentrations (50–200 mg L⁻¹). The mixtures were shaken using a mechanical shaker (150 rpm) for different periods of time exposures. At the end of each established contact time, the supernatant were analyzed for residual dye concentration. All experiments were carried out for at least three times with respect to each condition, mean values are presented. The amount of dye retained by the adsorbent (q_t) at each time interval t , was calculated using the following equation:

$$q_t = \frac{(C_0 - C_t)V}{m} \quad (1)$$

where

q_t is the amount of dye adsorbed per unit weight of adsorbent at time t (mg g⁻¹);

C_0 and C_t are the initial and liquid-phase concentrations of the dye solution at time t (mg L⁻¹), respectively;

V is the volume of the dye solution (L); and

m is the amount of the adsorbent (g).

When t is equal to the equilibrium agitation time (i.e., $C_t=C_e$, $q_t=q_e$), then the amount of dye adsorbed at equilibrium, q_e (mg g⁻¹), was calculated using Eq.1.

Regeneration study

For regeneration study, 1.0 g of the selected adsorbent particles were packed into glass columns. Solutions of both dyes with constant concentration of 20 mg L⁻¹ and optimum pH values (pH 4 for AG25 and pH 6 for AR14 dye) were passed through the columns at a constant flow rate of 3.0 mL min⁻¹.

The exhausted or dye uploaded columns were regenerated using different washing solutions including NaOH, HCl, NaCl (0.10 M each) and commercial ethanol (96%) at the rate of 3 (mL min⁻¹).

The column adsorption capacity (q_c , mg g⁻¹) was estimated as follows:²²

$$q_c = \frac{\sum(C_0 - C_i)V_{eff}}{m} \quad (2)$$

where

C_0 and C_i are the initial and effluent concentration of dye in the liquid phase (mg L⁻¹),

V_{eff} is the volume of the effluent solution (L) and m is the mass of adsorbent (g).

The regeneration efficiency (RE) was subsequently calculated using the following equation:

$$\%RE = \frac{V_b'}{V_b} \times 100 \quad (3)$$

where

V_b' is the breakpoint volume of the regenerated used column and

V_b is the breakpoint volume of the virgin SD/CTAB column.

It might be needed to mention that a plot of effluent concentration vs. time or volume of effluent usually yields an S-shaped curve referred to as a breakthrough curve. The point on the S-shaped curve at which the effluent concentration reaches to 5% and 95% of the influent concentration are usually called breakpoint and point of column exhaustion, respectively.

Adsorption isotherms

Adsorption isotherms, describe how adsorbate molecules interact with adsorbent particles and are thus critical in optimizing the use of chemically modified solid materials.²⁵⁻²⁷ It is possible to depict the equilibrium adsorption isotherms by plotting the concentration of the dye in the solid phase vs. that in the liquid phase. In the present study, experimental data were compared by using two well-known and widely applied isotherm models equations, namely Langmuir and Freundlich.²⁸⁻³⁰ The application of the Langmuir isotherm model suggests that adsorption takes place as monolayer coverage on homogeneous surface containing a finite number of vacant sites energetically equivalent to each other in respect of adsorption phenomenon and with negligible interaction between adsorbed molecules. The energy of adsorption is constant and does not depend on the degree of occupation of the adsorbent active centers. The empirical non linear Langmuir equation is given by Eq. (4) as shown in the following:

$$\frac{q_e}{q_m} = \frac{K_L C_e}{1 + K_L C_e} \quad (4)$$

where

q_e is the equilibrium dye concentration on the adsorbent (mg g⁻¹);

C_e , the equilibrium dye concentration in solution (mg L⁻¹);

q_m , the monolayer capacity of the adsorbent (mg g⁻¹);

K_L , the Langmuir constant (L mg⁻¹) related to energy of adsorption.

The linearized equation of Langmuir is represented as follows (Eq.5):

$$\frac{1}{q_e} = \frac{1}{q_m} + \frac{1}{K_L q_m} \frac{1}{C_e} \quad (5)$$

The values of K_L and q_m were determined from the slope and intercept of the representation $1/q_e$ versus $1/C_e$ of Eq. (5), respectively. The essential features of the Langmuir isotherm can be expressed in terms of a dimensionless constant called separation factor (R_L) which is defined by Eq. 6.

$$R_L = \frac{1}{1 + K_L C_m} \quad (6)$$

where C_m is the maximum initial dye concentration (mg L⁻¹).

The values of this parameter indicated the shape of the isotherm: for in which $R_L > 1$ is unfavorable, $R_L = 1$ is linear, $0 < R_L < 1$ is favorable, and $R_L = 0$ is irreversible. The Freundlich adsorption isotherm model can be applied for non-ideal adsorption on heterogeneous surfaces and multilayer adsorption. This model is the earliest known empirical equation and is shown to be consistent with exponential distribution of active centers, characteristic of heterogeneous surfaces. It is expressed by the following equation:

$$q_e = K_F C_e^{1/n} \quad (7)$$

where

q_e is the amount of dye adsorbed per unit of adsorbent (mg g⁻¹),

C_e is the concentration of non-retained dye at equilibrium (mg L⁻¹),

K_F (mg^(1-1/n)/g L^{1/n}) and $1/n$ are Freundlich empirical parameters relating to multilayer adsorption capacity and adsorption intensity, respectively.

For a suitable adsorption system $1/n$ value varies between 0 and 1.³¹ Linear form of the Freundlich isotherm model is given by Eq. 8. The values of K_F and $1/n$ can be obtained from the linear plot of $\log q_e$ versus $\log C_e$.

$$\log q_e = \log K_F + \frac{1}{n} \log C_e \quad (8)$$

Kinetics study

Adsorption kinetic studies are significant since they not only provide valuable insights into the reaction pathways, but also describe the solute uptake rate which in turn controls the residence time of adsorbate at the solid-liquid interface. The experimental data were processed on the basis of three of the most commonly used kinetic models suggested by Lagergren, Ho McKay, Weber and Morris.³²⁻³⁴ Pseudo-first order kinetic equation suggested by Lagergren shown by Eq. (9) is based on the assumption that the rate of change of adsorptive solute uptake with time is directly proportional to the difference in saturation concentration and the amount of adsorptive solid uptake with time.

$$\log(q_e - q_t) = \log q_{e1} - \frac{k_1}{2.303} t \quad (9) \quad \begin{array}{l} \text{w} \\ \text{here} \end{array}$$

q_e and q_t is the amount of dye adsorbed per unit of adsorbent (mg g⁻¹) at equilibrium and at time t ,

k_1 is the pseudo-first order rate constant (min⁻¹), and t is the contact time (min).

The pseudo-first order rate constant (k_1) was calculated from the plot of $\log(q_e - q_t)$ against t . Another commonly used kinetic model is the pseudo - second-order kinetic model (McKay Ho model) which its linear form can be expressed as:

$$\frac{t}{q_t} = \frac{1}{k_2 q_{e2}^2} + \frac{1}{q_{e2}} t \quad (10)$$

where k_2 is the pseudo-second order rate constant (g mg⁻¹ min⁻¹).

A plot of t/q_t against t provides second order adsorption rate constants k_2 and q_{e2} values from the slopes and intercepts. Both pseudo-first order equation or Lagergren's kinetics equation (Eq. 9) and pseudo-second order or HO and McKay (Eq.10) assume that adsorption rates are proportional to free available active sites on the surface of adsorbents for binding of adsorbate and Pseudo-second order equation which is based on the assumption that the adsorption process involves chemisorption mechanism. Weber and Morris proposed the intra-particle diffusion model to identify diffusion mechanisms of adsorption process. The effect of intra-particle diffusion resistance on adsorption can be determined by the following relationship.

$$q_t = k_{id} t^{1/2} + C \quad (11)$$

where k_{id} is the intra-particle rate constant (g mg⁻¹ min^{-1/2}), and the intra-particle rate constant k_{id} is a function of equilibrium concentration in solid phase q_e and intra-particle diffusivity. Adsorption mechanism follows the intra-particle diffusion model, a plot of q_t against $t^{1/2}$ should give a linear line with slope k_{id} and intercept C . Values of C give information about the thickness of the boundary layer, i.e.

the larger intercept the greater is the boundary layer effect.³⁵ If the plot of uptake, q_t , versus square root of time, $t^{1/2}$ passes through the origin, the intra-particle diffusion will be the sole rate limiting process.

Thermodynamic study

The equilibrium constant (K_c) is a measure of adsorption which is defined as the ratio of the quantity of the adsorbate retained by the adsorbent to the amount of the adsorbate remaining in solution.^{22,36,37} The equilibrium constant was calculated from the following equations (Eqs. 12-15):

$$\Delta G^0 = \Delta H^0 - T \Delta S^0 \quad (12)$$

$$\Delta G^0 = RT \ln K_c \quad (13)$$

$$\ln K_C = -\frac{\Delta H^0}{RT} + \frac{\Delta S^0}{R} \quad (14)$$

$$K_C = \frac{C_{Ae}}{C_e} \quad (15)$$

where

ΔG^0 , ΔH^0 and ΔS^0 are standard Gibb's free energy, enthalpy, and entropy changes, respectively.

R is universal gas constant (8.314 J mol K⁻¹),

T is absolute temperature (K),

K_c (L g⁻¹) is the adsorption equilibrium constant,

C_{Ae} is the amount of dye adsorbed on the adsorbent (mg g⁻¹),

C_e is the equilibrium or unadsorbed concentration of the dye in the solution (mg L⁻¹).

ΔG^0 is in fact the most fundamental criterion of spontaneity of any reaction. The slope and intercept obtained by the plot of $\ln K_c$ against $1/T$ were used to calculate the ΔH^0 and ΔS^0 , respectively.²² Gibbs free energy changes (ΔG^0) was then calculated from Eq. (12).

Results and Discussion

Effect of pH

The initial pH value of the solution is an important factor which can determine the surface charge of the adsorbent and the degree of ionization of the adsorbate.²¹ The effect of pH on the uptake of dyes was analyzed over the pH range from 2 to 10. In this investigation, 0.40 g of adsorbent was treated with 50 mL of dye solution (100 mg L⁻¹) for 1 h at room temperature. It was observed that maximum adsorption for SD/CTAB occurred at pH value of 4 for AG25 and pH 6 for AR14. Therefore all of the next adsorption experiments for dye removal using SD/CTAB adsorbent were carried out at the optimum pH values of 4 (for AG25) and 6 (for AR14), respectively. The pH of dye solutions was adjusted to value of 2 in the case of untreated sawdust because of its maximum adsorption at this pH value.

Effect of initial dye concentration

For this investigation, the adsorption experiments were carried out with initial dye concentration range of 50-200 mg L⁻¹, 0.40 g adsorbent dose, 298 K and 60 min contact time. The Figure 2 show that the amount of dye adsorbed increased with increasing the initial dye concentration in the case of modified sawdust. At higher concentrations, more dye molecules were left in solution due to the saturation of the limited binding sites on the adsorbent.

As the results show, adsorption capacities (mg g⁻¹) of SD/CTAB toward uptake of AG25 increased from 6.1 to 20.0 (~ 3.5 times improvement) and for uptake of AR14 dye, it was increased from 5.5 to 17.3 (~3 times improvement). In the case of untreated sawdust (SD), the dye uptake was slow and gradually increased to the maximum adsorption values of 3.3 and 3.8 mg g⁻¹ for AG25 and AR14, respectively.

As the data clearly show adsorption capacity of surfactant-modified sawdust (SD/CTAB) for both dyes is considerably higher than untreated sawdust (at least 5 times) especially at higher initial dye concentrations.

Effects of adsorbent dose

The effect of adsorbent dose on the removal of AG25 and AR14 at initial dye concentration of 100 mg L⁻¹, 298 K temperature and 60 min contact time for SD/CTAB and SD is shown in Fig. 3. Adsorbent dose was varied from 0.10 to 0.50 g for both adsorbents. The results obtained clearly indicate with increasing of adsorbent dose, the amount of dye uptake is increased and maximum adsorption of the dyes occurred by SD/CTAB at 0.40 g of adsorbent (Fig. 3). Therefore, further investigations were carried out using 0.40 g of adsorbent. SD/CTAB has also shows to be a more efficient adsorbent for the removal of acid dyes from aqueous solutions than the untreated SD. Increasing of adsorption with increasing of adsorbent dose can be due to the more availability of free binding sites with increasing of the amount of adsorbent.

Effect of contact time

In this investigation, fixed amounts of adsorbents (0.40 g) were agitated with constant volumes of dye solutions (50 mL) having initial dye concentration of 100 mg L⁻¹ at established pH values. The mixtures were shaken at room temperature for different periods of contact times (5-60 min). The results obtained are presented in Figure 4. As the results show, the adsorption rate of acid dyes in the first 5 min for SD/CTAB is very fast. Highest amount of dye retained is occurred within the initial 10 minutes of contact time. After reaching the saturation value in 60 min of contact, a continuous and smooth curve is obtained for both adsorbents. Based on these results, 60 min was taken as the equilibrium time in batch adsorption experiments. Again as the results of this part of investigation clearly show, the uptake rate and adsorption amount of acid dyes onto SD/CTAB is much higher than that of SD at any contact time. The difference in the equilibrium time for both adsorbents may be due to strong attractive forces such as electrostatic between the dye molecules and the surfactant-modified sawdust.

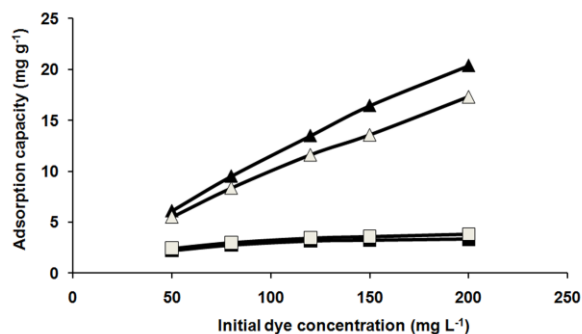


Figure 2. Effect of initial dye concentration on the adsorption of dyes by SD/CTAB (▲: AG25; △: AR14) and SD (■: AG25; □: AR14).

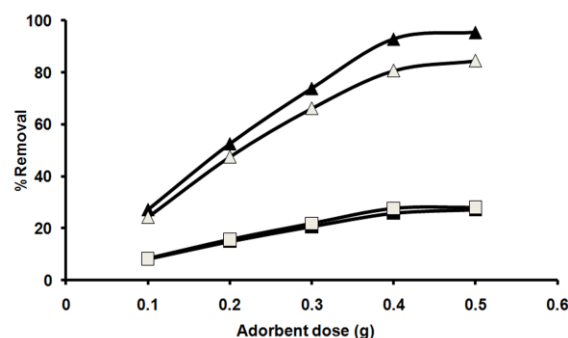


Figure 3. Effect of adsorbent dose on the adsorption of dyes by SD/CTAB (▲: AG25; △: AR14) and SD (■: AG25; □: AR14).

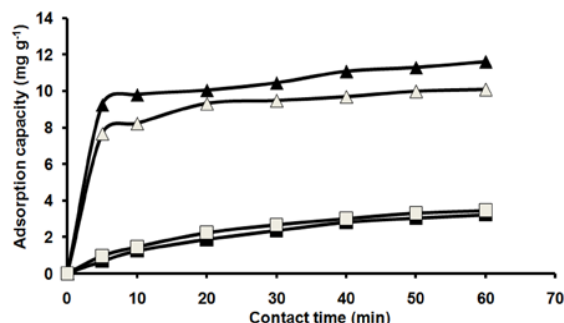


Figure 4. Effect of contact time on the adsorption of dyes by SD/CTAB (▲: AG25; △: AR14) and SD (■: AG25; □: AR14).

Effect of solution temperature

Investigation of temperature effect is very important from both kinetics and thermodynamic points of view. The effect of temperature (298-328 K) on adsorption of AG25 and AR14 by two selected adsorbents is illustrated in Fig. 5. In this investigation, constant amounts of adsorbents (0.40 g) were agitated with 50 mL of dye solutions with concentration of 100 mg L⁻¹. The results reveal (Fig. 5) that solution temperature does not affect the sorption efficiency. It might be concluded that the adsorption system investigated is not accompanied by considerable enthalpy changes. However, increasing of dye solution temperature seems to be more effective in the case of unmodified sawdust.

Table 1. Isotherm parameters obtained for adsorption of AG25 and AR14 dyes onto SD/CTAB and SD.

Adsorbent	Dye	Langmuir constants					Freundlich constants		
		q_m (mg g ⁻¹)	q_m (exp) (mg g ⁻¹)	K_L (L mg ⁻¹)	R_L	R^2	K_F (mg ^(1-1/n) /g L ^{1/n})	$1/n$	R^2
SD/CTAB	AG25	17.45	20.38	0.431	0.011	0.953	5.77	0.35	0.998
	AR14	18.87	17.30	0.066	0.070	0.986	2.33	0.48	0.997
SD	AG25	3.81	3.33	0.045	0.100	0.996	1.02	0.24	0.943
	AR14	4.33	3.83	0.041	0.108	0.999	1.00	0.27	0.979

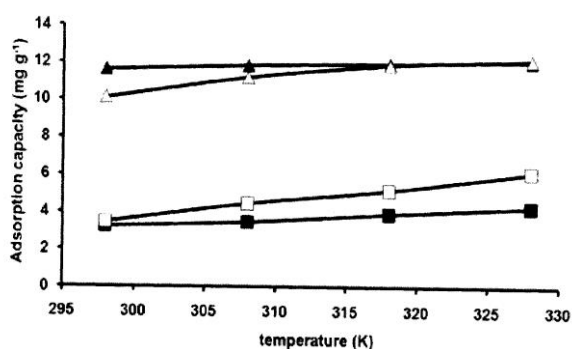
Table 2. Kinetic parameters obtained for adsorption of AG25 and AR14 dyes onto SD/CTAB and SD.

Adsorbent	Dye	Pseudo first-order model			Pseudo second-order model				Intraparticle diffusion model	
		q_{e1} mg g ⁻¹	k_1 min ⁻¹	R^2	q_{e2} mg g ⁻¹	q_e (exp) mg g ⁻¹	k_2 g mg ⁻¹ min ⁻¹	R^2	K_{id} g mg ⁻¹ min ^{-1/2}	R^2
SD/CTAB	AG25	3.20	0.043	0.949	11.89	11.60	0.032	0.997	0.420	0.981
	AR14	3.46	0.064	0.945	10.42	9.43	0.040	0.999	0.435	0.935
SD	AG25	3.82	0.057	0.975	4.97	3.22	0.006	0.996	0.472	0.991
	AR14	3.92	0.061	0.956	4.65	3.45	0.010	0.997	0.463	0.976

* q_{e1} and q_{e2} stand for calculated q_e based on pseudo first and second-order models respectively.

Isotherm investigation

The adsorption isotherm based on linear form of Langmuir and Freundlich equations were plotted (not shown) and the estimated parameters obtained from intercepts and slopes of the corresponding linear plots ($\log q$ versus $\log C$ and $1/q$ versus $1/C$) are summarised in Table 1. Based on the regression analysis (value of R^2), adsorption data obtained for CRAB/SD is better fitted with Freundlich model. The R_L and $1/n$ values (between 0 and 1) obtained for both adsorbents revealing the favorable adsorption too.

**Figure 5.** Effect of temperature on the adsorption of dyes by SD/CTAB (\blacktriangle : AG25; \triangle : AR14) and SD (\blacksquare : AG25; \square : AR14).

Kinetics investigation

The results of adsorption kinetics were processed based on the three kinetic models: pseudo-first order, pseudo-second and intraparticle diffusion models. The kinetic parameters related to each kinetic model were calculated from the intercepts and slopes of the corresponding linear plots (not shown) and the estimated parameters are summarised in Table 2.

The correlation coefficients (R^2) obtained for both adsorbents using pseudo-second-order model (0.996 and 0.999) are higher than those obtained for pseudo-first-order model (0.945-0.975). The calculated adsorption capacity value obtained from pseudo-second-order model (q_{e2}) agrees well with the related experimental value ($q_{e,exp}$). It could be concluded that the adsorption systems are fitted well to the pseudo-second-order model which confirms chemisorption mechanism. These results suggested that such adsorption of dyes might take place via surface ion exchange reaction until the surface function sites are fully occupied. The intraparticle diffusion plots for adsorption of AG25 and AR14 were linear but did not pass through the origin, indicated that the pore diffusion isn't the rate limiting step of the studied adsorption process.

Thermodynamic investigation

Thermodynamic study provides useful information about the spontaneity of a given adsorption processes point as well as calculating of fundamental thermodynamic parameters, such as ΔG^0 , ΔH^0 and ΔS^0 . The effect of temperature on the adsorption equilibrium constants and thermodynamic parameters of the adsorption equilibria derived from the linear plot of $\ln K$ versus $1/T$ (not shown) deduced from Fig. 6 and van't Hoff equation (Eq. 14) are presented in Table 3.

As the data show (Table 3), the value of K_c increases with increasing temperature from 298 to 328 K, suggested the endothermic nature of adsorption process ($\Delta H^0 > 0$). The negative values of ΔG^0 indicated the spontaneous nature of the studied adsorption system. The more negative values obtained for ΔG^0 with increasing temperature indicates that the adsorption process is more favorable at higher temperature. The positive values of ΔG^0 obtained for untreated sawdust (SD) as adsorbent indicate the presence of an energy barrier in the adsorption process.

Table 3. Thermodynamic parameters obtained for adsorption of AG25 and AR14 dyes onto SD/CTAB and SD.

Adsorbent	Dye	T, K	K _c	ΔG ⁰ , kJ mol ⁻¹	ΔH ⁰ , kJ mol ⁻¹	ΔS ⁰ , J mol ⁻¹ K ⁻¹
SD/CTAB	AG25	298	12.97	-6.35	18.52	83.56
		308	17.15	-7.28		
		318	20.73	-8.01		
		328	26.00	-8.88		
	AR14	298	4.17	-3.54	55.96	199.61
		308	8.38	-5.44		
		318	18.02	-7.64		
		328	32.05	-9.45		
SD	AG25	298	0.35	2.68	10.83	27.38
		308	0.38	2.47		
		318	0.45	2.12		
		328	0.51	1.68		
	AR14	298	0.38	2.39	24.23	73.42
		308	0.55	1.53		
		318	0.70	0.95		
		328	0.95	0.14		

Regeneration investigation

For desorption study, various chemicals such as dilute solutions (0.10 M) of NaOH, HCl, and NaCl. The regeneration efficiency (%RE) was calculated using Eq. (3). The results indicate that among the tested washing solutions, NaOH (0.10 M) led to obtaining the best results. Before regeneration experiment, a glass column was first packed with SD/CTAB (1.0 g) and dye solutions (AG25 and AR14) with initial concentration of 20 mg L⁻¹ were passed through the columns with flow rate of 3.0 mL min⁻¹. The dye uploaded columns were then washed with 0.10 M NaOH in order to regeneration and desorbing dyes. The results obtained for AG25 dye are illustrated in Fig. 6.

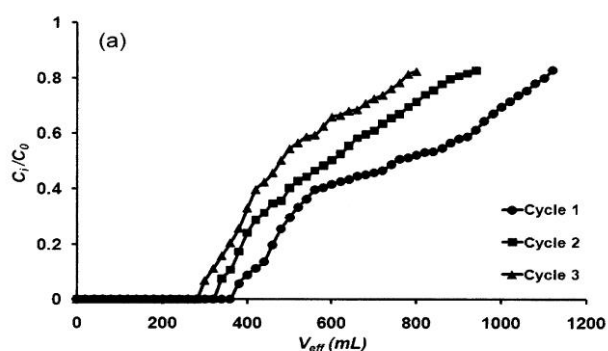


Figure 6. Breakthrough curves obtained for removal of AG25 by SD/CTAB regenerated column (●: Cycle 1; ■: Cycle 2; ▲: Cycle 3)

As the results represent the adsorption capacity of bed decreases as cycle proceeds and this is because of adsorbing sites, whose accessibility becomes difficult as the cycles progressed. Maximum decay observed after three run was about 20% of its initial performance. The results clearly indicate that both dyes retained good adsorption efficiency even after three runs. It was also found that simple pretreatment of the regenerated column with surfactant in each run leads to further improvement of sorption capacity of sawdust for dye removal.

Conclusion

Sawdust modified with cetyltrimethylammonium bromide (SD/CTAB) can be obtained by simple treatment of sawdust with surfactant solution and was proved to be an efficient low cost adsorbent for removal of AG25 and AR14 acid dyes. The adsorption process is influenced by some physical parameters such as solution pH, initial dye concentration, adsorbent dose, contact time and temperature. Adsorption capacity of the adsorbents increased with increasing initial dye concentration, contact time and temperature. The optimal pH of adsorption of AG25 and AR14 dyes onto SD/CTAB were found to be 4 and 6, respectively, while maximum adsorption capacity of these two dyes onto SD occurred at pH 2.

Freundlich isotherm described the equilibrium data of both dyes on SD/CTAB better than Langmuir isotherm, while Langmuir isotherm fitted better to the equilibrium data of dyes on untreated sawdust. The maximum adsorption capacity of SD/CTAB for AG25 and AR14 were found to be 17.5 and 18.9 mg g⁻¹, respectively, based on monolayer coverage of Langmuir model. Pseudo-second-order equation generated the best agreement with experimental data for adsorption systems for the two acid dyes. Thermodynamic analysis suggests that adsorption of dyes by SD/CTAB was a spontaneous and endothermic process.

High regeneration of the used SD/CTAB is quite possible using 0.01 M NaOH and the regenerated adsorbent can be reused without any considerable decay in its removal performance. Because of endothermic nature of the studied adsorption system, it may conclude that spontaneity is mainly governed by entropy factor ($\Delta S^0 > 0$). Upon simple treatment of agricultural wastes such as wood sawdust with cationic surfactants, it is possible to improve sorption capacity of sawdust toward anionic dyes from aqueous solution greatly. The same is true for removal of cationic dyes using sawdust pretreated with anionic surfactants as we have previously reported. The finding in this work seems to be a very important in order to be used in textile waste water treatment.

Acknowledgement

Partial support of this study by the Research Council of University of Guilan is acknowledged.

References

- ¹Mondal, S., *Environ. Eng. Sci.* **2008**, 25, 383.
- ²Garcia-Montano, J., Torrades, F., Perez-Estrada, L. A., Oller, I., Malato, S., Maldonado, M. I., Peral, J. *Environ. Sci. Technol.* **2008**, 42, 6663.
- ³Kar, A., Smith, Y. R., Subramanian, V., *Environ. Sci. Technol.* **2009**, 43, 3260.
- ⁴Koswojo, R., Utomo, R. P., Ju, Y.H.; Ayucitra, A. F., Soetaredjo, E., J., *Appl. Clay. Sci.* **2010**, 48, 81.
- ⁵Tuorma, T. E., *J. Orthomol. Med.* **1994**, 9, 225-243.
- ⁶Gaunt, I. F., Farmer, M., Grasso, P., Gangoli, S. D., *Food. Cosmet. Toxicol.* **1967**, 5, 179.
- ⁷Blackburn, R. S., *Environ. Sci. Technol.* **2004**, 38, 4905.
- ⁸Crini, G., *Bioresour. Technol.* **2006**, 97, 1061.
- ⁹Chakraborty, S., Purkait, M. K., Gupta, S. D., De, S., Basu, J. K., *Sep. Purif. Technol.* **2003**, 31, 141.
- ¹⁰Garg, V. K., Gupta, R., Yadav, A. B. Kumar, R., *Bioresour. Technol.* **2003**, 89, 121.
- ¹¹Allen, S. J., McKay, G., Porter, J. F., *J. Colloid. Interf. Sci.* **2004**, 280, 322.
- ¹²Jain, A. K., Gupta, V. K., Bhatnagar, A., Suhas, I. A., *J. Hazard. Mater.* **2003**, B101, 31.
- ¹³Chatterjee, S., Lee, D. S., Lee, M. W., Woo, S. H., *Bioresour. Technol.* **2009**, 100, 3862.
- ¹⁴Kadirvelu, K., Kavipriya, M., Karthika, C., Radhika, M., Vennilamani, N., Patabhi, S., *Bioresour., Technol.* **2003**, 87(1), 129.
- ¹⁵Suteu, D., Bilba, D.; Dorofte, F., Malutan, T., *Sep. Sci. Technol.* **2011**, 46, 1462.
- ¹⁶Arami, M., Limaee, N.Y., Mahmoodi, N. M., Tabrizi, N. S., *J. Hazard. Mater.* **2006**, B135, 171.
- ¹⁷Hameed, B. H., Ahmad, A. A., Aziz, N., *Chem. Eng. J.* **2007**, 133, 195.
- ¹⁸Ansari, R., Keivani, M. B., Delavar, A. F., *J. Appl. Polym. Sci.* **2011**, 122, 804.
- ¹⁹Ansari, R., Seyghali, B., Mohammad-khah, A., Zanjanchi, M. A., *Sep. Sci. Technol.*, **2012**, 47, 1802.
- ²⁰Ansari, R., Tehrani, S. M., Mohammad-Khah, A., *J. Wood Chem. Technol.* **2012**, 32, 198.
- ²¹Ansari, R., Tehrani, S. M., Keivani, M. B., *J. Wood Chem. Technol.* **2013**, 33, 19.
- ²²Ansari, R., and Dezhampannah, H., *Eur. Chem. Bull.* 2013, 2(4), 220.
- ²³Bingol, A., Aslan, A., Cakici, A., *J. Hazard. Mater.* **2009**, 161, 747.
- ²⁴Balistrieri, L. S., Murray, J. W., *Am. J. Sci.* **1981**, 281, 788.
- ²⁵Gupta, V. K., Sharma, S., *Environ. Sci. Technol.* **2002**, 36, 3612.
- ²⁶Anirudhan, T. S., Suchithra, P. S., *J. Environ. Sci.*, **2009**, 21, 884.
- ²⁷Al-Duri, B., *Adsorption modelling and mass transfer.* CRC Press, **1996**, 133.
- ²⁸Langmuir, I., *J. Am. Chem. Soc.* **1918**, 40, 1361.
- ²⁹Hall, K. R., Eagleton, L. C., Acrivos, A., Vermeulen, T., *Ind. Eng. Chem. Fundament.* **1966**, 5, 212.
- ³⁰Freundlich, H. M. F. , *Phys. Chem.* **1906**, 57A, 385.
- ³¹Coles, C. A., Yong, R. N., *Eng. Geol.*, **2006**, 85, 19.
- ³²Lagergren, S., *Kung. Sven. Vetenskapsak. Handl.* **1898**, 24, 1.
- ³³Ho, Y. S., McKay, G., *Process. Biochem.* **2009**, 34, 451.
- ³⁴Weber, W. J., Morris, J. C., *J. Sanit. Eng. Div. Am. Soc. Civ. Eng.* **1963**, 89, 31.
- ³⁵Vimonses, V., Lei, S., Jin, B.; Chow, C. W. K., Saint, C., *Appl. Clay Sci.* **2009**, 43, 465.
- ³⁶Lian, L., Guo, L., Guo, C., *J. Hazard. Mater.* **2009**, 161, 126.
- ³⁷Nigam, P., Armour, G., Banat, I. M., Singh, D., Marchant, R., *Bioresour. Technol.*, **2000**, 72, 219.

Received: 31.01.2013.

Accepted: 17.03.2013.



SPECTROPHOTOMETRIC DETERMINATION OF CINNARIZINE THROUGH CHARGE-TRANSFER COMPLEX FORMATION WITH POLYNITRO COMPOUNDS

Y. M. Issa^[a], A. F. A. Youssef^[a], W. F. El-Hawary^{[a,b]*}, E. A. Abdel-Ghaffar^[c]

Keywords: Spectrophotometric determination, Cinnarizine, Charge-transfer complexes, Polynitrobenzene π -acceptors

Spectrophotometric studies were carried out to investigate the charge-transfer reaction between cinnarizine and dipicrylamine (DPA) or 2,6-dinitrophenol (DNP). Simple and rapid spectrophotometric methods were suggested for the determination of cinnarizine (CN) in pure and in its pharmaceutical dosage forms. The colored products are quantified spectrophotometrically at 430 and 440 nm for cinnarizine complexes with DPA in a mixture of 15% dioxane in dichloroethane (I) and 15% ethyl acetate in chloroform (II), respectively. On the other hand, cinnarizine complexes formed with DNP in acetonitrile (III) and in a mixture of 30% dichloroethane in ethyl alcohol (IV) were quantified at 460 and 430 nm, respectively. The proposed procedures were successfully utilized for the determination of the drug in its pharmaceutical formulation using standard addition and calibration curve methods. Beer's law was obeyed in the concentration ranges 1.00-22.00, 1.50-36.80, 1.50-36.80 and 3.60-36.80 $\mu\text{g mL}^{-1}$ cinnarizine with molar absorptivities of 1.64×10^4 , 1.43×10^4 , 5.16×10^4 and 3.60×10^4 ($\text{L mol}^{-1} \text{cm}^{-1}$), for CN-DPA in mixture (I), CN-DPA in mixture (II), CN-DNP in acetonitrile (III) and CN-DNP in mixture (IV), respectively. The relative standard deviations are less than 1.02%. The results of analysis of commercial tablets (Cinnarizine-25) showed that there is no interference from any excipient. Statistical comparison of the results was performed with regard to accuracy and precision using student's t-test and F-ratio at 95% confidence level.

* Corresponding Authors

E-Mail: waheedfathi@yahoo.com

[a] Chemistry Department, Faculty of Science, Cairo University, Giza, Egypt

[b] Chemistry Department, Faculty of Science, Taif University, Taif, Saudi Arabia

[c] National Organization for Drug Control and Research, Giza, Egypt

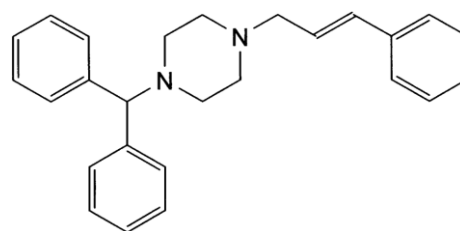


Figure 1. The structural formula of cinnarizine (CN).

Introduction

Cinnarizine (CN), 1-(diphenylmethyl)-4-(3-phenyl-2-propenyl) piperazine (Fig. 1), is a piperazine derivative with antihistaminic, sedative, and calcium channel blocking activity. It is used for the symptomatic treatment of nausea and vertigo caused by Menier's disease and other vestibular disorders. It is also used for the prevention and treatment of motion sickness.^{1,2} Several analytical methods have been reported for the determination of CN, either in pure form or in pharmaceutical preparations and biological fluids. These methods include non-aqueous titration,³ spectrophotometry,⁴⁻⁸ electrometry,^{9,10} high-performance liquid chromatography (HPLC),¹¹⁻¹⁴ gas chromatography (GC),¹⁵ titrimetry¹⁶ and capillary electrophoresis.¹⁷

The molecular interactions between electron donors and acceptors are generally associated with the formation of intense colored charge-transfer complexes, which absorb radiation in the visible region. The photometric methods based on these interactions are usually simple and convenient because of the rapid formation of the complexes.

The present article deals with the spectrophotometric determination of cinnarizine (CN) in pure form and in pharmaceutical preparations using dipicrylamine and 2,6-dinitrophenol as electron acceptors.

Experimental

Materials and reagents

All reagents and chemicals used were of analytical grade, and the solvents were of spectroscopic grade. Dipicrylamine and 2,6-dinitrophenol chemicals were provided by BDH chemical company. Cinnarizine standard powder was kindly provided by Edwic Chemical Company, Egypt and used as received and cinnarizine-25 tablets (1 mg/tablet) produced by Adco Drug Company were obtained from local market.

Stock solution of dipicrylamine, $10^{-2} \text{ mol L}^{-1}$, was freshly prepared by dissolving 0.4392 mg in 100 mL of 15% dioxane in dichloroethane, mixture (I) and 15%

ethyl acetate in chloroform, mixture (II). For 2,6-dinitrophenol reagent, a 10^{-2} mol L⁻¹ solution was prepared by dissolving 0.1841 mg in 100 mL acetonitrile (III) and in 30% dichloroethane in ethyl alcohol mixture (IV). These solutions are stable for 2 weeks. 10^{-2} mol L⁻¹ cinnarizine stock solutions were prepared by dissolving 0.3685 mg in a 100 mL of mixture (I), mixture (II), acetonitrile (III) and mixture (IV). These solutions are stable for 2 weeks.

Preparation of solid complexes

A solution contains 1 mmol CN was prepared in solvent mixture (I), (II) or (IV) and pure acetonitrile (III), while the DPA solutions contain 1.0 and 0.5 mmol were prepared in solvent mixtures (I) and (II), respectively. For DNP, solutions contain 1.0 and 2.0 mmol were prepared in pure acetonitrile (III) and solvent mixture (IV), respectively. The reagent solutions were added individually with constant stirring and left until solvent evaporated and then washed by petroleum ether.

Apparatus

The spectral measurements were carried out using a single beam spectrophotometer model 22 Spectro Labomed, with quartz cells of 1-cm optical path length. Elemental analysis of the resulting reaction products was carried out by atomic CHN analyzer (Perkin Elmer model 2400) in the Micro analytical Center, Faculty of Science, Cairo University, Giza, Egypt.

General recommended procedures

Using dipicrylamine (DPA)

Aliquots of CN solution containing 1.0-36.8 μ g were transferred into 10 mL measuring flasks. To each flask, 0.1 mL of DPA in mixture of 15% dioxane in dichloroethane or in mixture of 15% ethyl acetate in chloroform was added. The reaction mixture was mixed well and the volume was completed to 10 mL with the same solvent. The absorbance was measured against a blank solution, containing all additives except the drug, at 430 and 440 nm, in mixture (I) and mixture (II) respectively.

Using 2,6-dinitrophenol (DNP)

Different aliquots of the working standard solution containing 3.6-36.8 μ g were transferred into 10 mL measuring flasks. To each flask, 0.2 mL of DNP in pure acetonitrile or in 30% dichloroethane in ethyl alcohol was added. The reaction mixture was completed to 10 mL with the same solvent. The absorbance was measured against a blank, containing all additives except the drug, at 460 and 430 nm, in acetonitrile (III) and mixture (IV) respectively.

Pharmaceutical analysis

20 tablets were weighed and finely ground, then a weight equivalent to one tablet was dissolved in 15% dioxane in dichloroethane or in pure acetonitrile and

transferred into a 25 mL measuring flask. The solution was shaken and filtered to remove any undissolved excipients substances. The resulting solution was subjected to analysis as described in the general procedures.

Determination of the stoichiometric ratio of the complexes

The stoichiometry of the charge-transfer complexes formed between cinnarizine and both PDA and DNP were studied by the aid of continuous variation method,¹⁸ molar ratio method¹⁹ and elemental analysis.

For the Job's method of continuous variation, master equimolar (2×10^{-4} mol L⁻¹) aqueous solutions of CN and DPA or DNP were prepared. Series of 10 mL portions of the master solutions of CN and DPA or DNP were made up comprising different complementary proportions (0:10, 1:9, . . ., 9:1, 10:0) in 10 mL calibrated flasks. For the molar ratio method, the concentration of CN was kept constant by adding 0.2 mL of 2×10^{-4} mol L⁻¹ of CN while the concentration of the acceptors (DPA or DNP) was changed over a wide range. All solutions were further manipulated as described under the general recommended procedures. The solid charge-transfer complexes were subjected to elemental analysis and the results are presented in Table 1.

Table 1. Elemental analysis of the formed CN-DPA and CN-DNP charge-transfer complexes.

Formed complex	Molar ratio	(Found)% Calculated%		
		C	H	N
CN-DPA ^(a)	1:1	(55.10)	(3.78)	(14.22)
		56.40	3.83	15.59
CN-DPA ^(b)	2:1	(65.91)	(5.95)	(11.81)
		65.29	5.18	13.09
CN-DNP ^(c)	1:1	(69.99)	(5.95)	(10.04)
		69.48	5.60	10.13
CN-DNP ^(d)	1:2	(56.50)	(3.75)	(11.93)
		61.80	4.62	11.40

^a15% Dioxane in dichloroethane; ^b15% Ethyl acetate in chloroform; ^cAcetonitrile; ^d30% Dichloroethane in ethyl alcohol.

Results and discussion

The charge-transfer complex formation reactions are based on the π -acceptors that react with the basic nitrogenous compounds as donors to form charge-transfer complexes or radical anions according to the polarity of the solvent used.

Absorption spectra

The absorption spectra of CN-DPA and CN-DNP complexes were scanned in different solvents (acetonitrile, 1,4-dioxane, ethyl acetate 1,2-dichloroethane, and their mixtures with ethyl alcohol and chloroform). The results showed that a mixture of 15% (v/v) 1,4-dioxane in 1,2-dichloroethane and 15% ethyl acetate in chloroform are

the most suitable solvents for CN-DPA while pure acetonitrile and 30% dichloroethane in ethyl alcohol are the most suitable solvents for CN-DNP complexes. High molar absorptivity values (1.64×10^4 , 5.16×10^3 L mol⁻¹ cm⁻¹) for CN-DPA in mixture (I) and CN-DNP in acetonitrile have been obtained. The reaction between CN and DPA or DNP was performed and the absorption spectra of the products were recorded against reagent blank (Figs. 2 and 3). It was found that intense yellow-colored complexes, exhibiting λ_{\max} at 430 and 460 nm have been obtained for CN-DPA and CN-DNP in mixture (I) and acetonitrile (III), respectively.

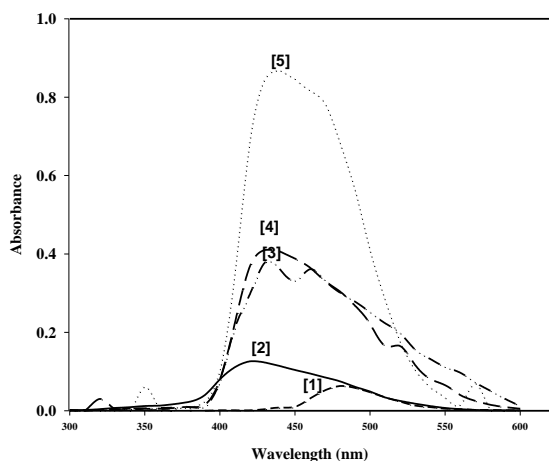


Figure 2. Absorption spectra for CN-DPA complexes in different solvents, [CN] = 5×10^{-5} mol L⁻¹; at room temperature. (1) 15% (v/v) Dioxane in ethyl alcohol, (2) Dioxane, (3) Ethyl acetate, (4) 15% (v/v) Ethyl acetate in chloroform, and (5) 15% (v/v) Dioxane in dichloroethane.

Spectral characteristics of the CT complex

The oscillator strength (f), which is a dimensionless quantity used to express the transition probability of the CT band,²⁰ and the transition dipole moment (μ_{EN}) of the CT complexes²¹ were calculated from the following

$$f = 4,32 \times 10^{-9} \left[\varepsilon_{\max} \Delta\nu_{1/2} \right] \quad (1)$$

$$\mu_{EN} = 0,0958 \left[\frac{\varepsilon_{\max} \Delta\nu_{1/2}}{\nu_{\max}} \right] \quad (2)$$

expressions:

where

$\Delta\nu_{1/2}$ is the band width at half absorbance and

ε_{\max} and ν_{\max} are the molar absorptivity and wave number at the absorption maximum of the complex, respectively.

In these equations, ν_{\max} has been expressed in cm⁻¹. The relative low values of f indicate a weak interaction between the donors-acceptor pairs.²² The R_N is the resonance energy of the complex in the ground state,

which is obviously a contributing factor to the stability constant of the complex (a ground state property), can be determined by the following equation²³:

$$\varepsilon_{\max} = \frac{7.7 \times 10^4}{h\nu_{CT} / |R_N| - 3.5} \quad (3)$$

where

ν_{CT} represents the frequency at maximum absorbance of the CT band.

Resonance energies for the CT complexes of CN with different electron acceptors, Table. 2, indicate that the probability and dipole moment of transition in case of CN-DPA in mixtures (I) and (II) are higher than those of CN-DNP in acetonitrile (III) and mixture (IV).

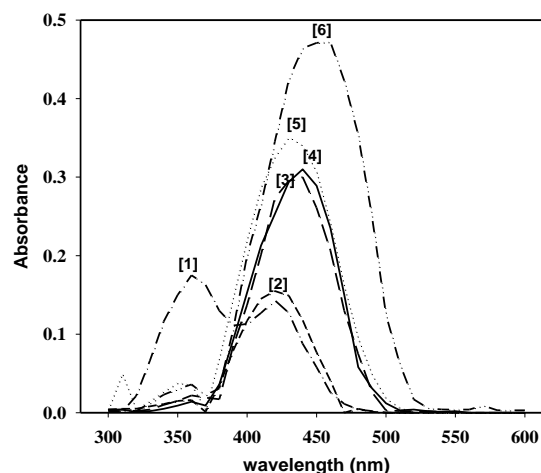


Figure 3. Absorption spectra for CN-DNP complexes in different solvents, [CN] = 1×10^{-4} mol L⁻¹; at room temperature, (1) 30% (v/v) Acetonitrile in dichloroethane, (2) 30% (v/v) dichloroethane in chloroform, (3) 30% (v/v) Acetonitrile in dichloromethane, (4) Dichloroethane, (5) 30% (v/v) Acetonitrile in dichloromethane, (6) 30% (v/v) Dichloroethane in ethyl alcohol and (6) Acetonitrile.

The probability of transition is the lowest for CN-DNP in mixture (IV), also values of resonance energy show that the stability of CN-DPA complexes in both mixtures (I) and (II) are higher than the stability of CN-DNP complexes in acetonitrile (III) and mixture (IV), and the CN-DNP complexes prepared in mixture (IV) exhibit the lowest stability.

Optimization of reaction variables

The spectrophotometric properties of the colored species as well as the different parameters affecting the color development were extensively studied to determine the optimum conditions for the analytical determination of the drug. The reactions were studied as a function of the volume of the reagents, nature of the solvents, effect of temperature and effect of time on the formation of the complex. Stability of colors and the molar ratio were also studied.

Table 2. Spectral properties obtained for CN-DPA and CN-DNP charge-transfer complexes.

Parameter	Method			
	DPA		DNP	
	I	II	III	IV
λ_{CT} , nm	430	440	460	430
$h\nu_{CT}$, eV	4.62	4.51	4.30	4.62
ϵ_{max} , L mol ⁻¹ cm ⁻¹	1.43×10^4	1.64×10^4	5.16×10^3	3.60×10^3
Stoichiometry (drug:reagent)	1:1	2:1	1:1	1:2
R_N (eV)	51.77×10^{-2}	55.08×10^{-2}	23.34×10^{-2}	18.56×10^{-2}
f	6.18×10^{-10}	7.08×10^{-10}	2.01×10^{-10}	1.09×10^{-10}
μ_{EN}^{Depye}	2.38×10^{-4}	2.57×10^{-4}	1.40×10^{-4}	9.97×10^{-4}

λ_{CT} - absorption maxima, ϵ_{max} - molar absorptivity, R_N - the resonance energy of the complex in the ground state stoichiometry, f - the oscillator strength, μ_{EN} - the transition dipole moment. I-15% dioxane :dichloroethane; II-15% ethyl acetate :chloroform; III-Acetonitrile; IV-30% dichloroethane: ethyl alc.

Effect of diluting solvent

Upon diluting the reaction solution with water, turbid solution with low color intensity was obtained indicating the incomplete solubility of CN-DPA or CN-DNP complexes in water. Therefore, water could not be used for dilution. In order to select the most appropriate solvent for diluting the reaction solution, different solvents were tested e.g. 1,4-dioxane, ethyl acetate, chloroform, acetone, acetonitrile, and mixture of these solvents with different proportions. The highest absorbance values were obtained when mixture of 15% dioxane in dichloroethane and pure acetonitrile were used as diluting solvents for CN-DPA and CN-DNP, respectively, Figs. 2 and 3.

Effect of reagent concentration

The effect of the reagents concentration on the intensity of the color production was studied by adding various amounts of the reagents to a fixed concentration of CN (1.0×10^{-4} mol L⁻¹). The results showed that, in case of using DPA in both mixtures (I) and (II), maximum and constant absorbance values were obtained using reagent concentration at least three times that of CN. While, in using DNP in acetonitrile (III) and mixture (IV), the maximum reproducible absorbances were obtained by using reagent concentration at least six times that of CN, Fig. 4.

Effect of temperature

The effect of temperature on the reaction was studied by carrying out the reaction at temperatures between 25-70 °C. The results revealed that complete color development is obtained at room temperature up to 30 °C and absorbance values decrease with increasing the temperature of the reaction medium. The decrease in the absorbance values may be attributed to the instability of the reaction product at high temperature.

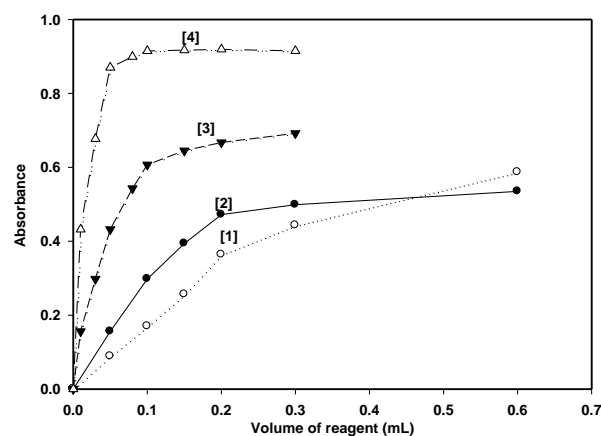


Figure 4. The effect of reagent concentration on the formation of the complexes. $[CN] = 0.1 \times 10^{-3}$ mol L⁻¹, (1) DNP in 30% (v/v) dichloroethane in ethyl alcohol, 430 nm, (2) DNP in acetonitrile, 460 nm, (3) DPA in 15% (v/v) ethyl acetate in chloroform, 430 nm, and (4) DPA in 15% (v/v) dioxane in dichloroethane, 440 nm.

Effect of time

Under the above mentioned optimum conditions, the reaction between CN and DPA or DNP was completed immediately at 25 ± 5 °C, and the absorbance no longer changes for standing up to 24 hours. The effect of time on the stability of the product was studied by following the absorbance intensity of the reaction solution (after dilution) at different time intervals. It was found that the absorbance of the product remains stable for at least 24 hours. This allows the processing of a large number of samples, and their comfortable measurements with convenience.

Stoichiometry of the reaction

Under the optimum conditions, the stoichiometry of the formed complexes was investigated using Job's continuous variation and molar ratio methods.

The results indicated that CN-DPA complex in mixture (I) and CN-DNP complex in acetonitrile (III) were formed in the ratio of 1:1. On the other hand, the ratio of the complexes CN-DNP formed in mixture (IV) and CN-DPA formed in mixture (II) are 1:2 and 2:1 drug : reagent ratio, respectively. The results obtained were confirmed by elemental analysis for the solid charge-transfer complexes, Table 1. The results are shown in Figs. 5 and 6.

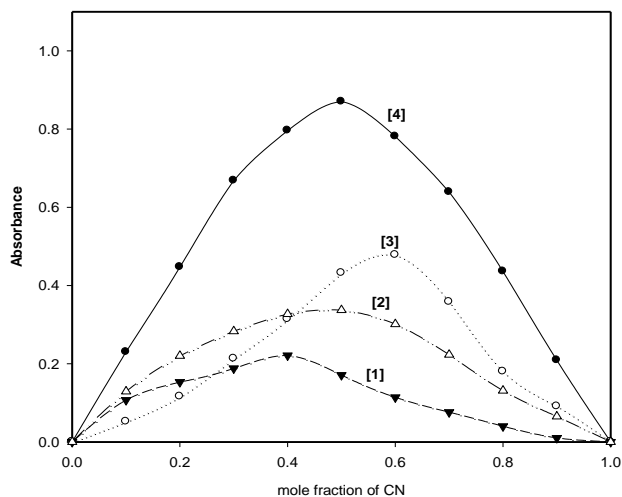


Figure 5. Continuous variation plots of CN-DPA and CN-DNP complexes; total molar concentration = 2×10^{-4} mol L⁻¹. (1) DNP in 30% (v/v) dichloroethane in ethyl alcohol, 430 nm, (2) DNP in acetonitrile, 460 nm, (3) DPA in 15% (v/v) ethyl acetate in chloroform, 430 nm, and (4) DPA in 15% (v/v) dioxane in dichloroethane, 440 nm.

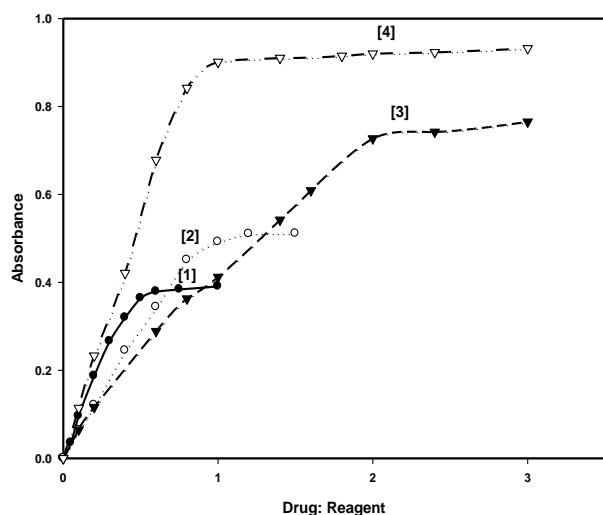


Figure 6. Molar ratio plots of CN-DPA and CN-DNP complexes. (1) DNP in 30% (v/v) dichloroethane in ethyl alcohol, 430 nm, (2) DNP in acetonitrile, 460 nm, (3) DPA in 15% (v/v) ethyl acetate in chloroform, 430 nm, and (4) DPA in 15% (v/v) dioxane in dichloroethane, 440 nm.

Association constants and standard free energy change

The association constants were calculated for 1:1 complexes using Benesi-Hildebrand²⁴ equation (4):

$$\frac{[A_0]}{[A_\lambda^{AD}]} = \frac{1}{\epsilon_\lambda^{AD}} + \frac{1}{K_C^{AD} \epsilon_\lambda^{AD}} \times \frac{1}{[D_0]} \quad (4)$$

where

A_λ^{AD} is the absorbance of the charge-transfer band,

ϵ_λ^{AD} is the molar absorptivity of the complex, $[A_0]$ and $[D_0]$ represent the initial acceptor and donor concentrations, respectively, and

K_C^{AD} is the association constant for the equilibrium.

Benesi-Hildebrand equations for 1:1 complexes of CN with DPA and DNP can be represented by equations 5 and 6, respectively.

$$\frac{[A_0]}{A_\lambda^{AD}} = (4.9 \times 10^{-5}) + (0.56 \times 10^{-8}) \times \frac{1}{[D_0]} \quad (5)$$

$$\frac{[A_0]}{A_\lambda^{AD}} = (1.4 \times 10^{-4}) + (0.27 \times 10^{-7}) \frac{1}{[D_0]} \quad (6)$$

The formation constants (K_f) of CN-DNP 1:2 ion-associate complexes formed in mixture (IV) and 2:1 CN-DPA complexes formed in mixture (II), were calculated, (Table 3) from the continuous variation data using the following equation²⁵:

$$K_f = \frac{\left[\frac{A}{A_m} \right]}{\left[\frac{1-A}{A_m} \right]^{n+1}} C^n n^n \quad (7)$$

where

A_m is the maximum absorbance obtained from Job's continuous variation curve,

A is the absorbance corresponding to the intersection of the two tangents of the continuous variation curve, C is the concentration corresponding to maximum absorbance,

n is the ratio of the drug in the reaction product.

The standard free energy change, ΔG° of the complex formation is related to the formation constant by the following equation²⁶:

$$\Delta G^0 = -2.303RT \lg K \quad (8)$$

where

R is the universal gas constant ($8.314 \text{ J mol}^{-1} \text{ K}^{-1}$),

T is the absolute temperature and

K is the formation constant of the CT complex.

The obtained values of $\varepsilon_{\lambda}^{\text{AD}}$, K_f and ΔG° for CN charge-transfer complexes are presented in Table 3. It is clear from the obtained results that, these charge-transfer reactions are spontaneous as indicated by the negative values of ΔG° and the high values of K_f .

Validation of the methods

Calibration and sensitivity

Calibration curves for the determination of CN by its reaction with both DPA and DNP were constructed by plotting the absorbances as a function of the corresponding concentrations. The regression equations for the results were $A=0.008+0.0425C$ ($r=0.9970$) and $A=0.0031+0.0371C$ ($r=0.9996$) with molar absorptivities (ε) 1.64×10^4 and $1.43 \times 10^4 \text{ L mol}^{-1} \text{ cm}^{-1}$ for DPA-CN complexes prepared in mixture (I) and mixture (II), respectively. The $A = -0.0071 + 0.0101C$ ($r = 0.9954$) and $A = 0.0033 + 0.0143C$ ($r=0.9996$) with molar absorptivities (ε) 5.16×10^3 and $3.60 \times 10^3 \text{ L mol}^{-1} \text{ cm}^{-1}$ for DNP-CN complexes prepared in acetonitrile (III) and mixture (IV) were found, respectively, where A is the absorbance at λ_{max} for each method, C is the concentration of CN in $\mu\text{g mL}^{-1}$, and r is the correlation coefficient. Optimization of the linear range (Ringbom) was evaluated by plotting the percentage transmittance versus the logarithm of concentration ($\mu\text{g mL}^{-1}$). The limit of detection (LOD) and limit of quantification (LOQ) were determined according to the International

Conference of Harmonization (ICH) guidelines for validation of analytical procedures.²⁷ The following formula was used: LOD or $LOQ = K SD_a$, where $K=3$ for LOD and 10 for LOQ , and SD_a is the standard deviation of the intercept. The values of LOD were 0.72 and 0.40, LOQ were 2.23 and 1.48 for CN-DPA in case of using 15% dioxane in dichloroethane and 15% ethyl acetate in chloroform, respectively. For CN-DNP LOD values were 0.54 and 2.08, and LOQ values were 2.35 and 5.27 in case of using acetonitrile and 30% dichloroethane in ethyl alcohol, respectively, Table 3.

Reproducibility

The reproducibility of the proposed methods was evaluated by replicate analysis of five separate solutions of the working standard at different concentration levels. The method gave satisfactory results; RSD did not exceed 2% indicating the good reproducibility of the proposed method. This precision level is adequate for routine analysis of the investigated drug in quality control laboratories.

Accuracy and interference liabilities

The accuracy of the proposed method was evaluated by the recovery studies for added concentrations. The recovery values were $98.77 \pm 0.9 - 100.00 \pm 1.1\%$, Table 4, indicating the accuracy of the proposed method. Interference liabilities of common excipients: starch, glucose, lactose, talc, and magnesium stearate were not necessary to be tested before proceeding with the analysis of CN in its dosage forms; the drug is extracted firstly by dissolving it in the appropriate solvent then filtering. The excipients are insoluble in such solvents.

Table 3. Analytical parameters for CT complexes of cinnarizine with DPA and DNP.

Parameter	Method			
	DPA		DNP	
	I	II	III	IV
λ_{max} , nm	430	440	460	430
Beer's law limits, $\mu\text{g mL}^{-1}$	1.00-22.00	1.50-36.80	1.50-36.80	3.60-36.80
Molar absorptivity, $\text{L mol}^{-1} \text{ cm}^{-1}$	1.64×10^4	1.43×10^4	5.16×10^3	3.60×10^3
Sandell sensitivity, $\mu\text{g cm}^{-2}$	0.0020	0.0269	0.0684	1.1111
Ringbom range, $\mu\text{g mL}^{-1}$	3.00-22.00	3.00-22.00	7.00-26.00	7.00-26.00
Slope	0.0496	0.0371	0.01446	0.0009
Intercept	0.0330	0.0007	0.0002	0.0001
LOD , $\mu\text{g mL}^{-1}$	0.72	0.40	0.54	2.08
LOQ , $\mu\text{g mL}^{-1}$	2.23	1.48	2.35	5.27
Correlation coefficient, r	0.9970	0.9996	0.9954	0.9996
K_c^{AD} (L mol^{-1})	4.20×10^3	--	5.36×10^3	--
K_f^{AD} (L mol^{-1})	3.15×10^4	1.05×10^9	1.46×10^4	1.75×10^4
ΔG° , k cal mol^{-1}	-2.59×10^4	-4.63×10^4	-2.40×10^4	-2.44×10^3

LOD : Limit of detection; LOQ : Limit of quantification; $n=5$; K_c^{AD} : the association constants calculated from Benesi-Hildebrand equation; K_f : the formation constants calculated from the continuous variation equation; I. 15% dioxane in dichloroethane; II. 15% ethyl acetate in chloroform; III. Acetonitrile; IV. 30% dichloroethane in ethyl alcohol.

Table 4. Recovery studies for determination of CN in standard solutions and pharmaceutical formulation applying calibration curve and standard addition methods.

Reagent	Proposed methods			Recovery±RSD% ^a	t-test ^b	F-test ^b	Reference method ²⁸
	Taken, µg	Added, µg	Found, µg				Recovery±RSD%
DPA							
Pure CN in 15% dioxane in dichloroethane							
	5.52	5.52	10.97	99.36±1.20	0.35	6.15	99.09±1.63
	3.68	--	3.67	99.72±0.92	2.25	1.82	99.80±2.01
	5.52	--	5.51	99.81±1.61	1.85	3.56	99.74±1.00
Cinnarizine-25 in 15% dioxane in dichloroethane							
	5.50	5.52	10.98	99.45±0.67	0.69	1.45	99.23±1.05
	18.00	--	17.78	98.77±0.90	2.25	0.96	99.06±0.69
Pure CN in 15% ethyl acetate in chloroform							
	5.52	5.52	10.97	99.36±1.44	1.32	2.09	
	3.68	--	3.66	99.45±1.63	1.51	3.11	
	5.52	--	5.49	99.40±1.81	1.02	2.15	
DNP							
Pure CN in acetonitrile							
	5.52	5.52	11.03	99.90±1.20	1.02	6.34	
	3.68	--	3.65	99.18±0.90	0.63	3.00	
	5.52	--	5.50	99.63±1.81	0.95	4.12	
Cinnarizine-25 in acetonitrile							
	5.50	5.52	10.96	99.27±0.51	1.12	1.24	
	18.00	--	17.84	99.11±1.20	0.83	1.00	
Pure CN in 30% dichloroethane in ethyl alcohol							
	5.52	5.52	11.00	99.63±0.12	0.98	2.51	
	3.68	--	3.68	100.00±1.11	1.01	4.03	
	5.52	--	5.50	99.63±1.80	1.00	3.52	

a. Mean ± relative standard deviation of five replicate analyses; b. Theoretical values for t- and F-tests are 2.77 and 6.39, respectively, for four degree of freedom and 95% confidence limit.

Robustness

Robustness was examined by evaluating the influence of small variation in the method variables on its analytical performance. In these experiments, the absorbances of the formed complex were determined at 5 minutes and at 15 minutes of the reaction time whereas the other conditions were kept unchanged. Similarly the temperature of the reaction was changed and the absorbance of the formed complex determined at 25 °C and 35 °C. The recovery percentage was calculated each time. It was found that small variation in the method variables did not significantly affect the procedures; recovery values were 97.90±1.95 – 100.50±1.02%, Table 5. This indicates the reliability of the proposed method during its routine application for the determination of cinnarizine.

Applications

The proposed methods were applied for the determination of Cinnarizine-25 tablets. Five replicate determinations were performed. Satisfactory results were obtained, Table 4. Moreover, to check the validity of the proposed methods, the standard addition method was applied by adding standard cinnarizine solution to a

previously analyzed tablet solution, and the recovery was calculated. The results of analysis of commercial dosage forms and the recovery study of the standard addition method of the cited drug reveals that the suggested methods give high recovery values.

For the sake of determining the accuracy and precision of the suggested methods, they were compared with a previously reported method.²⁸ Statistical comparison of the results was performed with regard to accuracy and precision using student's t-test and F-test at 95% confidence level, Table 6. The results showed that there is no significant difference between the reported²⁸ and proposed methods with regard to accuracy and precision.

Conclusion

The suggested methods for the determination of cinnarizine by using dipicrylamine and 2,6-dinitrophenol have the advantages of being simple, accurate, sensitive, rapid and suitable for routine analysis in control laboratories. These methods utilize a single step reaction, and no substantial differences among the proposed methods arise from analysis of the experimental results.

Table 5. Influence of small variations in the assay conditions on the analytical performance of the proposed spectrophotometric method for determination of CN using DPA and DNP.

Method ^b	Recovery% \pm SD ^a			
	Temperature		Time	
	25 °C	35 °C	5 minutes	15 minutes
DPA method				
I	99.15 \pm 1.02	100.10 \pm 0.84	100.02 \pm 0.99	100.50 \pm 1.02
II	98.20 \pm 0.98	98.15 \pm 1.01	100.50 \pm 1.02	98.21 \pm 0.96
DNP method				
III	97.90 \pm 1.95	97.90 \pm 1.95	97.90 \pm 1.95	97.90 \pm 1.95
IV	98.80 \pm 1.35	99.01 \pm 0.89	98.23 \pm 1.01	99.56 \pm 0.99

a Values are the mean of 3 determinations; b At the optimum conditions; I: 15% dioxane in dichloroethane; II: 15% ethyl acetate in chloroform; III: Acetonitrile; IV: 30% dichloroethane in ethyl alcohol.

Table 6. Statistical tests for accuracy and precision of the proposed methods on samples of pure CN with DPA and DNP, at 95% confidence level and $\nu=4$.

Parameters	DPA in 15% dioxane in dichloroethane	DNP in pure acetonitril
SD%	0.64%	0.66%
Coefficient of variation	0.71%	2.53%
RSD% ^a	0.32%	1.02%
F-test ^b	6.15	6.34
t-test ^b	0.35	1.02

a. Relative standard deviation of five replicate analyses; b. Theoretical values for t- and F-tests are 2.776 and 6.39, respectively, for four degree of freedom and 95% confidence level.

The complex formation of CN with DPA in mixture of 15% 1,4-dioxane in 1,2-dichloroethane is more sensitive than the other methods due to the higher molar absorptivity. These methods can be used precisely and accurately with high recovery ranged between 99.18 \pm 0.90 and 100.00 \pm 1.11, for the spectrophotometric determination of cinnarizine in the range of 1.00 - 36.80 μ g both in pure forms and in its pharmaceutical formulations.

References

- ¹Rahaway, N. J., *The Merk Index, an Encyclopedia of Chemicals, Drugs, and Biologicals*, Merck, USA, 12th Edn., **1996**.
- ²Parfitt, K., Martindale, W., *The complete drug reference*, 32th edn. Pharmaceutical Press, London, **1999**, 411.
- ³British Pharmacopoeia Commission, *British Pharmacopoeia*, vols. I and II. Her Majesty's Stationery Office, London (through electronic version), **2003**.
- ⁴Metwally, F. H., Elzeany, E. B. A. and Darwish, H. W., *J AOAC Int.*, **2005**, 88(6), 1666.
- ⁵Abdine, H., Belal, F. and Zoman, N., *Il Farmaco*, **2002**, 57, 267.
- ⁶El-Gindy, A., Emara, S. and Hadad, G. M., *Il Farmaco*, **2004**, 59, 703.
- ⁷El-Gindy, A., Emara, S. and Mostafa, A., *Il Farmaco*, **2004**, 59, 713.
- ⁸Xu, B. Z., Zhao, F. L. and Tong, S. Y., *Guangpuxue-Yu-Guangpu-Fenxi*, **1999**, 19(6), 886.
- ⁹Hassan, S. S. M., Abdel-Aziz, R. M. and Abbas, A. B., *Anal. Chim. Acta*, **1996**, 321(1), 47.
- ¹⁰Zeng, Y. H. and Sun, H. Y., *Fenxi-Huaxue*, **1993**, 21, 1185.
- ¹¹De Steene, J. C. V., Mortier, K. A. and Lambert, W. E., *J Chromatogr.*, **2006**, 1123, 71.
- ¹²Hassan, S. S. M., Elmosallamy, M. A. F. and Abbas, A. B., *J. Pharm. Biomed. Anal.*, **2002**, 28(3-4), 711.
- ¹³Rosseel, M. T. and Lefebvre, R. A., *Chromatographia*, **1993**, 36(1), 356.
- ¹⁴Sane, R. T., Sahasrabudhe, S. P., Nayak, V. G., Ladage, K. D., Kothurkar, R. M. and Nayak, V. G., *Indian Drugs*, **1989**, 26(9), 491.
- ¹⁵Xie, X. T., Wu, G. L. and Liu, C. H., *Sepu*, **1993**, 11, 315.
- ¹⁶Abdelal, A. A., Kitagawa, S., Ohtani, H., El-Enany, N., Belal, F. and Walash, M. I., *Pharm. Biomed.*, **2008**, 46(3), 491.
- ¹⁷El-Sayed, G. O., Yasin, S. A. and El-Badawy, A. A., *Anal. Lett.*, **2008**, 41(17), 3021.
- ¹⁸Job, P., *Ann. Chem.*, **1936**, 16, 97; Job, P., *Advanced physicochemical experiments*, 2nd Edn., Edinburgh, Oliner and Boyd, **1964**, 54.
- ¹⁹Yoe, J. H. and Jones, A. L., *Ind. Eng. Chem. Anal. Ed.*, **1944**, 16(14), 111.
- ²⁰Lever, A.B.P., *Inorganic Electronic Spectroscopy*, 2nd Edn., Elsevier, Amsterdam, **1985**, 166.
- ²¹Tsubomura, H. and Lang, R., *J. Am. Chem. Soc.*, **1961**, 83, 2085.

- ²²Pandeeswaran, M. and Elango, K.P., *Spectrochim. Acta A.*, **2006**, 65, 1148.
- ²³Briegleb, G. and Czekalla, J., *Z. Phys. Chem. (Frankfurt)*, **1960**, 24, 37
- ²⁴Bensi, H. A. and Hildbrand, J. H., *J. Am. Chem. Soc.*, **1949**, 71, 2703.
- ²⁵Incedy, J., *Analytical application of complex equilibria*, John Wiley, Budapest, **1976**.
- ²⁶Martin, A. N., Swarbrick, J. and Cammarata, A., *Physical Pharmacy*, 3rd Edn., Lea and Febiger, Philadelphia USA, **1983**, 344.
- ²⁷ICH Guideline, Q2 (R1), *Validation of analytical procedures: Text and methodology*, London, **2005**.
- ²⁸Feng-lin, Z., Bian-Zhen, X., Zhi-Quan, T. and Shen-Yang, Z., *J. Pharm. Biomed. Anal.*, **1999**, 21(2), 355.

Received: 27.02.2013.

Accepted: 25.03.2013.